Макрогетероциклы

Macroheterocycles
http://mhc-isuct.ru

Том 15 № 4
Декабрь 2022

Журнал является форумом специалистов, изучающих макрогетероциклические соединения. Он публикует оригинальные экспериментальные и теоретические работы (полные статьи и краткие сообщения) и обзоры по синтезу, строению, физической и координационной химии макрогетероциклов, а также их практическому применению.

The journal is a forum for the specialists investigating macroheterocyclic compounds. It publishes original experimental and theoretical works (full papers and short communications) and reviews on synthesis, structural characterization, physical and coordination chemistry as well as practical application of macroheterocycles.

Abstract and indexing information:
♦ CAS: Chemical Abstracts Service (ACS)
♦ Russian Index of Scientific Citation (РИНЦ)
♦ SCOPUS (Elsevier)
♦ Thomson Reuters Products:
- Current Contents®/Physical Chemical and Earth Sciences
- Science Citation Index Expanded (also known as SciSearch®)
- Journal Citation Reports/Science Edition

Адрес редакции:
Россия, 153000 Иваново,
Пр. Шереметевский, 7
Тел. 007 4932 324182
э-почта: macroheterocycles@isuct.ru
http://mhc-isuct.ru/

Editorial address:
Russia, RF-153000 Ivanovo,
Sheremetevskiy pr., 7
Tel. 007 4932 324182
e-mail: macroheterocycles@isuct.ru
http://mhc-isuct.ru/

Отв. секретарь *– С. С. Иванова*
Подготовка материалов *– Т. А. Агеева, Н. Л. Печникова*
Компьютерная верстка *– А. Л. Куленцан*
Дизайн обложки – *В. Б. Шейнин*

Editorial Assistant *– S. S. Ivanova*
Technical Assistants *– T. A. Ageeva, N. L. Pechnikova*
Computer make-up *– A. L. Kulenzan*
Cover design *– V. B. Sheinin*

Учредитель: ФГБОУ ВО «Ивановский государственный химико-технологический университет» (ИГХТУ)

Publisher: Ivanovo State University of Chemistry and Technology (ISUCT Publishing)

Периодичность – 4 выпуска в год

Published four times per year

ISSN 1998-9539, E-ISSN 2713-1092

Зарегистрирован Федеральной службой по надзору в сфере массовых коммуникаций, связи и охраны культурного наследия. Свидетельство о регистрации ПИ №ФС77-28655 от 22 июня 2007 г.

Подписной индекс «Пресса России» - 42140

2022
Том 15
№ 4

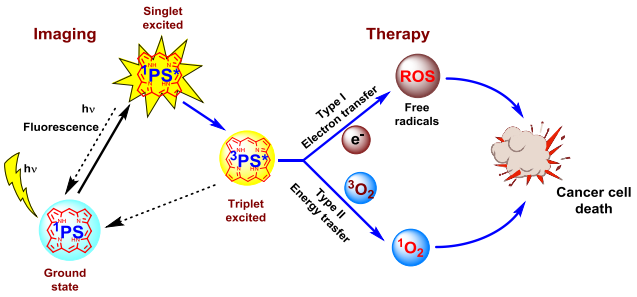

Content

DOI: 10.6060/mhc224870k

Synthesis Strategy of Tetrapyrrolic Photosensitizers for Their Practical Application in Photodynamic Therapy

Oskar I. Koifman[a,b@], Tatyana A. Ageeva[a], Natalia S. Kuzmina[c], Vasilii F. Otvagin[c], Alexander V. Nyuchev[c], Alexey Yu. Fedorov[c@], Dmitriy V. Belykh[d@], Nataliya Sh. Lebedeva[b], Elena S. Yurina[b], Sergey A. Syrbu[a,b], Mikhail O. Koifman[a], Yury A. Gubarev[b@], Dmitry A. Bunin[e], Yulia G. Gorbunova[e,f@], Alexander G. Martynov[e], Aslan Yu. Tsivadze[e,f], Semyon V. Dudkin[g@], Alexey V. Lyubimtsev[a@], Larissa A. Maiorova[a,h@], Maria V. Kishalova[a], Maria V. Petrova[a], Vladimir B. Sheinin[b], Vladimir S. Tyurin[e], Ilya A. Zamilatskov[e@], Eduard I. Zenkevich[i@], Philipp K. Morshnev[a,b], Dmitry B. Berezin[a@], Eduard A. Drondel[a], Andrey V. Kustov[a,b], Viktor A. Pogorilyy[k@], Alexey N. Noev[k,l@], Elizaveta A. Eshtukova−Shcheglova[k], Ekaterina A. Plotnikova[l], Anna D. Plyutinskaya[l], Natalia B. Morozova[l], Andrei A. Pankratov[l], Mikhail A. Grin[k], Olga B. Abramova[m@], Ekaterina A. Kozlovtseva[m], Valentina V. Drozhzhina[m], Elena V. Filonenko[l@], Andrey D. Kaprin[l], Anastasiya V. Ryabova[n,o@], Daria V. Pominova[n,o], Igor D. Romanishkin[n], Vladimir I.Makarov[n,o], Victor B. Loschenov[n,o], Kseniya A. Zhdanova[k@], Anastasia V. Ivantsova[k], Yulia S. Bortnevskaya[k], Natal'ya A. Bragina[k], Anna B. Solovieva[p@], Anastasya S. Kuryanova[p], and Petr S. Timashev[p,q]

[a]*Research Institute of Macroheterocyclic Compounds, Ivanovo State University of Chemistry and Technology, 153000 Ivanovo, Russia*
[b]*G.A. Krestov Institute of Solution Chemistry of the Russian Academy of Sciences, 153045 Ivanovo, Russia*
[c]*N.I. Lobachevsky State University of Nizhny Novgorod, 603950 Nizhny Novgorod, Russia*
[d]*Institute of Chemistry of Komi Republic Scientific Centre of the Ural Branch of Russian Academy of Sciences, 167000 Syktyvkar, Russia*
[e]*A.N. Frumkin Institute of Physical Chemistry and Electrochemistry, 119991 Moscow, Russia*
[f]*N.S. Kurnakov Institute of General and Inorganic Chemistry, Russian Academy of Sciences, 119991 Moscow, Russia*
[g]*A.N. Nesmeyanov Institute of Organoelement Compounds of the Russian Academy of Sciences (INEOS RAS), 119334 Moscow, Russia*
[h]*Institute of Pharmacoinformatics, Federal Research Center "Computer Science and Control" of Russian Academy of Sciences, Moscow, Russia*
[i]*Belarussian National Technical University, 220013 Minsk, Belarus*
[k]*MIREA-Russian Technological University, 119454 Moscow, Russia*
[l]*P. Hertsen Moscow Oncology Research Institute – Branch of the National Medical Research Radiological Centre of the Ministry of Health of the Russian Federation, 125284 Moscow, Russia*
[m]*Laboratory of Experimental Photodynamic Therapy, A.F. Tsyb Medical Radiological Research Center – Branch of the National Medical Research Radiological Center of the Ministry of Health of Russian Federation, 249034 Obninsk, Russia*
[n]*Prokhorov General Physics Institute, Russian Academy of Sciences, 119991 Moscow, Russia*
[o]*Department of Laser Micro-, Nano- and Biotechnologies, National Research Nuclear University MEPhI, 115409 Moscow, Russia*
[p]*N.N. Semenov Federal Research Center for Chemical Physics of the Russian Academy of Sciences, 119991 Moscow, Russia*
[q]*Institute for Regenerative Medicine, Sechenov University, 119991 Moscow, Russia*
E-mails: koifman@isuct.ru, afedorovnn@yandex.ru, belykh-dv@mail.ru, gua@isc-ras.ru, home_yuliya@mail.ru, sdudkin@ineos.ac.ru, lyubimtsev_av@isuct.ru, maiorova.larissa@gmail.com, joz@mail.ru, zenkev@tut.by, berezin@isuct.ru, pogorilviktor@gmail.com, aleksej-noev@yandex.ru, olyabramova@gmail.com, derkul23@yandex.ru, nastya.ryabova@nsc.gpi.ru, zhdanova_k@mirea.ru, ann.solovieva@gmail.com

This review presents a wide range of tetrapyrrole photosensitizers used for photodynamic therapy (PDT), antimicrobial photodynamic therapy, photoinactivation of pathogens. Methods of synthesis and design of new photosensitizers with greater selectivity of accumulation in tumor tissue and increased photoinduced antitumor activity are considered. The issues of studying the properties of new photosensitizers, their photoactivity, the ability to generate singlet oxygen, and the possibility of using targeted photodynamic therapy in clinical practice are discussed. The review examines the work on PDT by national and foreign researchers.

Keywords: Photodynamic therapy, antimicrobial photodynamic therapy, tetrapyrrolic macroheterocyclic compounds, porphyrins, phthalocyanines, chlorins, bacteriochlorins, synthesis, photosensitizers, optical properties, proteins, SARS-CoV-2, photoinactivation, optochemical diagnostics, self-assembling, nanostructures; Langmuir-Schefer films, extra-ligation, quantum dots, singlet oxygen generation, amphiphilic polymers, diagnostics, clinical application of PDT.

Стратегия синтеза тетрапиррольных фотосенсибилизаторов для их практического применения в фотодинамической терапии

О. И. Койфман[a,b@], Т. А. Агеева[a], Н. С. Кузьмина[c], В. Ф. Отвагин[c], А. В. Нючев[c], А. Ю. Федоров[c@], Д. В. Белых[d@], Н. Ш. Лебедева[b], Е. С. Юрина[b], С. А. Сырбу[a,b], М. О. Койфман[a], Ю. А. Губарев[b@], Д. А. Бунин[e], Ю. Г. Горбунова[e,f@], А. Г. Мартынов[e], А. Ю. Цивадзе[e,f], С. В. Дудкин[g@], А. В. Любимцев[a@], Л. А. Майорова[a,h@], М. В. Кишалова[a], М. В. Петрова[a], В. Б. Шейнин[b], В. С. Тюрин[e], И. А. Замилацков[e@], Э. И. Зенькевич[i@], Ф. К. Моршнев[a,b], Д. Б. Березин[a@], Э. А. Дрондель[a], А. В. Кустов[a,b], В. А. Погорилый[k@], А. Н. Ноев[k,l@], Е. А. Ештукова−Щеглова[k], Е. А. Плотникова[l], А. Д. Плютинская[l], Н. Б. Морозова[l], А. А. Панкратов[l], М. А. Грин[k], О. Б. Абрамова[m@], Е. А. Козловцева[m], В. В. Дрожжина[m], Е. В. Филоненко[n@], А. Д. Каприн[l], А. В. Рябова[n,o@], Д. В. Поминова[n,o], И. Д. Романишкин[n], В. И. Макаров[n,o], В. Б. Лощенов[n,o], К. А. Жданова[k@], А. В. Иванцова[k], Ю. С. Бортневская[k], Н. А. Брагина[k], А. Б. Соловьева[p@], А. С. Курьянова[p], П. С. Тимашев[p,q]

[a]*Институт макрогетероциклических соединений, Ивановский государственный химико-технологический университет, 153000 Иваново, Россия*
[b]*Институт химии растворов им. Г.А. Крестова РАН, 153045 Иваново, Россия*
[c]*Нижегородский государственный университет им. Н.И. Лобачевского, 603950 Нижний Новгород, Россия*
[d]*Институт химии Коми научного центра Уральского отделения РАН, 167000 Сыктывкар, Россия*
[e]*Институт физической химии и электрохимии им. А.Н. Фрумкина РАН, 119071 Москва, Россия*
[f]*Институт общей и неорганической химии им. Н.С. Курнакова РАН, 119991 Москва, Россия*
[g]*Институт элементоорганических соединений им. А.Н. Несмеянова РАН (ИНЭОС РАН), 119334 Москва, Россия*
[h]*Институт фармакоинформатики Федерального исследовательского центра «Информатика и управление» Российской академии наук, Москва, Россия*
[i]*Белорусский национальный технический университет, 220013 Минск, Беларусь*
[k]*МИРЭА - Российский технологический университет, 119454 Москва, Россия*
[l]*МНИОИ им. П.А. Герцена - филиал ФГБУ «НМИЦ радиологии» Минздрава России, 125284 Москва, Россия*
[m]*Медицинский радиологический научный центр им. А.Ф. Цыба – филиал ФГБУ «НМИЦ радиологии» Минздрава России, 249036 Обнинск, Россия*
[n]*Институт общей физики им. А.М. Прохорова РАН, 119991 Москва, Россия*
[o]*Национальный исследовательский ядерный университет «МИФИ», 115409 Москва, Россия*
[p]*Федеральный исследовательский центр химической физики им. Н.Н. Семенова РАН, 119991 Москва, Россия*
[q]*Институт регенеративной медицины Московского государственного медицинского университета им. М.М. Сеченова, Москва, Россия*
E-mails: koifman@isuct.ru, afedorovnn@yandex.ru, belykh-dv@mail.ru, gua@isc-ras.ru, home_yuliya@mail.ru, sdudkin@ineos.ac.ru, lyubimtsev_av@isuct.ru, maiorova.larissa@gmail.com, joz@mail.ru, zenkev@tut.by, berezin@isuct.ru, pogorilviktor@gmail.com, aleksej-noev@yandex.ru, olyabramova@gmail.com, derkul23@yandex.ru, nastya.ryabova@nsc.gpi.ru, zhdanova_k@mirea.ru, ann.solovieva@gmail.com

В обзоре представлен широкий спектр тетрапиррольных фотосенсибилизаторов, применяемых для фотодинамической терапии (ФДТ), антимикробной фотодинамической терапии, фотоинактивации патогенов. Рассмотрены методы синтеза и дизайн новых фотосенсибилизаторов, обладающих большей селективностью накопления в опухолевой ткани и повышенной фотоиндуцированной противоопухолевой активностью. Обсуждаются вопросы исследования свойств новых фотосенсибилизаторов, их фотоактивность, способность генерировать синглетный кислород, возможности применения таргетной фотодинамической терапии в клинической практике. В обзоре рассмотрены работы по ФДТ отечественных и зарубежных исследователей.

Ключевые слова: Фотодинамическая терапия, антимикробная фотодинамическая терапия, тетрапиррольные макрогетероциклические соединения, порфирины, фталоцианины, хлорины, бактериохлорины, синтез, фотосенсибилизаторы, оптические свойства, белки, SARS-CoV-2, фотоинактивация, оптохимическая диагностика, наноматериалы, самоорганизация, наноструктуры, пленки Ленгмюра-Шеффера, экстракоординация, квантовые точки, генерация синглетного кислорода, амфифильные полимеры, диагностика, клиническое применение ФДТ.

Introduction

The idea of this review was born as a result of a detailed discussion of the problems of photodynamic therapy at the “PDT Day” section at the XIV International Conference "Synthesis and Application of Porphyrins and Their Analogues" (ICPC-14), held at Ivanovo State University of Chemistry and Technology from 29th June to 4th July, 2022. The unique ability of porphyrins and related compounds to generate reactive oxygen species under the influence of light necessitates the synthesis of new photosensitizers with the required properties (such as selectivity, virulence, bacteriocide properties, *etc*.). Such properties are a crucial part of effective use of photosensitizers in photodynamic therapy, clinical laboratory diagnostics and photodynamic inactivation of bacteria and viruses that can be harmful to humans. Therefore, the review focuses on the synthetic aspects of tetrapyrrole macroheterocycles and their modification for the purposes of targeting photodynamic therapy. Leading specialists in the photosensitizers’ synthesis and research, as well as PDT practitioners were involved in writing this article.

List of Abbreviations:

$^1O_2$ – singlet oxygen
aPDT – antibacterial photodynamic therapy
BC – bacteriochlorin (7,8,17,18-tetrahydroporphyrin)
BSA – bovine serum albumin
CMPI – 2-Chloro-1-methylpyridinium iodide
DAMPs – damage-associated molecular patterns
DCC – dicyclohexylcarbodiimide
EDAC – 1-ethyl-3-(3-dimethylaminopropyl)carbodiimide
FLI – fluorescence imaging
FRET – fluorescence resonance energy transfer
FRET – foerster resonance energy transfer
GFC – gel filtration chromatography
GSH – glutathione
HCP1 – heme carrier protein 1
HDACi – histone deacetylase inhibitor
HDACs – histone deacetylases
HDL – high-density lipoproteins
HLB – hydrophilic-lipophilic balance
iBC – isobacteriochlorin (2,3,7,8-tetrahydroporphyrin)
LDL – low density lipoproteins
MAM – metastasis-associated macrophages
MDR – multiple drug resistance
MHC – macroheterocyclic compounds
MRI – magnetic resonance imaging procedure
NIR – near infrared
PBS – phosphate buffered saline
Pcs – phthalocyanines
PDT – photodynamic therapy
PL – photoluminescence
PSs – photosensitizers
QD – quantum dots
RBD – receptor-binding domain
ROS – reactive oxygen species
TAM – tumor associated macrophages
TFA – trifluoroacetic acid
TKI – tyrosine kinases inhibitors
TLC – thin-layer chromatography
TNTR – the tumor-to-normal tissue ratio
TOPO – tri-n-octyl phosphine oxide

1. The Key Role of Tetrapyrrole Macroheterocyclic Compounds in Photodynamic Therapy

Photodynamic therapy (PDT) is a perspective socially significant method of treatment successfully applied both for tumor neoplasms and microbial infections caused by poly-resistant pathogens.[1-9] This method requires the presence of three components: irradiation (including NIR radiation), photosensitizer (PSs, phototherapeutic agent) and molecular oxygen. Photosensitizers, substances selectively localized in tumor or microbial cells, produce reactive oxygen species (ROS)[4,10-13] when exposed to the red light in the presence of dioxygen.

In recent three decades, photodynamic therapy has attracted much attention due to its non-invasive features, low side effects and low systemic toxicity.[14-16] The photosensitizers are activated on exposure to light and become photosensitizers’ triplet, which, react with molecular oxygen to produce reactive oxygen species (Figure 1).[17,18] The hydroxyl radical is another reason which leads to the reaction between the photosensitizer and molecular oxygen. These cytotoxic molecules induce a series of biological reactions that ultimately lead to cell death. The outcomes of PDT depend on the nature of the cells, as well as the on the properties and localization of photosensitizer and the illumination conditions. Its obvious advantage is that cause negligible damage to the surrounding normal tissues and has little systemic effects.

Correspondingly, PSs is one of the key factors of PDT, and its physico-chemical properties (*e.g.* interaction with molecular oxygen, efficiency of singlet oxygen generation, solubility, successful targeting and delivery, *etc*.) largely determine the outcome of PDT. In this respect, it was evidently shown that tetrapyrrolic macrocycles (porphyrins, chlorins, bacteriochlorins, phthalocyanines) are potentially translatable PSs with exceptional properties, multifunctional uses and excellent biocompatibility for PDT, thus their special affinity to cancer cells makes them the ligands par excellence for anticancer drugs.[19-28] One of the prominent advantages of most porphyrins is that they have special affinity for cancer cells, which enables them to selectively remain in cancer cells, providing feasibility for the research of anti-tumor targeted drugs.[29–32]

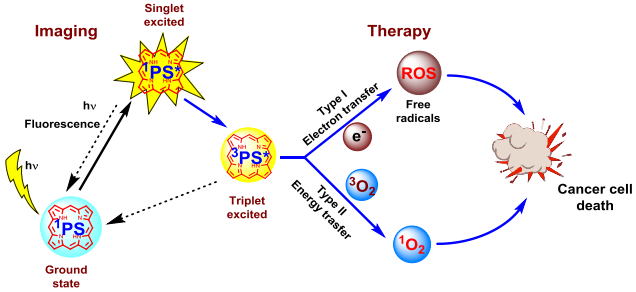

Figure 1. Schematic diagram of photodynamic therapy.

These tetrapyrrolic macroheterocyclic compounds are the focus of research because of their stability under a wide range of environmental conditions, absorption in the visible and near infra-red ranges of the electromagnetic spectrum (400–1000 nm), many derivatives possess long lived triplet excited states that sensitize singlet oxygen ($^1O_2$) formation to potentiate phototoxicity as anticancer and antibiotic agents. These macrocycles can chelate with nearly every metal in the periodic table which results in variable functional properties such as tuneable excited state lifetimes, redox potentials, catalytic activities, molar absorption coefficients, and molecular dynamics. Functional groups on the periphery of structurally rigid porphyrinoids provide topological diversity, making these pigments well suited for the engineering of supramolecular materials.[33-36]

Porphyrins and their analogues are organic heterocyclic macrocycles with photophysical properties well-suited for clinical phototherapy and cancer imaging. However, their wider application in the clinical management of disease is barred by poor aqueous solubility, bioavailability, tumour accumulation and skin phototoxicity. These limitations require the search of new photoactive systems devoid of these disadvantages

Chemists devoted many efforts to improving the efficiency and selectivity of the photosensitizers to prevent the side-effects of PDT over the last few decades. The perfect photosensitizers should meet several criteria: (1) pure and stable molecule, (2) no cytotoxicity in the dark, (3) optimal absorption, distribution, metabolism and excretion properties, (4) high molar absorption coefficient in the long wavelength region (650–800 nm) for maximum light penetration through tissue, (5) high $^1O_2$ quantum yield, (6) tumor selectivity and (7) ease of synthesis and a scalable process.[37-41] Today, numerous tetrapyrrole macroheterocyclic compounds that have been investigated as promising photosensitizers for use in PDT meet several necessary criteria, such as strong absorbing properties in the range from 650 to 700 nm, high quantum yield in the triplet state, high photostability and often minimal toxicity. In the world clinical practice, many tetrapyrrol photosensitizers have already found their application for the treatment of various forms of cancer.

As the PDT method was developing, all photosensitizers used in the clinical practice were grouped into several generations, mainly based on their spectral and photophysical properties.[17,23,42] The first generation of PS includes porphyrin derivatives, for example, hematoporphyrin isolated from blood (Figure 2). Based on this compound, the first domestic photosensitizer "Photogem"[43] was developed by Prof. A.F. Mironov, the founder of our scientific team. The second generation combines natural and synthetic compounds, including chlorins, bacteriochlorins, phthalocyanines, benzoporphyrins, and others. Finally, the third generation includes PS with enhanced spectral properties that absorb in the near-infrared range of the spectrum and show targeting against tumors of various genesis.

A huge number of reviews have been published on the chemistry, photochemical characteristics and clinical applications of PDT photosensitizers.[44–61] The number of publications devoted to tetrapyrrol photosensitizers, which are at different stages of development and clinical trials, is growing rapidly.

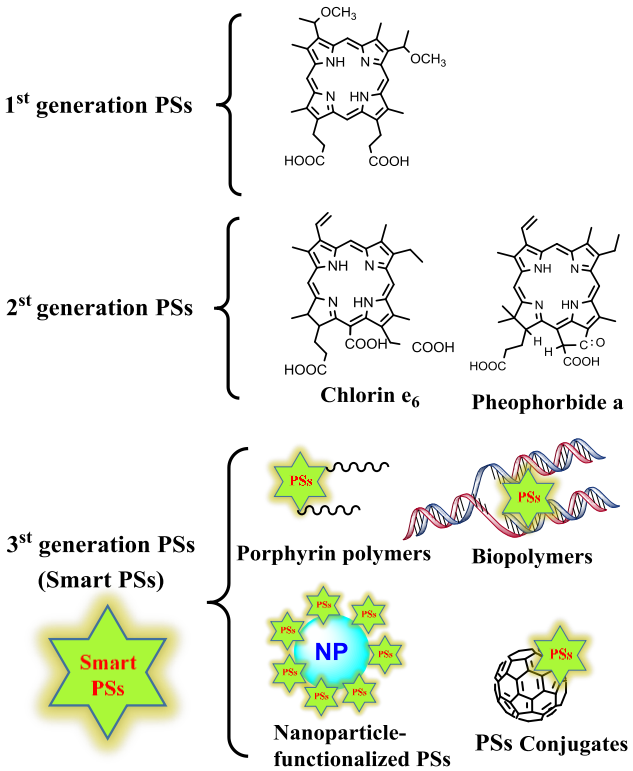

Figure 2. Classification of the generations of PSs developed so far.

The history of the development of PDT using tetrapyrrole photosensitizers dates back almost a hundred years. The starting date was an observation made in 1924 by A. Policard who revealed accumulation in animal tumors of endogenous porphyrins able to fluoresce under UV irradiation.[62] In 1942, H. Auler and G. Banzer recorded red fluorescence in the primary tumor and metastases in rats subjected to subcutaneous and intramuscular administration of hematoporphyrin.[63]

The modern stage of development of fluorescence diagnosis and photodynamic therapy began in the 1960s, when R. Lipson et al. (the United States) revealed the possibility to record the fluorescence of porphyrin in tumors of cancer patients who were administered the hematoporphyrin derivative prepared by acetylation and reduction of a porphyrin mixture enriched in hydrophobic oligomers.[64] It is commonlythat wide clinical use of photodynamic therapy of cancer began in 1978, when T. Dougherty *et al.* reported the results from application of this method for treatment of 25 patients with 113 primary, recurrent, and metastatic skin tumors.[65]

In Russia, photodynamic therapy of tumors has been the subject of experimental research for many years, but it was not until 1992 that it received development in clinical practice, when the first dosage form of the domestic photosensitizer Photohem from a group of hematoporphyrin derivatives was created. Successful clinical trials were conducted at Gertsen Moscow Research Oncological Institute and the State Scientific Center of Laser Medicine. After two years (in 1994), clinical trials of second generation photo-

sensitizer Photosens, on the base sulfonated aluminum phthalocyanine, developed at the SSC Research Institute of Organic Intermediates and Dyes, (Corresponding Member of RAS Prof. G.N. Vorozhtsov, Prof. E.A. Luk'yanets) were started. In 1999, clinical application of Alasens, a 5-aminolevulinic acid-based drug (GHTs NIOPIK, Corresponding Member of RAS Prof. G.N. Vorozhtsov, Prof. E.A. Luk'yanets) and in 2002 and 2004, that of drugs prepared from e6 chlorin, Radachlorin [Radafarma, Limited Liability Company, A.V. Reshetnikov], and Photoditazine (VETA–GRAND, Limited Liability Company, Prof. G.V. Ponomarev), respectively, were begun. Three decades of the history of the creation of tetrapyrrol photosensitizers that have received clinical use in Russia are reflected in Figure 3. The introduction of new treatment methods in Russia was facilitated by the development of appropriate domestic diagnostic and therapeutic equipment. The available instrumental base and domestic photosensitizers make photodynamic therapy not only a highly effective but also an economically feasible method.[66]

Although a few porphyrin/chlorin based PSs have been approved for clinical use, PDT is still limited by the low stability and poor tumor targeting capacity of the large majority of these macrocycles in vivo. The main obstacles in effective delivery of PSs are associated with these intrinsic properties. At present, two possible approaches to overcome this problem seem to be of interest in this direction.

One way is the supramolecular organic chemistry/photochemistry, a highly interdisciplinary field of science covering the chemical, physical, and biological features of chemical species held together and organized by means of intermolecular binding interactions of covalent and non-covalent nature. The resulting crossover has provided novel principles and concepts in physico-chemistry such as molecular recognition, self-organization, regulation, cooperativity, replication. A significant interest of numerous scientific groups in this direction has been devoted to the design and investigation of tetrapyrrole compounds that fold or assemble predictably in order to form multicomponent well-defined arrays which may be perspective in nanobiomedicine.[72-76]

On the other hand, small molecular PSs (including tetrapyrrolic macrocycles of various structure and physicochemical properties) can be attached to functional organic or inorganic nanomaterials to enhance the PS stability and tumor targeted delivery, and, in addition, some functionalized nanocarriers themselves can be directly used as PSs.[51,77,78] To date, nanostructures of different types and morphology (such as metal nanoparticles, semiconductor quantum dots, graphene-based nanomaterials, liposomes, ROS-sensitive nanocarriers and supramolecular nanomaterials)[79-88] have been tested as possible nanoplatforms for tetrapyrrolic PSs. Various nanomaterial systems have shown great potentials in improving PDT.[51,78,89]

The application of PDT is not only limited to oncology, but is also being explored for the treatment of cardiovascular, dermatological, ophthalmic and infectious diseases.[48] In accordance with the achievements of PDT today, five main areas of application can be distinguished. These are: (i) the anti-cancer agents for photodynamic therapy (PDT), (ii) the anti-cancer agents for photoimmunotherapy (PIT), (iii) the agents for photodynamic therapy (PDT) in ophthalmology, (iv) the agents for photodynamic therapy (PDT) in dermatology, and (v) the anti-microbial agents for photodynamic inactivation (PDI).

How to enhance the selective uptake and uniform distribution of photosensitizers in tumor tissues is still an urgent conundrum to be solved, especially the specific targeting of different cells and tumor tissues, to improve the efficacy and reduce their toxic and side effects on healthy tissues and organs. This may be a promising research direction, introducing functionally active groups into porphyrin photosensitizers to improve their targeting and anti-tumor activity, and then selectively delivering them to tumor tissues with transport carriers such as liposomes, magnetic nanoparticles and metal–organic frameworks. The advantages are as follows: photosensitizers bond with bioactive groups, which can exert synergistic therapeutic effects and improve the efficacy. Also, combining with a transport carrier having a bio-recognition function is conducive to improving the ability of the photosensitizers to penetrate tissues, enhancing the targeting of tumor tissues and increasing the drug-level concentration at the target site.

Further improvement of the photodynamic therapy technique requires finding new photosensitizers having higher photoactivity, possessing better tumor-tropic properties, and excitable in the near-infrared spectral region, as well as designing highly sensitive and reliable diagnostic and therapeutic equipment. Clinical experience with photodynamic therapy allows rating this method among the most promising directions in modern clinical oncology.

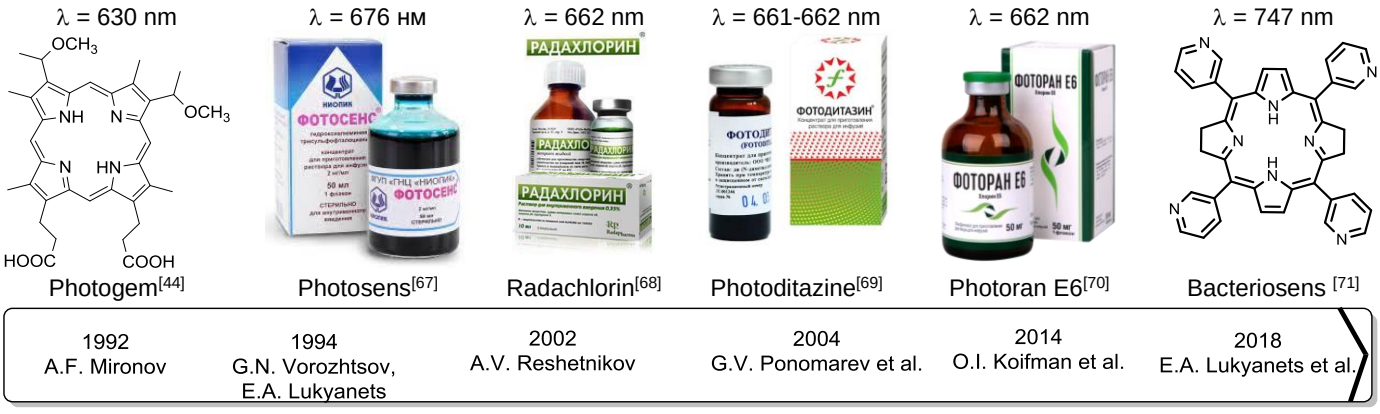

Figure 3. The Russian tetrapyrrolic photosensitizers that have received clinical use for PDT.

2. Conjugation of photosensitizers with cytotoxic molecules – an emerging trend in combination therapy

One of notorious problems associated with cancer diseases is a lack of the universal treatment protocol for patients diagnosed with a cancer. Due to genetic uniqueness of cancer cells, it is almost impossible to propose the treatment, whose outcome is completely predictable. In this regard, the combined therapy aimed to multiple cellular targets has many advantages over conventional chemotherapy.[90] Thus, combining various anticancer drugs it is possible to reverse drug resistance and fight metastatic cancers,[91] what is difficult for singular modalities. Moreover, combination therapy works in a synergistic manner, and therefore a lower therapeutic dosage of each individual drug is required. Among possible drug combinations the utilization of photodynamic therapy and chemotherapy together stands out as an emerging trend.[92,93] The successful outcome of PDT is highly dependent on a proper irradiation of a full area where cancer tissues are located. Combined treatment with a chemotherapeutic drug lowers this risk and inhibits pathogenic cells survived PDT.[94] Another notable advantage is the enhanced delivery of chemotherapeutic drugs after conjugation with porphyrinoid photosenstitizers. Due to binding with low density lipoproteins (LDL),[95] heme carrier protein 1 (HCP1)[96] or peripheral benzodiazepine receptor[97] the photosensitizing part can increase concentration of the chemotherapeutic counterpart in tumor cells. Therefore, along with therapeutic properties PS demonstrates a targeting delivery as well. Thus, such synergistic behavior can lead to reduce of a drug dose and systemic toxicity.[98,99] Another outstanding advantage of combining chemotherapy with PDT is the unique ability of PDT to induce an immune response to treatment.[100] Since the result of photodynamic action may be an inflammatory reaction, the resulting damage-associated molecular patterns (DAMPs) can be recognized by the corresponding receptors of neutrophils, which ultimately leads to the activation of the immune system in response to PDT.

Generally, there are many possible ways to connect PS with a chemotherapeutic molecule. The first way is administration of two or more drugs independently during one course of a treatment. To achieve a proper combinational effect in this case, a dosage has to be carefully chosen.[101] Another option is the incorporation of drugs in targeted systems - liposomes or nanoparticles.[91,102] One of the main problems associated with such approach is unpredictable properties arising during manufacturing of these delivery platforms. Thus, the procedures for surface modification may strongly modify the size, charge, shape, stability, drug loading, and releasing ability of the nanovectors,[103] what can cause undesirable side effects. In recent decades, covalent binding of a photosensitizer and a cytostatic agent demonstrated exceptional utility and efficiency (Figure 4).[92,104–107] Such platform operates with homogeneous, chemically pure and stable compounds, which satisfies the requirements for an ideal photosensitizer.[92,108] In addition, the structure of covalent conjugates can be easily varied over a wide range, thereby changing their biological activity. In order to create chemical bonding between active parts specific linkers are used, which provide sufficient separation in the space of the active fragments.

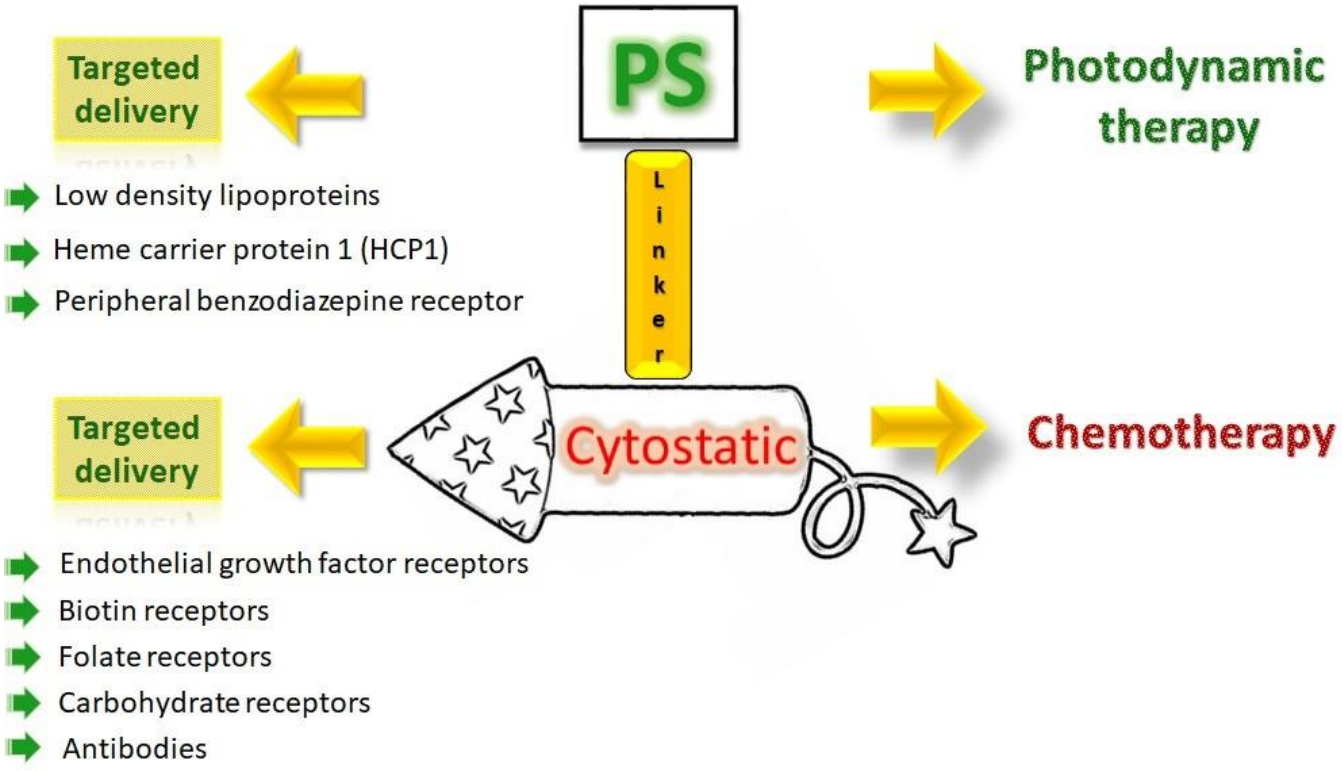

Figure 4. Combining chemotherapy with PDT in conjugated system.

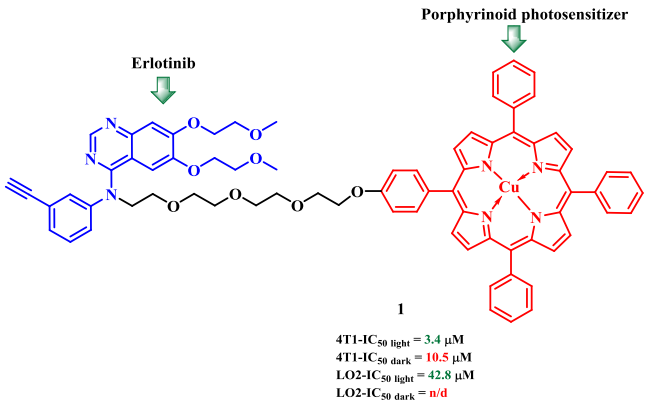

Scheme 1.

Interestingly, in some cases the chemotherapeutic part can also demonstrate binding to key proteins in cells and as a consequence improves delivery of PS.[106,109–111] Thus, tyrosine kinases inhibitors (TKI) have been proposed as a perspective cytostatic vector for the design of conjugates. One of the widely utilized TKI for construction of conjugates is erlotinib, which binds to the epidermal growth factor receptor (EGFR) known for its overexpression in many types of tumors.[103] Erlotinib provides targeted binding of the conjugate with EGFR and inhibits its activity what leads to a death of cancer cells.

One of the recent examples of photoactive conjugates designed with utilization of erlotinib is conjugate **1** (Scheme 1).[112] In this work Huang with colleagues suggested a conjugate **1**, where the copper(II) porphyrin moiety plays a dual role both as a photosensitizer and a sensor for glutathione-dependent apoptotic processes. The decrease of glutathione (GSH) level is an important benchmark during apoptotic processes.[113] Interestingly, paramagnetic copper being bound to NH fragments is capable to coordinate GSH which leads to fluorescence intensification.[114] However, when the concentration of glutathione is low, the copper(II) porphyrin exists in a fluorescence-quenching aggregation state.[114] This phenomenon was used to visualize apoptotic cells and monitor the therapeutic effect during PDT.[112] Copper tetraarylporphyrin and erlotinib were conjugated with the tetraethyleneglycol linker. The authors showed that the presence of erlotinib increases the selectivity of conjugate accumulation in murine breast cancer cells 4T1 (IC_{50} (**1**) = 3.4 μM against IC_{50} (Cu-porphyrin without erlotinib) = 25 μM) with an elevated level of EGFR compared to the non-tumor human hepatic LO2 line (IC_{50} (**1**) = 42.8 μM against IC_{50} (Cu-porphyrin without erlotinib) = 31.7 μM) with a low level of EGFR expression (LED, λ=540 nm). Furthermore, conjugate **1** could respond to intracellular glutathione fluctuations. Upon treatment of HepG2 cells with **1**, its fluorescence was restored, which can timely estimate the therapeutic efficiency of bimodal chemo- and photodynamic therapy.

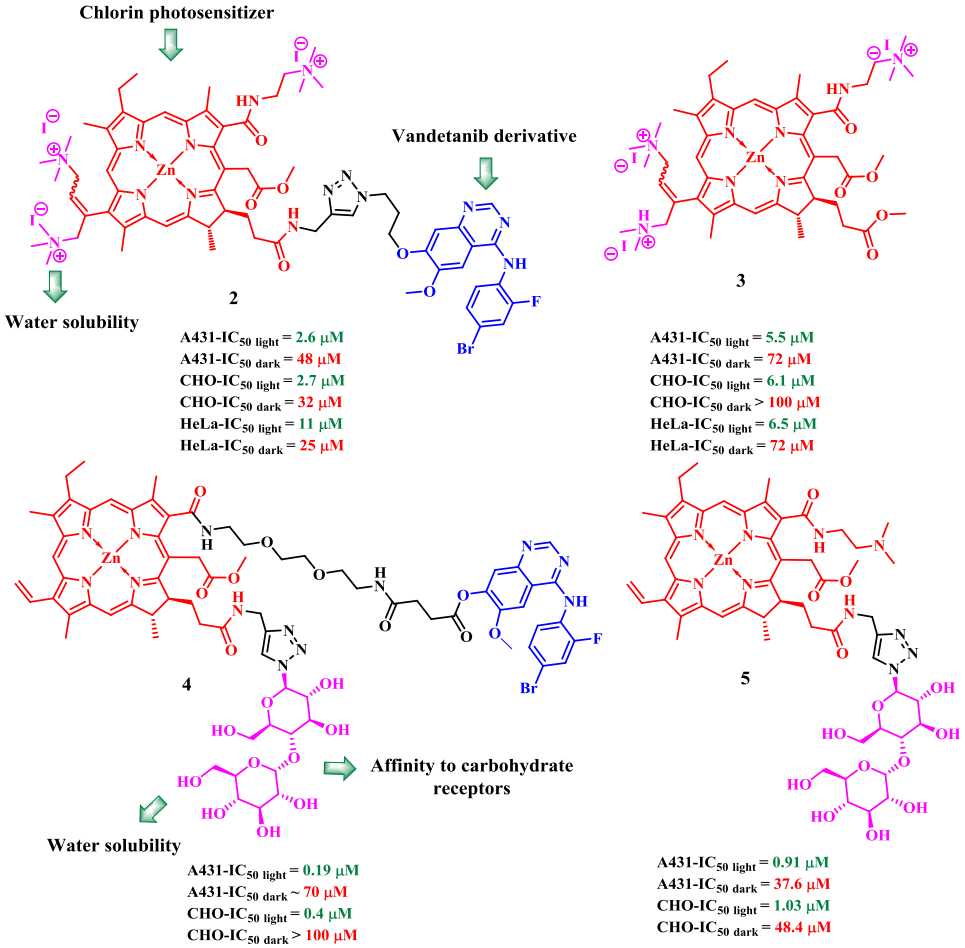

Scheme 2.

The research group under supervision of Prof. A.Yu. Fedorov is also interested in creation of various multifunctional conjugates with improved pharmacological parameters. Thus, the vandetanib derivative, another inhibitor of EGFR and VEGFR (vascular endothelial growth factor) tyrosine kinases, as part of a conjugated system based on the chlorin e_6 zinc complex **2** was used (Scheme 2).[110] Vanetanib was supposed to play the role of a dual agent of selective delivery due to preferential binding to VEGFR and EGFR receptors overexpressed by many types of tumors, as well as cytotoxic action due to inhibition of the activity of the mentioned tyronis kinases.[115] To increase water solubility, chlorin derivative was modified by the introduction of three ammonium groups in the form of quaternized salts. The conjugate **2** showed a selective accumulation in A431 cells (EGFR-positive, human epidermoid carcinoma), which was greater than in non-tumor CHO cells (EGFR-negative, chinese hamster ovary cells) and HeLa cells (human epidermoid carcinoma) with a low level of EGFR expression. Under the action of light (LED, λ= 615-635 nm), the conjugate **2** inhibited the growth of all cell lines at low micromolar concentrations, while without irradiation, the values of the half-inhibition index (IC_{50}) were approximately an order of magnitude higher. This indicates that when bound to chlorin-e_6, Vandetanib derivative is unable to inhibit cell growth. It should be noted that chlorin-e_6 without Vandetanib **3** had 2-3 times lower toxicity in all cell lines. In experiments performed on CT-26 tumor-grafted mice, the conjugate **2** also demonstrated selective accumulation in the tumor.

Then, it was decided to change the type of the linkage between vandetanib and chlorin-e_6 from an ether bond to an ester bond (Scheme 2). It is known that ester bonds in the body are easily destroyed by the action of esterase,[116] therefore, the modified conjugate may be capable of releasing vandetanib, which means that the synergistic effect of PDT and chemotherapy can be observed. The second change was to replace the tetramethylammonium groups with maltose-based carbohydrate moieties. Having hydrophilic properties, carbohydrates also selectively bind to their respective receptors (galectins and GLUT transporters) in tumor cells by the Warbug effect.[117-119] Although there was almost no selectivity for A431 cells compared to CHO, the conjugate **4** generally accumulated better in these cells than the conjugate with ammonium fragments **2**, and also showed less pronounced cytotoxicity in the dark compared to **2**. Under light irradiation (LED, λ = 655−675 nm) in A431 cells, the conjugate **4** was 2 times more active than in the CHO cell line and 2–5 times more active than unconjugated chlorin-e_6 **5**. An *in vivo* study of activity in mice with grafted A431 tumors showed a moderate selectivity for tumor-normal cells, as well as slight differences in the activity of the conjugate in the light and in the dark. This fact implies that the conjugate **4** enters the cells and releases vandetanib by esterase-mediated ester cleavage. Thus, the obtained results indicate different behavior of vandetanib-chlorin-e_6 conjugates depending on the type of bond between the key fragments.

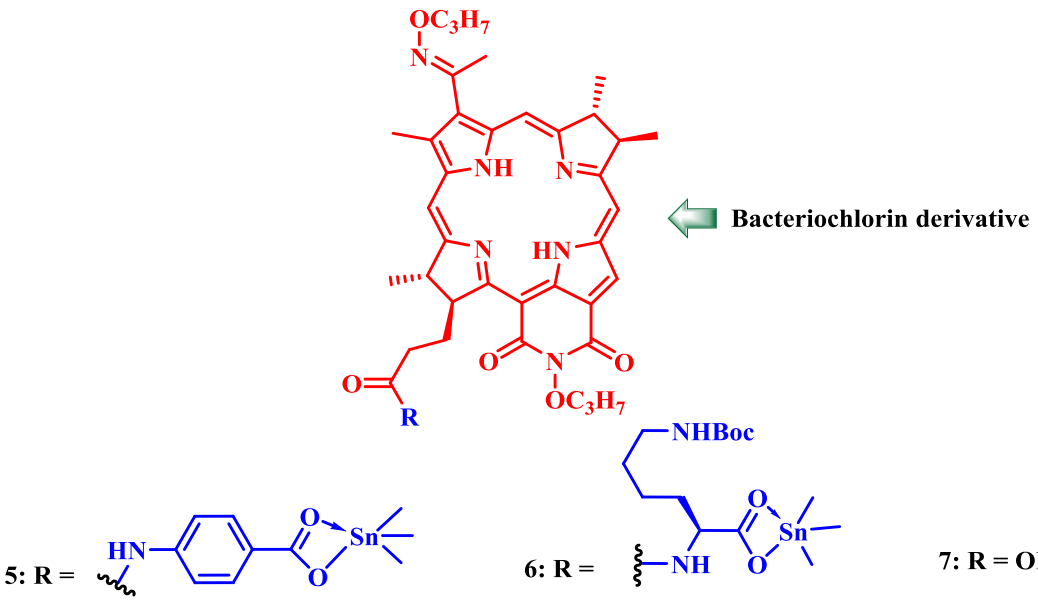

5: S-37-$IC_{50\ light}$ = 0.13 mmol/ml; S-37-$IC_{50\ dark}$ = 2.7 mmol/ml; PC-3-$IC_{50\ light}$ = 0.07 mmol/ml; PC-3-$IC_{50\ dark}$ = 1.1 mmol/ml; MCF-7-$IC_{50\ light}$ = 0.12 mmol/ml; MCF-7-$IC_{50\ dark}$ = 6.9 mmol/ml; A549-$IC_{50\ light}$ = 0.11 mmol/ml; A549-$IC_{50\ dark}$ = 3.0 mmol/ml; HeLa-$IC_{50\ light}$ = 0.41 mmol/ml; HeLa-$IC_{50\ dark}$ = 8.6 mmol/ml

6: S-37-$IC_{50\ light}$ = 0.06 mmol/ml; S-37-$IC_{50\ dark}$ = 3.1 mmol/ml; PC-3-$IC_{50\ light}$ = 0.06 mmol/ml; PC-3-$IC_{50\ dark}$ = 0.6 mmol/ml; MCF-7-$IC_{50\ light}$ = 0.05 mmol/ml; MCF-7-$IC_{50\ dark}$ = 3.1 mmol/ml; A549-$IC_{50\ light}$ = 0.09 mmol/ml; A549-$IC_{50\ dark}$ = 2.2 mmol/ml; HeLa-$IC_{50\ light}$ = 0.26 mmol/ml; HeLa-$IC_{50\ dark}$ = 3.0 mmol/ml

7: S-37-$IC_{50\ light}$ = 0.17 mmol/ml; S-37-$IC_{50\ dark}$ = 3.3 mmol/ml; PC-3-$IC_{50\ light}$ = 0.09 mmol/ml; PC-3-$IC_{50\ dark}$ = 1.0 mmol/ml; MCF-7-$IC_{50\ light}$ = 0.14 mmol/ml; MCF-7-$IC_{50\ dark}$ = 3.9 mmol/ml; A549-$IC_{50\ light}$ = 0.16 mmol/ml; A549-$IC_{50\ dark}$ = 2.8 mmol/ml; HeLa-$IC_{50\ light}$ = 0.62 mmol/ml; HeLa-$IC_{50\ dark}$ = 10.0 mmol/ml

Scheme 3.

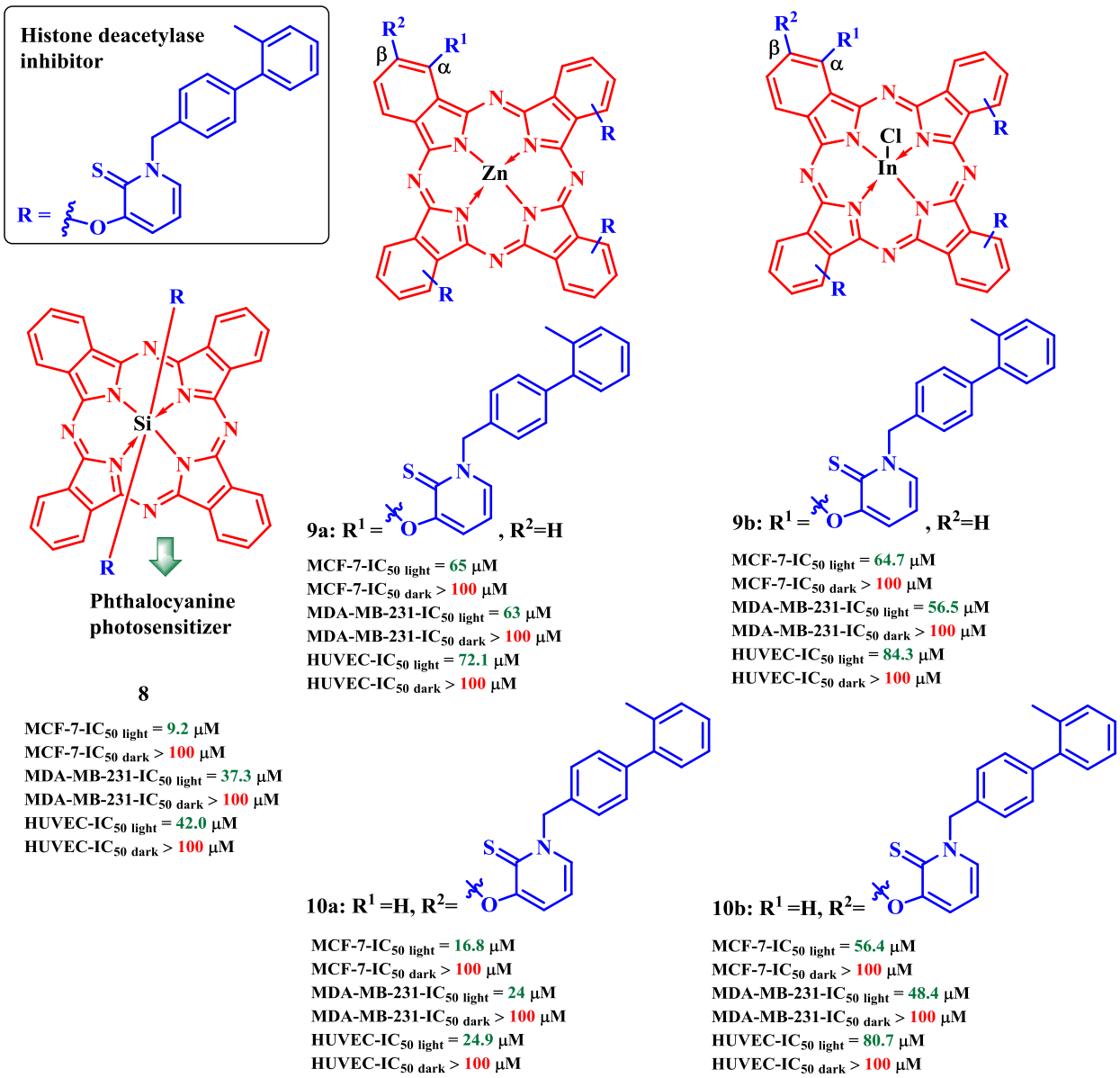

Scheme 4.

Metal-containing drugs are broadly known for their significant antitumor activity.[120] The conjugation of such metal complexes with PSs can modulate their hydrophilic properties. Due to the interaction with DNA, metal complexes[121] may serve as a vector to deliver PS to the cell nuclei. Organotin complexes are an attractive alternative to the known platinum-containing cytostatics because of lowered systemic toxicity.[122] Importantly, such complexes can be effective in cell lines possessing cisplatin resistance.[123,124] In 2021, two conjugates of bacteriochlorin derivative and a tin complex with amino acid ligands (*p*-aminobenzoic acid and L-lysine) **5-6** was obtained by Prof. Grin with colleagues (Scheme 3).[125]

The dark cytotoxicity of conjugates **5** and **6** in various cell lines (prostate gland adenocarcinoma (PC-3); breast adenocarcinoma (MCF-7); lung carcinoma (A549); cervix adenocarcinoma (Hela) and mouse sarcoma (S-37)) was 3-5 times higher than that of the corresponding organotin complexes. Based on studies *in vitro*, the authors concluded that the conjugation of tin-containing cytostatics with bacteriochlorin moieties promotes better internalization and accumulation of conjugates in tumor cells and therefore increased cytotoxicity. Among synthesized conjugates, the molecule **6** demonstrated exceptional photodynamic efficiency (2-3 fold increased IC_{50} under light) compared to referenced bacteriochlorin derivative **7** (halogen lamp, $\lambda \geq 720$ nm). The nature of the intracellular distribution of the obtained agents showed a diffuse granular distribution with predominant accumulation in the near nuclear region, but it was not possible to observe the localization of conjugates in the nuclei themselves. Thus, the authors conclude that the tin complexes act as target fragments for the delivery of bacteriochlorins into the cells.

Histone deacetylases (HDACs) are directly involved in carcinogenesis and therefore represent an attractive targets for anticancer therapy.[90,126] Inhibition of HDACs is shown to suppress growth of cancer cells, promote cell death, modulate immune responses, and inhibit formation

of new blood vessels.[127] Mainly approved for hematological malignancies, histone deacetylase inhibitor (HDACi) has been clinically tested for solid tumors and has shown better results when combined with another chemotherapy drug.[128] It is also known that, HDAC6 and HDAC8 are highly expressed in breast cancer cells, therefore their downregulation may be beneficial.[129] In 2020 Aru with colleagues reported the 3-hydroxypyridin-2-thione (3-HPT) substituted silicon phthalocyanine derivative **8** and evaluated its anti-cancer properties on two different breast cancer cell lines (non-invasive MCF-7 and invasive MDA-MB-231 cells) (LED, λ=700 nm). It was shown, that conjugate **8** activated programmed cell death pathways and induced cell cycle arrest which was accompanied by decreasing levels of HDAC6 and HDAC8 (Scheme 4).[130]

Among various breast cancers, its triple negative variant doesn't respond to classical hormone therapy and always associated with poor prognosis.[131] In this regard, promising results obtained after treatment of cell line MDA-MB-231 (triple negative breast cancer) with **8** can become a starting point for a novel treatment of such disease. Thus, the authors demonstrated pronounced inhibition of MDA-MB-231 cells with the highest late apoptotic cell population. Inspired by the obtained results, the authors evaluated how the substitution in α- or β-position of a phthalocyanine with HDACi inhibitor affects antitumor behavior of suggested conjugates.[132] Additionally, different metals were chosen for complexation with a phthalocyanine core. The influence of the central ion on the internalization of conjugates was different for zinc and indium derivatives. While for α-substituted indium conjugates **9b** and **10b** no differences were found in their cell uptake, β-substituted Zn-conjugate **10a** in demonstrated enhanced internalization and, therefore, a more pronounced antitumor effect compared to its α-analogue-conjugate ZnPc **9a** (LED lamp, red light). It was also noted that although all conjugates generated ROS in the mitochondrial network, only indium compounds **9b** and **10b** directly targeted mitochondria. Treatment of cells with obtained conjugates also led to cell cycle arrest in different phases of cell cycle.

Camptothecin **11** is a potent antitumor antibiotic whose action mechanism involves the inhibition of DNA relaxation by the stabilization of a covalent binary complex formed between topoisomerase I and DNA.[133] In 2022 Zhang and colleagues proposed the concept of a prodrug **12** based on the camptothecin derivative (Scheme 5).[134] As a photosensitizing part a BODIPY-based compound was chosen. At the same time camptothecin derivative was attached to the BODIPY through a labile phenyl benzoate group. The phenyl benzoate group is prone to cleavage by cell esterases what was exploited for the release of camptothecin **11**. Importantly, camptothecin **12** attached to the BODIPY photosensitizer can't inhibit tumor proliferation while its release could lead to pronounced cytotoxicity due to DNA binding. In addition, the fluorescence of conjugated camptothecin was dramatically reduced through the intramolecular fluorescence resonance energy transfer (FRET) process from camptothecin to the BODIPY photosensitizer. Monitoring the fluorescence level, the authors were able to observe the release of camptothecin **11**. Studies of esterase-mediated release of camptothecin **11** from conjugate **12** proved its liberation under action of exogenous carboxylesterase in phosphate-buffered saline and under action of endogenous carboxylesterase overexpressed in cancer cells. The authors showed a significant decrease in the IC_{50} values of the resulting conjugate against HepG2 human hepatocellular carcinoma and HeLa human cervical carcinoma cells upon irradiation (LED, λ=660 nm) compared with camptothecin and BODIPY as controls. The combined antitumor effects of the prodrug **12** were also observed in the mice bearing H22 murine hepatocarcinoma tumors.

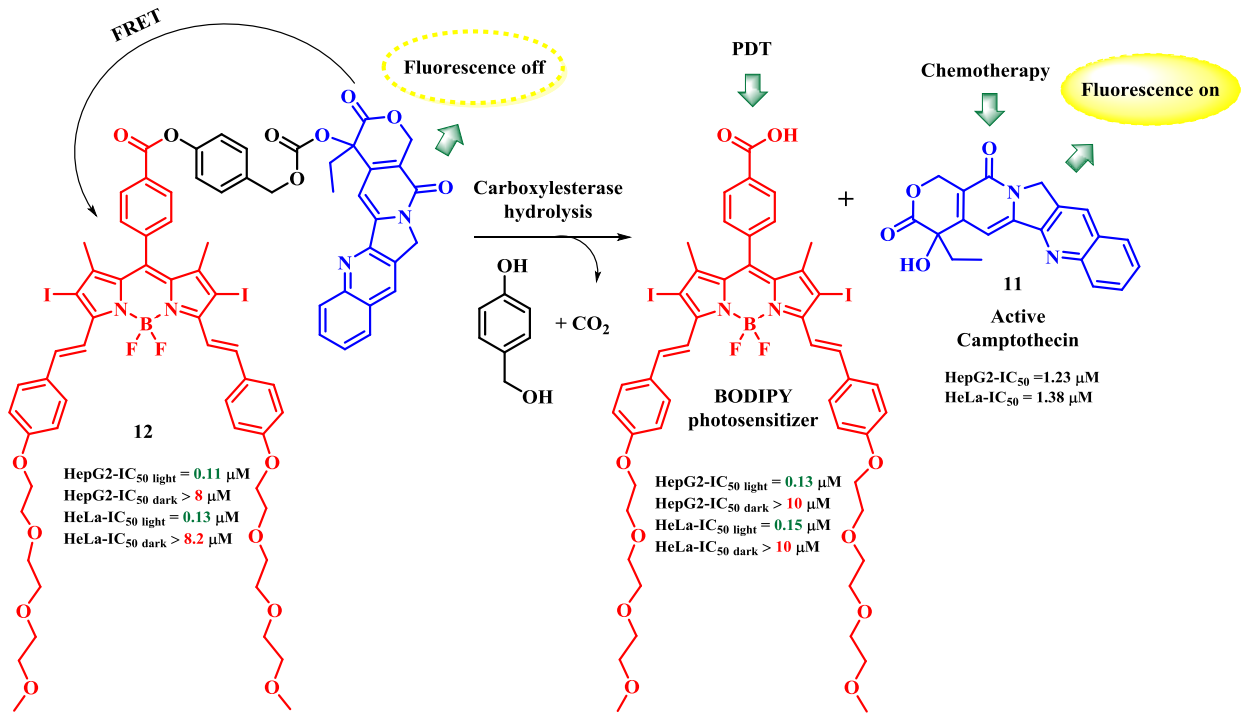

Scheme 5.

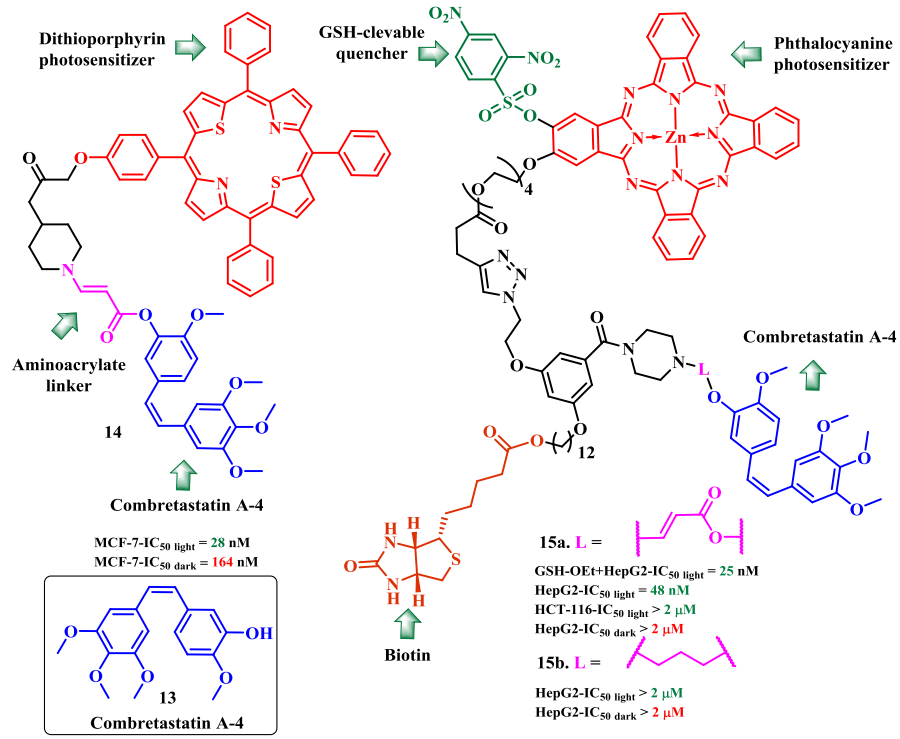

Scheme 6.

Combretastatin A-4 **13** (CA4) is a strong antimitotic agent that can bind to the colchicine-binding site and inhibit tubulin polymerization[135] (Scheme 6). CA-4 in Z-form exhibits cytotoxicity at the nanomolar level in various human tumor cell lines, (MCF-7-IC_{50} = 9 nM) including multi-drug resistant (MDR) tumor cells.[136] CA4 contributes to the blockage of tumor vessels, therefore serves as a vascular disrupting agent. In 2013, Bio with colleagues developed "photo-unclick chemistry", a novel chemical tool involving the cleavage of aminoacrylate linker by singlet oxygen ($^1O_2$). The researchers applied it to visible light-activatable prodrugs. The proposed delivery system includes a photosensitizer connected by an aminoacrylate linker to an antitumor drug (combretastatin A4) **14**[137] (Scheme 6).

The resulting prodrug **14** was activated by far-red light (diode laser, λ=690 nm) due to the destruction of the aminoacrylate linker by singlet oxygen formed upon irradiation of the dithioporphyrin photosensitizer. Thus, singlet oxygen acts not only as a cytotoxic agent, but also as a tool for activating the chemotherapy drug, resulting in synergistic dual chemo- and photodynamic therapy. In 2020, Bio with colleagues improved the above mentioned system by adding a 2,4-dinitrobenzenesulfonate (DNBS) quencher and biotin as a tumor-targeting ligand to it [138]. Due to the presence of the DNBS substituting group, zinc phthalocyanine quenching was achieved for $^1O_2$ production and fluorescence emission. When interacting with glutathione (GSH) in the cell environment, DNBS group had removed and prodrug had recovered photoactivity. In cells HepG2 (biotin receptor positive) conjugate **15a** demonstrated elevated uptake than that for HCT-116 cells (control, human colorectal carcinoma), therefore proving its ability to target biotin receptors. After GSH-OEt pre-treatment the fluorescence intensity increased. Under conditions of light irradiation (300 W halogen lamp, λ=610 nm) of HepG2 cells containing the conjugate **15a**, their growth was inhibited at a nanomolar concentration (Hep2G: $IC_{50\ light}$ = 48 nM), while in the dark it was inactive at a concentration of up to 2 μM. At the same time, the control conjugate without aminoacrylate linker **15b** had a much lower activity both with and without irradiation, confirming the proposed mechanism of activation of the conjugate system by singlet oxygen-induced destruction of the aminoacrylate linker in conjugate **15a**. The authors calculated the combination index (CI)[139] for **15a** (CI~0.25), which indicated strong synergism between photosensitizing and chemotherapeutic parts. Thus, the new delivery system is favorably distinguished by its dual action (PDT and chemotherapy) and high controllability.

Our research group decided to take advantage of combretastatin A-4's photoisomerization from a 1000-fold less active *trans*-isomer **17** (IC_{50} = 10^{-6}M) to a clinically active *cis*-isomer **13** (IC_{50} = 10^{-9}M)[140,141] (Scheme 7A). Combining *trans*-combretastatin with a porphyrin photosensitizer using a photoremovable *o*-nitrobenzyl linker,[142] we assumed that the action of one- or two-photon irradiation could trigger a cascade of processes: 1) destruction of the *o*-nitrobenzyl linker with simultaneous release of *trans*-combretastatin; 2) its photoisomerization into toxic *cis*-isomer **13**; 3) photoactivation of porphyrin and its generation of singlet oxygen.[143] As a result, we would be able to control the toxicity of the conjugates **16a-b** using light and enhance the therapeutic effect due to the simultaneous action of PDT and chemotherapy. To increase hydrophilicity, the porphyrin macrocycle was decorated with carbohydrate fragments (galactose and maltose, respectively). However, when using various light sources (UV-A, λ=365 nm, UV-B, λ=311 nm, and UV-C, λ= 254 nm, LED, λ = 450 nm), it was not possible to observe the desired release of combretastatin A-4. To determine the cause of the intactness of the conjugates **16a-b**, irradiation of the *trans*-combretastatin-

linker **18** model system without porphyrin was carried out. It turned out that this system is capable of releasing a therapeutic agent, which is immediately not only isomerized to active *cis*-combreatstatin, but further cyclized to a phenanthrene-type derivative **19** (Scheme 7B). TD-DFT calculations were also performed to identify the best type of binding between the porphyrin and the *o*-nitrobenzyl linker. It has been shown that the excitation of three orbitals (LUMO, LUMO+1, and LUMO+2) is possible when the conjugates are irradiated with 365 nm light, in which the maximum electron density is shifted towards the porphyrin fragment, which possibly complicates the photocleavage process. At the same time, if there are no additional functional groups between the porphyrin fragment and the *o*-nitrobenzyl linker, then on the LUMO + 2 orbital, which at the same time has an energy higher than for all considered types of binding, the electron density shifts towards the linker, which increases the probability of photodegradation. Our result is consistent with the experimentally photocleaved porphyrin-*o*-nitrobenzyl linker-fluorouracil conjugate by Lin,[144] for which we also calculated the corresponding orbitals. Thus, further research will focus on an updated design that eliminates linkers between the photosensitizer moiety and the *o*-nitrobenzyl group, and the replacement of combretastatin A-4 with azo analogs that do not undergo cyclization.[145].

Thus, the substantial progress made in the development of multifunctional drugs opens broad possibilities for the creation of efficient antitumor agents. Even though there are no approved conjugated drugs so far on the market, their further investigation will undoubtedly lead to new treatment options for people suffering from oncological diseases. Among main beneficials hiding in this concept the one can point out: 1) broad variability arising from unlimited tools for conjugation including cytostatics, cleavable linkers, quenchers etc.; 2) predictability of cellular targets for main active parts of conjugate; 3) possibility to exploit multiple mechanisms leading to the death of cancer cells, including MDR-cells; 4) selective delivery to tumors through decoration with specific oncovectors or targeted TKI utilization.

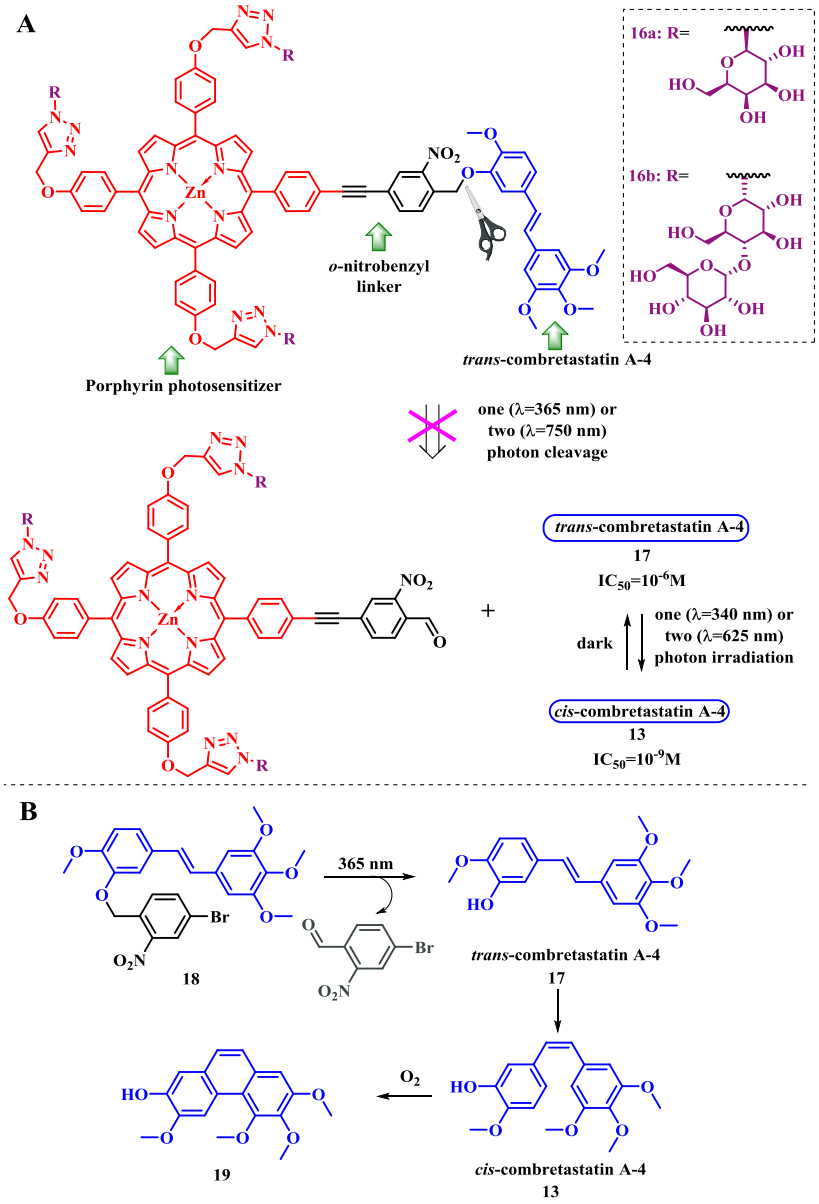

Scheme 7.

3. Formation of Cationic Groups at the Natural Chlorins Macrocycle Periphery in the Synthesis of Potential Antitumor and Antibacterial Photosensitizers

It is known that the introduction of cationic groups to the periphery of the chlorin PS macrocycle not only increases hydrophilicity, but also promotes interaction with the cell membrane of gram-negative bacteria.[42,47,92,146-161] Chlorophyll *a* derivatives have spectral properties suitable for use as antitumor and antibacterial PSs and relatively low toxicity; therefore, they are widely used as a basis for the synthesis of new PSs for medical purposes.[42,47,92,146-161] One of the possible directions of chlorophyll *a* and its derivatives chemical modification is the introduction of cationic substituents to the macrocycle periphery. It should be noted that a positive charge can arise both in the protonation of nitrogen atoms (as a rule, nitrogen atoms of peripheral substituents[47,150,153,162-164]) and in the presence of p*H*-independent cationic groups on the macrocycle periphery.[47,146,148–153,159,165] The dependence on p*H* of the charge presence at the macrocycle periphery can reduce the effectiveness of the PS, so the formation of cationic substituents with a constant charge is more preferable. This review considers methods for the formation of cationic groups at the periphery of the macrocycle of chlorophyll *a* derivatives. It should be noted that not all cationic chlorins, which will be discussed below, have been studied as potential PS, however, the methods used in their synthesis can be applied in the synthesis of potential PS, and these chlorins themselves are potential PS. Only cationic derivatives with a quaternary nitrogen atom have been described for *a*-series chlorins. The key step in the formation of a cationic group is the introduction of an amino group substituted to varying degrees (usually it is tertiary amino group). Quaternization of this group allows the formation of a charged group and is usually not difficult. Next, will be considered the main ways of introducing the previous nitrogen-containing groups and their subsequent transformation into cationic groups.

The Introduction of Cationic Substituents by Forming an Ester Bond

To introduce cationic groups by forming an ester bond the action of an alcohol with a tertiary nitrogen atom on the activated carboxyl groups of chlorine is used, followed by quaternization of the nitrogen atom. When chlorin e_6 is treated with 2-(N,N-dimethylamino)ethanol (choline) or 3-hydroxymethylpyridine, followed by alkylation with methyl iodide, the corresponding chlorins with three cationic substituents are obtained. Because when using dicyclohexylcarbodiimide (DCC) and 1-ethyl-3-(3-dimethylaminopropyl)carbodiimide (EDAC) the products are usually a mixture of mono-, di-, and tri-substituted chlorin e_6, mostly mono- and di-substituted chlorin e_6, probably because the structure of intermediates is too bulky to esterify all of the three carboxyl groups, the carboxyl groups "activation" is carried out with oxalyl chloride. The corresponding acid chloride is forms, which makes it possible to carry out the reaction at all three carboxyl groups of chlorin e_6[166] (Scheme 8).

Insertion of Cationic Substituents through the Formation of an Amide Bond

The formation of an amide bond upon the introduction of a tertiary amino group to the periphery of the chlorine macrocycle is carried out both using the usual reactions of "activated" carboxyl groups and using the reactions of chlorophyll *a* derivatives associated with the features of their chemical structure. When, for the introduction of the N,N(dimethyl)ethylenediamine fragment in reactions with various 17-carboxy derivatives of chlorophyll *a*, in most cases, carbodiimide "activation" (DCC, EDC) is used (Schemes 9-12). The quaternization of the tertiary nitrogen atom is carried out by the action of CH_3I, if it is necessary, the exchange of the counterion is carried out on an ion exchange resin. So, for the synthesis of the cationic derivative of pheophorbide *a*, the DCC-activated carboxyl group of the substrate is treated with (N,N-dimethyl)ethylenediamine[167] (Scheme 9).

A similar reaction of pyropheophorbide *a*[168] (Scheme 10), pyropheophorbide *d*[169] (Scheme 11), and phorbin, which is the active substance of Photochlor PS[170] (Scheme 12), is carried out with EDC "activation".

If it is necessary to carry out some additional modifications of chlorin (for example, the synthesis of a complex or the reduction of the aldehyde group,[169] Scheme 11), quatrainization is carried out at the final stage, since it is not so convenient to work with a compound with a cationic group due to its increased hydrophilicity and also the possibility of uncontrolled exchange of the counterion and its participation in side reactions. As will be seen from what follows, this technique is quite universal and is used regardless of the method of introducing a substituent with a tertiary nitrogen atom.

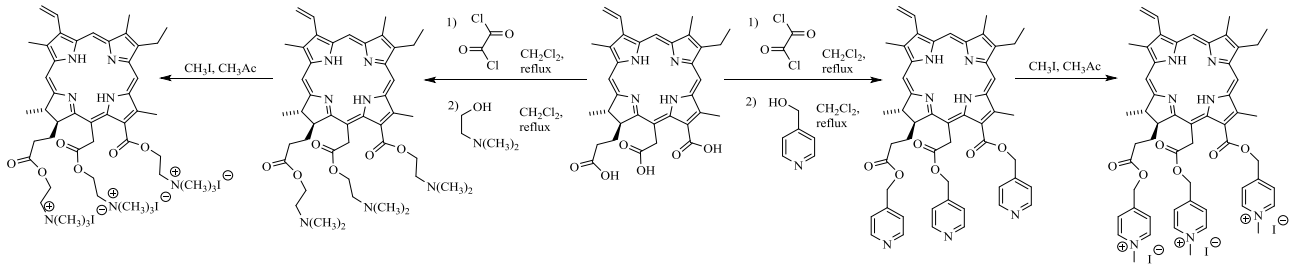

Scheme 8.

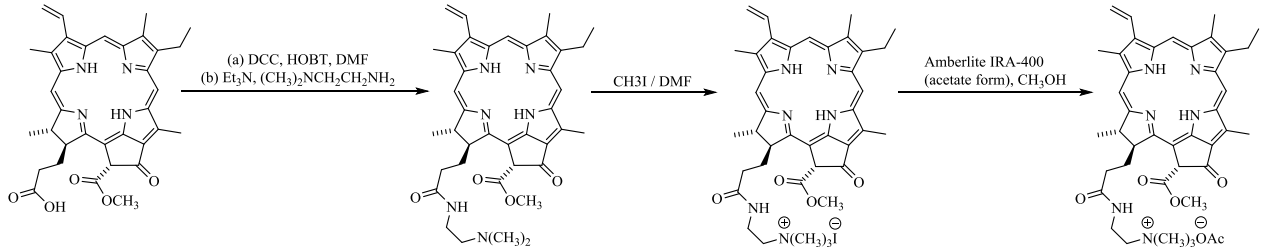

Scheme 9.

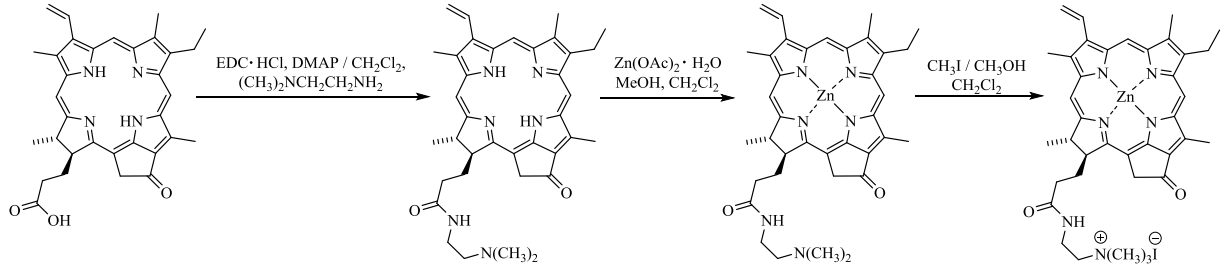

Scheme 10.

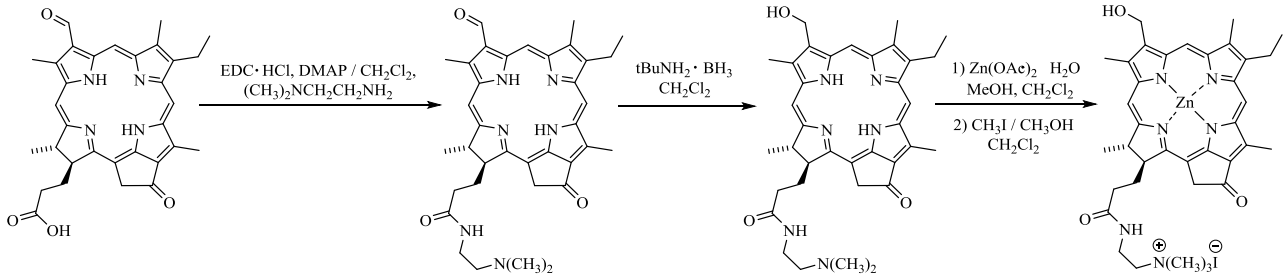

Scheme 11.

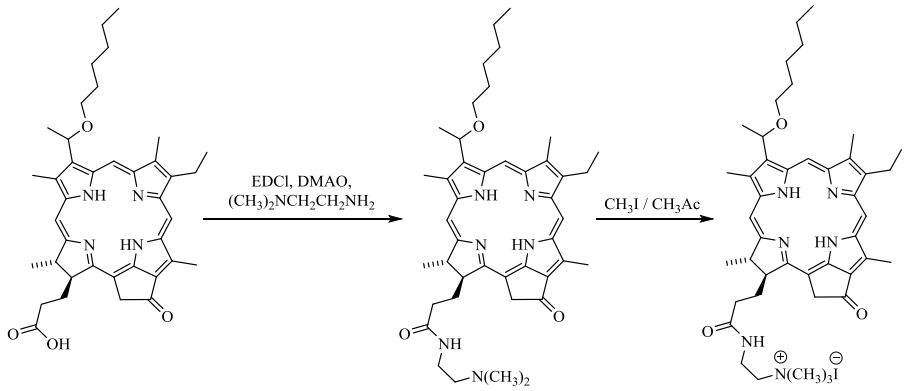

Scheme 12.

The interaction of amines with esters to form the corresponding amides is a well-known reaction that is possible for compounds of various classes, including natural chlorins. Amidation of chlorophyll *a* derivatives ester groups in most cases, is carried out after the formation chlorin e_6 13-amide derivatives after the exocycle opening (see below). However, amidation of the phytylpropionate substituent of pheophytin *a* by the action of N,N,N,N,N,N-hexapropylpenta(aminoethyl)amine (amine oligoamine with five tertiary nitrogen atoms) is possible before exocycle opening[161] (Scheme 13). The reaction is carried out under the action of a small molar excess of amine in the presence of

about 10-fold molar excess of TFA. It is known,[161] that the same amine can open the pheophytin *a* exocycle with the formation of the corresponding 13-amide derivative (see below), but this reaction does not occur under amidation conditions. The selectivity of amidation can be provided not only by a small excess of amine, but also by the presence of TFA. The role of TFA the authors of[161] do not comment on. Possibly, the presence of a small amount of TPA provides an "acidic" catalysis of amidation, which, along with a slight excess of amine, results in the selectivity of the process. The target compound in this synthesis was the cationic zinc complex, as in the cases described above, quaternization is carried out at the last stage.

A similar reaction of the amide's formation occurs upon the action of amines on cyclic lactones formed during the oxidation of chlorines with a carboxyl group in position 17.[171,172] As a result of the reaction, the lactone exocycle opens and the corresponding hydroxychlorines are forms. This reaction can be used to insert the N-methylpyridyl group[173] (Scheme 14).

It is known that the exocycle of pheophytin *a*, methyl pheophorbide *a*, pheophorbide *a* and a number of other similar natural chlorins is relatively easily opened under the action of nucleophilic agents such as amines. This reaction can be used to form cationic groups if the opening is performed with an amine containing tertiary nitrogen atoms or additional amino groups that can be alkylated. The exocycle opening under the action of (N,N-dimethyl)ethylenediamine allows the introduction of a tertiary amino group, the quaternization of which gives a cationic substituent (Scheme 15). This pathway was implemented for pheophytin *a*, methylpheophorbide *a* and a number of its derivatives with fragments of biomolecules to increase hydrophilicity.[110,118,174-178] Alkylation of the dimethylamino group is usually carried out with CH_3I.[110,174-178] However, other alkylating agents, such as C_2H_5Br, are also possible[118] (Scheme 15).

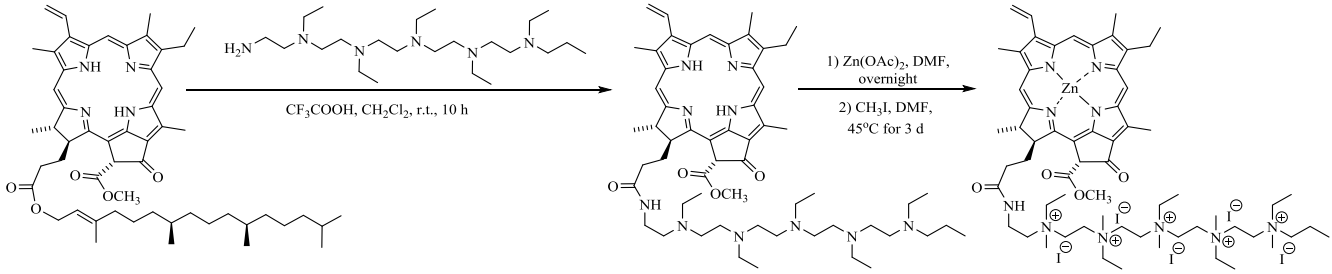

Scheme 13.

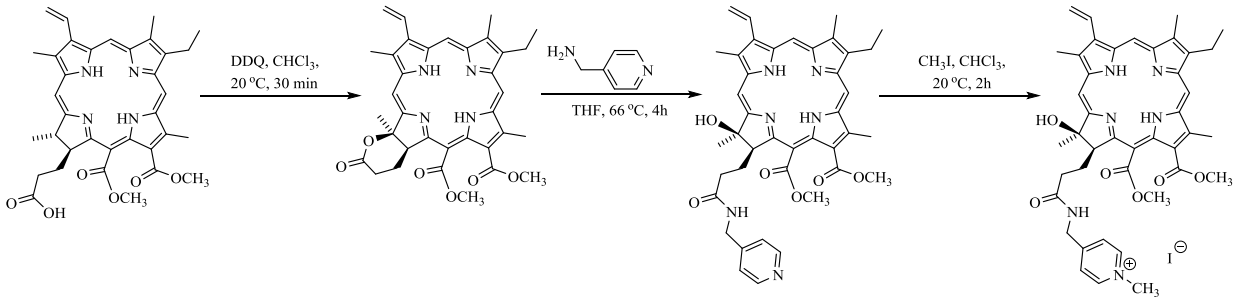

Scheme 14.

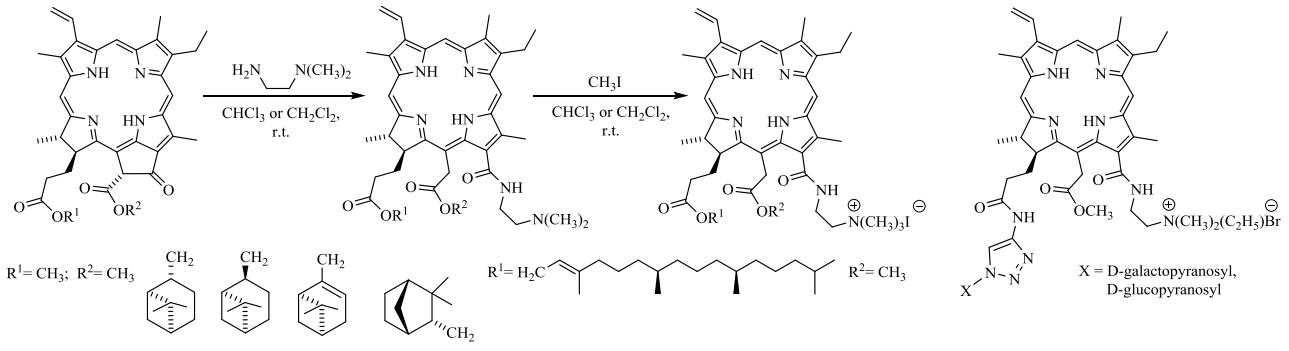

Scheme 15.

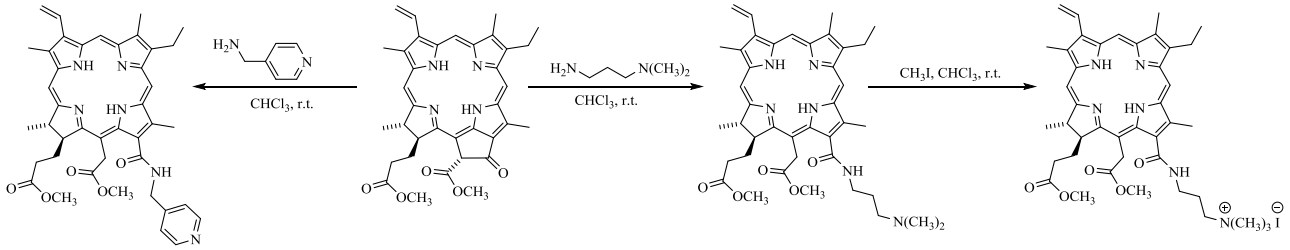

Scheme 16.

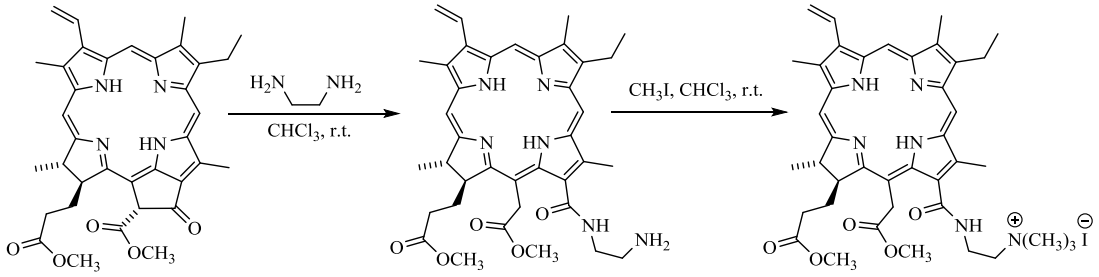

Scheme 17.

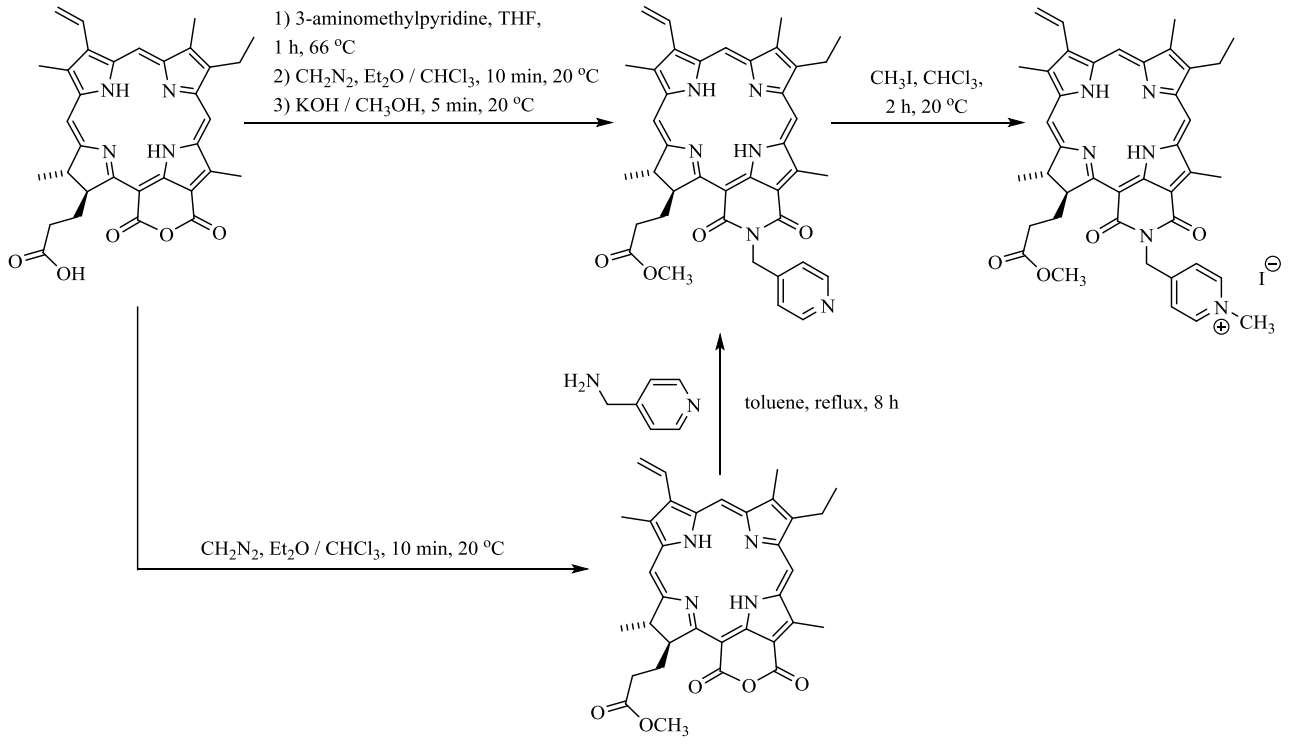

Scheme 18.

The use of (N,N-dimethyl)ethylenediamine analogs with a large number of methylene units between the primary and tertiary amino groups makes it possible to synthesize chlorin e_6 derivatives with a cationic group remote from the macrocycle to varying degrees. For example, the reaction with 1-(N,N-dimethylamino)-3-aminopropane[179] makes it possible to lengthen the spacer by one methylene group (Scheme 16).

The exocycle opening with 4-aminomethylpyridine can be used to introduce the pyridinium fragment[180] (Scheme 16), but the authors did not perform further alkylation. The cationic group formation is also possible from a primary amino group. For example, chlorin with a cationic group is synthesized by the action of a large excess of CH_3I on the 13-amide derivative of chlorin e_6, obtained by the action of ethylenediamine on methyl pheophoride *a*[181] (Scheme 17).

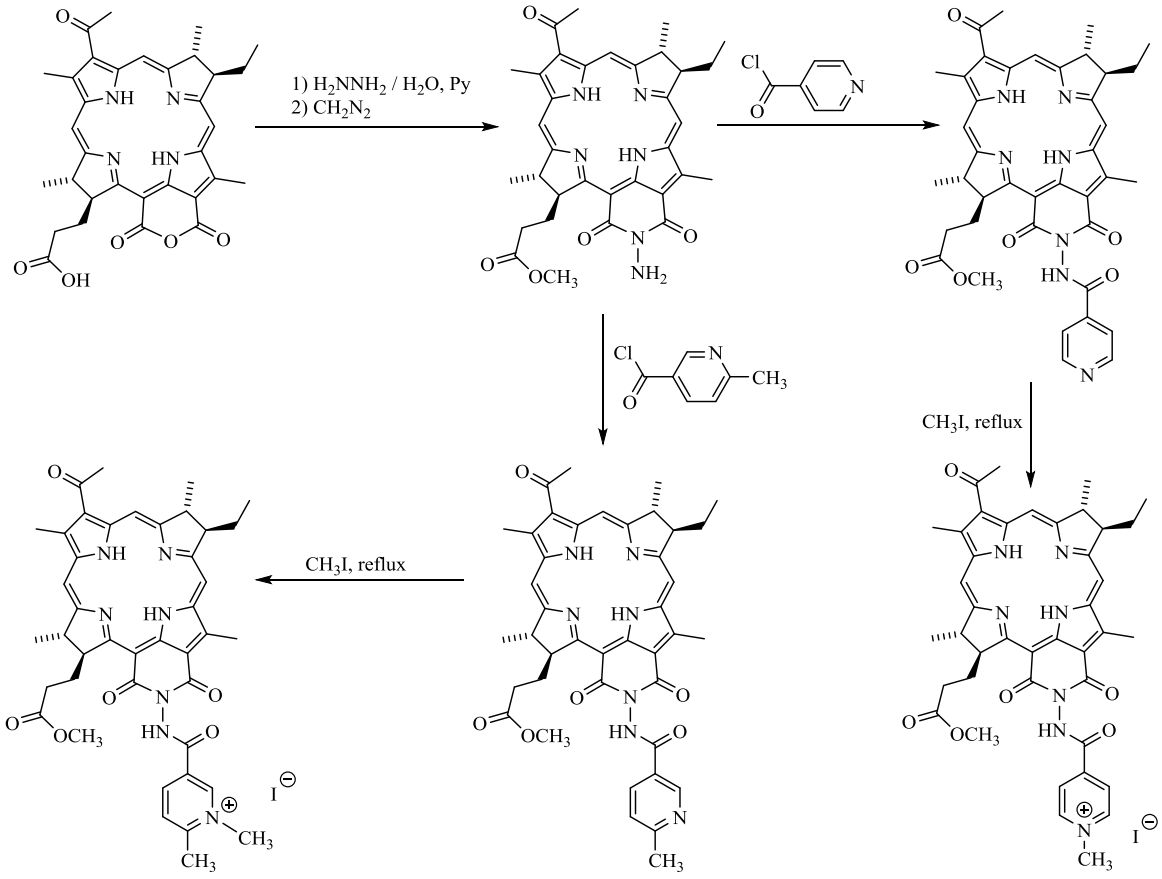

Scheme 19.

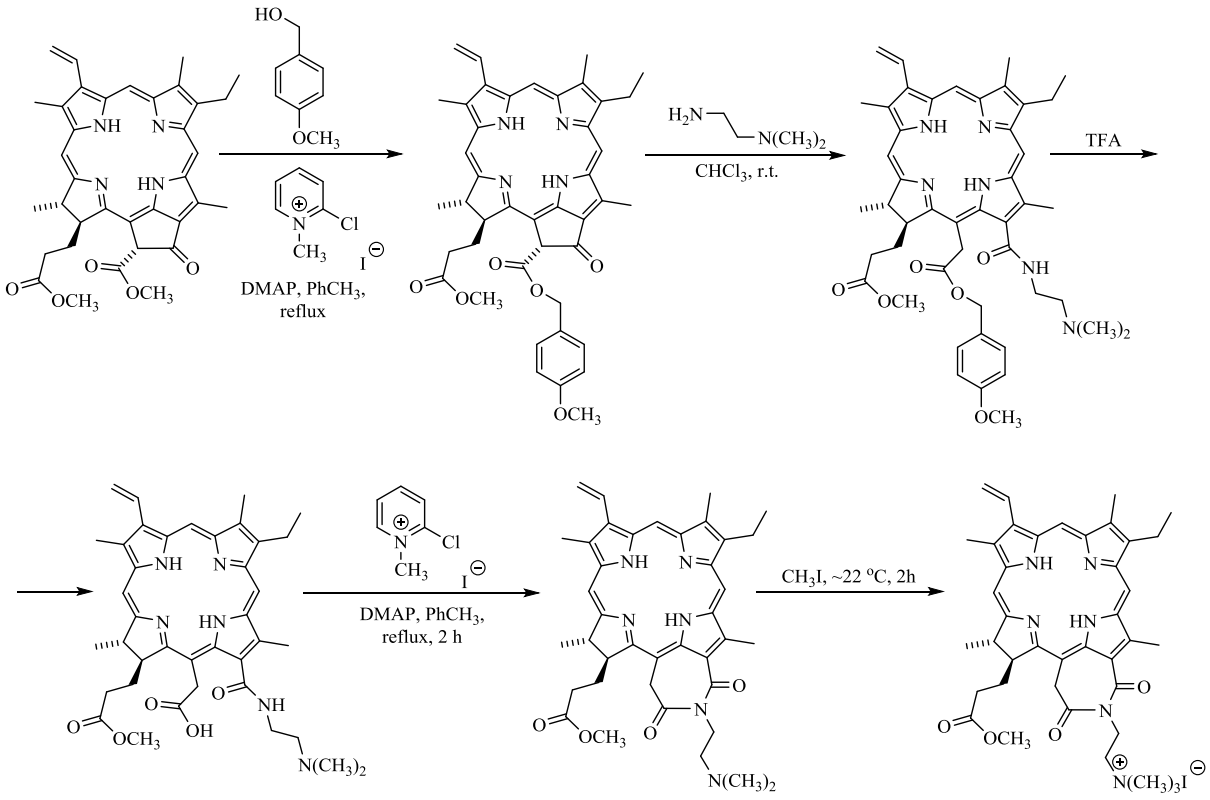

Scheme 20.

The interaction of purpurin 18 and its analogs with amines giving cycloimide derivatives not only significantly improves the spectral characteristics of chlorin, but also introduces an additional functional group.[182] This reaction can be used both for the directly insertion of a substituent with a tertiary nitrogen fragment[173] and for the formation of a reaction center, which can then be used to synthesize a derivative with a tertiary nitrogen fragment. The purpurin methyl ester 18 cycloimide derivative is obtained from purpurin 18 by the action of 4-aminomethylpyridine in three stages performed "in one flask", subsequent alkylation of the pyridine substituent with CH_3I gives the target cationic derivative[173] (Scheme 18). Starting from purpurin methyl ester 18, a similar derivative can be obtained in one step by refluxing in toluene with 4-aminomethylpyridine[180] (Scheme 18). In addition to the direct introduction of a substituent with a tertiary nitrogen atom, the formation of cycloimide can be used to introduce an additional reaction center. The action of hydrazine on bacteriopurpurin methyl ester 18 gives a cycloimide derivative with a reactive amino group, acylation of which with pyridinecarboxylic acids leads to derivatives with a pyridinium fragment[183-185] (Scheme 19). Quaternization of pyridinium fragments by the action of CH_3I gives the corresponding cationic derivatives.

Chlorins with a seven-membered exocycle closed by an imide bond can be synthesized by the action of CMPI on 13-amd-15-carboxy derivatives of chlorin e_6, provided that the amide group at position 13 is secondary or primary.[186] In the case when there is a dimethylaminomethyl group at the amide nitrogen atom, cyclization results in the formation of chlorin, the action of which with CH_3I gives the corresponding cationic derivative[186] (Scheme 20).

Formation of C-N(amine) Bonds in the Synthesis of Cationic Chlorins

The formation of C-N(amine) in a number of cases is used to introduce substituents with a tertiary nitrogen atom, the subsequent quaternization of which gives a cationic substituent. Epoxidation of the vinyl group of chlorin with meta-chloroperoxybenzoic acid followed by treatment of the in situ formed polyamine epoxide gives chlorin with a polyamine fragment in position 3, a precursor of the pentacation substituent[161] (Scheme 21). Quaternization of tertiary nitrogen atoms in the molecule by the action of CH_3I is carried out at the last stage.

Cationic derivatives with a pyridinium group were synthesized by the action of heterocyclic compounds with a pyridinium fragment, I_2 and $AgPF_6$, on vinylchlorins; the cationic group is immediately formed in the course of chemical oxidative pyridylation[152,187] (Scheme 22). Using the reaction involving pyridine as an example, it was shown[187] that more accessible silver salts, for example, halides, can be used instead of $AgPF_6$.

A similar reaction can also be carried out in a series of bactriochlorophyll *a* derivatives after the formation of a vinyl group in position 3[187] (Scheme 23).

In the absence of a vinyl group, the insertion of a cationic substituent during chemical oxidative pyridylation occurs in *meso*-positions[188] (Scheme 24). As a result, a mixture of regioisomers with comparable isolated yields is formed, which significantly complicates the use of this reaction for the synthesis of cationic PSs.

A similar reaction can also be carried out in a series of bactriochlorophyll *a* derivatives after the formation of a vinyl group in position 3[187] (Scheme 23).

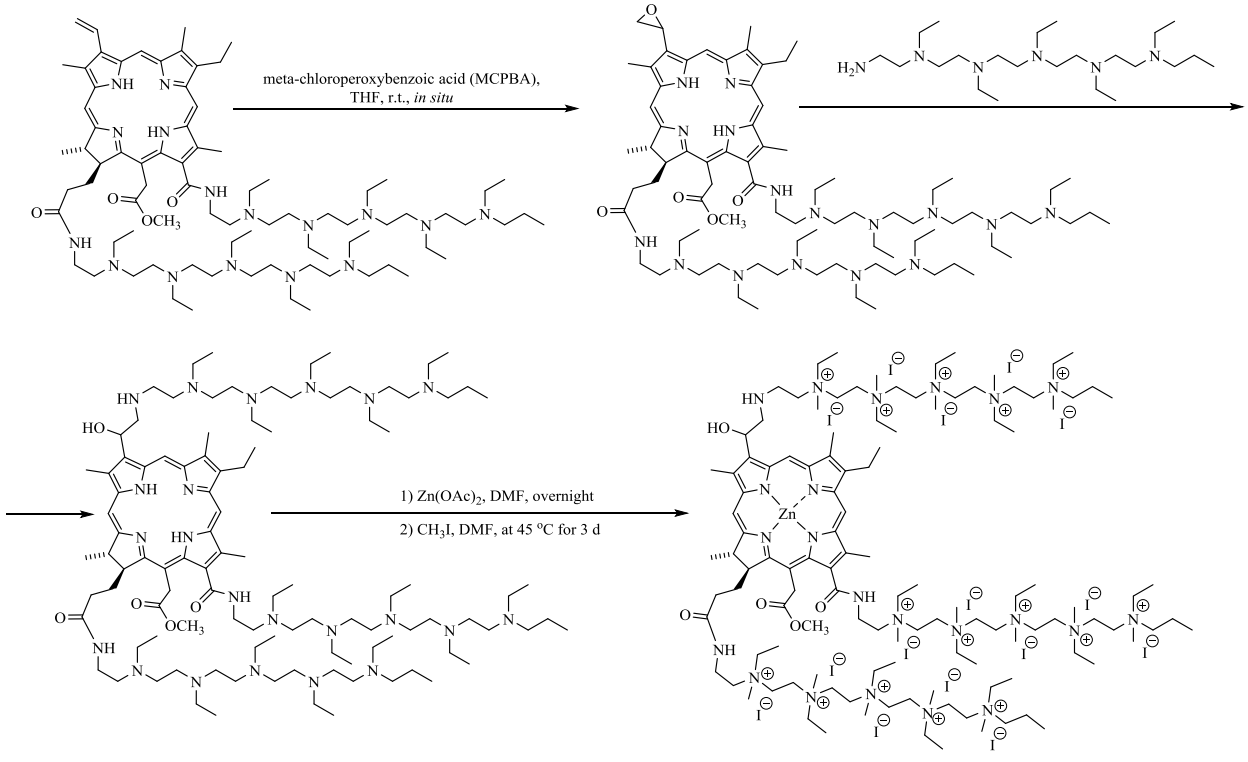

Scheme 21.

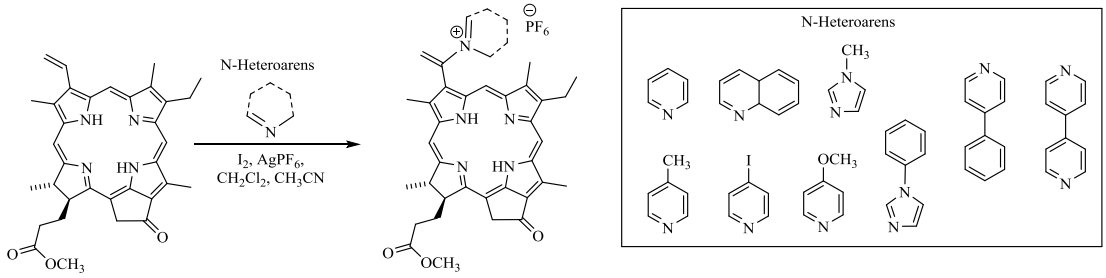

Scheme 22.

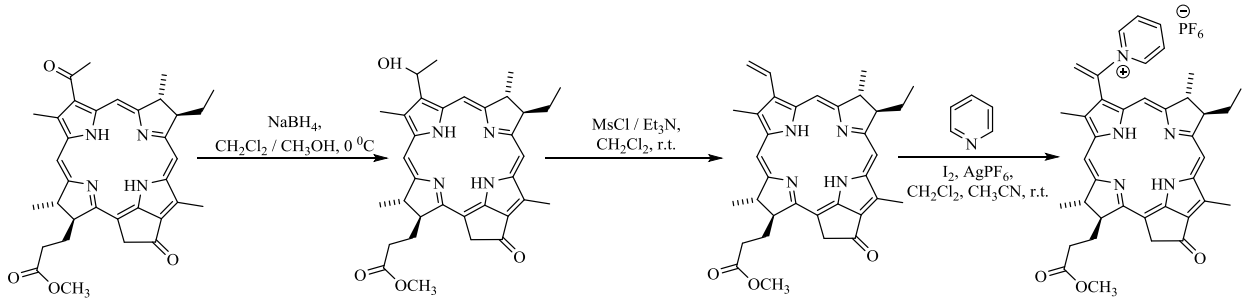

Scheme 23.

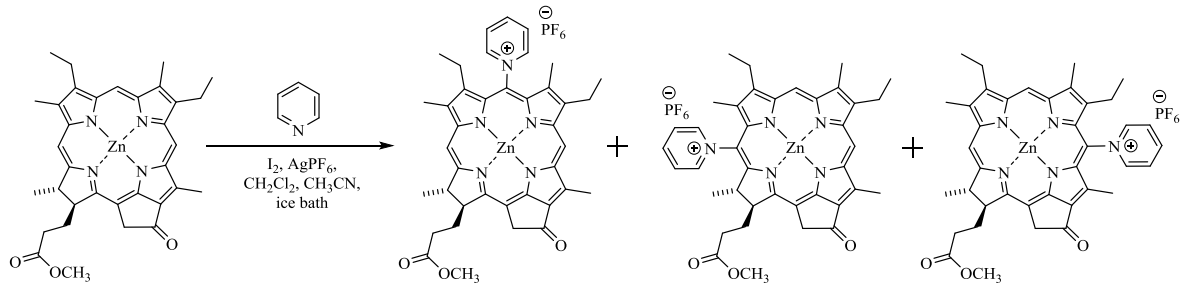

Scheme 24.

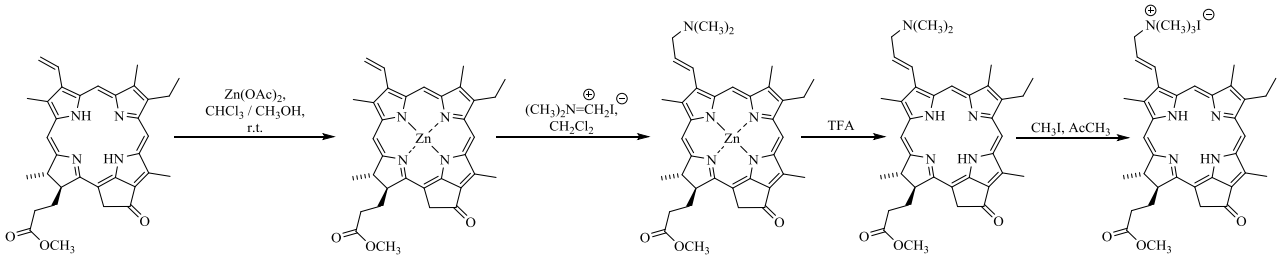

Scheme 25.

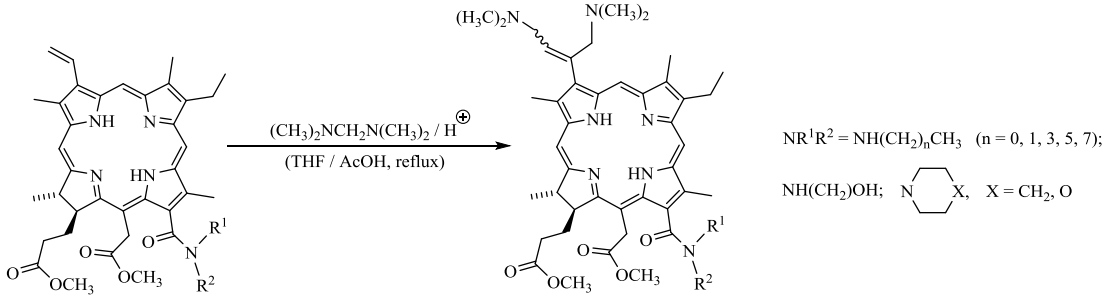

Scheme 26.

In the absence of a vinyl group, the insertion of a cationic substituent during chemical oxidative pyridylation occurs in *meso*-positions[188] (Scheme 24). As a result, a mixture of regioisomers with comparable isolated yields is formed, which significantly complicates the use of this reaction for the synthesis of cationic PSs.

C-C and C=C Bonds Formation in the Synthesis of Cationic Chlorins

The formation of a carbon-carbon bond is considered to be the most preferred when introducing a substituent with a tertiary nitrogen atom. In the chemical modification of chlorins in this direction, both some "classical" reactions (variants of the Mannich reaction, other condensations) and relatively recently discovered cross-coupling reactions are used. Under the action of Eschenmoser's reagent on zinc porphyrinates obtained from methyl pheophorbide *a*, methyl pyropheophorbide *a*, and chlorin e_6 trimethyl ester, stereoselective aminomethylation of the vinyl group occurs[189-193] (Scheme 25, methyl pyropheophorbide *a* as an example). As a result of the reaction, *trans*-isomers are formed, subsequent demetallation with trifluoroacetic acid and alkylation of the dimethylaminomethyl group of the obtained derivatives with CH_3I gives the corresponding metal-free monocationic chlorins.

It was shown[194] that, in contrast to Eschenmoser's reagent, the action of bis(N,N-dimethylamino)methane on metal-free 13-amide derivatives of chlorin e_6 by refluxing in acetic acid results in the nonstereoselective insertion of two dimethylaminomethyl substituents into the vinyl group (Scheme 26).

A similar reaction occurs at room temperature with the participation of zinc[195] and nickel[196]) complexes of *a*-series vinyl-chlorins.

The vinyl group aminomethylation reaction[194-196] is used to synthesize dicationic chlorins containing additional hydrophilic and hydrophobic fragments[197] (Scheme 27), as well as dicationic derivatives of chlorin e_6 with membranotropic substituents (myristic acid fragments[198] (Scheme 28) and phytol[176,177] (Scheme 29). In addition to aminomethylation, the introduction of a cationic group can be carried out using palladium-catalyzed cross-coupling reaction. This reaction was used to insert a pyridine moiety at position 20 of mesomethylpyropheophorbide *a*, which was then quaternized by the action of iodo triethylene oxide[199-201] (Scheme 30).

Condensation of the methylpyropheophorbide *d* aldehyde group with methyl groups of the corresponding heterocycles is used to introduce a heterocyclic fragment with a pyridyl nitrogen atom. The heterocyclic fragment of the substituted vinyl group formed as a result of condensation is quaternized by the action of CH_3I[202] (Scheme 31).

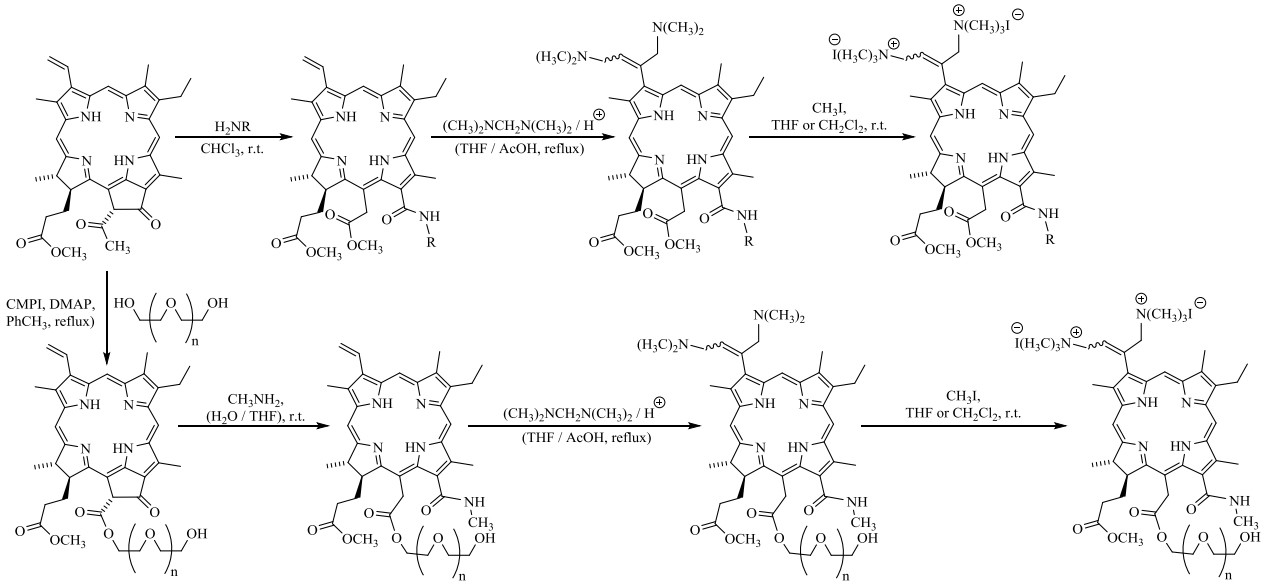

Scheme 27.

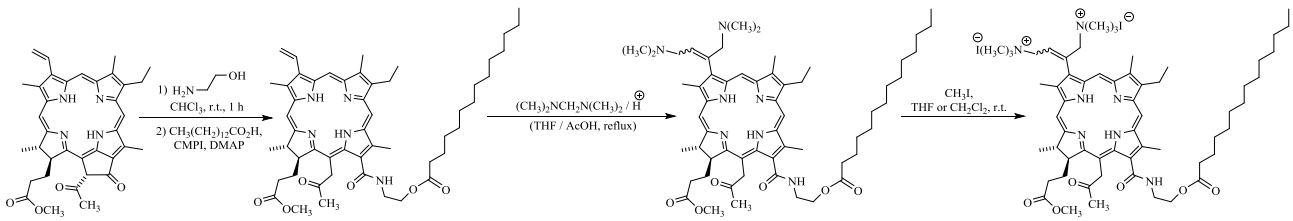

Scheme 28.

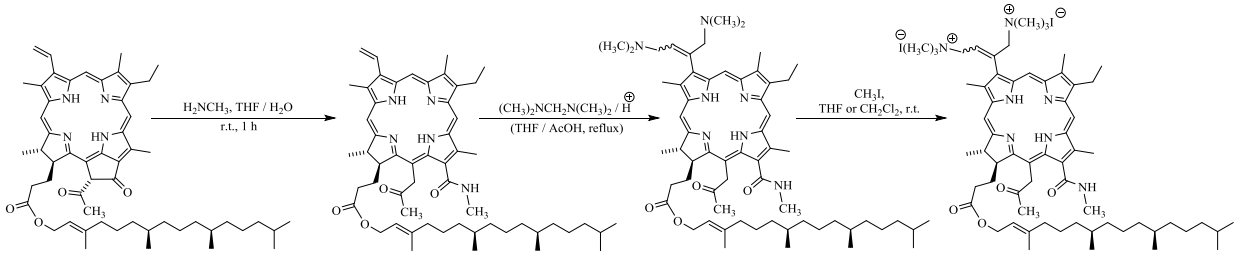

Scheme 29.

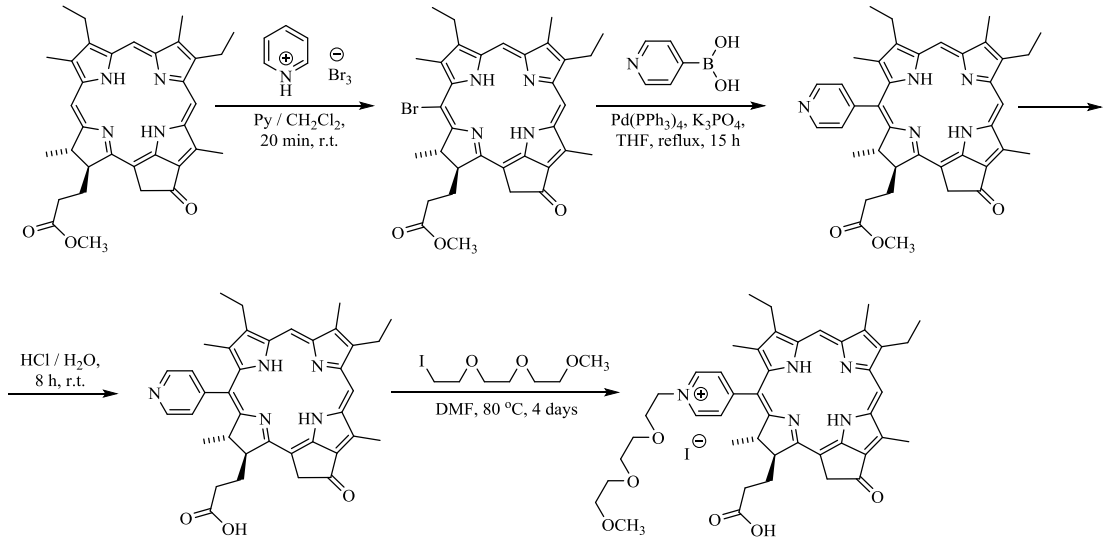

Scheme 30.

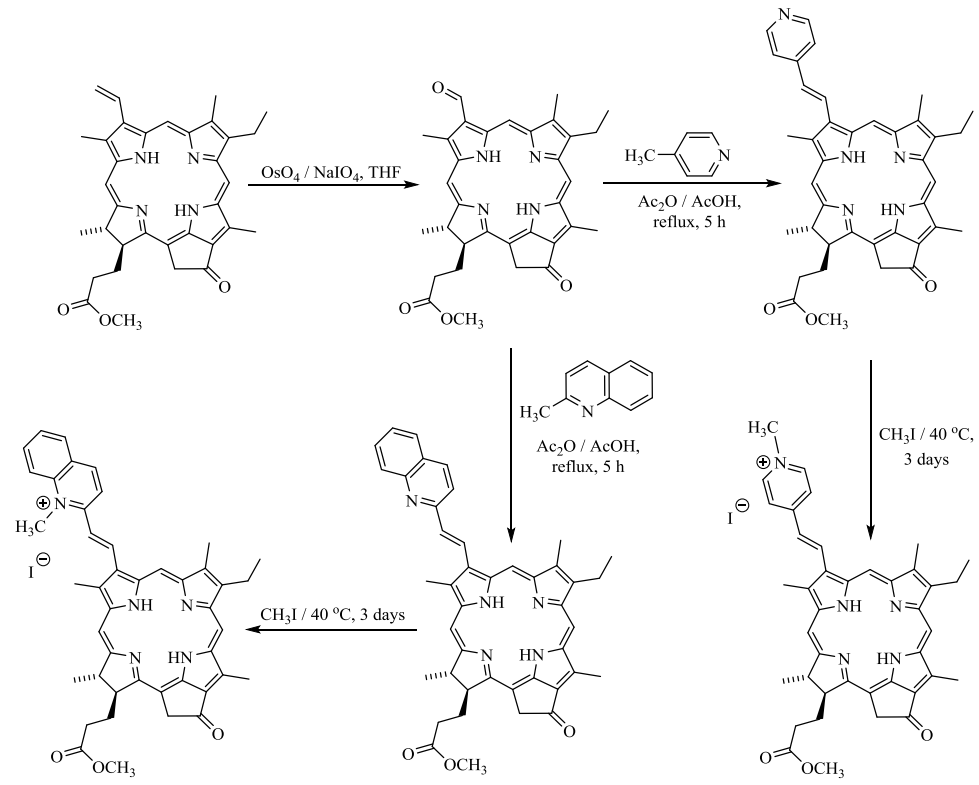

Scheme 31.

Combination of Reaction Centers of Various Chlorophyll a Derivatives in the Synthesis of Cationic Chlorins

It often becomes necessary to synthesize chlorins with different natures, amounts, and positions of cationic substituents to reveal structure-activity relationships. Combinations of modifications using reactions of various reaction centers allow not only to increase the number of introduced cationic groups, but also to synthesize chlorins with different arrangement of cationic groups on the periphery of the macrocycle, which is widely used in the synthesis of cationic PSs based on chlorophyll *a* derivatives. The chlorin e_6 diamide derivative with ten cationic groups was synthesized by combining the amidation of the pheophytin *a* phytylpropionate substituent with the action of N,N,N,N,N,N-hexapropyl-penta(aminoethyl)amine leads to the opening of the exocycle of the 17-amide derivative containing a fragment of the same amine[161] (Scheme 32). As in all previous cases, the cationic groups are formed by the action of CH_3I in the last step.

Opening of the cyclic lactone in combination with the formation of cycloimide makes it possible to synthesize the purpurin 18 cycloimide derivative with two cationic groups[173] (Scheme 33).

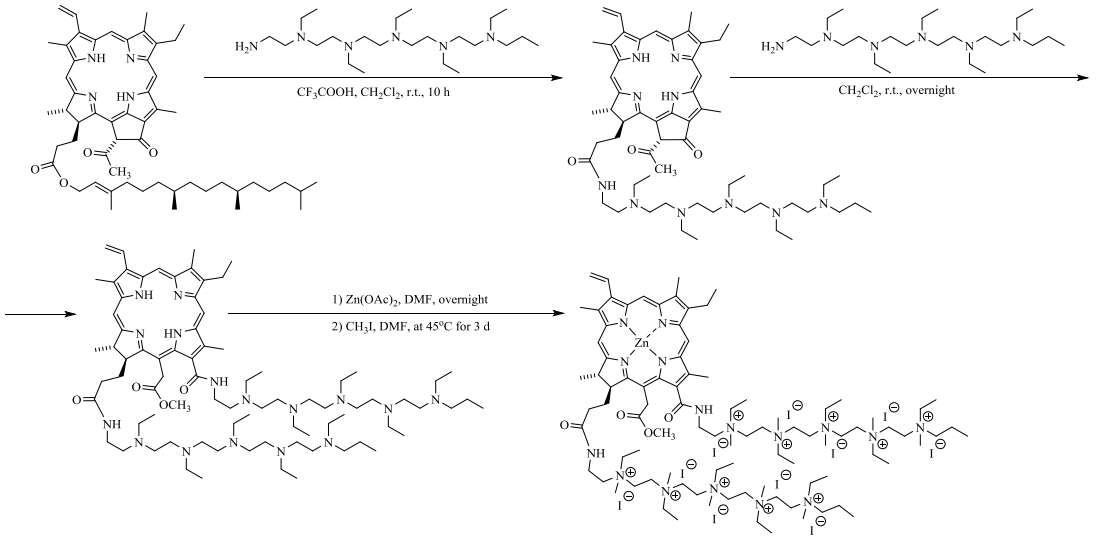

Scheme 32.

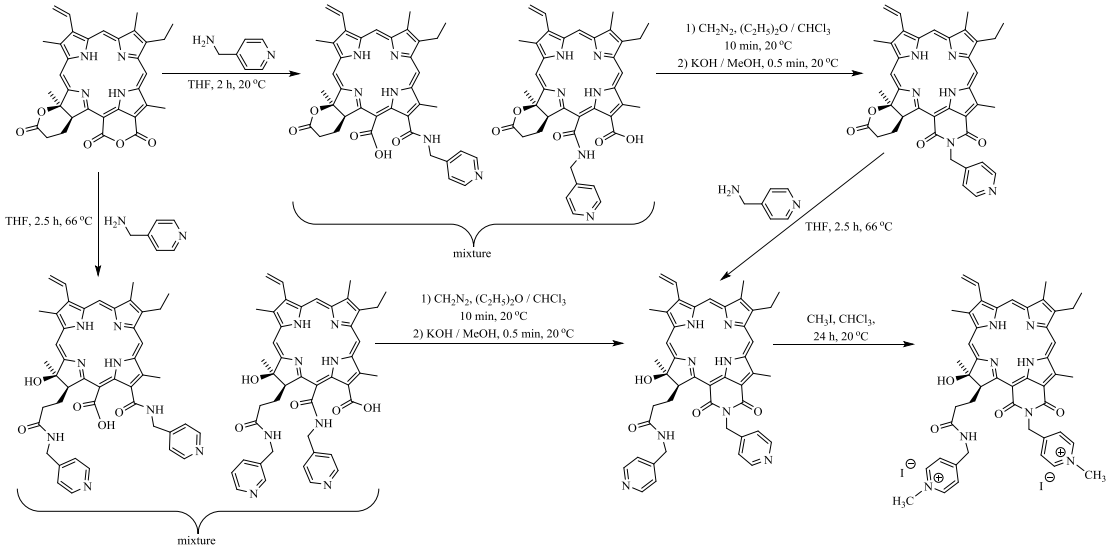

Scheme 33.

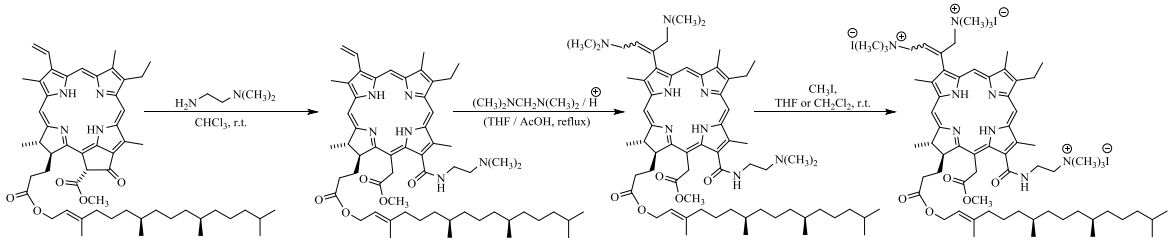

Scheme 34.

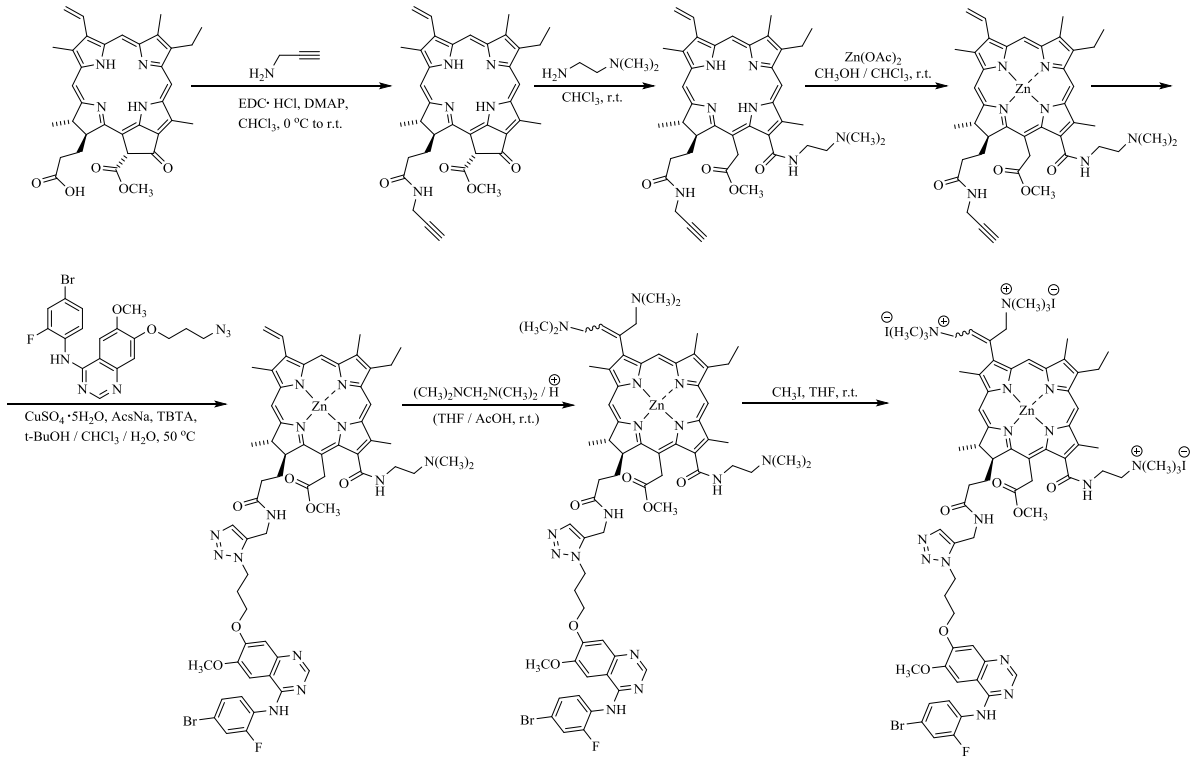

Scheme 35.

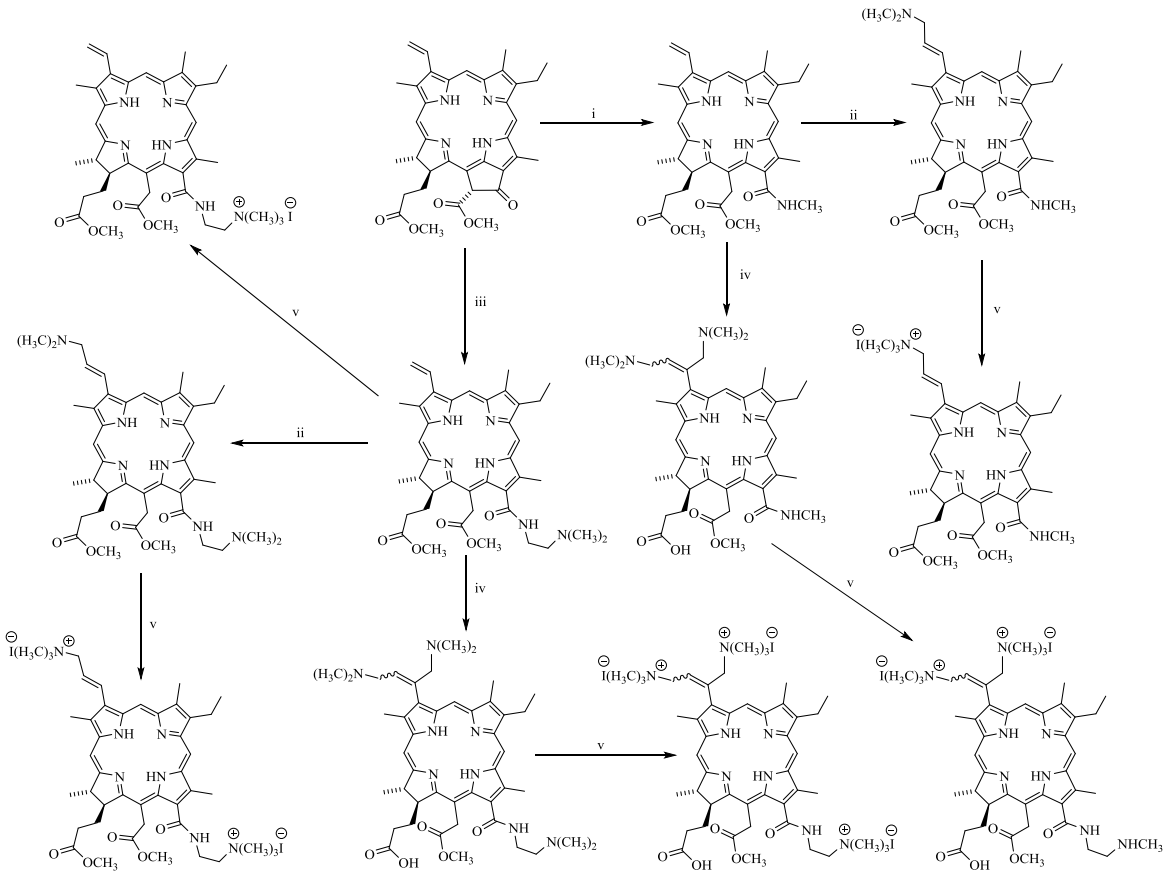

Reaction conditions: i: CH_3NH_2-H_2O/THF, r.t., 3 h; ii: $[(CH_3)_2N{=}CH_2]^+I^-$, CH_2Cl_2, r.t., 12 h; iii: $H_2NCH_2CH_2N(CH_3)_2$, CH_2Cl_2, r.t.; iv: $CH_2(N(CH_3)_2)_2$, AcOH-THF, boiling for 30 min; v:[92] CH_3I, CH_2Cl_2, r.t.

Scheme 36.

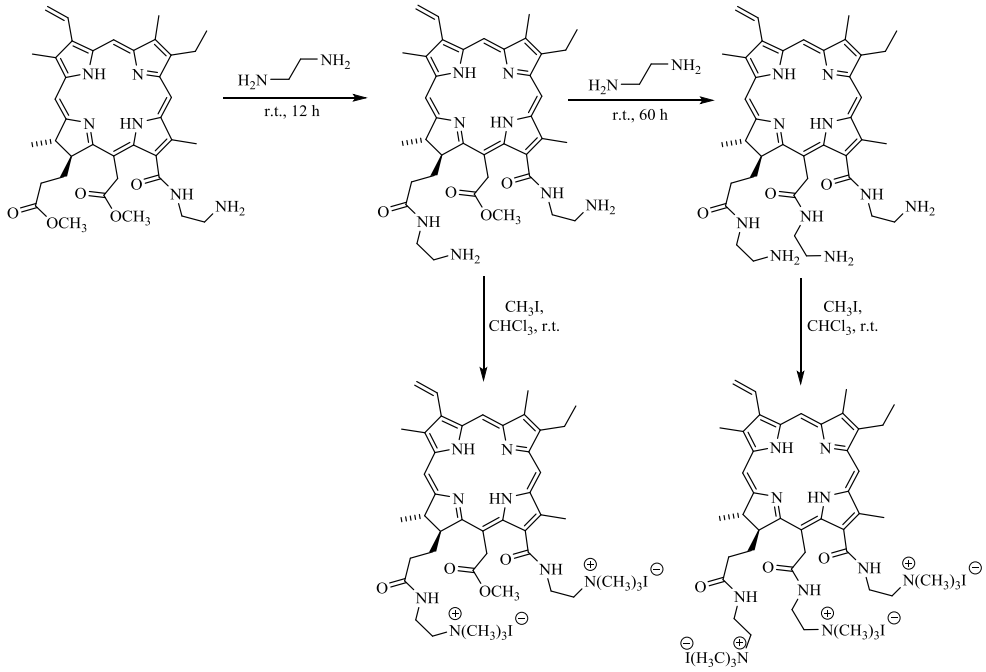

Scheme 37.

The combination of exocycle opening with aminomethylation of the vinyl group by the action of bis(N,N-dimethylamino)methane makes it possible to synthesize tricationic chlorin with a membranotropic phytol fragment[176] (Scheme 34). The same reactions were used for the synthesis of tricationic chlorin with 4-arylaminoquinazoline moiety[110] (Scheme 35).

The combination of different variants of the vinyl group aminomethylation with the exocycle opening makes it possible to synthesize chlorins with a different number of cationic groups and their arrangement in the macrocycle[178] (Scheme 36).

Alkylation of amino groups in chlorin e_6 di- and triamide derivatives allows the formation of two and three cationic groups, respectively[181] (Scheme 37).

Thus, chlorophyll a and its derivatives, having a number of convenient reaction centers in the molecule, are a good basis for the synthesis of cationic photosensitizers for medical purposes.

4. Water-Soluble Cationic Porphyrins for Photoinactivation of Pathogens

The ability of porphyrins and related compounds to generate reactive oxygen species under the action of light necessitates the synthesis of new photosensitizers with the required properties (selectivity, virucidality, bactericidality, etc.) for their effective use in photodynamic therapy, clinical laboratory diagnostics, pharmacopoeia,[203] antimicrobial water and air purification,[204] photodynamic inactivation of bacteria and viruses dangerous to humans and plants.[205]

Photodynamic inactivation of bacteria and viruses is considered the most promising treatment for drug-resistant bacteria[206] and zoonotic viruses.[207] The method of photoinactivation is based on the reactions of biomolecules, biosubstrates, and pathogens with ROS, which are generated with the participation of PS. It should be noted that, in addition to tetrapyrrole macroheterocyclic compounds, other classes of compounds are also considered as PS for photoinactivation of pathogens.[208] For example, the well-known cationic methylene blue or anionic rose bengal also show an antibacterial photoelectric effect, but their effectiveness is much lower than that of porphyrin photosensitizers. To date, it is reliably known that cationic tetrapyrrole MHCs more effectively damage pathogens than anionic and neutral PSs. The positive charges of PS promote the electrostatic binding of porphyrin to negatively charged sites on the outer membrane of bacteria and induce damage that enhances the penetration of the photosensitizer into the cell.[209,210]

The structure of the outer shell of the pathogen is no less significant. In general, gram-positive bacteria show a higher susceptibility to photoinactivation than gram-negative ones. This is probably the result of differences in the structure of the cell membranes of these two microbial groups. gram-positive and gram-negative bacteria have a cytoplasmic membrane. The membrane of gram-positive bacteria is more permeable; peptidoglycan structure is porous, filled with teichoic and teichuronic acids. The main structural difference between gram-positive and gram-negative bacteria is the thickness of the peptidoglycan and the presence of an outer membrane. The outer membrane is present only in gram-negative species. It is a very effective barrier to the penetration of exogenous substances. This membrane is very dense, the porins present in it ensure the passage of only small hydrophilic substances.[211,212] In addition, due to the presence of lipopolysaccharides, the outer membrane has a strong negative charge and a high surface potential.[204]

In order to damage a bacterium, PS must reach the cytoplasmic membrane after passing through the outer membrane.[213] Differences in the structure of the cell membrane of gram-negative and gram-positive bacteria determine the

possibility of photoinactivation of the latter with the help of not only cationic, but also anionic and neutral PS, while gram-negative bacteria are more resistant to photoinactivation.

Photoinactivation of viruses by MHC is a less explored topic compared to photoinactivation of bacteria, but as with bacteria, singlet oxygen generated (type II photooxidation) and radicals (type I photooxidation)[214, 215] play a key role in virus inactivation. Potential targets for photosensitizer binding are the protein capsid, nucleic acids, and virion envelopes.

It is a priori clear that the intracellular localization/binding site of a cationic PS is highly dependent on the structure and intramolecular charge distribution of the porphyrin compound and is an important factor in photodynamic antimicrobial chemotherapy. Therefore, the purpose of this work was to summarize the literature data and our own data obtained recently and reflecting the interaction of cationic porphyrins with biosubstrates in the context of photoinactivation of the corresponding pathogens.

Very interesting data were obtained in a study[217] that evaluated the efficiency of photoinactivation of bacteriophage T4 using tetra-, tri-, and dicationic porphyrins. The efficiency of photoinactivation of this virus depends on the charge of the MHC: the greater the charge, the greater the virucidality of the MHC. The authors attribute the revealed pattern to the fact that the T4 phage capsid in aqueous solutions with a pH of about 7 is negatively charged; therefore, tetracationic porphyrins interact electrostatically with the surface of the virus, and partially oxidize it upon photoirradiation. Tricationic porphyrins are also able to interact with the bacteriophage capsid, in contrast to dicationic MHCs. The significance of the positive charge of MHC for photoinactivation can also be traced on the example of trisubstituted porphyrins: 5-(4-methoxycarbonylphenyl)-10,15,20-tris(N-methylpyridinium-4-yl)porphyrin tri-iodide and 5-(4-carbonylphenyl)-10,15,20-tris(N-methylpyridinium-4-yl)porphyrin tri-iodide. These porphyrins differ only in the nature of the substituent in one of the phenyl rings. The carboxyl group of 5-(4-carbonylphenyl)-10,15,20-tris(N-methylpyridinium-4-yl)porphyrin tri-iodide dissociates $-CO_2H \leftrightarrow -CO_2^- + H^+$[218] in an aqueous medium, unlike $-CO_2CH_3$ group, which is part of 5-(4-methoxycarbonylphenyl)-10,15,20-tris(N-methylpyridinium-4-yl)porphyrin tri-iodide and is incapable of dissociation. As a result, the total formal charge of a porphyrin with a carboxyl group and virucidal activity are lower than those of a porphyrin with a $-CO_2CH_3$ group.

Results for 5-(4-methoxycarbonylphenyl)-10,15,20-tris(N-methylpyridinium-4-yl)porphyrin triiodide and 5-(pentafluorophenyl)-10,15,20-tris(N-methylpyridinium-4-yl)porphyrin triiodide demonstrate that the presence of a lipophilic aryl group in one of the meso positions of the tetrapyrrole macrocycle contributes to phage inactivation.[219] This conclusion is consistent with the results of the study of photoinactivation of hepatitis A virus and bacteriophage MS2 with PS differing in the length of the side alkyl chain (tetrakis(N-[*n*-butyl]-4-pyridiniumyl) porphyrin, tetrakis(N-[*n*-hexadecyl]-4-pyridinium tetrayl)porphyrin, tetrakis(N-methyl-4-pyridiniumyl)porphyrin, tetrakis(N-[*n*-octyl]-4-pyridiniumyl) porphyrin).[203] At the same concentration of PS and identical conditions for complete photoinactivation of the hepatitis A virus using tetrakis(N-[*n*-butyl]-4-pyridiniumyl) porphyrin, irradiation was required for 30 min, while when using tetrakis(N-[*n*-octyl]-4-pyridiniumyl)porphyrin took 1 min to achieve the same effect.[203]

The introduction of lipophilic fragments has a positive effect on the bactericidal activity of PS. Photodynamic effect of meso-substituted cationic porphyrins, 5-[4-(trimethylammonium)phenyl]-10,15,20-tris(2,4,6-trimethoxyphenyl)porphyrin iodide, 5,10-di(4-methylphenyl)- 15,20-di(4-trimethylammoniumphenyl)porphyrin iodide and 5-(4-trifluorophenyl)-10,15,20-tris(4-trimethylammoniumphenyl)-porphyrin iodide have been studied in vitro in gram-negative *Escherichia coli* bacteria.[220] It turned out that after the washing step, only 5-(4-trifluorophenyl)-10,15,20-tris(4-trimethylammoniumphenyl)porphyrin iodide had bactericidal activity.

The authors,[221] while studying the antibacterial properties of *meso*-substituted tetracationic pyridylporphyrins quaternized with hydroxyalkyl and haloalkyl residues against gram-negative and gram-positive microorganisms, hypothesized that the main factor of photoinactivation is the presence of positively charged groups in the PS molecule, which have electrostatic interaction with negative groups on the surface of bacterial cell membrane. The final binding of PS to cells is regulated by the lipophilicity of functional groups, which contributes to the strong association of PS with the cytoplasmic membrane.

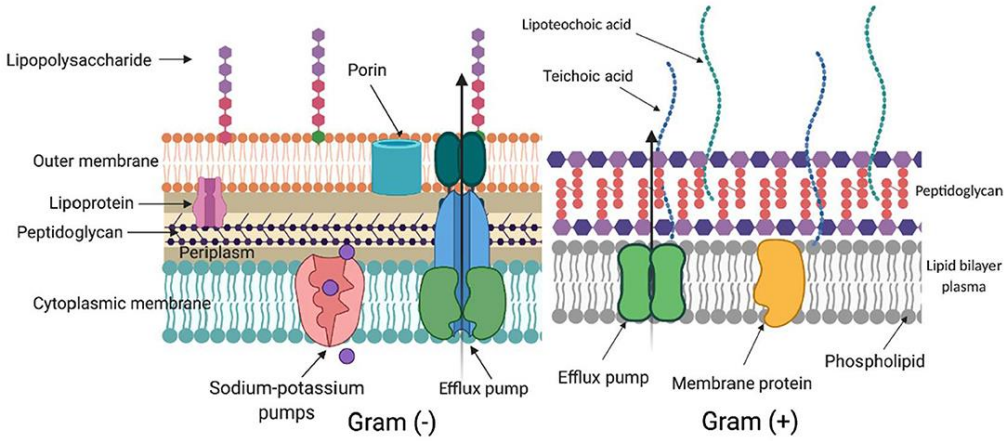

Figure 5. The structure of cell membrane.[216]

When designing a PS, it is also necessary to take into account the fact that the introduction of a lipophilic substituent can lead to a shift in aggregation equilibria in porphyrin solutions towards self-association, which will adversely affect antibacterial activity. It is this phenomenon that was discovered by the authors[222] when studying the photophysical properties and antibacterial activity of a number of derivatives of 5,10,15,20-tetrakis-(4-N-methylpyridyl)porphine, in which one N-methyl group is replaced by a hydrocarbon chain in the range from C6 to C22. It turned out that the antibacterial photoactivity of porphyrins increased with an increase in the length of the N-alkyl chain to C14, which led to complete inhibition of the growth of *E. coli* even at doses of 0.8 μM. A further increase in the size of the substituent to C18 and C22 was accompanied by a decrease in the photosensitizing efficiency.

It is known that an asymmetric charge distribution in the peripheral position of a porphyrin leads to an increase in the amphiphilic nature of MHC, which can contribute to a better accumulation in cells during PDT,[223] as well as inactivation of bacteria. For example, 5-(4-trifluorophenyl)-10,15,20-tris(4-trimethylammoniumphenyl)porphyrin iodide,[224] which has a lipophilic trifluoromethyl group in its composition, exhibits the ability to bind with high affinity to *E. coli* (gram-negative) and provides effective photoinactivation. At the same time, 5,10-di(4-methylphenyl)-15,20-di(4-trimethylammoniumphenyl)porphyrin iodide is able to cause photodamage of *E. coli* in a lesser extent, and after washing out the PS, it does not inhibit the growth of bacteria at all. This fact suggests that the dicationic porphyrin does not enter the cell.

The inactivation of gram-positive and gram-negative bacteria with 5,10,15-tris(1-methylpyridinium-4-yl)-20-(pentafluorophenyl)porphyrin tri-iodide is reported in the work,[225] which also emphasizes the importance of the lipophilic substituent in the PS molecule for photoinactivation of gram-negative bacteria.

Quite interesting data were obtained by the authors[209] in the study of photoinactivation of gram-negative bacteria *Vibrio anguillarum* and *E. coli* by porphyrins. Tetra(4-sulfonatophenyl)porphine, tetra(4N-methyl-pyridyl)porphine tetraiodide and the tetra(4-N,N,N,-trimethyl-anilinium)porphine were evaluated as PS. All three porphyrins show a similar pattern of subcellular distribution, localizing mainly in protoplasts. However, only cationic porphyrins have photoinactivating ability.

It is known that the mechanism of photooxidation with the participation of PS can proceed in two types: type I, with the participation of radical forms, and type II, with the participation of singlet oxygen. As the data show,[226] photoinactivation of gram-negative bacteria of the genus *Salmonella* is carried out to a greater extent due to the generation of superoxide anion and hydroxyl radical upon irradiation of tetracationic porphyrin containing $[Ru(bpy)_2Cl]^+$ - peripheral groups. The results obtained are credible, since the formation of radical forms was confirmed by the EPR method.

As noted above, the cell membrane of gram-negative bacteria is characterized by low permeability for large molecules. Nevertheless, the authors[227] succeeded in obtaining an effective PS for the gram-negative bacterium *E. coli* based on a conjugate of tricationic porphyrin with cyclodextrin, which, judging by the information presented by the authors, penetrates into the bacterial cell. The work[228] emphasizing the significance of the influence of the charged group position and the bridging heteroatom in porphyrin conjugates with cyclodextrin on the efficiency of *E. coli* photoinactivation is quite indicative. The authors of this publication found that the replacement of thiopyridine by methoxypyridine units in the conjugates leads to a significant decrease in the antibacterial effect.

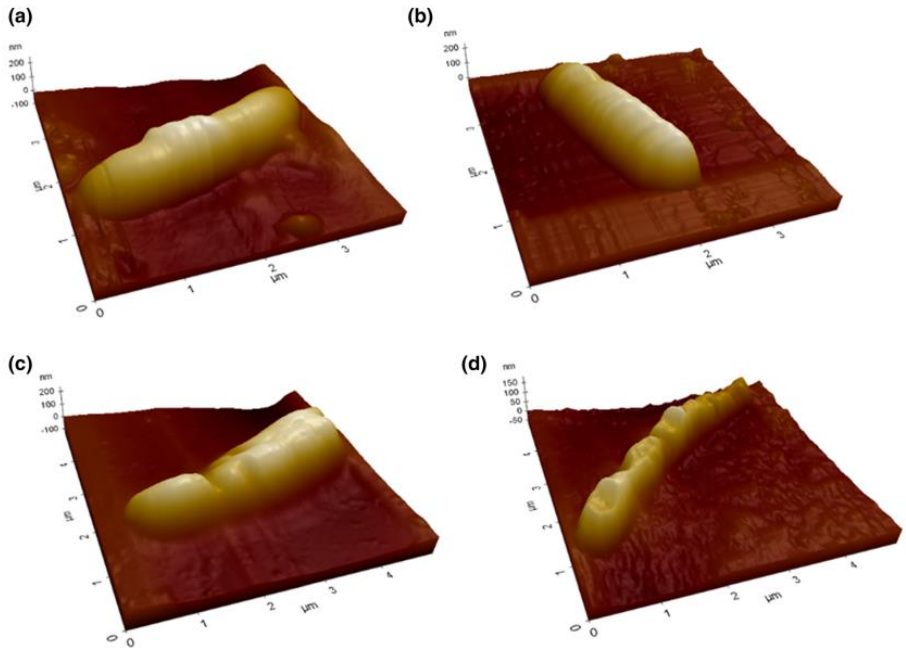

Figure 6. Atomic force microscopy for a mycobacterium in the initial state (a), after light exposure (b), after treatment with tetracationic ZnTMPyP (c), after treatment with tetracationic ZnTMPyP and light exposure (d).

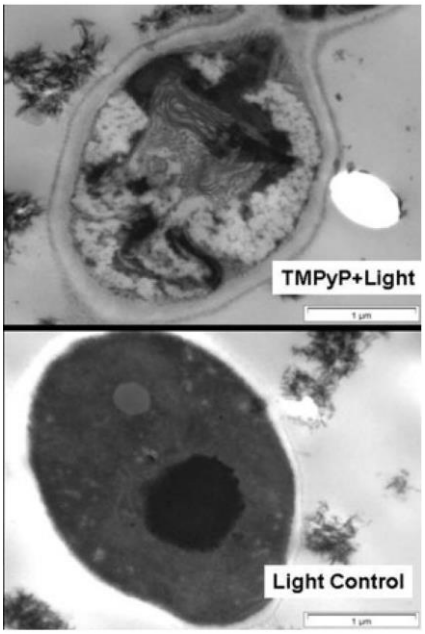

Figure 7. Effect of photosensitization by the exogenous porphyrins on the ultrastructure of *C. albicans* cells. TEM images of *C. albicans* cells treated with 3.5 μM TMPyP illuminated with 12 J·cm^{-2} (TMPyP+Light). *C. albicans* cells illuminated with 12 J·cm^{-2} without an exogenous porphyrin (Light Control) served as control.[234]

Establishing the localization and accumulation sites of PS in virions and most bacterial cells is a complex and unresolved issue in most cases. For bacterial cells, it is extremely difficult to analyze individual structural elements of the cell, for example, by flow cytometry methods, where the bacterial cells themselves are often at the limit of the resolution of the method[216]. Obtaining information about the role or behavior of individual cell structures in the process of photoinactivation of bacteria requires the use of complex methods. In some cases, it is possible to establish the localization of a PS by the presence of its own fluorescence[229]. Recently, atomic force microscopy[230-232] or transmission electron microscopy[323] has been used to prove the localization of PS in the bacterial cell wall. Figure 6 shows, as an example, atomic force microscopy data for a mycobacterium in the initial state (a), after light exposure (b), after treatment with tetracationic zinc(II) 5,10,15,20-tetra-[4-N-methylpyridyl]porphine (ZnTMPyP) (c), after treatment with tetracationic ZnTMPyP and light exposure (d), as well as TEM results for *C. albicans* with 5,10,15,20-tetra-[4-N-methylpyridyl]porphine (TMPyP) porphyrin.[230]

TEM makes it possible to detect ultrastructural changes in the cell, so in the presented photo (Figure 7), after treatment with PS and light, disorganization of the cytoplasm is visible, there is a lack of a nucleus and the appearance of white spots, a massive accumulation of wall-like material in the cytoplasm and damage of cells with a rupture of the membrane, which reflects the leakage of intracellular components.[234]

However, few such data have been obtained so far, which does not allow us to analyze the dependence of the PS structure and its predominant localization in the pathogen. Nevertheless, the conducted mini-review of the literature data allows us to conclude that for the effective interaction of *meso*-substituted porphyrins with pathogens and their subsequent inactivation, three cationic groups in the photosensitizer composition are sufficient, and the fourth peripheral substituent must have a lipophilic character and can provide the required selectivity. Based on this conclusion, we attempted to design a cationic porphyrin capable to binding with the SARS-CoV-2 spike protein in the receptor-binding domain (RBD).[235,236] The ultimate goal was to obtain a porphyrin capable of causing photodestruction of the RBD S-protein, which would make it impossible for the SARS-CoV-2 virion to bind to the surface enzymes of human cells. As a result of theoretical studies,[235-239] the some porphyrins were designed, which, according to the results of molecular docking with the S-protein, are localized between the RBDs of three S-protein polypeptide chains. Using the C-H-activation method,[240] a targeted synthesis of porphyrins was carried out: 5-[4′-(1″,3″-benzothiazol-2″-yl)phenyl]-10,15,20-tris(N-methylpyridinium-3′-yl)porphyrin triiodide (S-Por), 5- [4′-(1″,3″-benzoxazol-2″-yl)phenyl]-10,15,20-tris(N-methylpyridinium-3′-yl)porphyrin triiodide (O-Por), 5-[4-(N-Methyl-1″,3″-benzimidazol-2″-yl)phenyl]-10,15,20-tris(N-methylpyridinium-3′-yl)-porphyrin triiodide (N-Por). For the compounds obtained, the quantum yields of singlet oxygen were determined, which amounted to 0.61-0.86.[235,241] In monohetaryl substituted porphyrins, the replacement of a heteroatom has almost no effect on both the quantum yield of fluorescence (0.17–0.21) and singlet oxygen, and the lifetime (8.3–9.8 ms) in the triplet state.

To confirm the results of molecular docking, a spectral study of S-protein binding to the synthesized monoheteryl substituted porphyrins was performed. Quantitative characteristics reflecting the affinity[242,243] of the S-protein to hetaryl porphyrins were obtained by spectrophotometric titration of the S-protein with asymmetrically monosubstituted hetaryl porphyrins (Table 1).

Table 1. The affinity parameters of S-protein with hetaryl porphyrins according to fluorescent titration data.

System	Affinity	The number of binding sites
S-protein·N-por	$5.94 \cdot 10^5$	3.6
	$1.18 \cdot 10^5$	4.7
S-protein·O-por	$1.2 \cdot 10^6$	2.4
S-protein·S-por	$7.96 \cdot 10^5$	2.6
S-protein·ACE2·N-por	$1.56 \cdot 10^5$	2.2
	$1.25 \cdot 10^5$	2.4

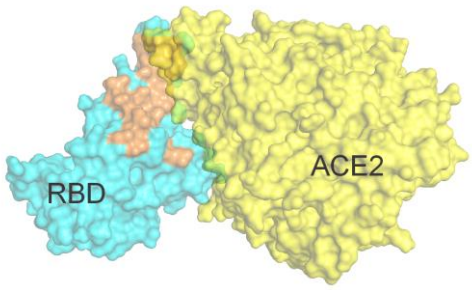

Figure 8. Structure of the ACE2-RBD (6vw1) complex with N-por according to X-Ray data. Yellow ACE2, blue RBD. Orange indicates the RBD region responsible for binding to the N-por.[244]

The results of competitive titration[243] of the S-protein·ACE2 complex with N-por (Figure 8) clearly demonstrated that N-por leads to the destruction of the S-protein complex with ACE2. The competitive influence of N-por and ACE2 for binding to the S-protein confirms that the binding of porphyrin occurs precisely in the RBD site of the S-protein.

Determination and evaluation of the bactericidal activity of porphyrins was carried out on the surface of a dense nutrient medium (Columbian Agar with sheep's blood) contaminated with museum strains of microorganisms - *S.aureus ATCC 29213* and *S.epidermidis ATCC 14990*. It was found that the synthesized compounds upon photoactivation exhibit antibacterial activity against staphylococci (Figure 9, Table 2). Thus, the conducted microbiological study showed that with photoirradiation for 15', monoheteryl substituted porphyrins containing benzothiazole and N-methylbezimidazole residues provide complete lysis of *S.aureus* and *S.epidermidis* strains. In the case of a hetaryl substituted porphyrin with a benzooxazole residue, complete lysis was observed in the *S.aureus* strain and incomplete lysis was observed in the *S.epidermidis* test strain. Increasing the exposure time to 30' ensured complete lysis in the *S.epidermidis* strain.

This review of literature data showed that tri- and tetra-cationic porphyrins are effective photosensitizers; reactive oxygen species generated by them initiate oxidative destructive reactions in biomolecules and biostructures of pathogens. Variation of the lipophilic nature of the PS makes it possible to adjust the bactericidal and virucidal activity of MHC. To increase the efficiency of photoinactivation of pathogens, further studies are needed to study the influence of the nature of photosensitizers, their interaction with cells and subcellular structures, biomolecules, and the assessment of photoinduced damage.

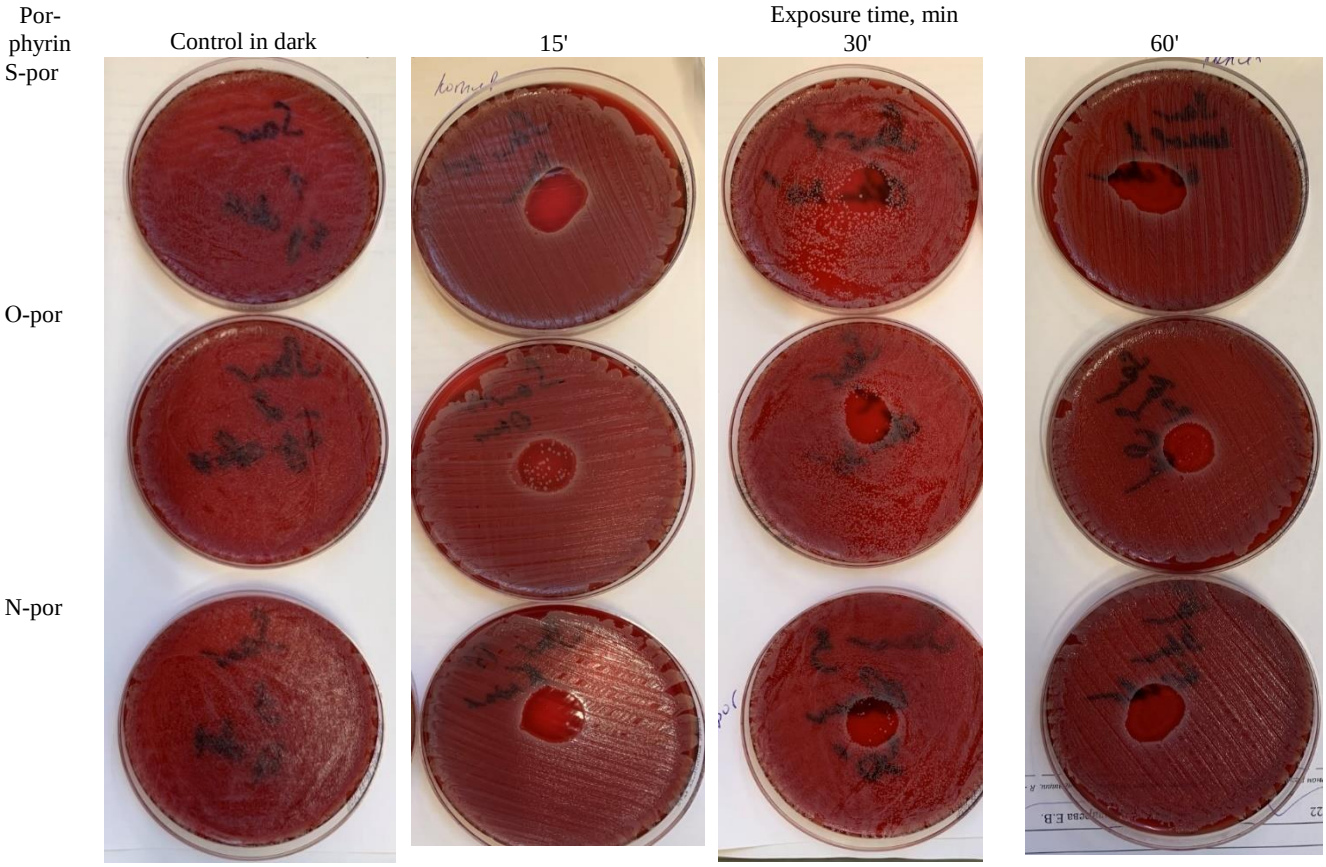

Figure 9. The results of the bactericidal effect of porphyrins in the dark and upon activation by light on the *S. aureus ATCC 29213* test culture.

Table 2. Evaluation of lytic activity on a five-point scale ("-" no lytic activity; "+" low activity; "++" formation of a lysis zone with a large number of colonies of secondary growth of the bacterium; "+++" lysis zone with single colonies of secondary growth ; "++++" transparent zone of lysis without secondary growth colonies).

Porphyrin	S-por			O-por			N-por		
Exposure time	15'	30'	60'	15'	30'	60'	15'	30'	60'
S.aureus	++++	++++	++++	+++	++++	++++	++++	++++	++++
S.epidermidis	++++	++++	++++	++++	++++	++++	++++	++++	++++

5. Approaches toward Cationic Photosensitizers Based on Phthalocyanines

One of the most attractive photosensitizers in PDT are phthalocyanines (Pcs) and their metal complexes.[10,98, 245–248] The singlet oxygen mediated process is predominant for Pcs that possess strong absorbance in the visible region between 600 nm and 700 nm (referred to as the Q-bands) resulting from the HOMO → LUMO (π→π*) excitations.[249,250] This part of spectrum favours the optimal penetration of the light through a tissue. Moreover, Pcs, compared with porphyrins, have low absorbance at wavelengths between 400 nm and 500 nm, where daylight intensity is highest. The presence of a heavy atom in the phthalocyanine leads to the enhancement of singlet oxygen generation due to an increase in spin-orbit coupling owing to so called "heavy atom effect", and consequently, the transition of the photosensitizer from the excited singlet state to the excited triplet state. Outstanding photophysical properties of phthalocyanines are tailorable through variation of the central cation, axial ligands, nature of substituents and their position in the Pc aromatic ring.[98,251–253] Introduction of cationic substituents into phthalocyanine's rings may provide better solubility in water as well as decrease their tendency to aggregation [254,255]. In addition, many cationic Pcs show a higher photodynamic efficiency than anionic or uncharged hydrophilic Pcs [255] due to better binding to DNA molecules.

Cationic function in Pc can be formed *via* different ways, such as: quaternization of the nitrogen atom in aliphatic and aromatic substituents,[256–258] quaternization of pyrido(pyrazo)porphyrazines [255] and exocyclic metalation,[259] introducing of pnictogenes(V) in the cavity of phthalocyanine ring,[260–264] or via meso-N-protonation of phthalocyanines bearing alkoxy-groups in non-peripheral positions[265] (Figure 10).

The synthesis and photophysical properties of some cationic Pcs bearing quaternized nitrogen-containing groups have been summarized in two comprehensive reviews.[266,267] This chapter of the review is an attempt to illustrate novel examples of Pcs with quaternized nitrogen-containing groups and other pathways to others types of cationic Pcs.

N-Centered Cationic Charges

Intriguing examples of cationic phthalocyanines with four and eight extremely bulky 2,6-di(*N*-methylpyridine-3-yl)phenoxy substituents were reported by P. Zimcik group (Figure 11).[257] These Pcs exist as monomers in water and phosphate buffered saline (PBS) and exhibit moderate fluorescence quantum yields (0.17 and 0.16) both in DMF and PBS that may be used for bioimaging. Also, high values of phototherapeutic indices were obtained. The ratio of dark toxicity to light toxicity (TC_{50}/EC_{50}) for HeLa cell line was found to be 1409 and 5691 for tetra- and octa-substituted complexes respectively.

Introduction of imidazolium units into Pcs's macroheterocycles was accomplished by Lioret *et al.* through S_N2 reaction of 4,5-dichlorophthalonitrile and imidazole in the presence of K_2CO_3 at 50 °C yielding 75 % of the diimidazolyl derivative. The further template cyclotetramerization of the resulting phthalonitrile with $Zn(OAc)_2$ lead to octa-imidazolyl Pc derivative (Figure 12).[258] After quaternization with methyliodide, the target zinc octa(*N*-methylimidazolium)phthalocyaninate was obtained in almost quantitively yield. For latter complex photocytotoxicity studies were carried out on murine melanoma B16F10 cancer cells and IC_{50} = 5.379 mM was determined.

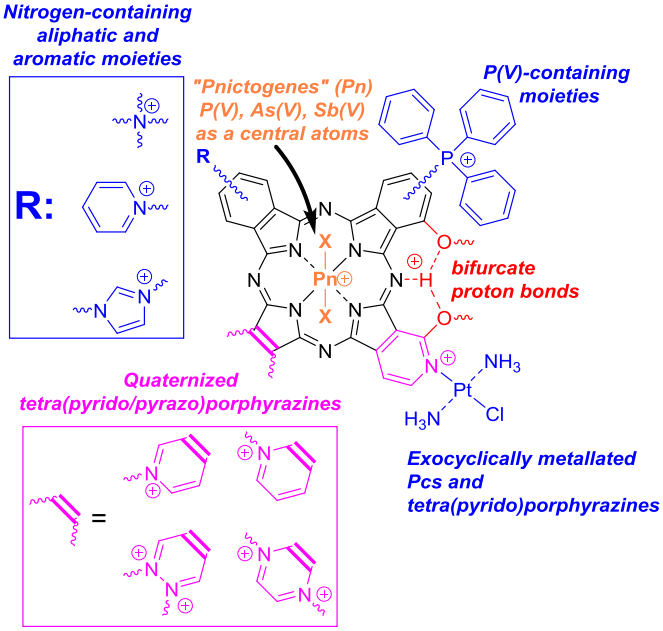

Figure 10. Approaches toward cationic phthalocyanines and tetra(pyrido/pyrazino)porphyrazines.

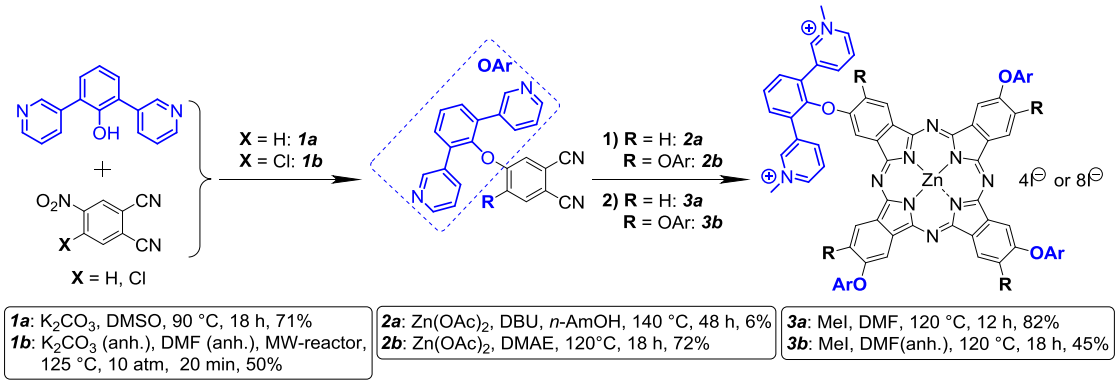

Figure 11. Synthesis of quaternized zinc complexes with tetra-[257] and octa-substituted[268] [2,6-di(3-pyridyl)phenoxy]phthalocyanines.

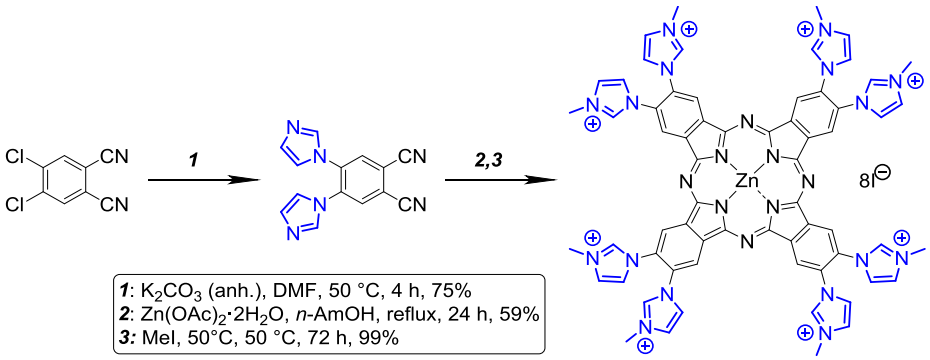

Figure 12. Synthesis of zinc octa(N-methylimidazolium) phthalocyaninate.[258]

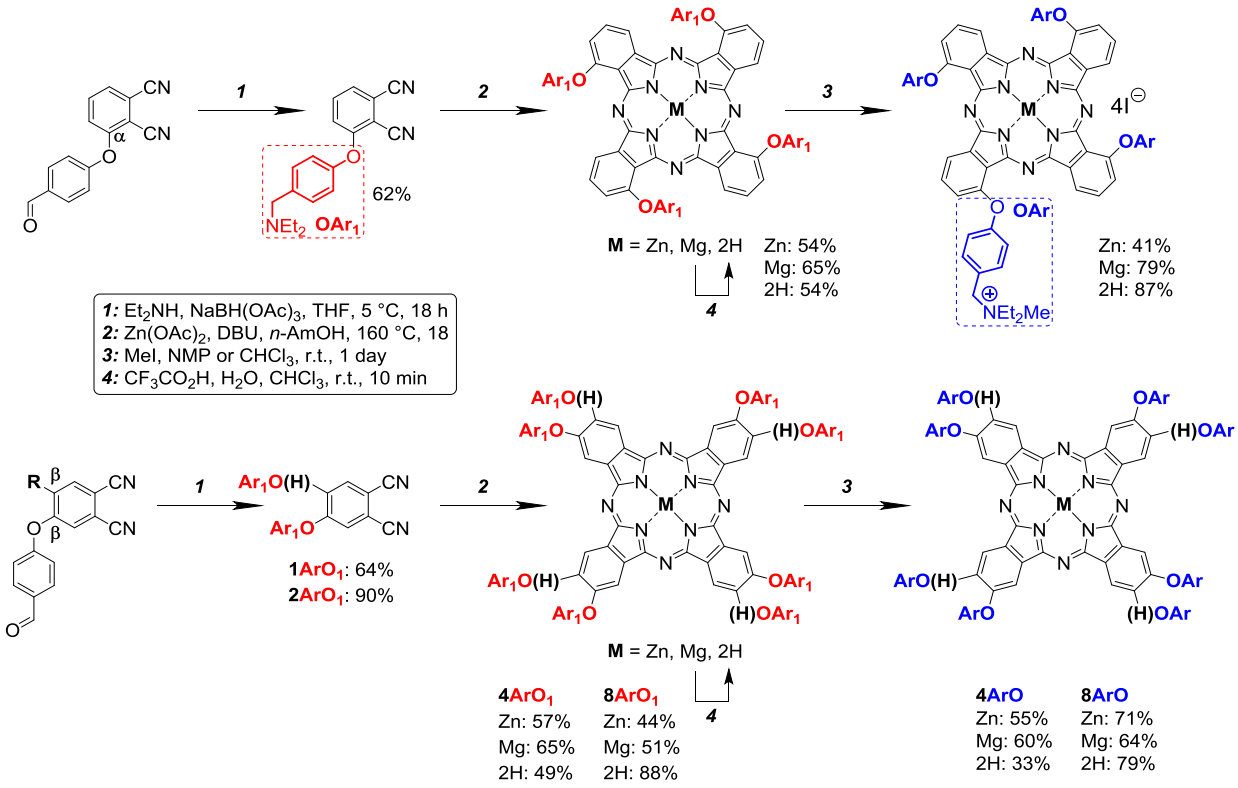

Figure 13. Robust route toward cationic phthalocyanines through reductive amination.[256]

Recently Bunin *et al*. developed robust route toward cationic phthalocyanines through reductive amination.[256] In the synthesis of cationic Pcs reductive amination was used for the first time. Thus, reaction of 3- and 4-(formylphenoxy)phthalonitriles with diethylamine and sodium trisacetoxyborohydride in THF resulted in corresponding diethylamino-derivatives of phthalonitriles isolated in high yields (Figure 13). New Zn(II), Mg(II) and metal-free phthalocyanines containing four or eight cationic groups in non-peripheral (α-) or peripheral (β-) positions were synthesized starting from the aminated phthalonitrile derivatives followed by quaternization with CH_3I. All novel cationic Pcs exhibited strong absorption in the phototherapeutical range from 670 to 700 nm and high quantum yields of singlet oxygen generation in DMSO where all phthalocyanines existed in monomeric forms. Also, cationic complexes showed moderate solubility in water with high tendency to aggregation, however α-substituted Zn(II) and Mg(II) complexes existed in water in predominantly monomeric states. Further monomerization of tetra-α-substituted Zn(II) complex in aqueous solution was achieved by interaction either with non-ionic surfactant Tween-80 or bovine serum albumin (BSA). The advantage of these results was not limited to new convenient synthetic approach to the cationic phthalocyanines but it also consisted in preparation of new promising phototherapeutic agents with good photophysical and photochemical properties.

Cationic Charges Centered on Other Atoms

Schneider *et al*. report the first example of exocyclic metalation of tetra(pyrido)porphyrazine (Figure 14).[259] In this

intriguing work, zinc complex with tetra(pyrido)porphyrazine (as a mixture of regioisomers) was coupled with transplatine fragments via reaction with fivefold excess of tetrakis-[*trans*-Pt(NH_3)$_2$Cl]NO_3, derived *in situ* from transplatine (tetrakis-(*trans*-Pt(NH_3)$_2$$Cl_2$)) and $AgNO_3$ in DMF. Mass-spectrometry in combination with ^{195}Pt-NMR spectrum for platinated compound indicates the formation of the tetraplatinated derivative as a sole product. This exo-platinated Pc demonstrate red shift of Q-band in UV-Vis spectra up to 682-692 nm in comparison with 663-674 nm for its non-platinated precursor. Interesting, platinated complex of demonstrated low absolute quantum yield of fluorescence (0.01 in DMF) expectedly due to large percentage of inter system crossing (ISC) that provides «heavy atom effect» of Pt-atoms, but no generation of singlet oxygen was also indicated (by direct method in which luminescence of $^1O_2$ was registered at 1270 nm in DMF-d_7). However, in phototoxicity experiments with HeLa cell line this complex exhibited IC_{50} value at 1.6 μM at the light and 12 μM in the dark. These results could be rationalized by production of other forms of reactive oxygen species (ROS) rather than singlet oxygen. Notably, for zinc complex of tetra(pyrido)porphyrazine light and dark toxicities IC_{50} were 28 and 34 μM respectively. Difference in dark toxicity of precursor and platinated complex was explained by DNA-binding ability of transplatine fragments, which was shown in this work; after irradiation difference in toxicity was explained by «double-punch» effect (photoxicity in combination with DNA-binding ability) provided by platinated complex. Thus, authors proposed further investigation of this novel exocyclically platinated tetra(pyrido)porphyrazine as a photosensitizer.

Also, positive charges can be obtained by introduction of quaternized phosphonium moieties (Figure 15).[269–271] For example, such complexes were synthesized with the intention to be used for enhanced mitochondria penetration owing to four triphenylphosphonium units, they demonstrated both photodynamic and sonodynamic efficacy against MCF-7 and HeLa cell lines (IC_{50} = 12.7 – 45.0 μM).

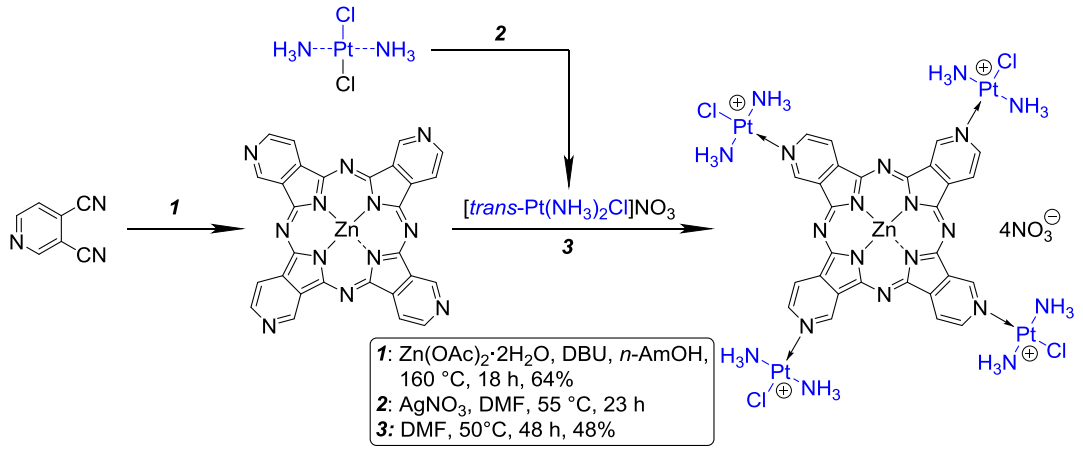

Figure 14. Synthesis of phthalocyaninate modified by four transplatine units.[259]

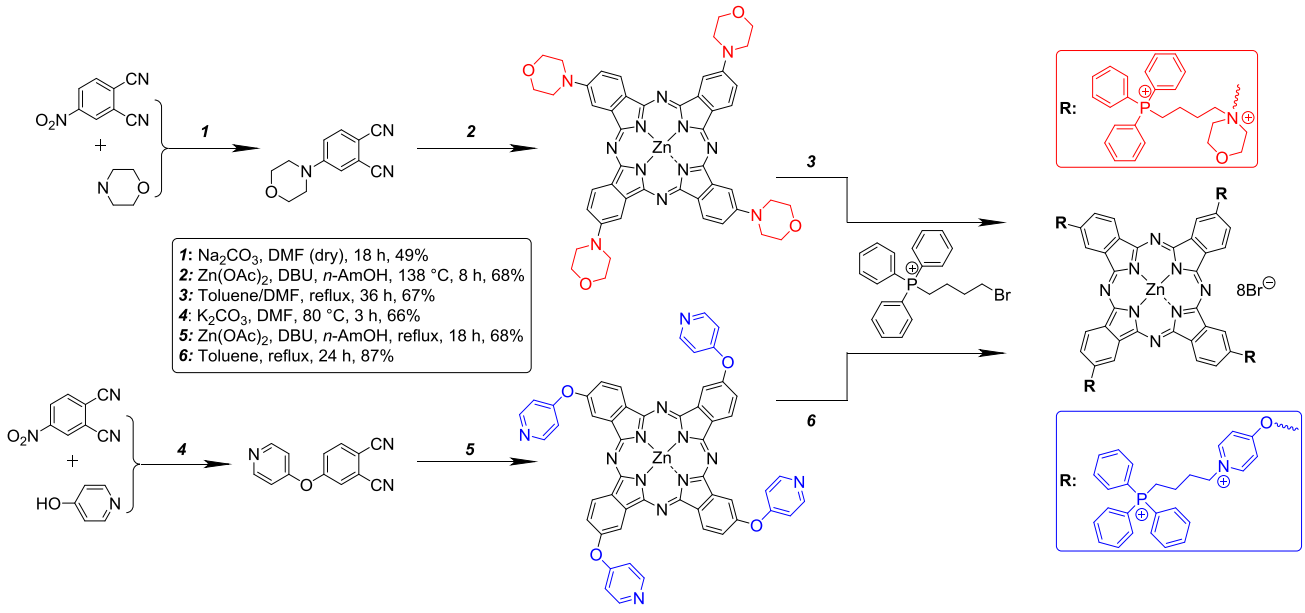

Figure 15. Synthesis of phthalocyanines with trisphenylphosphonium moieties.[269–271]

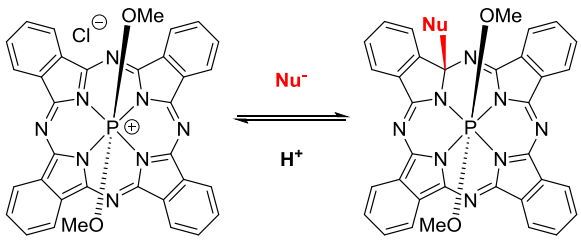

Figure 16. Reversible nucleophilic addition to phosphorus(V) phthalocyaninate (Nu^- = OH^- or MeO).[264]

Recently Kolomeychuk *et al*. performed detailed investigation of phthalocyaninate where the cationic phosphorus(V) centre was placed *into* the cavity of the macrocycle[264] in order to compare its photophysical properties with corresponding porphyrin derivatives.[272,273] During this study the authors discovered the unprecedent switching of aromaticity (Figure 16),[264] which could be "turned off" by reversible aromatic nucleophilic addition of OH^- or OMe^- to the α–pyrrole C-atom affording the nonfluorescent adduct. Aromaticity and fluorescence could be restored by acidic treatment of the adduct. Structure of the adduct was confirmed by single crystal X-ray analysis.

Kobayashi *et al.* demonstrated the prospective of cationic phthalocyanines with endocyclic pnictogene atoms. They synthesized non-peripherally substituted octa(2,6-dimethylthiophenoxy) phthalocyaninates of P(V), As(V) and Sb(V) and thoroughly investigated their optical properties (Figure 17).[260–262] Absorption maxima of these complexes (Q-bands) were found at 1018, 1032 and 1056 nm, respectively, whereas the analogous zinc complex had a Q-band located at 790 nm (in CH_2Cl_2). Such strong shifts of Q-bans into near-IR region for P(V), As(V) and Sb(V) complexes occurred due to decrease in HOMO–LUMO gap that was confirmed by DFT calculations. In addition, the insertion of electron-donating S-atoms in non-peripheral positions also contributed to the narrowing of the HOMO–LUMO gap.

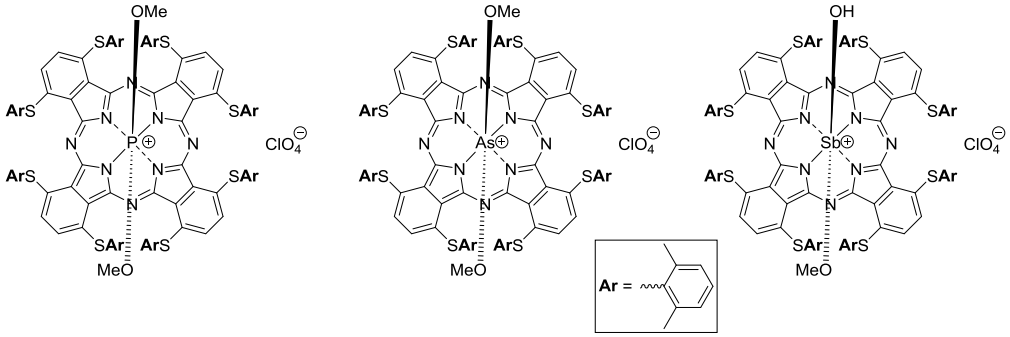

Figure 17. Complexes of P(V), As(V) and Sb(V) with non-peripherally 2,6-dimethylthiophenoxy-substituted phthalocyanine.[261]

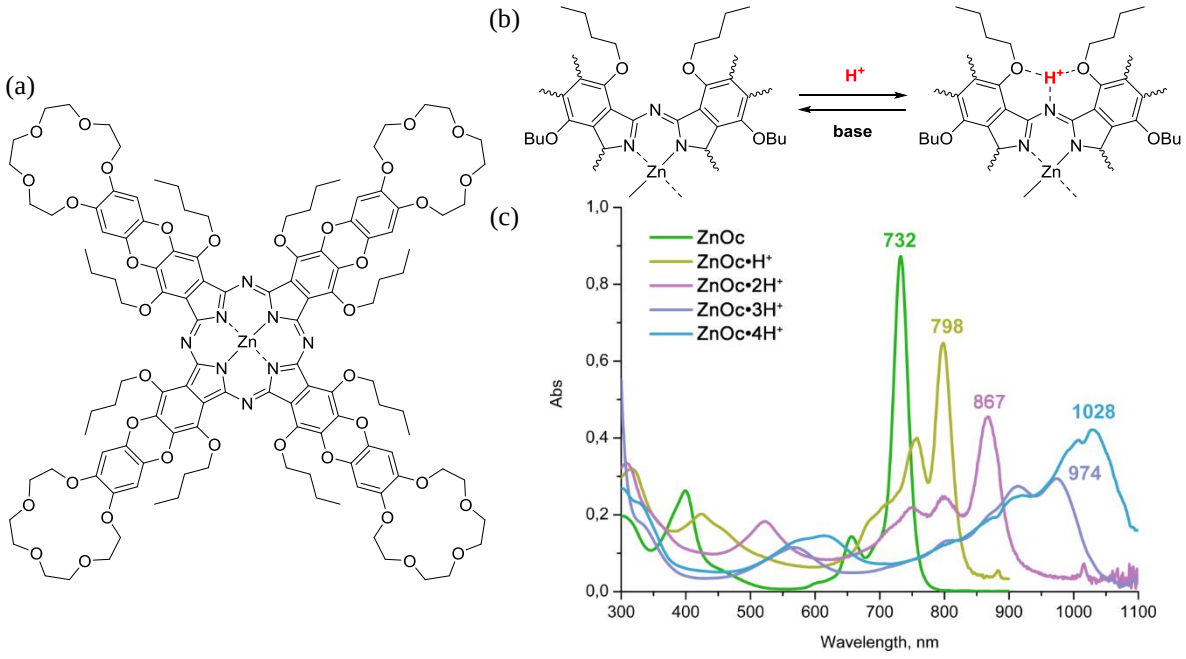

Figure 18. (a) – Zinc(II) complex with crown-substituted oxanthrenocyanine **ZnOc**; (b) reversible formation of bifurcate proton bonds upon acidic treatment; (c) UV-vis spectra of **ZnOc** and its protonated forms in $CHCl_3$.[265] Adapted with permission from ref. [265] Copyright 2016, American Chemical Society.

Apart from strong bathochromic shifts of Q-bands non-peripheral substitution provides phthalocyanines with enhanced basicity of their *meso*-nitrogen atoms.[274,275] Protonation has profound effect on optical properties of phthalocyanines resulting in strong bathochromic shifts of their Q-bands and quenching of fluorescence.[276] For example, Safonova *et al.* developed approach toward tetra-15-crown-5-annelated zinc oxanthrenocyaninate **ZnOc** (Figure 18a,b) and demonstrated consecutive formation of four protonated forms having absorption maxima at 798, 867, 974 and 1028 nm respectively whereas non-protonated form had maximum of absorbance at 732 nm (Figure 18c).[265] Notably, this protonation is reversable and neutral form can be recovered under addition of amines. Such proton-susceptible compound can serve as a molecular switcher for optoelectronic materials, sensors as well as switchable photosensitizers.

To conclude, cationization of phthalocyanines is an effective way to complexes, that are soluble in water and exist in aqueous solutions predominantly as monomeric species. Also, some cationic phthalocyanines and their analogs have absorbance beyond 1000 nm due to complexation with pnictogens or formation of protonated species. These properties of cationic Pcs in conjunction with excellent photodynamic efficiency may be useful in photomedicine and also, cationic Pcs might be suitable NIR dyes, molecular switchers and sensors.[277]

6. Effective Near-Infrared Photosensitizers for PDT and aPDT Based on meso-Tetrakis(3-pyridyl)bacteriochlorin

The reduced derivatives of porphyrins such as, chlorins and bacteriochlorins, are used as photosensitizers (PSs) for photodynamic therapy (PDT) of cancer due to their high-intensity optical absorption and luminescence in the red and near-IR range.[46,148,278-281] Thus, well-known photosensitizers based on hydrogenated porphyrin derivatives such as Foscan® (Temoporfin, *meso*-tetrakis(3-hydroxyphenyl)porphyrin),[282,283] Visudyne® (Verteporfin),[46,284] and Tookad[285, 286] have been designed (Scheme 38).

A porphine molecule has a multiple-contour conjugated system; its interior chromophore contains 18 π electrons. Two peripheral C_β=C_β' bonds are quasi-isolated, and their hydrogenation does not disrupt the main macrocyclic aromatic π-conjugated system (Scheme 39).[287–290]

Reduction of the double bond in one of the pyrrolyc moieties of porphine gives chlorin (2,3-dihydroporphyrin); reduction of double bonds in two opposite pyrrole moieties give rise to bacteriochlorin (7,8,17,18-tetrahydroporphyrin, BC), while hydrogenation of two adjacent pyrrole moieties yields isobacteriochlorin (2,3,7,8-tetrahydroporphyrin, iBC) (Scheme 40).[291]

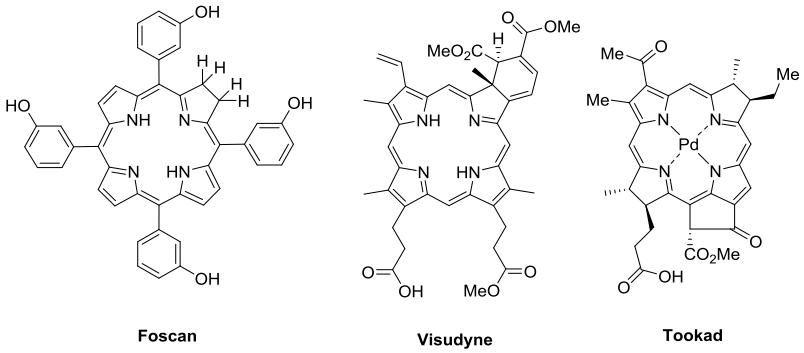

Scheme 38.

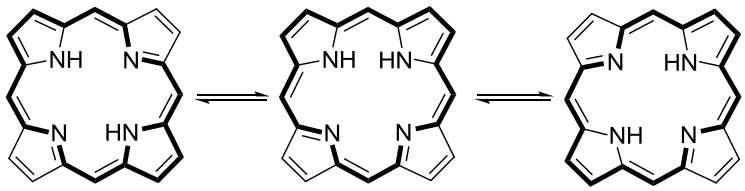

Scheme 39.

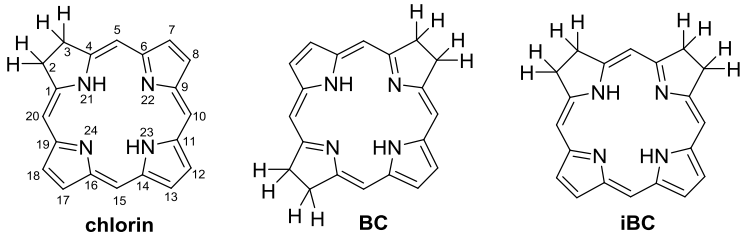

Scheme 40.

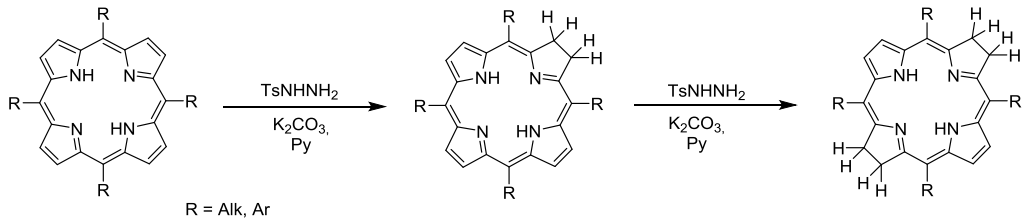

Scheme 41.

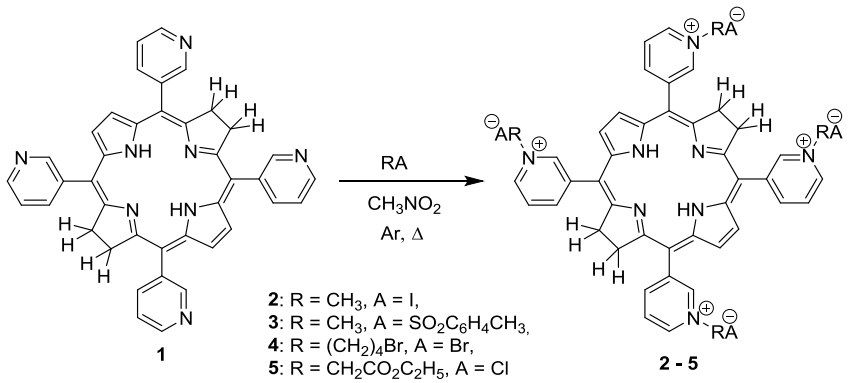

Scheme 42.

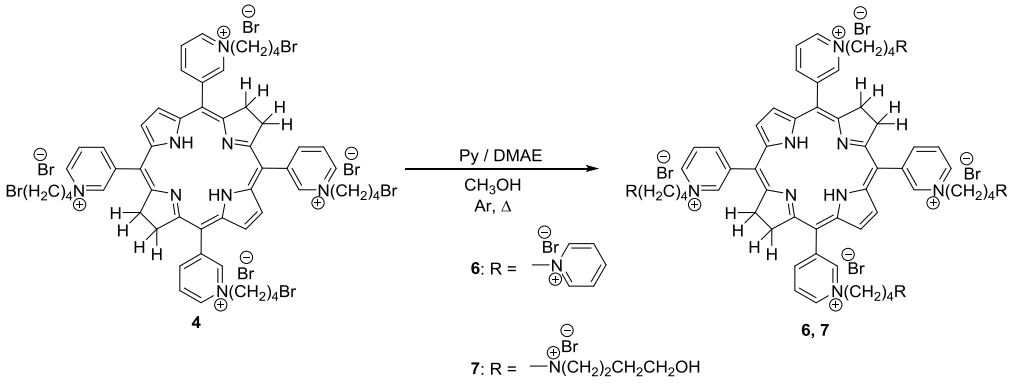

Scheme 43.

The main data on preparation of synthetic chlorins and bacteriochlorins have been summarized in reviews.[292-294] The simplest and most available method for preparation reduced porphyrin derivatives is Whitlock reduction (reduction by diimide generated *in situ* from *p*-toluenesulfonyl hydrazide, $TsNHNH_2$) (Scheme 41).[295]

Solubility in bodily fluids, and water in particular, is one of the key requirements posed on PSs, along with the high quantum yield generation of singlet oxygen and tropicity to tumor cells [14,296-299]. Therefore, *meso*-tetrakis(3-pyridyl)bacteriochlorin is a promising platform for designing novel photosensitizers: on the one hand, this compound is characterized by strong light absorption in the long-wavelength region (λ_{max} = 747 nm; ε ~ 112,000 mol^{-1} L cm^{-1}; chloroform [300]), while on the other hand, quaternary ammonium salts can be produced by quaternization of pyridyl nitrogen atoms upon exposure to various alkylating agents, giving rise to water-soluble species.

The initial *meso*-tetra(3-pyridyl)bacteriochlorin (BC **1**) was synthesized using the conventional method: by Whitlock reduction of *meso*-tetrakis(3-pyridyl)porphyrin (Scheme 41, R = 3-Py), and its two water-soluble salts (tetraiodide (BC **2**) and tetratosylate (BC **3**)) were immediately produced by boiling of BC **1** with excess amount of methyl iodide or methyl-*p*-toluenesulfonate, respectively (Scheme 42).[301]

Later on, it was shown that other water-soluble quaternary salts can be produced by boiling BC **1** with excess amount of 1,4-dibromobutane (BC **4**) or ethyl chloroacetate (BC **5**), respectively, in nitromethane under an inert atmosphere (Scheme 42).[300] Aqueous solutions of tetracationic salts are stable under dark conditions for up to 6 months.[302]

The presence of bromine atoms in the alkyl chain of BC **4** made it possible to conduct further quaternization and increase the number of cationic sites to n = 8. Boiling BC **4** with excess amount of dry pyridine or dimethylaminoethanol (DMAE) in methanol under an inert atmosphere for 4.5 h yielded octabromide (BC **6**) and octabromide (BC **7**), respectively (Scheme 43).[300]

Hermann *et al.*[303] found that tetratosylate BC **3** generates singlet oxygen *via* type I photosensitization. During type I photosensitization reactions, an electron is detached from the substrate by a photoexcited photosensitizer molecule, which is accompanied by formation of hydroxyl radicals, superoxide anion radicals, and hydrogen peroxide;[304,305] in turn, these species can easily penetrate biological membranes, are highly reactive in oxidation processes, and can further generate radical particles, thus ensuring an oxidation cascade.

Tetratosylate BC **3** exhibited high photodynamic activity (> 86% dead cells) with respect to bile duct cancer (BDC, GBC) cell lines in *in vitro* and *in vivo* experiments; furthermore, it possesses low systemic toxicity and dermatological toxicity.[306] Later, *in vivo* experiments showed that BC **3** is rapidly absorbed by human choroidal melanoma cells and has low dark toxicity after 24 h incubation.[307] The studies of pharmacokinetics and biodistribution of BC **3** *in vivo* (in live mice) and *ex vivo* (in resected organs) in Balb/c colon-26 carcinoma tumor-bearing mice showed that BC **3** is predominantly accumulated in the tumor compared to most normal tissues except for the kidneys: the tumor-to-normal tissue ratio (TNTR) for the liver, colon, muscle, and spleen tissues ranged from 8 to 50.[307]

Physicochemical properties, biodistribution in animal tissues and photoinduced antitumor efficacy of BC **4** and BC **6** were studied using epidermoid carcinoma of the larynx (Hep2) cell culture and the Lewis lung carcinoma (LLC) animal tumor model. *In vitro* studies showed that photosensitizers remained stable for a long time and exhibited a high photoinduced activity with respect to HEp2 cell culture (IC_{50} varied from 0.34±0.07 to 0.71±0.09 μM)[308]. These compounds were shown to be rapidly accumulated in tumor tissue in mice (the tumor-to-normal tissue ratio being 2.3–3.3), exhibit a high photoinduced activity against LLC tumor cells – for BC **4** and BC **6** in the *in vitro* (IC_{50} is 0.34±0.03 and 0.37±0.08 μM, respectively) and *in vivo* system (inhibition of tumor growth and response rate are 100%).[308]

Along with being used as conventional photosensitizers for PDT, BC **1** and its water-soluble derivatives exhibit antibacterial activity against various pathogens. Thus, BC **3** was used against Gram-positive *S.aureus* strains (MSSA and MRSA) and Gram-negative *E.coli* and *P. aeruginosa* strains.[309,310] BC **3** was found to strongly bind to the cell wall of both Gram-positive and Gram-negative bacteria and exhibit no inhibitory activity against *S.aureus* in the dark, while irradiation causes almost complete inactivation of the pathogen.[309] Incubation of the *S. aureus* MRSA strain in phosphate-buffered saline (PBS) in the presence of BC **3** for 30 min followed by irradiation causes almost complete death of the pathogen.[310]

Along with quaternary ammonium salts, lyophilisate for solution for infusion based on BC **1** and containing a non-ionogenic surfactant, Bacteriosens drug, can be used as a water-soluble photosensitizer.[311] This lyophilisate is stable during storage under dry conditions for 6 months. Bacteriosens exhibits a moderate *in vitro* hemolytic activity, does not possess dark cytotoxicity against cultured human and mouse cancer cells, and exhibits high specific activity when exposed to light.[312,313]

Loschenov *et al.* described the application of BC **1** as a photobactericidal coating for a hydroxyapatite implant and demonstrated that this coating was resistant to washout of photosensitizer particles over time.[314]

The Intrachlorin composition based on *meso*-tetrakis(3-pyridyl)bacteriochlorin and being a mixture of water-soluble *meso*-tetra(3-pyridyl)bacteriochlorin and *meso*-tetra(3-pyridyl)chlorin (88 : 12, wt. %) was designed.[315,316] The mixture was prepared by Whitlock reduction of *meso*-tetrakis(3-pyridyl)porphyrin, and pyridyl nitrogen atoms were subsequently quaternized using methyliodide.[316] The resulting composition is characterized by stability, high-intensity long-wavelength optical absorption, and high quantum yields of singlet oxygen generation (~ 0.45±5).[317] The Intrachlorin composition was active when used at a dose of 5–15 mg per 1 g of tumor against model Lewis tumors, spontaneous pituitary cancer, and breast cancer.[318] Rzhevskii *et al.* reported using the Intrachlorin composition for photodynamic therapy of C26 colon carcinoma subcutaneously grafted to Balb/c mice.[319] The recurrence-free efficacy during 6 months was 70 %. A systemic toxicity study of the Intrachlorin composition in Wistar mice was conducted.[319] The 10 mg/kg dose of the Intrachlorin composition was found to be safe when administered daily during 7 days, both intravenously and subcutaneously; the dose > 20 mg/kg repeatedly administered intravenously and the dose > 50 mg/kg repeatedly administered subcutaneously were found to induce toxic effects.[319]

7. Spectral Properties of Photosensitizers Based on Tetra(pyridin-3-yl)porphine and Its Reduced Forms in Solutions and Thin Films

There are numerous tetrapyrrolic compounds that are used as PSs in PDT, whereas porphyrins and phthalocyanines are the most frequently used PSs in antibacterial photodynamic therapy (aPDT). Cationic porphyrins like TMPyP (5,10,15,20-tetrakis(1-methyl-4-pyridinium)porphyrin tetra(*p*-toluenesulfonate)) have fourfold positive charge. Collins *et al.* used TMPyP against *Pseudomonas aeruginosa* biofilms both wild and mutant strains.[320,321] It was postulated that this effect might be due to the large molecular structure of TMPyP or strong electrostatic interaction between the fourfold positive charge of cationic porphyrin and negative charge of extracellular polymeric substance molecules.[322]

Nowadays cationic antimicrobial peptides or cell penetrating peptides are conjugated to porphyrins to improve their efficiency. These conjugated porphyrins show a great cell inactivation during aPDT. Recent studies strongly uphold the hypothesis that aPDT can be a satisfactory alternative since there is a substantial difference in the mode of action of PSs than that of antibiotics. The key benefits of aPDT can be outlined as follows: a broad spectrum of action compared to antibiotics since PS can act on diverse organisms such as bacteria, protozoa, fungi; bactericidal effects independent of antibiotic resistance pattern; more limited adverse effect profile and damage to the host tissue;

no resistance following multiple sessions of therapy. The synthetic photosensitizers of the porphyrin series,[323,324] conjugates of porphyrins with amino acids[325] and saccharides[326,327] are the most studied. A special place in this range of compounds is occupied by reduced forms of porphyrins - chlorins and bacteriochlorins, which can compete with existing photosensitizers used in clinical practice.

During the last decade, nanotechnology has had a great impact on PDT. Most of these studies have used nanoparticles to improve the efficacy of classical PDT while a few of them have been done on the antimicrobial aspects.[328] The results with nanoparticles were more satisfactory than with the PS alone. Furthermore, PS bound to a nanoparticle penetrates through the membrane better than free PS. Nanoparticles themselves can act as PS.[329] To date, low-dimensional porphyrin-based nanostructures with promising properties have been obtained in three-dimensional (3D) environments, on solid surfaces using two-dimensional (2D) templates, exploiting covalent bonding[330,331] or various non-covalent intermolecular interactions.[332,333] Self-assembly is a key player in materials nanoarchitectonics.[334–336] The nanostructures formed in this way arise from molecules carrying side groups that promote the process. Supramolecular polymers were created using diverse self-assembly strategies.[337,338] Formation of different kinds of supramolecular assemblies from some compounds at the water surface,[339] during electrochemical deposition on electrodes[340] and in metal-organic frameworks[341] was reported.

Previously, we demonstrated the possibility of supramolecular design at the air-water interface by controlled self-assembly of porphyrins into 2D and 3D nanoaggregates.[342–349] The concept of nanostructuring of organic compounds at the air-water interface and a model of a floating layer, the structural units of which can be both individual molecules (Langmuir's approach, special case) and their major nanoaggregates (so-called M-nanoaggregates, general case), were presented.[342,350] The formation of the porphyrin nanoparticles from magnesium porphine, a functional element of chlorophyll, was reported.[342] The formation of nanoparticles of biological and bioactive compounds is a non-trivial, but very important and urgent task. Recently, we have established the possibility of formation of nanoparticles by a hydrophobic derivative of vitamin B_{12} (porphyrin-type compound) whose properties differ from the properties of the parent molecules. They were formed at the water-air interface. This was important for pharmacology because this derivative is a neuroprotective agent.[351] Micro- and nanocapsulation technologies occupy an important place in the development of means for targeted delivery of hydrophilic and hydrophobic drugs and modulation of their biological properties.[352-354] It was found that vitamin B_{12} itself can also form nanosized ensembles in delivery systems.[354]

However, nanostructures of photosensitizers based on 3-pyridylporphine, which is parent compound of such important photosensitizers as chlorin and bacteriochlorin, have not yet been obtained.

The aim of this work is to synthesize and characterize the 5,10,15,20-tetra(pyridine-3-yl)chlorin **(T3PyCh)** and 5,10,15,20-tetra(pyridine-3-yl) bacteriochlorin **(T3PyBCh)**, which are the products of 5,10,15,20-tetra(pyridine-3-yl)porphine (**T3PyP)**[355] reduction according to the procedure of Whitlock[†][295] (Figure 19). The possibility of forming **T3PyP** nanostructures by self-assembly at the water-air interface and in thin films on solid supports was studied.[‡]

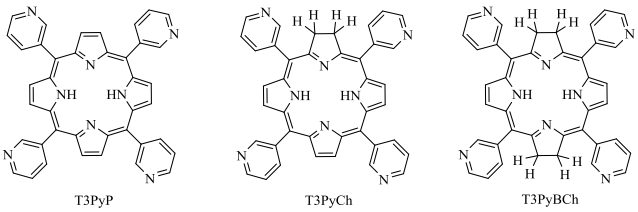

Figure 19. Structural formulae of 5,10,15,20-tetra(pyridine-3-yl)porphine (**T3PyP**); 5,10,15,20-tetra(pyridine-3-yl)chlorin (**T3PyCh**); and 5,10,15,20-tetra(pyridine-3-yl) bacteriochlorin (**T3PyBCh**).

[†] **T3PyP** in pyridine was heated at 100-105 °C in the presence of potassium carbonate with p-toluenesulfonylhydrazide (pTSH); the latter was added gradually. The reaction was carried out until the maximum ratio of optical densities at 745 and 653 nm (absorption maxima of bacteriochlorin and chlorin, respectively) was reached. It was shown that this ratio is inconstant and reaches a maximum (8-10) between 12 h and 16 h.

[‡] The layers at the water-air interface were formed on a Langmuir setup (NT-MDT, Russia). A solution of **T3PyP** in dichloromethane with $C = 0.88 \cdot 10^{-4}$ M was applied to the surface of bidistilled water using a syringe with a graduation value of a 1 μL (Hamilton, Sweden) at (20±1) ºC. The solution was taken in such a volume that the initial degree of surface coverage, assuming perpendicularity of the planes of molecules and the water surface (ISCD c_{edge}, the ratio of the area occupied by the molecules of the substance to the surface area of water) was between 25 and 51%. Also the ISCD c_{face} value for the parallel arrangement of the molecular planes and the surface was calculated. Surface pressure was measured using Wilhelmi sensor with an accuracy of 0.02 mN/m. In 15 minutes after the application of the solution, the formed layer was compressed at a rate of $v=2.3$ cm$^2 \cdot$min^{-1}.

Langmuir-Schefer (LS) films were prepared at (17±1) ºC. For this purpose, the barriers compressing the layer on the water surface were stopped at the selected pressure value, and then the layers were successively transferred onto the quartz substrate by the horizontal lift method. To obtain optimal optical density, the number K of times the substrate was in contact with the layer was varied from 20 to 60. The electronic absorption spectra of LS films and solutions were recorded on a Shimadzu-Uv-1800 spectrophotometer (wavelength resolution ±1 nm), fluorescence spectra were measured with the Solar spectrophotometer.

The structure of the layers at water–air interface was analyzed by using quantitative analysis of compression isotherms of a nanostructured M-monolayer, based on the concept of a layer as a real two-dimensional gas with structural elements representing two-dimensional nanoaggregates 5–20 nm in diameter (M-nanoaggregates).[342] The method allows determination of the critical characteristics of floating layers: the area per molecule in a nanoaggregate, the number of molecules in nanoaggregates, *etc*. The stable state of the layer is described by equation $\pi(A-A_{mol}) = kT/n$ (1) where π is the surface pressure, A is the area per molecule in the layer, A_{mol} is the area per molecule in the aggregate, n is the number of molecules in the aggregate, k is the Boltzmann constant and T is the absolute temperature. When plotted in πA–π axes, a compression isotherm of the floating layer has both linear (corresponding to the single-phase states of the layer) and nonlinear regions. The A_{mol} and n are the main characteristics of a floating monolayer; these values may be determined by approximating the πA–π plot using a linear function (the least squares method was used and the πA error did not exceed 3%).

Geometric parameters of the molecule, determined using the Hyperchemistry software, are as follows: a = 1.5 nm, b = 1.4 nm, c = 0.7 nm; the projection areas Aproj(face) = 1.55 nm^2, Aproj(edge) = 0.7 nm^2; the areas of circumscribed rectangles Arec(face) = 2.2 nm^2 and Arec(edge) = 1.2 nm^2. The areas per molecule in the most densely packed monolayer are Apack(face) = 2 nm^2 and Apack(edge) =1 nm^2.

Although the Whitlock procedure is now the main method for obtaining chlorins from porphyrins, its course has not been systematically studied. In turn, understanding the principles of this interaction would be useful for identifying reaction conditions in which the target product is either **T3PyCh** or **T3PyBCh**. To this end, we quantitatively monitored the diimide reduction of **T3PyP** in the course of the Whitlock reaction by measuring the optical density of the reaction mass at 653 and 745 nm after adding each portion of the reducing agent (pTSH).

The reaction can be divided into two steps: the reduction of porphyrin to chlorin and the formation of bacteriochlorin. In the first stage, chlorin is predominantly formed, which is accompanied by an increase in absorbance at 653 nm (Figure 20a). In the second stage, chlorin is converted to bacteriochlorin; absorbance decreases at 653 nm and increases at 745 nm (Figure 20b).

The concentration of chlorin in the mixture initially increases, reaches a maximum after 7.5 h, and then decreases. On the other hand, the concentration of bacteriochlorin increases insignificantly in the beginning, but starts to increase sharply after 6 hours. Therefore, if the target product of the reaction is chlorin, the reaction should be stopped at the moment when bacteriochlorin absorption starts to grow rapidly. Maximum conversion to bacteriochlorin is expected when the maximum ratio of optical densities at 745 nm and 653 nm is reached.

Taking this data into account, we individually isolated the reduced products. The hydrogenated products, **T3PyCh** and **T3PyBCh**, were isolated by column chromatography.[356] Chromatographic separation was performed on aluminum oxide, and for the first time on silica gel using chloroform or dichloromethane and their mixtures (up to 5%) with methanol. In general, chromatography on both sorbents leads to almost identical results, however, separation on silica gel is more efficient in terms of product yield.

Figure 21 shows the absorption and fluorescence spectra of the initial porphyrin **T3PyP** and its reduced forms, **T3PyCh** and **T3PyBCh**.

As can be seen, the transition from porphyrin **T3PyP** to chlorin **T3PyCh** results in significant changes in the electronic spectra of their solutions. In particular, the Soret band decreases significantly and broadens with the formation of the "shoulder", with a simultaneous increase in the intensity and a slight bathochromic shift of the last band in the Q-region. Changes in the spectrum of bacteriochlorin **T3PyBCh** solution are even more noticeable: intensive absorption bands appear in the short-wave region at 355 nm and 378 nm and in the long-wave region at 745 nm.

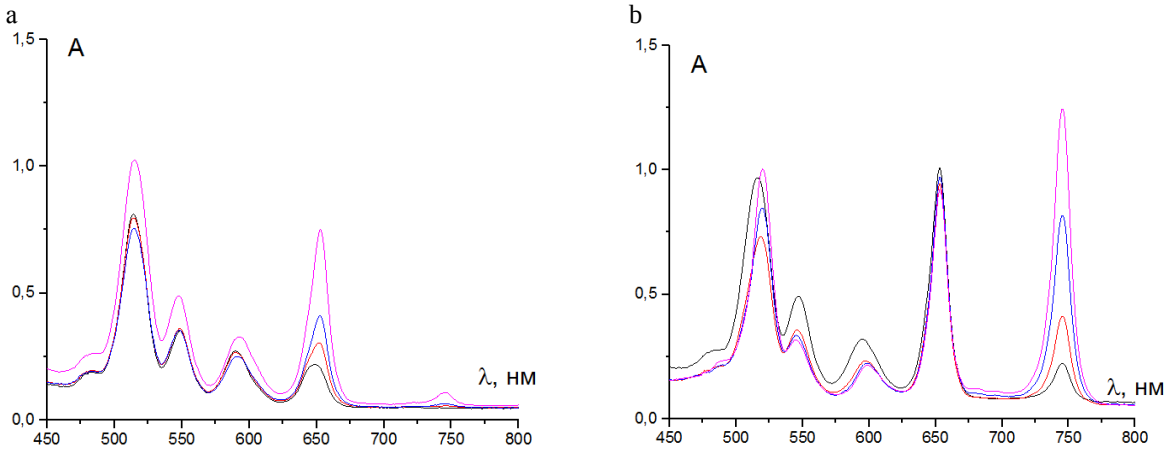

Figure 20. Electronic absorption spectra (DCM) of the reaction mixture during the first 6 h (a) and the last 6 h (b) of the reaction.

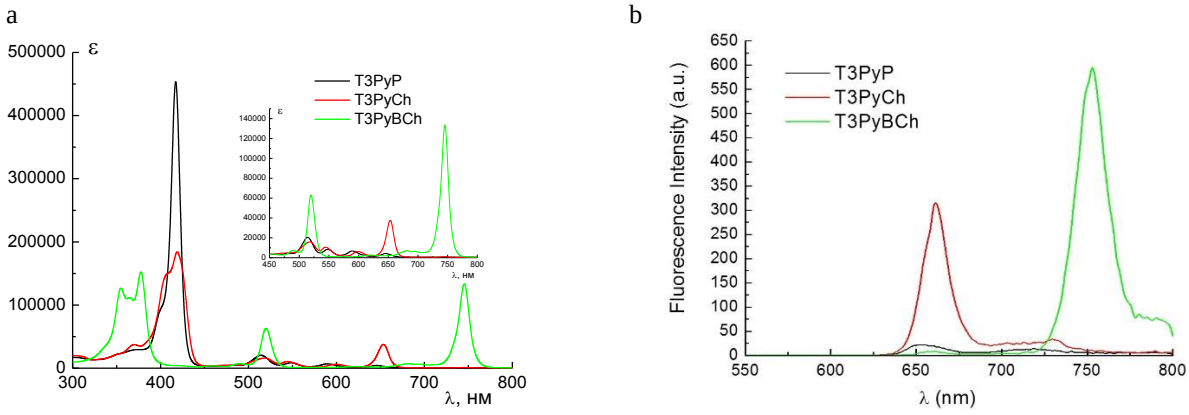

Figure 21. UV-Vis absorbance spectra (DCM) (a) and emission spectra (DCM) (b) at 520 nm of **T3PyP**, **T3PyCh** and **T3PyBCh.**

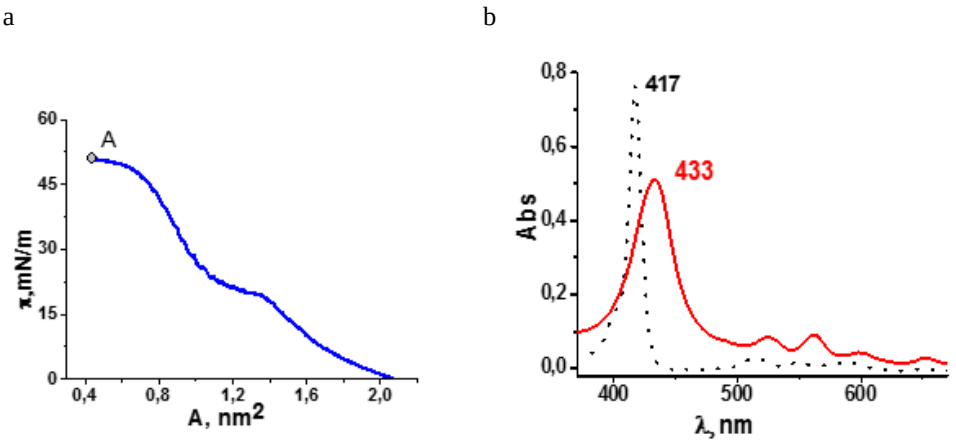

Figure 22. (a) The π-A isotherm of tetra(pyridine-3-yl)porphine. Point A shows the conditions of layer transfer onto the solid support. (b) UV-Vis absorption spectra of solution in dichloromethane (C=1·10^{-6} M, dotted line) and of the LS film formed from nanostructured layers (solid line).

As part of the search for a solution to the problem of formation of nanoarchitectures of bioactive porphyrin-type compounds, studies have begun on the possibility of forming nanoparticles of these compounds. The compression isotherm for the layer formed at c_{edge}=51% is presented in Figure 22a. The structure of the layers was analyzed within the framework of the author's model of a nanostructured M-monolayer using the quantitative method of isotherm analysis [342]. It was found that **T3PyP** forms nanostructured layers at the water-air interface. The conditions for the formation and the main characteristics of monomolecular layers obtained at small values of the ISCD are determined. In particular, at low surface pressures (less than 1 mN/m) the number of molecules (n) of **T3PyP** in the M-nanoaggregate is 270-330; aggregate diameter (D_{aggr}) is 2-28 nm; the area per molecule in the nanoaggreagate (A_{mol}) is 1.1 nm^2; the pressure range of existence of a stable monolayer is 0.1-0.5 mN/m; water content in the nanoaggregate (when molecules are arranged vertically in stacks) 25%; the degree of surface coverage by aggregates at the beginning of the region of stable monolayer is 83 %.

Three-dimensional tetralayer nanoaggregates formed on the water surface were transferred to a quartz plate by the Langmuir-Schaefer method at the surface pressure of 50 mN/m (point A in Figure 22a). The positions of the main bands in the absorption spectrum of **T3PyP** film (Figure 22b, solid line) are shifted batochromically compared to the spectrum of the monomer solution (dash-and-dot line in Figure 22b): the Soret band by 16 nm and Q bands by 8-12 nm. The half-width of the Soret band in the film spectrum is twice as large as in the monomer solution. The ratio of intensities of Q bands has also changed. These results indicate intermolecular interactions stronger than the van der Waals ones in the nanostructures formed within the films of tetra(pyridine-3-yl)porphine.

Thus, 5,10,15,20-tetra(pyridine-3-yl)chlorin (**T3PyCh**) and 5,10,15,20-tetra(pyridine-3-yl) bacteriochlorin (**T3PyBCh**), the products of 5,10,15,20-tetra(pyridine-3-yl)porphine reduction, were synthesized and fully characterized, and their photophysical properties were studied. The first stable **T3PyP** nanostructures, whose properties differ from properties of original substance were obtained by its controlled self-organization within layers at the air-water interface and films on solid supports.

8. Derivatives of *meso*-Formylporphyrins: Synthesis and Application as Components of Optical Sensors and Photosensitizers

The production of porphyrin materials with target specific structures is based on various methodologies, differing in that natural or synthetic porphyrins are used. Synthetic porphyrins such as *β*-octaethylporphyrin (OEP) and *meso*-tetraphenylporphyrin (TPP) are considered as a good alternative to the natural porphyrins due to their availability by simple synthesis. The porphyrin core, which is easily obtained by tetrapyrrole condensation,[357] then needs to be functionalized to impart the required properties to the porphyrin molecule.[358-360] The free *meso*-positions of *β*-octaethylporphyrin and *meso*-arylporphyrins can be functionalized by a variety of methods, among which the formylation is especially prolific.[361] The advantage of this functionalization methodology is based on that the aldehyde group is rich in the possibilities of further transformations leading to the addition of functional fragments. There are reported examples of formylporphyrins utilization in a wide variety of reactions including, but not limited to the Wittig,[362-364] Grignard,[364-366] McMurry,[367] cycloaddition,[368] Knoevenagel[369] reactions and Schiff bases preparation.[370] The products of the formylporphyrins transformations are potential optical sensors[371] and photosensitizers.[46,372,373]

meso-Functionalization of porphyrins by electrophilic formylation of tetrapyrrole macrocycle

Although a formyl group can be inserted into a tetrapyrrole macrocycle by various ways, the “old-fashioned’’ classical aromatic electrophilic substitution reaction, namely the Vilsmeier-Haack formylation reaction stands out, as it allows the formyl group to be inserted into the porphyrin core with simple procedure and affordable reagents (DMF/$POCl_3$ (Scheme 44).[361,374] The Vilsmeier reagent is

an electrophilic agent, the iminium cation, formed by the interaction of $POCl_3$ with DMF. To promote the reaction of an electrophilic Vilsmeier reagent with a nucleophilic porphyrin substrate, the tetrapyrrole aromatic system is activated by the formation of metal complexes in which the porphyrin core has a formal charge of -2, and thus it is enriched with electrons. Porphyrin complexes with Ni(II), Cu(II), Pd(II), Pt(II) resistant to HCl released during the reaction, are usually formylated.[361]

meso-Formylporphyrins formed during the formylation of *β*-substituted porphyrins differ significantly in physical and chemical properties from *β*-formylporphyrins - products of the formylation of *β*-unsubstituted porphyrins.[374] This is explained by the fact that the aldehyde group in *β*-formyl derivatives is conjugated with the tetrapyrrole macrocycle and exhibits all the properties of arylaldehydes, while the aldehyde group in *meso*-formylporphyrin is largely out of conjugation with the macrocycle due to steric hindrances caused by neighboring pyrrole substituents.[361] There is an additional wide long-wavelength band in the region of 650-670 nm in the UV-Vis spectra of *meso*-formylporphyrins.

In the process of formylation with a Vilsmeier reagent, prepared from 3-(dimethylamino)acrolein instead of DMF, the corresponding acrolein derivatives of porphyrins were formed. These derivatives were easily cyclized to form annelated six-membered cycles, when heated in an acidic medium. Smith et al. obtained Ni(II) *meso*-acroleinyl-*β*-octaethylporphyrin **1**, which was cyclized by the action of sulfuric acid at room temperature for two hours into benzochlorin **2** (Scheme 45).[375]

The absorption spectrum of such annulled porphyrins is significantly bathochromically shifted, which makes them promising photosensitizers for photodynamic therapy (PDT).[46,372,373,376] Thus, the product of the double cyclization of *meso*-bis-acroleinyl-*β*-octaethylporphyrin **3** – dibenzobacteriochlorin **5** [375] possesses a strong absorption band in the region of 752 nm, which fully corresponds to the tissue transparency window (Scheme 46).[373,378] The conjugates of the similar benzochlorin with carbohydrates were screened using the galectin-binding-ability assay and exhibited an enhancement of about 300-400-fold compared to lactose. All conjugates were also shown to possess good photosensitizing efficacy with fibrosarcoma tumor cells.[379]

The McMurry reaction

The McMurry reaction, first described in 1974, is a reaction of an organometallic derivative of aldehydes and ketones to form alkenes, which is based on the use of low-valent titanium. Peripherally carbonyl-substituted metal porphyrins were subjected to this reaction with the formation of the variety of bis-porphyrins and their homo- and hetero-bimetallic complexes.[367] Cu(II) *meso*-formyl-*β*-octaethylporphyrin (CuOEP-CHO) was dimerized under the action of $TiCl_3$ and Zn/Cu to form of the copper complex of bisporphyrin **6** bound by the ethene bridge with a 64%yield in the form of a mixture of *cis* and *trans* isomers (Scheme 47).[375]

A similar reductive dimerization reaction was carried out with acrolein derivatives, resulting in the formation of the dimer with a hexatriene bridge. The dimerization of the benzochlorin acrolein derivative **4** led to the dimer **7**, for which a significant bathochromic shift of the Q band up to 706 nm was observed.

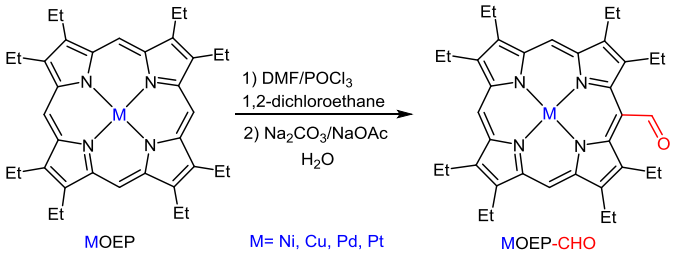

Scheme 44. The Vilsmeier-Haack formylation reaction.

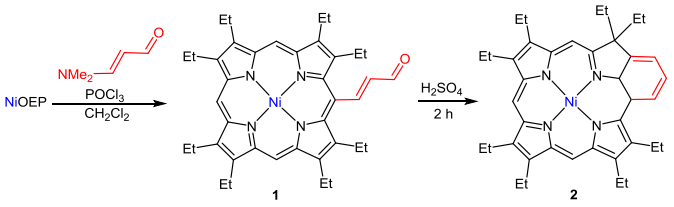

Scheme 45. Transformation of Ni(II) *β*-octaethylporphyrin (NiOEP) into Ni(II) benzochlorin **2**.

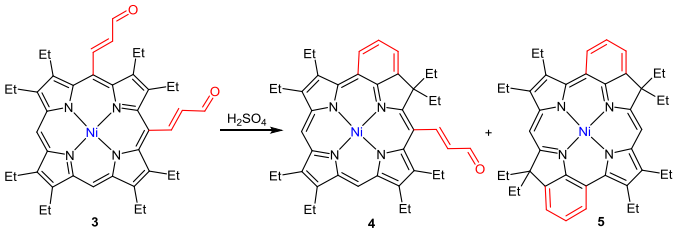

Scheme 46. Preparation of dibenzobacteriochlorin.

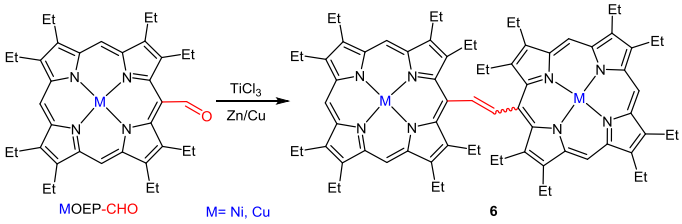

Scheme 47. McMurry reaction of Ni(II) and Cu(II) *meso*-formylporphyrins.[375]

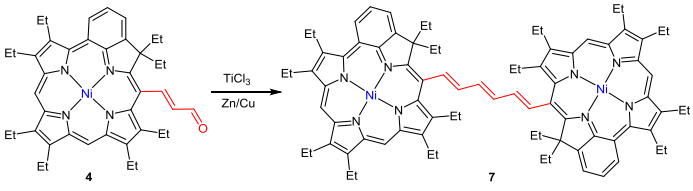

Scheme 48. McMurry reaction of Ni(II) *meso*-acroleinylbenzochlorin.

Grignard and Wittig reactions

Johnson and Arnold[366] performed the Grignard reaction between Ni(II) *meso*-formyl-*β*-octaethylporphyrin (NiOEP-CHO) and MeMgI, obtaining, as expected, Ni(II) 5-(1-hydroxyethyl)-*β*-octaethylporphyrin **8**, by eliminating water from which Ni(II) 5-vinyl-*β*-octaethylporphyrin **9** was obtained (Scheme 49). Smith et al. carried out a similar reaction with a free base and a zinc complex of *meso*-formyl-*β*-octaethylporphyrin, which resulted in 15-alkylated products (**10**), and the formyl group remained intact (Scheme 50). A regioselective attack of the C-nucleophile to the 15-carbon of the macrocycle of Zn(II) 5-formyl-*β*-octaethylporphyrin was also observed in the case of the methyllithium reaction, while with the free base *β*-octaethylporphyrin, a product of the attack to the carbonyl group 5-(l-hydroxyethyl)-*β*-octaethylporphyrin was obtained. The Wittig reaction is more reliable in this regard, with the help of which the *meso*-formyl group of porphyrins is easily transformed into a *meso*-vinyl (Scheme 49), 2-(ethoxycarbonyl)ethenyl, 2-cyanoethenyl, and others.[361,364]

The *meso*-vinyl group can further be functionalized with the conjugation extension. The direct C-H borylation of the *meso*-vinyl group in **9** was performed with Cu(II) complex as a catalyst, yielding the *meso*-(2-pinacolboronylethenyl)porphyrin **11**, which was shown to act as nucleophilic partner in the Suzuki cross-coupling leading to porphyrin derivatives with an extended π-conjugation through the carbon-carbon double bond.[380] The oxidative homocoupling of the borylporphyrin **11** produced the dimer **13** (Scheme 51).[381] Thus, this strategy of the *meso*-formyl group transformations allows to attach various aromatic chromophores through the ethene and butadiene bridges. The products of couplings possess bathochromic shift of absorption bands.

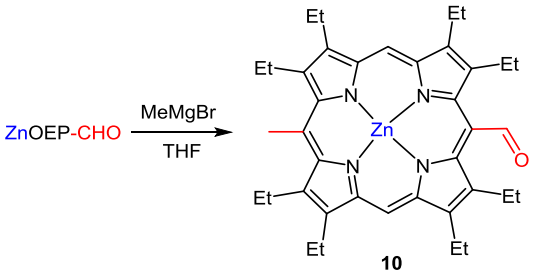

Scheme 50. The Grignard reaction of Zn(II) *meso*-formyl-*β*-octaethylporphyrin.

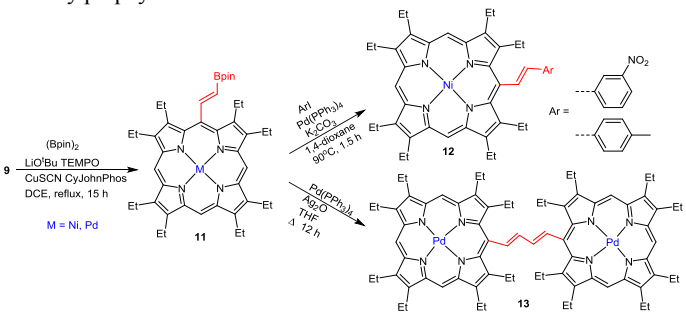

Scheme 51. The borylation of the vinyl-porphyrin with the subsequent coupling reactions.

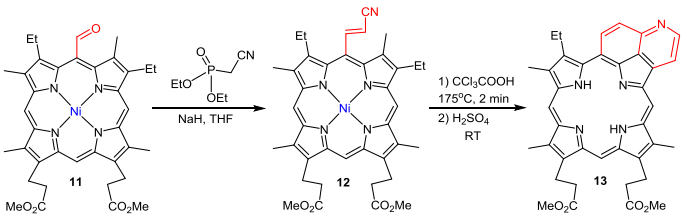

Scheme 52. Preparation of an exocyclic derivative of the dimethyl mesoporphyrin IX.

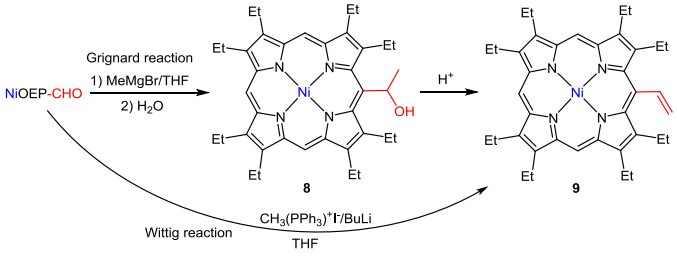

Scheme 49. The Grignard and Wittig reaction of Ni(II) *meso*-formyl-*β*-octaethylporphyrin.

Lugtenburg et al. obtained a 2-cyanoethenyl derivative **12** from the dimethyl *meso*-formyl-mesoporphyrin IX (**11**), which was then cyclized when heated in an acidic medium to a quinoline-annelated product **13** (Scheme 52).[382] The product **13** strongly absorbed light at 685 nm and it was tested as a photosensitizer in the PDT of the tumor cells of the ovary of the Chinese hamster (Cricetulus griseus), providing a good antitumor activity.

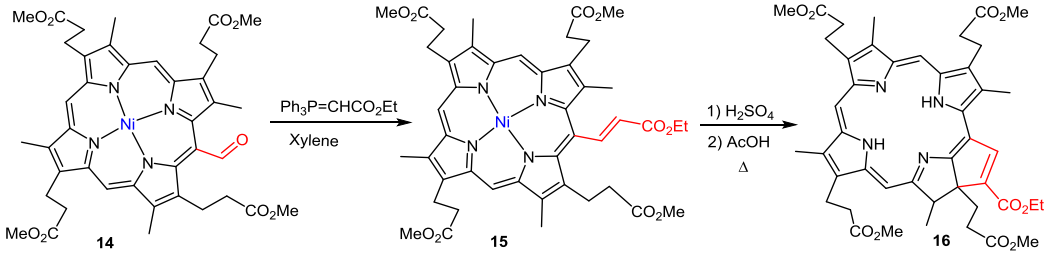

Scheme 53. Preparation of copropurpurin I from coproporphyrin I.

The formyl group in NiOEP-CHO and Ni(II) tetramethyl ester of *meso*-formyl-coproporphyrin I (**14**) was transformed by Wittig reaction with ethoxycarbonylmethylenetriphenylphosphoran into 2-(ethoxycarbonyl)ethenyl group.[383] After demetallation in sulfuric acid, the obtained products were heated for 24 hours in glacial acetic acid in an argon atmosphere, causing the cyclization with the formation of etiopurpurin I and copropurpurin I (**16**), respectively (Scheme 53).

The authors of the work conducted a study on rats with the bladder cancer induced. The obtained etiopurpurin I and tetramethyl copropurpurin I photosensitizers were emulsified and injected intravenously to the rats. The PDT of the cancer cells proceeded efficiently with both compounds. However, it was noted that the copropurpurin I has a lower cytotoxic effect, and selective accumulation of etiopurpurin I in tumor cells was also observed.

The Knoevenagel reactions

The Knoevenagel reaction, like the Wittig reaction, is used to transform formylporphyrins into the corresponding derivatives of acrylic acid. *Meso*-formyl-triarylporphyrin derivatives were usually synthesized under standard conditions of basic catalysis. The *meso*-cyanoacrylate derivative of Zn(II) *meso*-formyl-tri(*p*-tolyl)porphyrin was obtained by boiling in piperidine with methanol for 16 hrs.[384] *meso*-Formyl-diarylporphyrin reacted with nitromethane, dimethylmalonate and malononitrile in a mixture of piperidine, acetic acid and toluene.[385] The product of the reaction of *meso*-formyldiarylporphyrin with malononitrile containing *meso*-dicyanovinyl group was shown to act as a fluorescence ‘‘turn-on’’ cyanide probe.[386] *meso*-Nitroethylene derivative was utilized as fluorescence turn-on probes for biothiols as it exhibited fast fluorescence enhancement and high selectivity towards thiols based on the Michael addition mechanism.[385] It was also successfully applied to fluorescent cell imaging in the NIR wavelength range.

meso-Formyl-*β*-octaethylporphyrin (NiOEP-CHO) is less reactive and also easily degraded under basic conditions, therefore it requires a special approach. Activation of the carbonyl group with $TiCl_4$ in pyridine promoted the reaction.[369] Using the Knoevenagel reaction with NiOEP-CHO, heterocyclic derivatives of porphyrins were obtained.[387] First, upon condensation with malonic ester, the corresponding malonate derivative (**17**) was obtained, which reacted with hydrazine in the presence of sodium ethoxide, resulting in formation of pyrazolidine-3,5-dione linked to the Ni(II) *β*-octaethylporphyrin with ethane bridge (**18**) (Scheme 54).

Direct synthesis of the porphyrin conjugates with thiohydantoin, and thiobarbituric acid (Scheme 55) was also performed via the Knoevenagel reaction.

The UV-Vis spectra of the heterocyclic conjugates contain new bands arose from the interaction of the conjugated chromophores as well as bathochromically shifted original absorption bands. Particularly dramatic changes were observed in the UV-Vis spectrum of the thiobarbituric acid conjugate, which exhibited substantial increase of absorption in green and red spectral region. Such combinations of porphyrin dyes with such heterocyclic chromophores and sensing fragments can be of interest as potential promising photosensitizers and sensor dyes.

Synthesis and properties of Schiff bases derivatives of meso-formylporphyrins

Synthesis of Schiff bases from formylporphyrins is a promising direction of functionalization, since a huge number of various tetrapyrrole compounds with desired properties can be obtained from azomethine derivatives, including photosensitizers and sensor dyes with the required photophysical characteristics.[388] There are two main approaches to the synthesis of Schiff bases: 1) interaction of formylporphyrins with amines; 2) interaction of amines with the so called "phosphorus complex" formed during the Vilsmeier-Haack reaction.[370] The classical reaction of the preparation of Schiff bases by the reaction of amines with the aldehyde group of porphyrin was first investigated in the synthesis of oximes, which were formed within a few hours from the *meso*-formylporphyrin with hydroxylamine hydrochloride in boiling pyridine.[366,389] Oximes are of interest as precursors for the production of cyanoporphyrins,[390] which can be consequently transformed to carboxyl derivatives. Intramolecular cyclizations of *meso*-substituted porphyrins often leads to porphyrinoids with fused exocycles like purpurins and benzochlorins. Treatment of nickel complex of *meso*-oxime **21** with lead tetraacetate (1.2 eq.) in methylene chloride in the presence of an excess of triethylamine at room temperature for 5 min gives the product **22** with fused 1,2-oxazin ring with an overall yield of 77%.[391] When a solution of Zn(II) complex of *meso*-oxime **23** was stirred in methylene chloride with a small amount of water, after a few hours the starting complex was transformed to hydroxy-1,2-oxazinochlorin **24** (Scheme 56).[392] Oxidative hydroxylation of the intermediate 1,2-oxazinochlorin possibly occurred via a peroxide mechanism leading to the stable hydroxychlorin. Ni(II) complex of the oxime vinylog *meso*-(*trans*-formylvinyl)-*β*-octaethylporphyrin **25** underwent similar intramolecular cyclization producing a condensed eight-membered exocycle **26** (Scheme 57).[393] Such annulated products are of interest as photosensitizers due to their strong absorption in red region. The electronic absorption spectrum of 1,2-oxazocine fused porphyrinoids **26** shows a significant bathochromic shift by 50 nm of all absorption bands compared to the spectra of the corresponding chlorins.

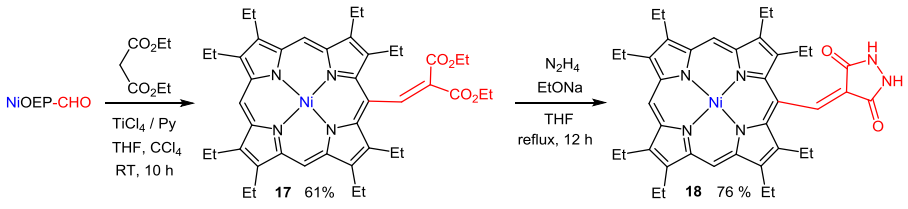

Scheme 54. Synthesis of the conjugate of Ni(II) *β*-octaethylporphyrin with pyrazolidine-3,5-dione.

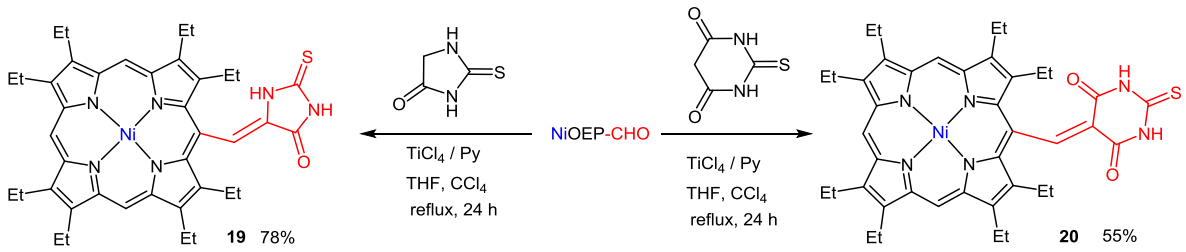

Scheme 55. Synthesis of the conjugate of Ni(II) *β*-octaethylporphyrin with thiohydantoin and thiobarbituric acid.

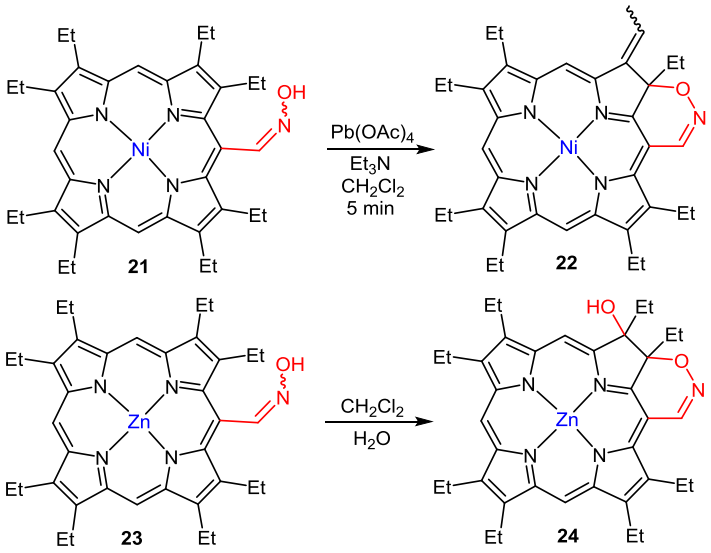

Scheme 56. Synthesis of the porphyrinoids with fused 1,2-oxazin ring via oxime cyclization.

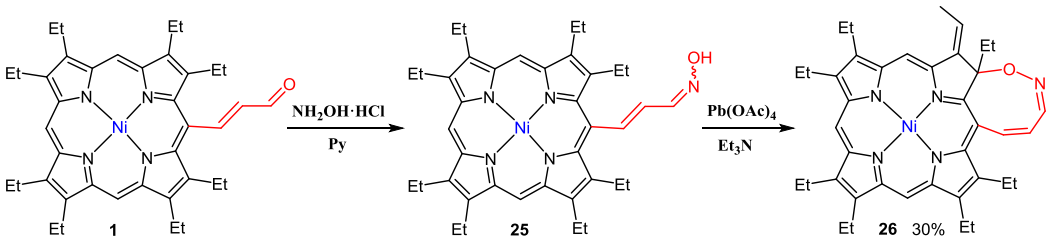

Scheme 57. Synthesis of the porphyrinoid with fused 1,2-oxazocine ring **26** via vinylogous oxime cyclization.

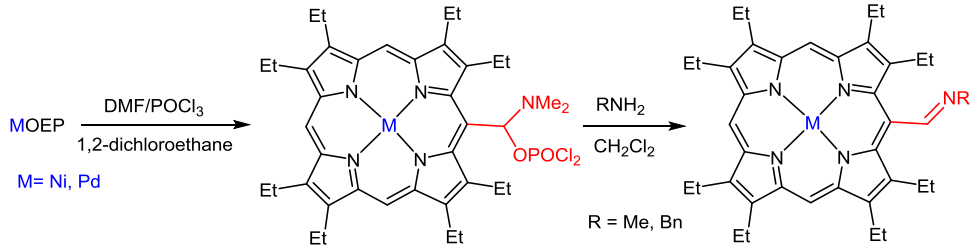

Scheme 58. Preparation of azomethine derivatives of octaethylporphyrin from the phosphorus complex.

Despite the large number of examples of the utilization of the interaction of formylporphyrins with an amino group for preparation of Schiff bases, the reaction of the "phosphorus complex" with amines has become more widespread. Ponomarev et al. was the first to isolate phosphorus complexes of various porphyrins.[370] Azomethine deriva-

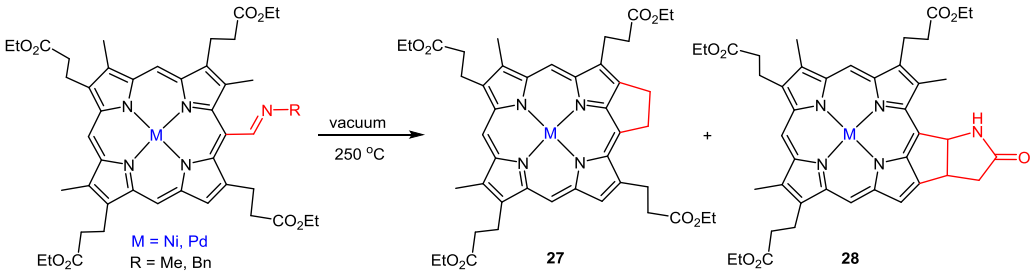

Scheme 59. Preparation of cyclopentane-annelated derivatives.

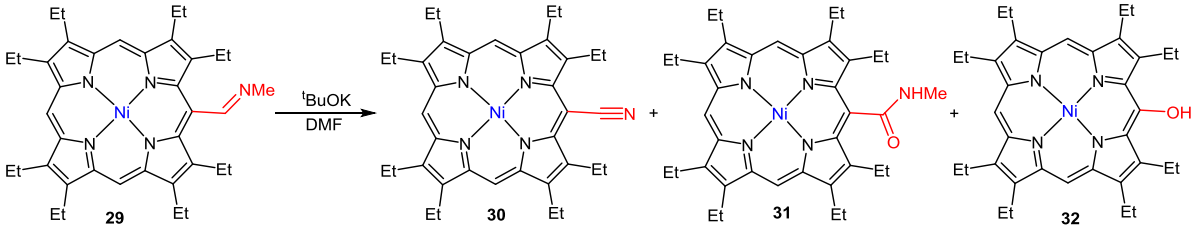

Scheme 60. Treatment of the N-methylimine derivative of the Ni(II) β-octaethylporphyrin **(29)** with a strong base.

tives of nickel and palladium complexes of various porphyrinoids including *β*-octaethylporphyrin, tetraalkyl esters of coproporphyrins I and II, mesoporphyrin IX and mesochlorin e6 were obtained by direct interaction of "phosphorus complexes" with amines (Scheme 58).[388,389,395]

The metal complexes of azomethine derivatives, obtained by this way, were investigated as potential photosensitizers for photodynamic therapy (PDT).[388] A number of Schiff bases, in particular, Pt(II) and Pd(II) complexes of *β*-octaethylporphyrin and tetramethyl coproporphyrin I, were investigated as sensor dyes for determination of oxygen concentration and acidity.[396,397] An optochemical probe for cellular diagnostics using phosphorescent determination of oxygen and pH in living cells was developed based on the Pt(II) complex of *meso*-(N-methylimino)-*β*-octaethylporphyrin.[398]

Upon studying the thermolysis of azomethine derivatives of porphyrins, it was found that the cyclization occurs with the formation of cyclopentane-fused derivatives (Scheme 59).[399-401] During thermolysis of metal complexes of *meso*-imines of tetraalkyl ester of coproporphyrin I the formation of both cyclopentane and cyclopentane-lactam bicycle was observed.[395]

Treatment the Ni(II) complexes of the azomethine derivatives of *β*-octaethylporphyrin with t-BuOK led to the formation of the corresponding *meso*-nitrile (**30**), *meso*-amide (**31**) and *meso*-hydroxy (**32**) derivatives (Scheme 60). The latter was demetalated with sulfuric acid (Scheme 61), resulting in the phlorin **33** with strong light absorption in the region of 700 nm which could be useful for the photosensitizing applications.[395]

meso-Hydrazone derivatives were obtained by reaction of *meso*-formyl derivatives of *β*-octaethylporphyrin and coproporphyrin I with hydrazine and N-substituted hydrazines catalyzed by trifluoroacetic acid (Scheme 62).[402] Hydrazones **34**, **35** were formed as a mixture of E- and Z-isomers.

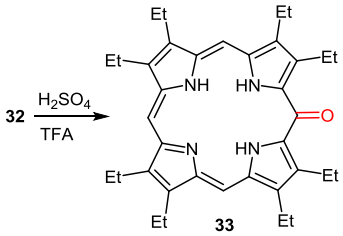

Scheme 61. Demetalation of the Ni complex of *meso*-hydroxy-*β*-octaethylporphyrin (**32**).

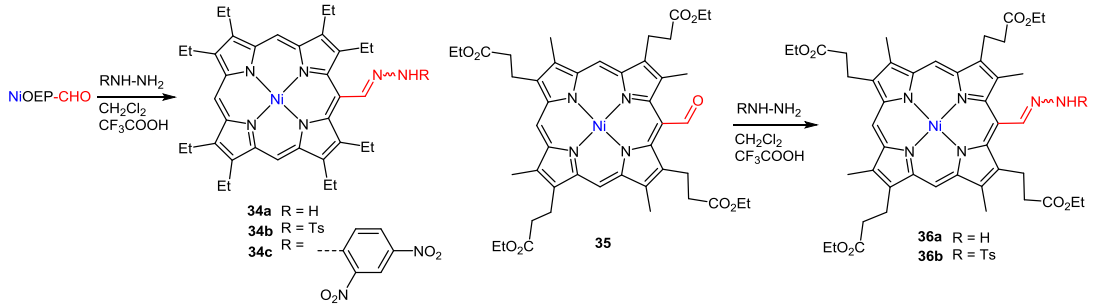

Scheme 62. Synthesis of hydrazones from formyl porphyrins.

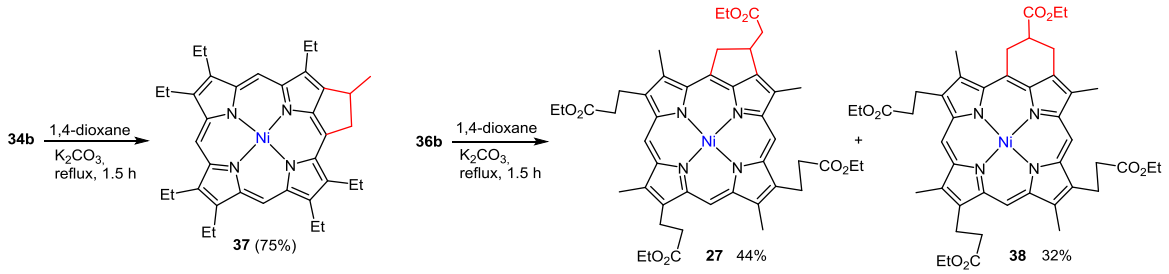

Scheme 63. Preparation of cyclopentane fused porphyrins by thermolysis of *meso*-tosylhydrazones.

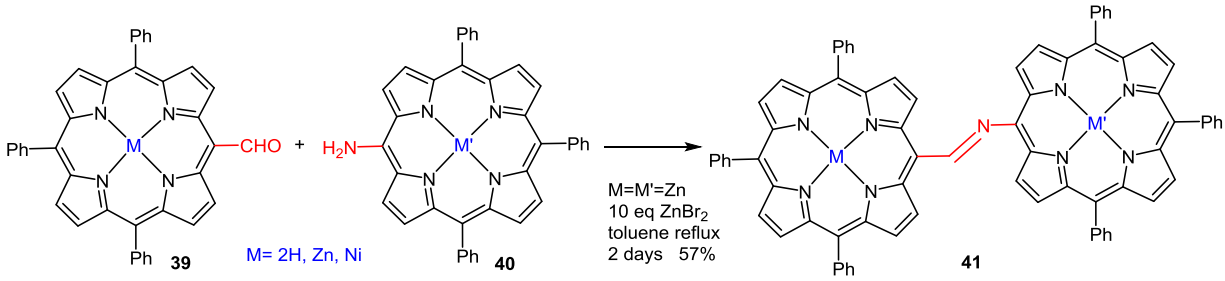

Scheme 64. Synthesis of the porphyrin dyads linked with the imino group.

Thermolysis of N-tosylhydrazones in the presence of a base produced *meso*-carbenes that were cyclized leading to the corresponding cyclopentane fused porphyrinoids *via* intramolecular carbene C–H insertion.[403] The cyclopentane fused products **27**, **37** obtained were the same as in the thermolysis of azomethines, however, the second product in the N-tosylhydrazone of the coproporphyrin I thermolysis was 6-member ring fused **38** instead of bicyclic lactam **28**,[395] and yields of the products in the carbene based reaction were higher (Scheme 63).

By the interaction of metal complexes of *meso*-formyltriarylporphyrin **39** and *meso*-aminotriarylporphyrin **40**, dyads **41**, linked *via* an imino group, were obtained (Scheme 64).[404] However, due to the low activity of the *meso*-amino group and its degradation under sufficiently harsh reaction conditions, yields were low. A satisfactory yield of 57% was achieved for the zinc complex by catalysis with a tenfold excess of $ZnBr_2$. Such dyads can be used in the two-photon excited PDT, which provides a highly targeted treatment.[405]

Unsubstituted *meso*-hydrazones of *β*-octaethylporphyrin and *β*-octaethylchlorin were used in the preparation of azines **42** by reaction with various aldehydes (Scheme 65).[406]

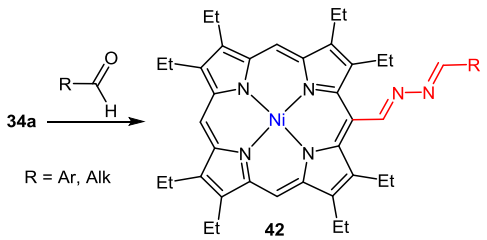

Scheme 65. Preparation of azines from the Ni(II) complex of the *meso*-hydrazone of *β*-octaethylporphyrin.

In using chlorins containing an aldehyde group (methyl pyropheophorbide-a (PPPa) and methyl pyropheophorbide-d (PPPd)) as aldehyde components in the reaction with Ni(II) *meso*-hydrazone of *β*-octaethylporphyrin **34a**, porphyrinoid dyads **43**, **44** were obtained (Scheme 66).[406] In the excited state of the dyads the energy was efficiently transferred from the OEP moiety to the pyropheophorbide chromophore.

One-pot formylation, hydrazone and azine formation was realized for the *meso*-amino substituted octaethylporphyrin.[407] Amino-group was preliminarily protected with trifluoroacyl group. It was found that under the conditions of formylation of *meso*-(trifluoroacetamido)-*β*-octaethylporphyrin (**45**), the amide fragment was oxidized to form hydroxamic acid **49** (Scheme 67). Combination of trifluoroacetamide and arylazine groups in the products **47**-**49** led to the strongly increased absorption near 500 nm and considerably red-shifted Q-bands up to 650 nm.

Further expansion of the π-electron system of the azine functionalized disubstituted *β*-octaethylporphyrin was achieved through the conjugation with another tetrapyrrole. Interaction of the hydrazone **46a** with methyl pyropheophorbide-*d* (PPPd), containing formyl group at *β*-position of the tetrapyrrole ring resulted in formation of the azine bridged porphyrin-chlorin conjugate **50** (Scheme 68). The resulting compound features the substantial growth of the Q-band intensity as well as red-shifting Soret band. The azine bridged dyad could be of interest as potential photosensitizers, sensor dyes and biologically active compounds.

Porphyrins with meso-fused heterocycles

Interaction of the aldehyde group with 1,2-dithiol is often used to protect it by the formation of the 1,3-dithiolane. A family of push–pull quinoidal porphyrin was obtained from a *meso*-formyl porphyrin through the at-

tachment of 1,3-dithiolane (benzo-1,3-dithiolane) and malononitrile fragments at the opposite meso-positions of the 5,15-diarylporphyrin (Scheme 69).[408]

Porphyrins with *meso*-fused 2-imidazolyl heterocycles 53 were obtained from the *meso*-formylporphyrins as carbonyl components in the heterocyclic condensation. 5-formyl-10,20-diarylporphyrins as well as their Cu(II) complexes reacted with phenanthrene- or phenanthroline-5,6-dione and ammonium acetate leading to the corresponding imidazolyl-porphyrin conjugates with high yields (Scheme 70).[409] Ruthenium complex of the free base porphyrin-imidazo[4,5-f]phenanthroline conjugate **56** showed good binding ability to DNA, which facilitated DNA photocleavage.[410] Thus, it could be a potential photosensitizer for PDT.

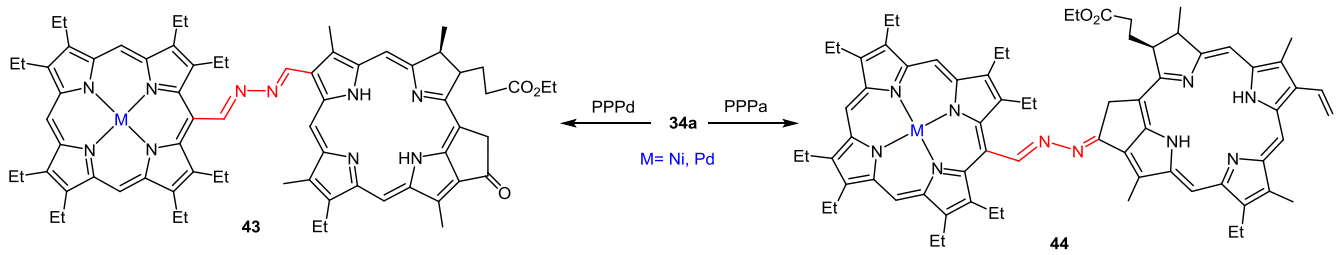

Scheme 66. Synthesis of porphyrin-chlorin dyads linked by the azine bridge.

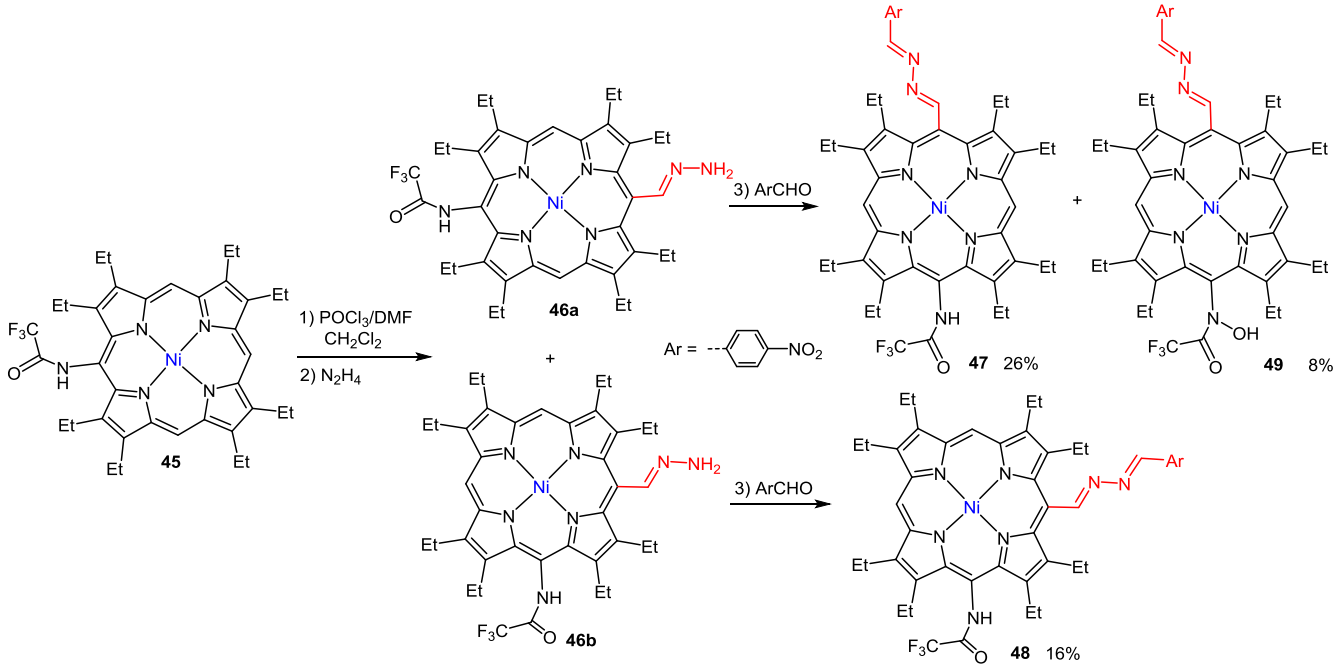

Scheme 67. Synthesis of trifluoroacetamide and arylazine oppositely substituted *β*-octaethylporphyrin.

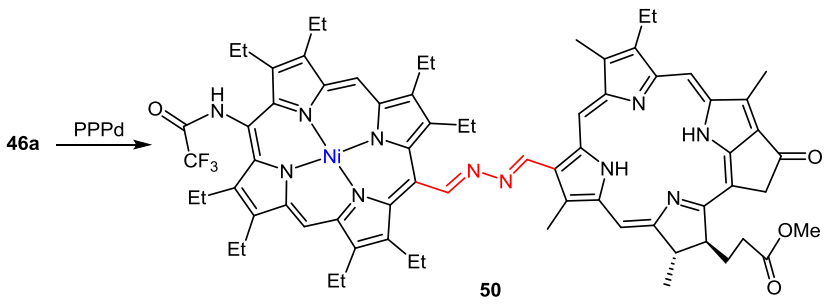

Scheme 68. Synthesis of the azine bridged dyad **50**.

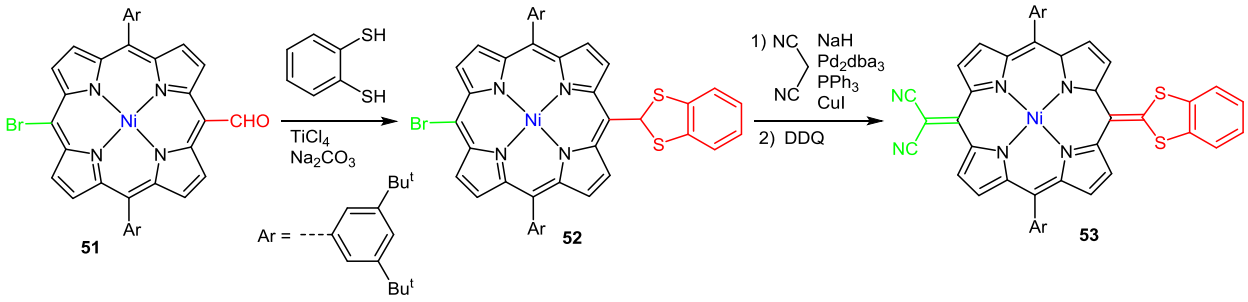

Scheme 69. Synthesis of the porphyrins with *meso*-fused 2-imidazolyl heterocycles.

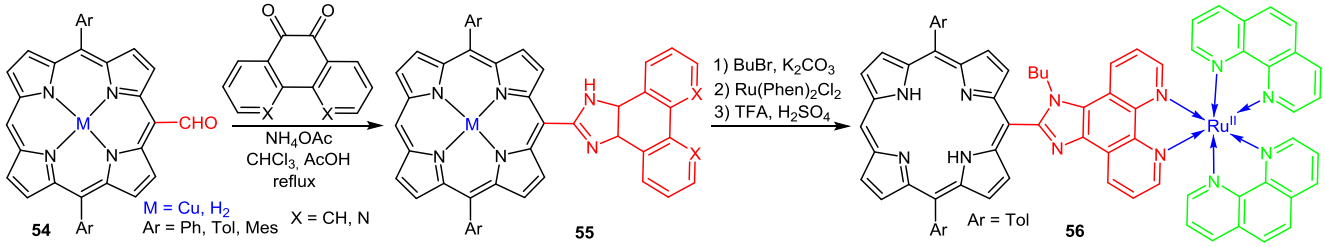

Scheme 70. Synthesis of the porphyrins with *meso*-fused 2-imidazolyl heterocycles.

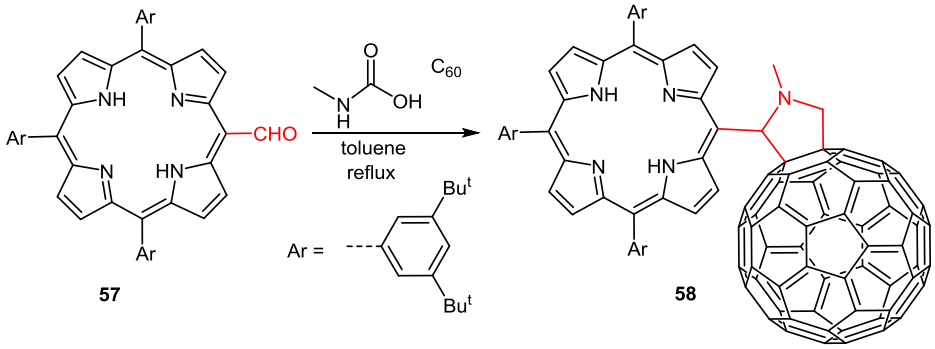

Scheme 71. Synthesis of the *meso*-linked porphyrin – fullerene conjugate **58**.

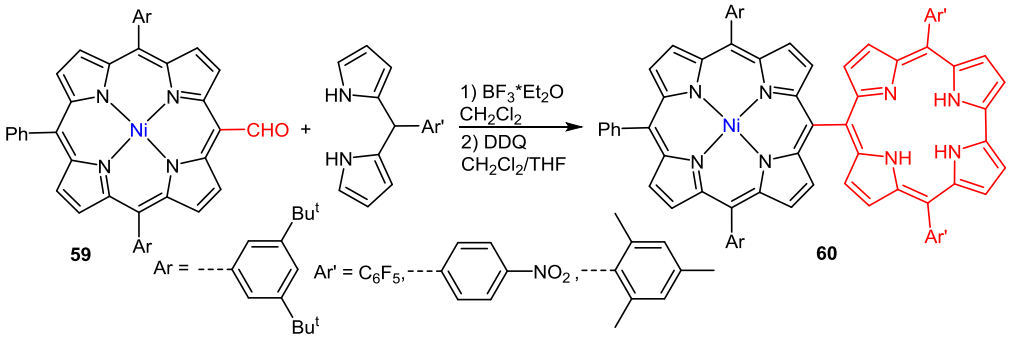

Scheme 72. Synthesis of the porphyrin-corrole dyads **60**.

meso-Formylporphyrins can form azomethine ylide after interaction with N-methylglycine. 1,3-dipolar cycloaddition of the intermediate azomethine ylide to the double bond leads to the porphyrins with *meso*-fused heterocycles. The porphyrin – fullerene conjugate **58** was obtained by this way from *meso*-formyltriarylporphyrin **57**, N-methylglycine and C60 fullerene (Scheme 71).[368] The excitation of the dyad led to the extremely fast formation of the exci-

plex due to the strong interaction between the porphyrin and C60 moieties placed at close proximity.

Directly linked porphyrin-corrole dyads **60** were obtained by the condensation of the *meso*-formyltriarylporphyrin **59** and dipyrromethane (Scheme 72).[411] The strong exciton coupling between porphyrin and corrole and reversible energy transfer were shown to exist in the dyads. When 5,15-bisformylporphyrin was used in the condensation, the corrole–porphyrin–corrole triad was formed.[412] Similar directly *meso*-*meso* linked porphyrin dimers and oligomers were obtained using condensation of *meso*-formylated porphyrins with pyrrole.[413] Such porphyrin dimers and oligomers were shown to act as prospective photosensitizers.[414]

To sum up, *meso*-functionalization of porphyrins with formyl group provides powerful tool for development of the diverse porphyrin derivatives possessing valuable properties. In particular, promising photosensitizers with strong red-shifted absorption bands, including NIR bands, were obtained from the *meso*-formyl porphyrins *via* formation of the annulated cycles such as benzochlorins and dibenzobacteriochlorins. *meso*-Imino derivatives were applied as sensor dyes in the multi-modal, multi-analyte optochemical sensing platform for cell diagnostics. Easily formed with the help of the formyl group porphyrin conjugates with heterocycles can be used as biologically active compounds and in sensing applications. Imino- and azino- bridges represent two alternatives for bonding porphyrins into dyads, utilizing various pathways for energy transfer between the chromophores. Currently, the post-derivatization of the *meso*-formylporphyrins is under intense development.

9. Interaction of Multiporphyrin Complexes and Nanoassemblies with Molecular Oxygen in Solutions: Mechanisms and Some Specific Effects

Together with the formation of supramolecular complexes of tetrapyrrole photosensitizers, which have already found application in biomedicine,[72-76] another approach to the formation of possible platforms of tetrapyrrole photosensitizers of the third generation can be implemented by combining tetrapyrroles of various structures with functional nanocarriers of organic or inorganic nature. Both approaches are promising for increasing the stability of PSs and their targeted delivery to the tumor.

From the photophysical background it should be noted that in both approaches, the first necessary step is connected with the quantitative experimental analysis of the influence of molecular oxygen O_2 on deactivation of excited singlet and triplet states of the given PS which is included in multimolecular complex or attached to nanocarrier. Keeping in mind this idea, within German-Belarus scientific collaboration such comparative study was carried out for various multicomponent nanoassemblies containing tetrapyrrolic macrocycles.[74,75,79,80,88] Herein, we aim to review main results of this study and provide a comprehensive understanding of O_2 interaction with multicomponent species in liquid solutions at ambient temperature. At the first step, excited S_1- and T_1-states quenching by molecular oxygen was studied for a set of Zn-porphyrin and Zn-chlorin chemical dimers in which π-conjugated macrocycles are covalently linked via spacers of various nature and flexibility ($-CH_2-CH_2-$ bond or phenyl ring in mesoposition, cyclodimers) in non-polar toluene with and without pyridine admixture. At the second step, self-organized multiporphyrin triads and pentads were formed via non-covalent binding interactions of Zn-porphyrin or Zn-chlorin chemical dimers with di- and tetrapyridyl containing porphyrin or chlorin extra-ligands, and the main peculiarities of the interaction of $O_2$with the triads and pentads of various and controlled geometry were evaluated. Then, we consider perspectives of semiconductor quantum dots (QD) as well as their nanoassemblies with porphyrin molecules as possible PDT photosensitizers, and provide quantitative comparative results on efficiencies of the singlet oxygen generation by QD-porphyrin nanoassemblies. Finally, as far as in many experiments the intensity of the singlet oxygen ($^1O_2$ or $^1\Delta_g$) emission at λ_{max} = 1.27 μ is measured in various solvents, some specific reasons (described in literature) are discussed which may change the rate constant of the radiative transition $^1\Delta_g \rightarrow {}^3\Sigma^-_g$ in $^1O_2$ molecule.

All objects under study (including monomeric porphyrins, chemical dimers, triads, pentads as well as QD-porphyrin nanoassemblies) were synthesized, prepared and characterized according to methods comprehensively described in our earlier publications,[74,75,79,80,88,416 and references herein] the details of experimental setup, steady-state and time-resolved spectral measurements, direct detection of intensity and kinetics for singlet oxygen IR-emission as well as theoretical calculations one may find in these publications also. Below some necessary information in this respect as well as the corresponding structures will be presented directly in appropriate places of the text.

Interaction of Zn-porphyrin and Zn-chlorin chemical dimers with molecular oxygen

Typically, in degassed liquid solutions for monomeric Zn-porphyrins and Zn-chlorins as well as for chemical dimers on their basis the deactivation of excited S_1-states takes place within τ_S^0=1.2-1.6 ns,[416,417] and, thus these excited states are hardly influenced by the presence of oxygen at normal atmospheric pressure at 293 K (see data in Table 3). It is not the case with long-lived excited T_1-states, and correspondingly, Table 3 collects experimental τ_T values and bimolecular rate constants k_T showing the specificity of T_1-states quenching by molecular oxygen for the studied dimers and their complexes with pyridine.

For all dimers collected in Table 3, it was shown[416,417] that at 77-293 K fluorescence and intersystem crossing quantum yields as well as the rate constants of the internal conversion S_1~>S_0 are hardly dependent on the interactions between coupled macrocycles. In addition, it follows from Table 3 that coordination of pyridine to the central Zn ion in the dimers moiety has not a substantial effect on fluorescence quantum yields and lifetimes. It means that additional non-radiative deactivation processes of S_1-states are not enhanced in pyridinated dimers. In contrast, there are some noticeable features for triplet states for pyridinated dimers: (i) phosphorescence lifetimes and quantum yields exhibit a decrease by 1.5 - 2.5 times compared to uncomplexed dimers;[416,417] (ii) an additional T_1-state quenching is found for pyridinated complexes which diminishes upon the tri-

plet level lowering for a set of the investigated dimers, $(ZnOEP)_2Ph \rightarrow$ Zn-3^1,3^1-cyclodimer $\rightarrow (ZnOEP)_2 \rightarrow$ $\rightarrow (ZnHTPP)_2 \rightarrow (ZnOEChl)_2$. In the result, the basic conclusion is as follows. The dimers $(ZnOEP)_2Ph$, Zn-3^1,3^1-cyclodimer and $(ZnOEP)_2$ with high-energy triplet states and relatively long phosphorescence decays τ_{Ph} are sensitive to the coordination with pyridine leading to enhancing non-radiative deactivation of T_1-states. This quenching is attributed to several reasons: accepting role of the extra-ligand vibrations, the enhanced spin-orbit coupling due to the singlet σ,π^* states energy lowering and the out-of-plane distortion of porphyrin macrocycle. However, for the dimers $(ZnHTPP)_2$ and $(ZnOEChl)_2$ with low-energy triplet states and relatively short lifetimes τ_{Ph} the rate constants of intrinsic non-radiative deactivation processes $T_1 \sim> S_0$ (due to Frank-Condon factor presumably) are so large that additional channels of the non-radiative deactivation of T_1-states caused by the extra-ligation seem in comparison not very effective.

According to[417,418] the process of T_1-states quenching by O_2 is realized via non-radiative transitions between electronic states in an intermediate short-living weak collision complex formed as a result of a diffusional contact of a given excited organic molecule with an oxygen molecule. From this point of view, the quenching of T_1-state of the organic molecule ($^3M_1$) may take place via different ways depending on the spin state of the collision complex:

$$^3M_1 + {}^3O_2 \underset{k_{dis}}{\overset{g_1 k_{diff}}{\rightleftarrows}} {}^1\left[{}^3M_1 \ldots {}^3O_2\right] \overset{k_\Delta}{\sim\!\sim>} {}^1\left[{}^1M_0 \ldots {}^1O_2\left({}^1\Delta_g\right)\right] \xrightarrow{k_{dis}} {}^1M_0 + {}^1\Delta_g\,, \qquad \text{(I)}$$

$$^3M_1 + {}^3O_2 \underset{k_{dis}}{\overset{g_3 k_{diff}}{\rightleftarrows}} {}^3\left[{}^3M_1 \ldots {}^3O_2\right] \overset{k_{TS}}{\sim\!\sim>} {}^3\left[{}^1M_0 \ldots {}^3O_2\right] \xrightarrow{k_{dis}} {}^1M_0 + {}^3O_2\,. \qquad \text{(II)}$$

Table 3. Lifetimes of S_1- and T_1-states and bimolecular rate constants for quenching of excited T_1-states by molecular oxygen O_2 found for monomeric precursors and chemical dimers in toluene (TOL) and toluene+pyridine (TOL+PYR) at 293 K. For clarity, the structures of the compounds under study are presented also, central Zn ions are not shown.

Compound	Structure	Solvent	τ_S, ns	τ_T, ns	k_T, [a] $10^9\,M^{-1}s^{-1}$	$k_T(lig)/k_T$ [b]
ZnOEP-CH_3	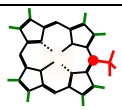	TOL TOL+PYR	1.6 1.45	330 285	1.65 1.95	1.18
$(ZnOEP)_2$	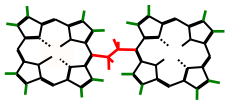	TOL TOL+PYR	1.3 1.2	440 205	1.2 1.9	1.6
ZnOEP-Ph	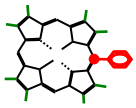	TOL TOL+PYR	1.5 1.4	335 370	1.6 1.5	0.94
$(ZnOEP)_2Ph$	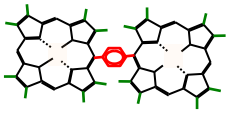	TOL TOL+PYR	1.2 1.1	495 490	1.1 1.1	1.0
ZnHTPP	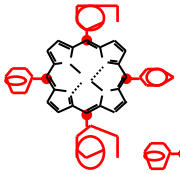	TOL TOL+PYR	1.6 1.5	570 530	1.0 1.05	1.05
$(ZnHTPP)_2$	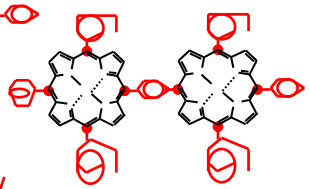	TOL TOL+PYR	1.5 1.4	590 500	0.95 1.05	1.10
ZnOEChl-CH_3	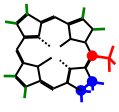	TOL TOL+PYR	1.3 1.25	290 265	1.9 2.1	1.10
$(ZnOEChl)_2$	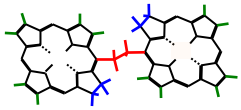	TOL TOL+PYR	1.2 1.2	350 285	1.6 2.0	1.25
ZnOEP-cycle=CH_2	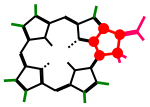	TOL TOL+PYR	2.6 2.5	310 275	1.9 2.0	1.05
Zn-3^1,5^1-cyclodimer	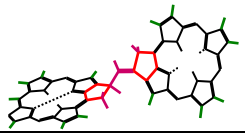	TOL TOL+PYR	2.5 2.5	355 295	1.6 1.9	1.2

[a] The corresponding values of bimolecular rate constants of the excited S_1-and T_1-states quenching by molecular oxygen were calculated using oxygen solubility in methylcohexane and toluene (TOL) at 293 K and the following expression $k_{TS} = [(\tau_{T,S})^{-1} - [(\tau^0_{T,S})^{-1}]/[O_2]$, where τ_T and τ_S are the corresponding decays of T_1- and S_1-states of the given compound in the presence of molecular oxygen, τ^0_T and τ^0_S are decays in degassed solutions, $[O_2]$ is the concentration of dissolved molecular oxygen at 293 K.

[b] $k_T(lig)$ is the rate constant of triplet state quenching for extra-ligated compound in toluene+pyridine (TOL+PYR) solution.

Here, k_{diff} is a diffusion rate constant, k_{ST} is a non-radiative intersystem crossing rate constant, and k_Δ is a the singlet oxygen generation rate constant. g_1=1/9 and g_3=1/3 are spin-statistical factors reflecting the rate constants of the formation of the complex states $^1[^3M_1...^3O_2]$ and $^3[^3M_1...^3O_2]$, correspondingly; k_{dis} is the rate constant of the complex dissociation. In the case of porphyrins and chlorins $k_{dis} \approx k_S$ where k_S is the bimolecular rate constant of S_1-state quenching by O_2.[418] From the considerations presented in[417,418] it follows that at the same quenching mechanism (exchange and donor-acceptor interactions) the quenching scheme may differ. Scheme (I) with generation of singlet oxygen ($^1O_2$ or $^1\Delta_g$) corresponds to the case when the ratio $\beta = k_T/k_S = 1/9$, while scheme (II) without $^1O_2$ generation is operative at $\beta = k_T/k_S = 1/3$.

It follows from the data collected in Table 3 that in toluene at 293 K, all non-pyridinated dimers exhibit a noticeable decrease (by 15-30%) of bimolecular rate constants k_T compared to with those known for the corresponding precursor monomers with the same side substituents. The reason of that is connected with the fact[74,415] that in chemical dimers containing Zn-porphyrin subunits coupled by the phenyl spacer, the non-radiative exchange triplet-triplet energy transfer realizes at distances R_{DA}=12.6-17.0 Å with rate constants of $k^{ET} \approx 5 \cdot 10^6$ s^{-1}, while rate constants of T_1-state quenching by dissolved O_2 for porphyrin monomers are of $k_q = k_T \cdot [O_2] \approx 3 \cdot 10^6$ s^{-1} in these conditions. Correspondingly, the T-T energy transfer between porphyrin halves in the dimers competes with quenching of T_1-excited macrocycle by molecular oxygen leading to the relative decrease of the experimental bimolecular rate constants k_T for the dimers with respect to those found for monomeric precursors at the same conditions.

It is seen also from Table 3 that k_T values for the dimers increase sequentially in the following set: $(ZnOEP)_2$Ph, $(ZnHTPP)_2 \rightarrow (ZnOEP)_2 \rightarrow$ Zn-3^1,3^1-cyclodimer, $(ZnOEChl)_2$. It is known [415,416,418] that T_1-state quenching by O_2 is an electron donor-acceptor by nature $[M^+ \ldots O_2^-]$ and thus correlates with one electron oxidation potentials ($E^{ox}_{1/2}$) of porphyrins and chlorins. According to[419] $E^{ox}_{1/2}$ values (measured vs SCE) for Zn-*meso*-phenylporphyrins are higher than $E^{ox}_{1/2}$ =0.63 V for ZnOEP, and values $E^{ox}_{1/2}$ =0.20 V for ZnOEChl and Zn-cyclopentaneporphyrins are lower than that for ZnOEP. Therefore, the observed sequential increase of k_T values in the presented set of the dimers reflects qualitatively the corresponding $E^{ox}_{1/2}$ values lowering. Finally, the most pronounced oxygen-induced T_1-state quenching (by 60%, Table 3) is found for pyridinated dimer $(ZnOEP)_2$ with a flexible -CH_2-CH_2- bridge. There are two factors that come into play here. Firstly, electron-donating ethane bridge in the dimer may strengthen the pyridine action in oxygen-induced T_1-state quenching (effect of $E^{ox}_{1/2}$ decrease). Secondly, it is known[415,416] that pyridine-coordinated dimer $(ZnOEP)_2$ is in the opened fully staggered conformation. It means that the cross-section of the dimer-oxygen interaction becomes larger thus leading to the increase of the experimentally detected quenching.

Finally, based on results obtained in[415,416] one may conclude that quantum efficiencies γ_Δ of singlet oxygen $^1\Delta_g$ generation for both monomeric precursors and chemical dimers of Zn porphyrins coincide practically (within experimental errors) with the corresponding values of quantum efficiencies γ_T of the non-radiative intersystem crossing $S_1 \sim\sim> T_1$. It means that for Zn-porphyrin dimers, T_1-states quenching by oxygen O_2 is realized according to scheme (I) followed by the formation of singlet oxygen $^1\Delta_g$ molecule.

Interaction of porphyrin triads and pentad with molecular oxygen

The formation of self-assembling porphyrin triads and pentads (based on a "key-hole" principle) was realized via two-fold extra-ligation of both central Zn ions of Zn-porphyrin chemical dimers with two nitrogens of meso-pyridyl rings in the corresponding di- and tetra-pyridyl-containing porphyrin free bases.[74,420-422] The structures of monomeric and dimeric precursors as well as optimized geometries of multiporphyrin arrays under study are presented in Figure 23. For these multiporphyrin arrays with known morphology, the main pathways and mechanisms of the primary photoinduced relaxation processes were evaluated using steady-state and time-resolved luminescence/absorption measurements and theoretical analysis, and are properly described in our earlier publications.[420-422] Based on this results, photophysical events leading to the formation of the final excited states of the triad or pentad subunits are the following. The fast non-radiative relaxation of the dimer S_1-state (within 1.6 ps) is caused by two competing processes: (i) the resonance energy S-S transfer dimer→extra-ligand, and (ii) the photoinduced electron transfer from the dimer to the extra-ligand leading to the singlet radical ion pair state formation. It means that the population of the dimer T_1-state via intersystem crossing $S_1(^1\text{dimer}^*) \sim\sim> T_1(^3\text{dimer}^*)$ with a rate constant of $k_{ISC} \sim (5\text{-}7) \cdot 10^7 s^{-1}$ is low probable. In its turn, because of charge transfer events, the extra-ligand T_1-state in triads and pentads cannot be populated via simple $S_1 \sim\sim> T_1$ process in ligand subunit. The population of the locally excited T_1-state of porphyrin extra-ligands in triads and pentads ($^3H_2P^*$) takes place from the upper-lying triplet radical ion pair state $^3(\text{dimer}^+ \ldots H_2P^-)$ or directly from the singlet radical ion pair state $^1(\text{dimer}^+ \ldots H_2P^-)$. Concluding, after any excitation of the triad or pentad the final lowest locally excited state is the extra-ligand T_1-state. Namely this state should be taken into account upon examination of the interaction of triads and pentad with O_2 in liquid solutions.

The obtained experimental data are collected in Table 4. It is seen that at 293 K in degassed solutions, fluorescence quantum yields φ_F^0 and lifetimes τ_S^0 do practically not differ for all pyridyl substituted porphyrin free base derivatives (exta-ligands). In these conditions T_1-state decays are practically the same (τ_T^0= 1.2-1.4 ms) for individual extra-ligands, triads and pentad. It was shown also[423] that in triads and pentads containing dimers $(ZnHTPP)_2$ and $(ZnTPP)_2$, the locally excited T_1-state (E_T=1.44 eV) of extra-ligands lies essentially lower than the CT state. Therefore, in these multiporphyrin arrays the upper lying CT-state does not influence the deactivation of the locally excited T_1-state of the extra-ligand.

In the presence of oxygen, both S_1- and T_1-states quenching is observed for individual pyridyl substituted porphyrin free bases and those including in triads and pentad. Notably, Table 4 shows that for all extra-ligands and multiporphyrin arrays under consideration the ratio

$\beta = k_T/k_S$ is within 0.11-0.15. It corresponds to the spin-statistical factor of g=1/9 reflecting the situation[417,418] where triplet states of the compounds are quenched by triplet molecular oxygen, $^3O_2$ (see Scheme 73).

The role of structural organisation of triads and pentads is most readily understood upon their interaction with molecular oxygen in liquid solutions at 293 K. The comparative analysis of data summarised in Table 4 shows that both k_S and k_T values for extra-ligands in the triads and pentad are smaller than those obtained for the corresponding individual pyridyl substituted porphyrins. Therefore, it is reasonable to connect the relative decrease of k_S and k_T values upon transition from monomeric extra-ligands to those including in the triads and pentad with screening effects depending on the mutual arrangement of subunits in multiporphyrin complexes. In fact, the Zn-porphyrin dimer in the triad (without any populated excited states) plays a screening role limiting the access of oxygen molecule to the excited extra-ligand. For the "opened" triad $(ZnHTPP)_2 \otimes H_2P\text{-}(p\text{^}Pyr)_2$ (see Figure 23) this screening effect is minimal, and the measured decrease of k_T value for this triads is minimal with respect to that obtained for individual $H_2P\text{-}(p\text{^}Pyr)_2$. In contrast, for "closed" triads, $(ZnHTPP)_2 \otimes H_2P\text{-}(m\text{^}Pyr)_2$ and $(ZnHTPP)_2 \otimes H_2P\text{-}(m\text{-}Pyr)_2$, the access of oxygen molecule to the excited extra-ligand becomes more limited thus resulting in more pronounced decrease of the observed k_S and k_T values in comparison with those found for the corresponding monomers. Consistent with this interpretation is the fact that for pentad $2(ZnOEP)_2Ph \otimes H_2P\text{-}(m\text{-}Pyr)_4$ where screening effects due two dimers $(ZnOEP)_2$ are higher with respect to those in triads, the relative decrease of k_T values is maximal in comparison with the triads at the same experimental conditions (see Table 4).

Finally, quantum yields of singlet oxygen generation by triad (γ_Δ= 0.80) and pentad (γ_Δ=0.70) are high in toluene and comparable with those known for monomeric free bases (γ_Δ= 0.68 - 0.73[418]). In fact, for triads or pentads it means that the quenching of extra-ligands excited states by O_2 takes place with the same efficiency practically like for monomers, but with smaller bimolecular constants because of screening effects. In fact, the observation of singlet oxygen generation by triads and pentads in liquid solutions at room temperature serves the independent direct proof of the existence of locally excited triplet states in these arrays.

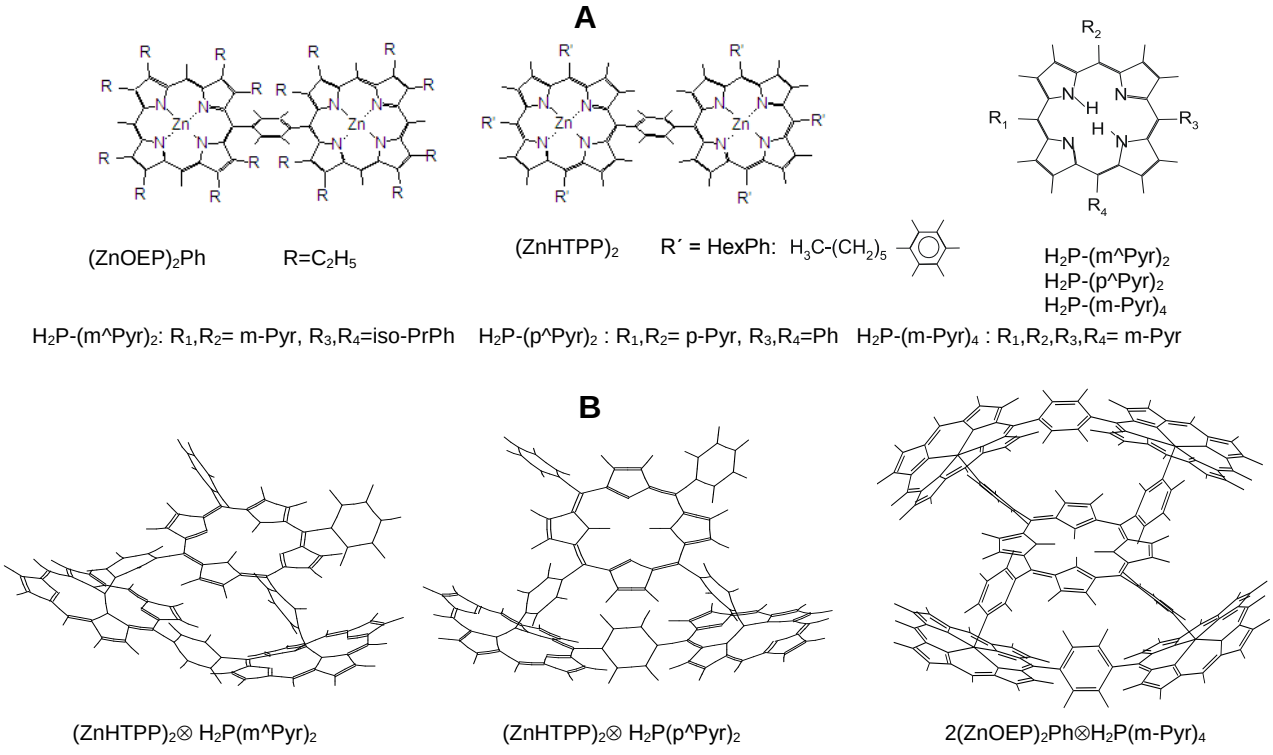

Figure 23. A: Structures of chemical dimers with phenyl spacer, $(ZnOEP)_2Ph$, $(ZnHTPP)_2$, and pyridyl-containing monomeric porphyrins $H_2P(m\text{^}Pyr)_2$-(iso-PrPh)$_2$, $H_2P(p\text{^}Pyr)_2(Ph)_2$ and $H_2P(m\text{-}Pyr)_4$ used as extra-ligands upon formation of triads and pentad. The corresponding extra-ligands were used: i) porphyrin, H_2P containing two meso-phenyls and two meso-pyridyl rings with different positions of both pyridyl rings (adjacent) and pyridyl nitrogens N (meta and para): i) adjacent meta-pyridyl rings - $H_2P(m\text{^}Pyr)_2$-(iso-PrPh)$_2$ and adjacent para-pyridyl rings - $H_2P(p\text{^}Pyr)_2(Ph)_2$; ii) porphyrin, H_2P containing four meso-pyridyl rings with meta-nitrogens. **B**: Mutual arrangement of the dimers, $(ZnHTPP)_2$, $(ZnOEP)_2Ph$ and various extra-ligands in triads and pentad (optimized geometry, HyperChem software package, release 4, semiempirical methods AM1 and PM3). For simplicity, mesophenyl rings in $(ZnHTPP)_2$ are omitted. Mark ⊗ denotes what porphyrin subunits are included in self-assembled triads and pentad.

Table 4. Photophysical parameters and bimolecular rate constants of excited S_1- and T_1-states quenching by molecular oxygen for pyridyl-substituted porphyrin free bases, triads and pentad in methylcyclohexane (MCH) and toluene (TOL) at 293K

Compound	Solvent	τ_S, ns	τ_S^0, ns	k_S, 10^{-9} $M^{-1}s^{-1}$	φ_F	φ_F^0	τ_T, ns	k_T,10^{-9} $M^{-1}s^{-1}$	$\beta=k_T/k_S$	τ_T (77K), ms
H_2P-(m^Pyr)$_2$	MCH	8.9	11.4	9.3	0.070	0.104	275	1.40	0.14	4.2
H_2P-(p^Pyr)$_2$	MCH	9.1	12.8	12.0	0.064	0.098	280	1.37	0.11	4.2
H_2P-(m-Pyr)$_4$	MCH	8.4	10.5	9.3	0.071	0.098	260	1.45	0.15	4.1
(ZnHTPP)$_2$ ⊗H_2P-(p^Pyr)$_2$	MCH	8.0	10.4	11.3	-	-	340	1.15	0.10	4.1
(ZnHTPP)$_2$ ⊗H_2P-(m^Pyr)$_2$	MCH	8.2	10.3	9.6	-	-	365	1.05	0.12	3.1
H_2P-(m^Pyr)$_2$	TOL	9.5	-	-	0.075	-	380	1.45	-	-
(ZnOEP)$_2$Ph ⊗H_2P-(m^Pyr)$_2$	TOL	7.7	-	-	0.05	-	550	1.0	-	-
2(ZnOEP)$_2$Ph ⊗H_2P-(m-Pyr)$_4$	TOL	-	-	-	0.04	-	680	0.80	-	-

τ_S, φ_F and τ_S^0, φ_F^0 are fluorescence decays and quantum yields in the presence and absence of O_2 in solution, correspondingly; k_S and k_T are bimolecular rate constants of the excited S_1-and T_1-states quenching by molecular oxygen (for definition see Table 3); τ_T (77K) is T_1-states decay in rigid solutions at 77 K. Mark ⊗ denotes which porphyrin subunits are included in self-assembled triads and pentad.

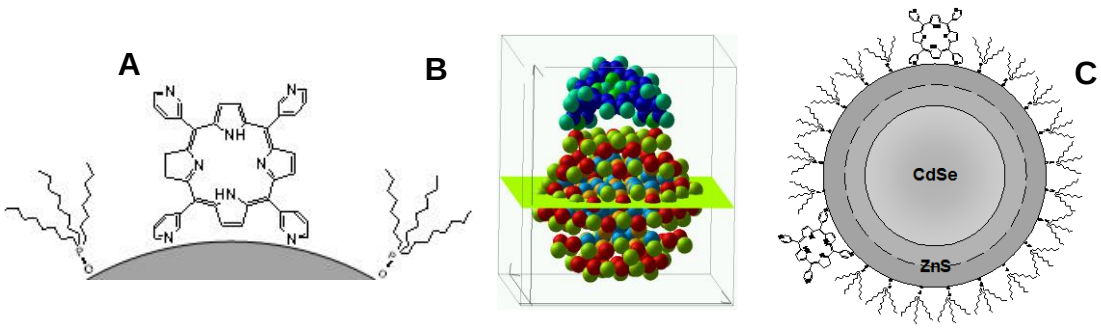

Figure 24. Structural properties of nanoassemblies based on semiconductor CdSe/ZnS QDs capped with n-trioctylphosphine oxide (TOPO)and H_2P(m-Pyr)$_4$ molecules. **A**: Schematic presentation of QD-porphyrin nanoassemblies. **B**: An optimized geometry for $Cd_{33}Se_{33}$ + H_2P(m^Pyr)$_2$ (B, optimization by HyperChem 7.0; simulations by ab initio density functional theory, DFT, with the VASP code[424]). **C**: the scales of CdSe core, ZnS shell, porphyrin and TOPO molecules corresponding to relative sizes of the main components of the arrays.

Interaction of "Quantum Dot – Porphyrin" nanoassemblies with molecular oxygen

Like for multiporphyrin complexes described in the previous section, a controllable formation of nanoassemblies based on semiconductor quantum dots (QD) and porphyrins was realized using also a "key-hole" principle upon quantitative titration experiments in toluene at ambient conditions.[74,75,79,80] In this case, "QD-Porphyrin" nanoassemblies with various porphyrin/QD ratio were successfully prepared upon two-point coordination interactions of two nitrogens of meso-pyridyl rings in the tetra-pyridyl-containing H_2P(m-Pyr)$_4$ or H_2P(p-Pyr)$_4$ porphyrin free bases, and surface Zn ions of colloidal core/shell CdSe/ZnS QDs passivated by tri-*n*-octyl phosphine oxide (TOPO) (Figure 24).

From the photochemical point of view, the generation of singlet oxygen by "QD-porphyrin" nanoassemblies should involve two steps. First, after excitation of QD the energy transfer QD→porphyrin should be organized resulting in S_1-state formation followed by the intersystem crossing into porphyrin T_1-state via the intersystem crossing S_1~~>T_1 pathway. Second, for porphyrin acting as PS, the diffusional controlled triplet-triplet energy transfer PS(T_1)→oxygen($^3O_2$) should take place resulting in $^1O_2$ generation in the surrounding media. This section provides a description of the obtained basic results and a discussion of all necessary steps what should be realized upon quantitative analysis of QD PL quenching processes in "QD-porphyrin" nanoassemblies and efficiencies of the singlet oxygen generation.

Typically, the formation and "QD-porphyrin" nanoassemblies manifests itself in a pronounced quenching of QD photoluminescence (PL).[74,79,80,424] Correspondingly, for nanoassemblies consisting of TOPO-capped CdSe/ZnS QDs (d_{CdSe} = 3.0 nm, 2 ZnS monolayers, C_{QD} = 4×10^{-7} M) and H_2P(m-Pyr)$_4$ molecules in toluene, the direct quantitative comparison of QD PL quenching results and sensitization data for porphyrin fluorescence was carried out using a complete set of titration points. Our results showed[79,80,424] that in "QD-porphyrin" nanoassemblies under consideration, Foerster resonance energy transfer (FRET) QD→porphyrin

occurs with low quantum efficiency of Φ_{FRET} =0.10-0.15, while the main part of the observed QD PL quenching is due to non-FRET nature ($\Phi_{non\text{-}FRET}$ =0.85-0.90). We quantitatively argued for the first time that a mechanism clearly distinct from the photoinduced charge transfer and FRET may be responsible for the QD PL quenching in QD-porphyrin nanocomposites upon the coordinative attachment of the extra-ligand on QD surface.[74,425] This process is correlated with the extension of the exciton wave function beyond the interface between the QD and the attached porphyrin molecule. Based on comparison of experimental data and quantum mechanical calculations it follows that the specificity of the exciton non-radiative decay in QD-porphyrin nanoassemblies (that is QD PL non-FRET quenching) is connected with the charge tunneling through ZnS barrier in the conditions of quantum confinement.

Keeping in mind these results, a comparative studying the quantum yields γ_Δ of the singlet oxygen generation by alone QDs and "CdSe/ZnS QD-porphyrin" nanoassemblies was performed using the direct spectral-kinetic measurements of $^1O_2$ near-IR emission.[79,80,424] It follows from these experiments (Figure 25B) that at ambient temperature most of alone QDs are hardly perspective to the direct generation of singlet oxygen (the quantum efficiency γ_Δ =1.5%), and without attached organic PSs cannot be used in clinical practice.

Figure 25 evidently shows that upon laser excitation at the same experimental conditions and concentrations in air-saturated toluene, "QD-porphyrin" nanoassemblies do indeed produce singlet oxygen with essentially higher efficiency in comparison with alone QDs or even with alone $H_2P(m\text{-}Pyr)_4$ molecules. The radiative relaxation of $^1O_2$ detected at λ_{reg}=1270 nm is characterized by the same decay value of $\tau(^1\Delta_g)$ = 30-31 μs that is typical for $^1O_2$ emission in non-polar liquid solutions.[415,416] It seems to be reasonable to connect this findings with FRET QD→porphyrin in nanoassemblies. Thus, for clear understanding the role of FRET namely in the increase of the quantum yields γ_Δ of $^1O_2$ generation by nanoassemblies one should take into account the role of the excitation conditions and then carry out the quantitative analysis of the whole experimental data.

Typically, photoluminescence measurements are carried out at lower excitation energies with respect to experiments with essentially higher laser pulse energies being used for $^1O_2$ generation, and this thing was taken into account. From Fig. 25C it is evidently seen that the PL intensity for QDs in "QD-porphyrin" nanoassemblies (curve 1, λ_{em}=558 nm) and for alone CdSe/ZnS QDs is not a linear function of the laser pulse energy. In the case of alone porphyrin solutions, the above dependence is linear practically (not shown), while in contrast, this dependence for porphyrin counterpart in the "QD-porphyrin" nanoassembly is non-linear (curve 2, λ_{em}=720 nm). The linear dependence for alone porphyrin solutions in the whole range of nanosecond laser energies is explained by the minor role of the singlet-singlet and triplet-triplet annihilation processes at low solute concentrations[426] (C=10^{-5}-10^{-6} M in the given case). Non-linear dependence obtained for alone QDs and QDs in "QD-porphyrin" nanoassemblies reflects the well-documented pump-intensity dependence of the amplitudes of the single-exciton caused by non-radiative intraband Auger processes mediated by Coulomb electron-electron interactions in the conditions of the spatial confinement.[427] In this respect, the non-linear dependence of fluorescence measured for porphyrin being attached to QD surface (Figure 25C, curve 2, λ_{em}=720 nm) presents itself a direct proof of the realization of namely FRET process QD→porphyrin competing with both radiative electron-hole recombination and non-radiative Auger process in the conditions of powerful excitation.

The above results evidently show that the relative increase of the efficiency of $^1O_2$ generation by "QD-porphyrin" nanoassemblies with respect to that for alone QDs coincides with the observed sensitized increase of the fluorescence intensity for the attached porphyrins caused by FRET. Therefore, understanding and ultimately controlling the energy of laser excitation we have carried out the quantitative estimation of FRET efficiency in the nanoassemblies based on singlet oxygen generation experiments presumably.[79]

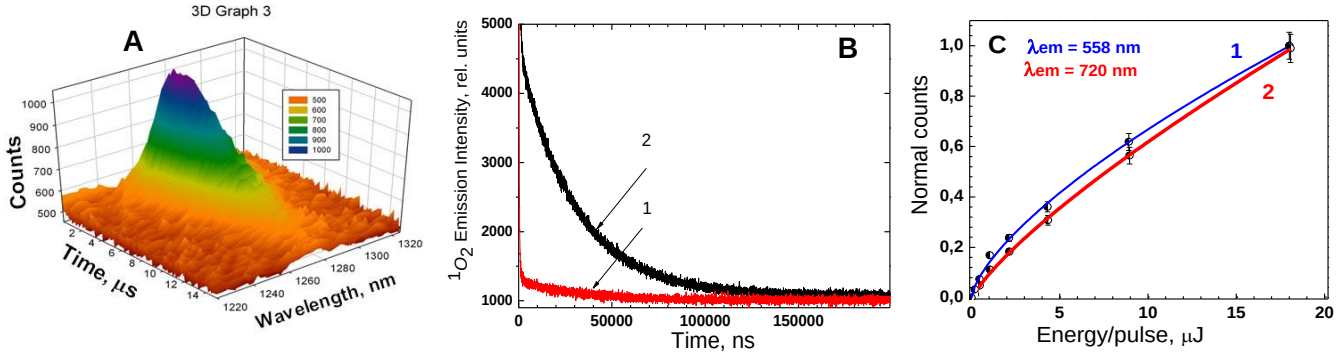

Figure 25. Singlet oxygen detection upon laser excitation of ZnS/CdSe QDs and "QD-porphyrin" (1:4) nanoassemblies in air-saturated toluene. **A**: 3D presentation of spectrum of singlet oxygen $^1O_2$ emission. **B**: Comparative presentation of singlet oxygen $^1O_2$ luminescence decay sensitized by individual CdSe/ZnS QDs (1) with respect to that measured for nanoassemblies (2) at the same molar concentrations of QDs and laser excitation conditions (λ_{exc}=532 nm, pulse duration $\Delta t_{1/2}$= 0.7 ns, λ_{reg}=1270 nm). **C**: Dependencies of the normalized emission intensities on the energy of laser excitation for CdSe/ZnS QDs (1, λ_{em}=558 nm) and $H_2P(m\text{-}Pyr)_4$ molecules (2, λ_{em}=720 nm) being coupled in nanoassemblies.

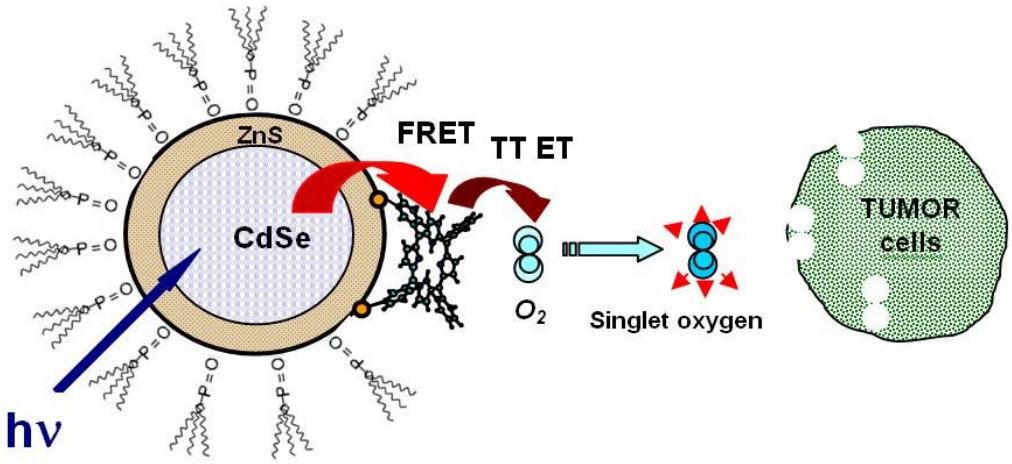

Scheme 73.

Our findings have shown that within the experimental accuracy the for these nanoassemblies, the values of FRET efficiencies obtained via the direct $^1O_2$ emission measurements at low laser excitation (Φ^{Δ}_{FRET} = 0.12 ± 0.03), are in a good agreement with FRET efficiencies found from the direct sensitization data for porphyrin fluorescence (Φ_{FRET} = = 0.14 ± 0.02, discussed above). Such quantitative analysis was done for the first time and shows that namely FRET process QD→porphyrin is a reason of singlet oxygen generation in the given nanoassemblies according to the following Scheme 73.

To our knowledge, such an approach is a first example showing quantitatively the role of FRET effects in the singlet oxygen generation by QD – PS nanoassemblies. The obtained results may be considered as a direct proof of the realization of namely FRET QD→porphyrin process followed by the singlet oxygen generation via porphyrin triplet states. This conclusion has been proven also for the same nanoassemblies using two-photon excitation.[428] All these facts raise the conclusion that "CdSe/ZnS QD-porphyrin" nanoassemblies may be considered as PSs of a novel type for PDT. However, nanoassemblies based on TOPO capped CdSe/ZnS QDs and porphyrins are not soluble in water and contain toxic elements, what limits their biological applications. Recently, we examined water-soluble glutathione capped AgInS/ZnS QDs with electrostatically attached Zn-porphyrins and showed that upon UV excitation, these nanoassemblies are capable to generate $^1\Delta_g$ (via FRET QD→porphyrin in ps time scale).[88] These preliminary results together with a specific dependence of spectral-kinetic parameters of AgInS /ZnS QDs on p*H* and local polarity, studied by us also,[429] make these nanoassemblies more perspective in various biomedical applications (drug delivery carriers, the distant testing the local pH, PDT treatment, *etc.*).

Finally, taking into account that in a lot of investigations the direct experimental measurements of the singlet oxygen ($^1O_2$ or $^1\Delta_g$) emission at λ_{max} = 1.27 μ are realized in various solvents, one should pay attention to some specific effects which may change the rate constant of the radiative transition $^1\Delta_g \rightarrow {}^3\Sigma^-_g$ in $^1O_2$ molecule. Luminescence of singlet oxygen $^1\Delta_g$ in solvents is difficult to observe[430,431] because of fast quenching of $^1O_2$ molecules by solvent vibrations, and the rate constant of the radiative transition $^1\Delta_g \rightarrow {}^3\Sigma^-_g$ in $^1O_2$ molecule is strongly dependent on the solvent properties (e.g. refractive index and polarizability)[432-434] including interface boundaries[435] and biological dielectrical nanoobjects.[436] Correspondingly, it is important to know all physico-chemical factors determining the singlet oxygen $^1\Delta_g$ lifetime (or the rate constant of the radiative transition $^1\Delta_g \rightarrow {}^3\Sigma^-_g$ in $^1O_2$ molecule) in various environments including systems *in vivo*. In[437] radiative rate constants k_r of the radiative transition $^1\Delta_g \rightarrow {}^3\Sigma^-_g$ have been determined for the photoluminescence of singlet oxygen $^1O_2$ in solutions with regularly changed refractive indexes using laser kinetic spectroscopy. The observed changes in the radiative rate constants k_r are shown to be caused both by inherent properties of the emitting $^1O_2$ molecule and by characteristics of an external environment, which defines the local field factor and the density of photon states of the field. In addition, the dielectric dipole moment of the transition $^1\Delta_g \rightarrow {}^3\Sigma^-g$ increases significantly as a result of the contact of $^1O_2$ molecule with solvent molecules.

Nevertheless, in spite of numerous experimental studies in this direction during last decade, some peculiarities of electronic mechanisms of $^1O_2$ luminescence decay remain still under the question.[438] Recently,[439] the molecular modeling of the influence of 10 solvents on the radiative rate constant k_r was carried out. The data obtained indicate that the correlation of k_r values with molecular polarizability that occurs in a number of cases is associated, on the one hand, with its effect on the strength of dispersion interactions in the complex, and, on the other hand, with the fact that, to certain extent, it reflects the position of the upper occupied orbitals of the solvent molecule. Both factors affect the degree of mixing of π-orbitals of $^1O_2$ molecule, which promotes the activation of the radiative transition $^1\Delta_g \rightarrow {}^3\Sigma^-_g$. Only taking into account all the above factors one may give a consistent explanation what happens with the intensity of $^1O_2$ in various solvents.

Conclusions

The interaction of molecular oxygen O_2 with various multicomponent complexes and nanoassemblies containing tetrapyrrolic compounds was quantitatively analyzed using set of steady-state and time-resolved experimental data ob-

tained in liquid solutions at ambient temperature. It was found that for Zn-porphyrin and Zn-chlorin chemical dimers, the extra-ligation of central Zn ions of the porphyrin macrocycles by pyridine leads to the enhancement of the non-radiative T_1~~>S_0 intersystem crossing rate constant (the most pronounced for the dimers with higher lying T_1-states). This effect is attributed to several reasons: accepting role of the extra-ligand vibrations, the enhanced spin-orbit coupling due to the singlet σ,π^* states energy lowering and the out-of-plane distortion of porphyrin macrocycle. For pyridinated dimers, their T_1-states quenching by molecular oxygen depends on the spacer flexibility and donor-acceptor interactions with pyridine.

In the case of self-assembled triads and pentads containing Zn-porphyrin dimers and pyridyl substituted porphyrin free bases (extra-ligand), the cooperative existence of energy and electron transfer processes results in the population of the final locally excited S_1- and T_1-states of porphyrin extra-ligands. The quenching of these states in triads and pentads by O_2 is noticeably weakened with respect to that for individual pyridyl substituted porphyrins, and is caused by the screening action of a strongly quenched Zn-porphyrin dimer subunit in triads and pentads limiting the access of oxygen molecule to the excited extra-ligand. These facts have to be taken into account upon the analysis of natural dark and photoinduced reactions of porphyrin supramolecular systems with molecular oxygen (oxygenation and deoxygenation in haemoglobin, singlet oxygen generation in tissues and PDT of cancer).

For inorganic-organic nanoassemblies based on TOPO-capped semiconductor quantum dots CdSe/ZnS and tetra-pyridyl porphyrins and formed via a two-fold coordination Zn….N-pyr "key-hole" principle in toluene at ambient conditions, the photoluminescence quenching for QD with superficially attached porphyrin molecules is caused by two main competitive reasons: the electron tunneling in the conditions of quantum confinement (the efficiency of 0.85-0.90) as well FRET QD→porphyrin (the efficiency of 0.10-0.15). On the basis of near-IR photoluminescence detection of singlet oxygen $^1O_2$ emission, it was proven that the experimental efficiencies γ_Δ of $^1O_2$ generation by "QD-porphyrin" nanoassemblies are essentially higher than those obtained for alone QDs. It was found that in "QD-porphyrin" nanoassemblies (1:4), FRET efficiencies $\Phi^{\Delta}_{FRET} = 0.12 \pm 0.03$ obtained via the direct $^1O_2$ emission measurements at low laser excitation, are in a good coincidence with FRET efficiencies $\Phi_{FRET} = 0.14 \pm 0.02$ evaluated from the direct sensitization data for porphyrin fluorescence in nanoassemblies. It means that namely FRET process QD→porphyrin is a reason of singlet oxygen generation by QD-porphyrin nanoassemblies. Taking into account experimental data and structure of excitonic states for QDs, it was concluded that at ambient temperature most of alone QDs are hardly perspective to the direct generation of singlet oxygen. On the other hand, "QD-porphyrin" or "QD-chlorin" nanoassemblies may be considered as good candidates for ''see and treat'' PDT or for oxygen sensing over physiological oxygen ranges.

Concluding, dealing with the direct quantitative measurements of the singlet oxygen $^1\Delta_g$ emission ($\lambda_{max} = 1.27$ μ) in various solvents, one should take into account changes in the rate constants k_r of the radiative transition $^1\Delta_g \rightarrow {}^3\Sigma^-_g$ in $^1\Delta_g$ molecule which may be caused as discussed in[417-419] by inherent properties of the emitting singlet oxygen molecule and by characteristics of an external environment (nature of solvent).

10. Hydrophilic-Lipophilic Balance and Interaction of Chlorin Type Photosensitizers with a Transport Proteins of Blood

The trend towards the search of new effective photosensitizers, best meeting the requirements applied to drugs is of current interest for decades and up to the present time.[6,10,440–448] The ability to generate ROS is one of the most important characteristics of potential PS designed for PDT. However, the singlet oxygen as a highly reactive oxidative form has a very short lifetime (≤ 40 ns) limiting its ability to diffuse inside biological tissues (20~40 nm).[6,12,448] Accordingly, pharmacodynamics of PS and, namely, mechanisms of its biodistribution in the human body including intracellular localization, play a crucial part in of PDT efficacy increase.[6,448-451] These biological features are fairly determined by the structure and hydrophilic-lipophilic balance (HLB) of the PS molecule, or, in fact, by the pigment affinity to a cell membrane and ability to penetrate it.[444, 452-454] In this regard, design of a new antitumor drug for PDT should involve an estimation of the affinity and accumulation selectivity of PS in malignized or pathogenic cells, as well as the control of specificity of passive transport of the drug *in vivo* and its localization on the target cell sites.[84,455,456]

Our scientific group is involved in extensive and continuing series of multidisciplinary studies on the development and investigation of new and already known potential sensitizers for antitumor and antimicrobial PDT[6,9,11,13,75,444,451,453,457-463] based on the porphyrin, chlorin and some other macroheterocyclic platforms. Our experimental efforts in this field are aimed at finding the ways to improve efficacy of PDT in terms of pharmacodynamics and selective biodistribution of potential PSs. Current work is a brief of literature and own recently obtained results, related to the influence of the structural features and amphiphilicity of the chlorin photosensitizers on the mechanisms of these drugs distribution and transport by proteins of human blood.

The main emphasis on PSs of chlorophyll-like nature is made here due to several factors. Naturally derived chlorins have an intense absorption ($\lg\varepsilon$ = 4.5-4.6) in a long-wavelength part of visible spectrum (~665 nm), a sufficient quantum yield of singlet oxygen,[6,10-13,373,448] a good amphiphilicity[453,454] due to asymmetric location of polar and non-polar substituents in the molecule and a susceptibility of macrocycles to chemical modification.[6,373,464,465] Some chlorin-based drugs like Foscan, Talaporfin, Radachlorin, Photoditazine or Photoran e_6 are currently used in clinical oncology as antitumor PSs.[6,9,10]

Hydrophilic-lipophilic balance of naturally derived chlorin photosensitizers

The balance of hydrophilic and lipophilic properties of PS plays an important part both at the stage of drug administration in its dosage form when the covalent or non-covalent binding of PS to a different type of nanocarriers is

often used[84,451,455-460] and during its delivery to the surface of the target cell.[6,448,465] The interaction of photosensitizer with a cellular constituents starts from the main primary target – membrane of the atypical cell.[466] The generation of ROS by irradiated cell-localized PSs results in oxidation of membrane lipids and proteins. The important chemical targets for photoactivated PS are double bonds of membrane unsaturated phospholipids.[10,467] The accumulation of lipid hydroperoxides and oxidased forms of cholesterol in membrane is a trigger for the lateral phase separation of lipids, perturbation of their functions and, as a result, a decrease of membrane permeability and cell death.[468-470] Although the mechanism of oxidative transformation of lipid membranes during PDT remains still poorly established[466] the most of authors are inclined to state a key role of $^1O_2$, formed at the photochemical reaction of PS with molecular oxygen, in the oxidation of unsaturated membrane phospholipids.[467] However, regardless of the type of photooxidation mechanism,[10,75,373,447] the efficacy of a sensitizer in the deactivation of a malignant or pathogenic cells depends on the proximity of molecular contact between the PS and the membrane lipid.[469] Therefore optimized PS molecule have to possess a certain HLB, to be well soluble in water or aqueous solutions of carriers,[84,455-457] but not to be too hydrophilic and not weaken its affinity and transfer through lipid membranes of cells.[84,444,454]

The human body can be represented as a set of lipid-like membrane barriers divided by water-like environment.[26,28,30] The *P* coefficient[3,452-454,469-475] reflecting partition of the substance between two immiscible phases is the main parameter for the comparative quantitative estimation of the hydrophilic-lipophilic balance (HLB) of any potential drug.[146,452,471,472] *P* value of the later give an important information about its ability to interact and penetrate cell membranes and, furthermore, about drug bioavailability and biodistribution pathways. The results of experimental determination of *P* values for tetrapyrrole photosensitizers and their theoretical evaluation obtained by various computational methods are widely presented in the literature.[3,473,474]

Usually the hydrophobic core of lipid membrane is modeled by 1-octanol (OctOH) and phosphate buffered saline (PBS, p*H* 7.4) is used to mimic water-like media for simulating transfer through the surface of lipid membranes and experimental evaluation of the hydrophilic-lipophilic balance of the drug.[452,454,461,462] To calculate partition coefficients (*P*) the isothermal saturation method is normally applied. This quantity is determined from the ratio of the equilibrium concentrations of PS in the lipid-like phase and in the PBS according to equation (1):

$$P = C_{m\ OctOH} / C_{m\ aq}, \quad (1)$$

where $C_{m\ OctOH}$ and $C_{m\ aq}$ are equilibrium solute molal concentrations in 1-octanol and aqueous phase, respectively.

Our experiments to determine *P* values were carried out in thermostatically controlled 50 ml glass cells filled with a PS solution with the initial concentration within 20 - 90 μmol/kg in a phosphate saline buffer or OctOH. Then the second component of the immiscible solvent system was added in a volume ratio of OctOH and PBS equal 40:60. After 36 hours of magnetic stirring at 298 K the solution was kept until complete phase separation before the probe was taken from the lipid-like layer. The equilibrium concentration of PS was analyzed by the spectrophotometric method using previously obtained calibration graphs. The solute concentration in the aqueous phase was estimated as the difference between the initial and lipid-like phase equilibrium concentration of the pigment. Values of the partition coefficients calculated according to the eq. (1) are presented in the Table 5.

All the chlorin PSs investigated (compounds **2**-**9**) were synthesized by chemical modification of methylpheophorbide *a* (**1**).[451,454,476-478] Methylpheophorbide *a* and clinically used photosensitizing agents as "Photoditazin" (**8**) and "Photoran e_6" were purchased from companies "CHLORIN", "VETA-GRANT LLC" and "RANFARMA", respectively. Trisodium salt of chlorin e_6 (**9**) was obtained by precipitation of "Fotoran" from aqueous solution of HCl (p*H* ~ 6) followed by solid powder dissolution in diluted NaOH solution (pH ~ 8) and further complete water evaporation.[451] All the compounds were identified using ^{1}H NMR spectroscopy and mass spectrometry technics.

The analysis of the previously measured at 298 K and newly obtained partition coefficients of chlorin PSs at the interface of OctOH and PBS clearly demonstrate these quantities differentiate strongly depending on the substitution pattern of the macroheterocyclic molecule. Thus, a metal-free chlorophyll *a* appeared to be the most hydrophobic natural chlorin studied (*P* = 326.0[453]) with a highly pronounced affinity to the lipid surrounding. Transesterification of this PS with the replacement of a hydrophobic phytyl tail with a methyl group (methylpheophorbide *a*, **1**) leads to a rather significant decrease in the *P* value down to 210.1.[444,454,476] An additional structural factor contributing to the chlorin hydrophilic properties is the opening of the cyclopentanone ring accompanied by the transformation of phorbine (**1**) to chlorin (**2**-**9**) molecular structure.

Table 5. Partition coefficients (*P*, 298K) for compounds **1**–**9** in the 1-octanol/phosphate saline buffer biphasic system and PSs distribution between transport proteins of human blood (%).

	Photosensitizers								
	1	**2**	**3**	**4**	**5**	**6**	**7**	**8**	**9**
	Partition in OctOH – PBS system								
P	210.1± 6.0 [444]	29.3 ± 0.9 [454]	20.1 ± 0.9 [451]	8.7 ± 0.2 [476]	1.04 ± 0.2 [476]	0.97 ± 0.3 [476]	19.0 [478]	2.03 ± 0.21 [9]	1.88 ± 0.09 [9]
Proteins	Serum proteins binding, %								
LDL	-	52 [479]	45	53	NB	NB	38 [479]	2	1
HDL	-	31 [479]	53	40	NB	NB	44 [479]	4	5
Albumin	-	17 [479]	2	7	NB	NB	18 [479]	94	94

NB – no binding

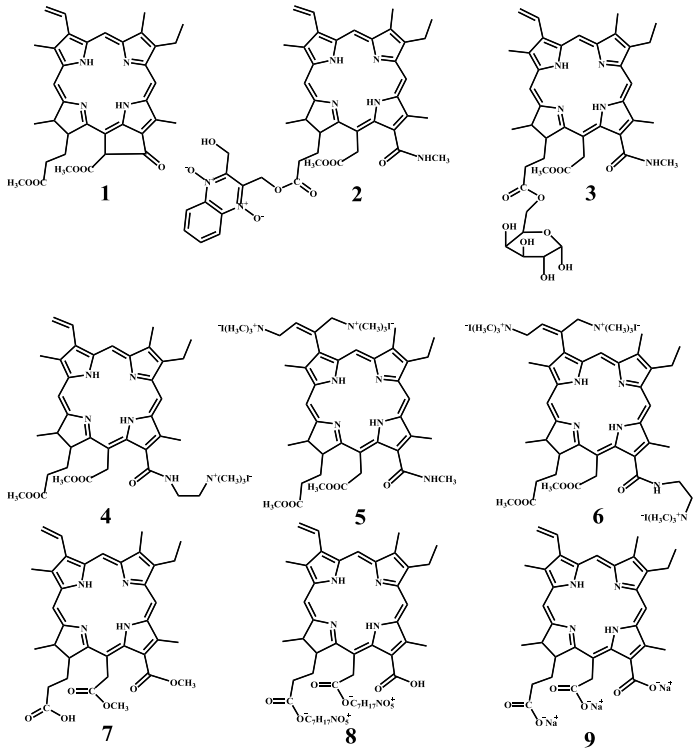

Figure 26. Molecular structures of PSs studied: **1** — Pheophorbide *a* 17(3)-methyl ester, **2** — Chlorin e_6 13(1)-N-methylamide-17(3)-(1'-(2'-hydrohymethyl-3',8'-dioxy-quinoxalinyl)methyl ester)-15(2)-methyl ester, **3** — Chlorin e_6 13(1)-N-methylamide-15(2)-methyl ester-17(3)-O-6'-galactopyranosyl ester, **4** — Chlorin e_6 13(1)-*N*-(2-*N',N',N'*- trimethylammonioethyl iodide) amide-15(2),17(3)-dimethyl ester, **5** — Chlorin e_6 3(1),3(2)-*bis*(*N,N,N*-trimethylaminomethyl iodide)-13(1)-*N'*-methylamide-15(2),17(3)-dimethyl ester, **6** — Chlorin e_6 3(1),3(2)-*bis*(*N,N,N*-trimethylaminomethyl iodide)-13(1)-*N*′-(2-*N*″,*N*″,*N*″-trimethylammonioethyl iodide) amide-15(2),17(3)-dimethyl ester, **7** — Chlorin e_6 13(1),15(2)-dimethyl ester, **8** — Chlorin e_6 dimeglumine salt, **9** — Chlorin e_6 trisodium salt.

For instance, at the disclosure of phorbine exo-cycle in the molecule of macrocyclic PS conjugate with diethylene glycol an intense decrease of the partition coefficient from 77.7 to 32.6 is observed at 298K.[444]

Any conjugation of one or higher number of hydrophilic groups to a chlorin macroheterocycle decreases *P* parameter (Table 5). At the same time, the incorparation of a single non-ionic or zwitterionic substituent, such as resedues of glycol[444] or carbohydrate,[451] N-oxide[454] or amino acid[451] into the PS structure promotes an amphiphilicity of the molecule without essential increase in water solubility. Usually, the naturally derived chlorins carrying one of the substituents listed above (Table 5, compounds **2**, **3**), demonstrate partition coefficients ranged from 15 to 30. Meantime, chlorin molecules containing one or more ionic groups (**4**-**6**, **8**, **9**) and characterized by *P* values less than 10 acquire solubility in water to achieve therapeutic concentrations of PS.[6,7,9,10] So, the solubility of dicationic chlorin (**5**) reaches to 0.04 mol/kg at 298K. [477] Comparison of partition coefficients of cationic (**5**, **6**) and anionic (**8**, **9**) type PSs with two and three charged groups in the OctOH – PBS system in both cases demonstrates the proximity of the *P* values within pairs of PSs with a positively and negatively charged groups (Table 5). At the same time, these quantities are slightly lower for cationic PS **5** and **6** revealing more hydrophilic character of trimethylammonia groups (P = 0.97-1.04)[476] as compared to carboxylic ones (P = 1.9-2.0).[9] The HLB of the monocationic chlorin (**4**, P = 8.6) differs significantly from di- and three charged derivatives.[457] Meantime, having moderate amphiphilicity, comp. **4** retains a sufficiently high solubility in water. The monocarbaxylate derivative of chlorin e_6 (**7**) is significantly less hydrophilic (P = 19.0[478]), localized mainly in a lipid-like phase and almost insoluble in water. An increase in the number of charged groups in the PS molecule provides the pronounced enhancement of macrocycle affinity towards a water-like pool. Nevertheless, even tricationic chlorin e_6 (**6**) is still equally distributed between lipid-like octanol and water-like PBS phase[476] due to the bulky non-polar macrocyclic part of the molecule.

Hydrophilic chlorin PSs[476] in contrast to more hydrophobic ones[444,451,454] demonstrate only modest Arrhenius dependence already at P < 30. So, for such a compounds partition coefficients measured at standard temperatures can be attributed to physiological conditions.[476] It should also be taken into account the *P* parameter of chlorin PSs with an acidic groups depends on p*H* significantly.[475] In particular, it is found, that an affinity to a water-like compartment in the case of anionic carboxylic derivatives of chlorin e_6 decreases with p*H*.[475] This information could be important for tumor-localized anionic PSs.

Thus, the *P* value is a reliable quantitative characteristics of the hydrophilic-lipophilic balance of porphyrin and chlorin-type macroheterocyclic PSs. Knowledge about the HLB of photosensitizing agents is critically important for understanding mechanisms of their delivery and pharmacodynamics.[84,95,449-451] Partition coefficients provide not only the information about PS affinity towards a water-like or lipid-like surrounding but also an ability to bind to a different kind of blood proteins determining the mechanisms of drug biodistribution in organism and, finally, the efficacy of PDT. That is why in the next section of the paper the effect of the structure and HLB of chlorin PS on the mechanisms of their transport by blood proteins, as well as on their affinity to the membranes of atypical cells will be analyzed.

Equilibrium distribution of chlorin PSs between transport proteins of blood

Extensive material devoted to the study of the interaction of PSs of various structure with blood proteins using a wide range of spectroscopic, chromatographic and quantum chemical methods [75,480-485] are accumulated in the literature. Entering biological tissues the drug participates in the process of equilibrium redistribution on the molecules of bio-environment, primarily on the blood transport proteins – "light" albumins (M = 66.5 kDa) or "heavy" lipoproteins of low and high densities (LDL and HDL, M = >230 kDa and ~180, respectively).[478] Redistribution occurs regardless of whether the PS is taken as a pure compound or as molecular complex of the drug with any non-covalently bound delivery vehicle.[75,84,455,456,486]

It is known that the selectivity of PS for tumor cells is several times higher compared to healthy mammalian ones.[6,448] The most of photosensitizers are mainly hydro-

phobic molecules, therefore, in human circulatory system they bind predominantly to the lipophilic protein fraction like low-density lipoproteins (LDL).[6,296,483,486,487] Lipoproteins play an important role in supplying cells with cholesterol, which is used to form membranes during cell division. Since tumor cells have an abnormal growth rate, they require a large excess of cholesterol and the number of LDL receptors in them per surface unit increases significantly compared to healthy cells.[488] Thus, the binding of PS to LDL in the bloodstream is one of the main reasons of the pigments tumor selectivity due to their targeted delivery.[486]

High-density lipoproteins (HDL) and albumins are also used as a transport proteins of human blood.[449] HDL are able to deliver the drug to the tumor tissue, but, compared to LDL, they are accumulated in tumor macrophages, which can negatively influence the efficacy of the same PS.[487] In turn, albumins have a less pronounced affinity for malignant cells, so PS associated with this type of transport proteins will be accumulated both in target tumor and healthy mammalian cells, providing less selectivity.

PS molecules of various structures have different pharmacodynamics and bind to transport proteins in individual ways. It can be expected that essentially hydrophilic PS bind mainly to albumins, the amphiphilic ones interact with both HDL and albumins and hydrophobic molecules make a complex selectively with LDL.[449,451,478,489] This hypothesis is in a good agreement both with a previously published results and our data (Table 5).[451,479] Thus, three types of transport proteins of the circulatory system compete for binding with PS molecule, therefore, and the efficacy of the antitumor agent mainly depends on its hydrophilic-lipophilic balance (Table 5).

There are a number of ways to determine the nature of PS binding to various types of proteins, including transport ones. One of the most common is the titration of the PS solution with a specific protein using spectral methods to obtain both equilibrium constants and thermodynamic parameters of the process, as well as structural characteristics such as binding sites and geometrical features of the complex.[75,490,491] However, in relation to the study of PS interaction with transport proteins of blood the spectral approach has some disadvantages. Albumins are commercially available and chemically stable proteins, therefore titration using spectral measurements is the most preferable in this case.[296,480,481] At the same time, low- and high-density blood lipoproteins are hardly separable from each other and because of the low stability require immediate use after the sample preparation. In addition, the titration using spectroscopic methods in the case of LDL and HDL is also of little use because it requires separate experiments for different types of proteins and does not allow to work with a mixture to assess the competitive distribution of PS between transport proteins. At the same time, information about the competitive interaction of potential PS with proteins is important for understanding the real picture of their redistribution and transport *in vivo*.

To solve the above problems, the gel filtration chromatography (GFC) capable to separate complexes of transport human serum proteins with PS divided into fractions according to the size of macromolecules is used.[478,479,482,483,485,489,492] (Figure 27) Spectrophotometric or fluorescence analysis of fractions gives the gel-filtration chromatogram or separation curve which is the dependence of the relative optical density (A/A_{max}) measured on the absorption maxima of tryptophan (280 nm, available in all types of transport proteins), and naturally derived chlorin PS, absorbing at ~665 nm, from the volume of the solution (V, mL) eluting from the chromatographic column. Figure 28 demonstrates an example of gel chromatographic separation on the column (1.6×70 cm) filled with polyacrylamide gel Acrilex P-200. Three pronounced peaks of blood proteins are observed usually on the gel-chromatogram (curves 1, Figure 28), where the first one corresponds to LDL (with an admixture of HDL), while the second and third represent HDL and albumins, respectively. This finding is confirmed by the biochemical analysis of the obtained fractions (Figure 27).[478,489] The area under the PS curve on the gel chromatogram, measured for individual peaks corresponding to specific types of blood proteins, allows to calculate the percentage of pigment in each fraction (Table 5).

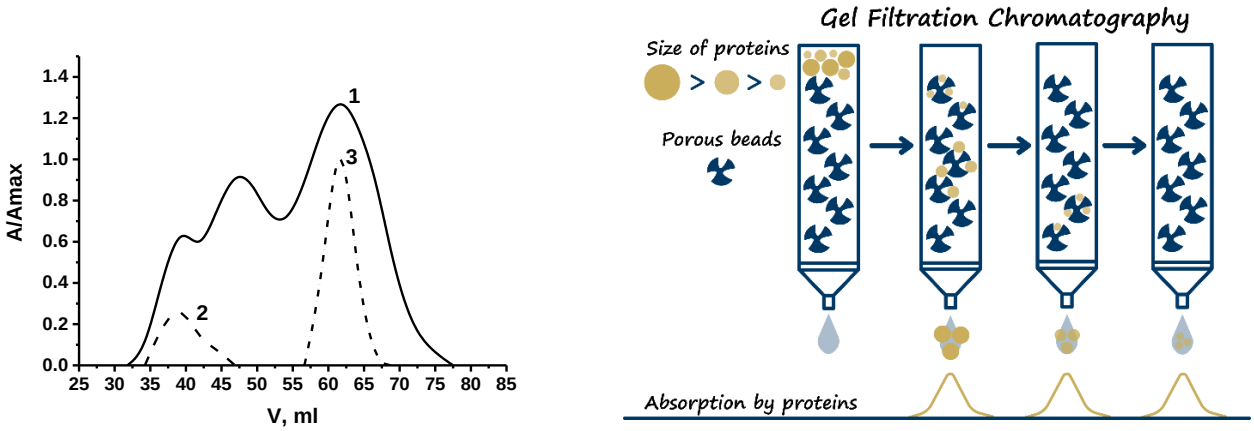

Figure 27. Detection of protein components of human blood by biochemical analyzer "COBAS" (*left*, 1 – blood protein sample, 2 – low-density lipoproteins, 3- albumins) and the principle of gel-filtration chromatographic separation of proteins depending on the size of the molecule (*right*).

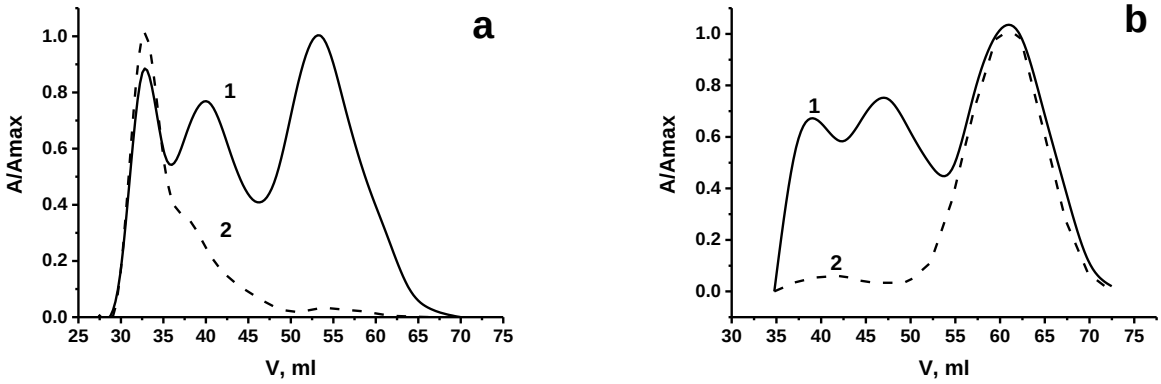

Figure 28. Gel filtration chromatograms of 70% blood serum (1 mL) with addition of $9 \cdot 10^{-5}$ mol/kg of PSs **4** (a) or **8** (b): 1 – main protein (absorption at 280 nm), 2 - analyzed PS (665 nm). Column elution rate is 0.2 mL/min, the volume of each collected fraction is 2.5 mL.

As mentioned above, the degree of amphiphilicity affects significantly the biodistribution of drugs, including PS, using blood transport system.[478,489] As can be seen from the literature and our data[9,475,478,479] (Table 5), hydrophilic chlorin molecules **8** and **9** containing two and three anionic groups, respectively, are accumulated to a greater extent in the albumin structure (94%). An increase in the partition coefficients *P* and affinity of PS to a lipid-like compartments, on the contrary, leads to preferential binding of drug molecule to a less polar lipoprotein fractions. So, more hydrophobic compound **7** (*P* = 19.0[478]), containing the only carboxyl group is about equally distributed between both LDL and HDL (Table 5) with a total binding to lipoproteins of 82%. Amphiphilic conjugates of chlorin e_6 with an antimicrobial drug "Dioxidine" (**2**) and D-galactose (**3)** behave in approximately the same way due to a relatively similar HLB (*P* = 20 – 30). Binding of the compound **3** to lipoproteins is overwhelming and reaches 98% (Table 5).

Based on close *P* values and HLB of di- and trianionic (**8**, **9**) and di- and tricationic PSs (**5**, **6**) an identical picture of blood proteins binding could be expected for them. However, it was found that molecules **5** and **6** carrying two and three cationic trialkylammonia groups, respectively, do not demonstrate interaction to any types of transport proteins during GFC. The reason of that is the most important characteristic affecting the equilibrium distribution of PS across transport proteins is not only the number, but also the sign of the charged substituents presented in the molecule. As known from the literature[478] the at the pigment interaction with albumin, the nonpolar macrocyclic core is embedded into the hydrophobic pocket of the transport protein surrounded by positively charged groups.[478] Therefore, anionic PSs strongly bind to albumins, whereas cationic pigments such as compounds **4**, **5** or **6**, are repulsed electrostatically from these transport molecules. At the same time, the moderate hydrophobicity of monocationic chlorin **4** (*P* = 8.3) allows it to form stable complex with blood lipoproteins (in total 93%, see Table 5). Mainly hydrophilic (*P* ~ 1) PSs **5** and **6** are not able to be transported by lipid transport proteins due to its high affinity for the water-like phase.

Thus, based on the fact that LDL is the most preferred PS transport agent, it can be assumed that cationic pigments with an appropriate HLB estimated by partition coefficient of about 10, such as the compound **4**, should demonstrate a good efficacy as photosensitizing agents in antitumor PDT. In addition, due to the amphiphilic structure and the presence of a cationic group in the molecule PS **4** is more versatile compared to neutral or anionic chlorins, since it can be used both in antitumor and antimicrobial PDT.[3,5,6,75,447,476]

Amphiphilic PSs with non-ionic or zwitterionic functional groups (**2**, **3**) interact effectively with LDL and HDL (Table 5), however, provide negligible solubility in water and pronounced aggregation in aqueous solutions. The later factor affects negatively their ability to generate ROS and reduces PS bioavailability.[10-13,373,447] The application of micellar, polymer and other types of nanocarriers for PS binding and solubilization is an effective way to achieve its therapeutic concentrations in aqueous solutions.[84,471]

The results presented above allow us to draw the following important conclusions:

1. The structural features of photosensitizing molecules designed for PDT determine their polarity, amphiphilic properties and significantly affect the biodistribution of pigments, mechanisms of their transport in the system bloodstream and the selectivity of accumulation in the membranes of malignazed or pathogenic cells.

2. PS distribution coefficients reflecting the state of its hydrophilic-lipophilic balance are correlated with the type of their distribution between blood transport proteins. Thus, highly hydrophilic anionic-type chlorins give a stable complex with blood albumins, whereas a decrease in the affinity of PS to the aqueous phase leads to the predominant binding to lipoprotein fractions of the blood. Cationic PSs carrying two or more charged groups do not interact with any type of transport proteins.

3. Gel filtration chromatography is a reliable method of primary evaluation of the mechanism of PS biodistribution between proteins of the circulatory system.

Chlorin-type monocationic pigments with moderate HLB (*P* ~10) are the most promising photosensitizing agents, which, on the one hand, maintain the solubility in water, and, on the other hand, are transported mainly by lipoproteins in the system bloodstream of human. Thus, due to the number and sign of the charges PS **4** demonstrates higher versatility compared to neutral or anionic chlorins and can be applied both in antitumor and antimicrobial PDT.

11. Sulfur-Containing Derivatives of Natural Bacteriochlorophyll *a* as Promising Photosensitizers for PDT of Cancer

The development of antitumor drugs is one of the most important areas in the modern medicinal chemistry.[1] The World Health Organization (WHO) defines cancer as a broad group of pathological processes that can begin in almost any organ or tissue and can be accompanied by uncontrolled division of abnormal cells. Despite the variety of existing therapeutic agents, all of them have a number of drawbacks, including non-selectivity of action, high toxicity, and resistance of tumors to these agents. Since oncological diseases continue to threaten the people's health and quality of life around the world, there is a need for innovative targeted therapeutics aiming at specific targets in tumor cells in order to implement a personalized approach in oncology.[2]

The development of sulfur-containing pharmaceutical substances plays an important role in the development of medicinal chemistry. There are more than 300 sulfur-containing drugs approved by the US Food and Drug Administration (FDA), the most popular of which include sulfonamides, thioethers, sulfones, penicillin, *etc*.[493] Photosensitizers that acquire new useful properties upon incorporation of sulfur-containing groups or individual sulfur atoms into their structure also attract attention.

One of the most desirable groups of PS includes natural bacteriochlorins with absorption maxima in the near-infrared spectral range, which expands the capabilities of treating deep-seated tumors.[494] Moreover, they have a relatively high yield of singlet oxygen and low toxicity along with increased tropism to tumor tissues.[106,495]

The glutathione system is one of the key protective cell systems affecting the efficiency of its photoinduced death.[496] This system is vitally important for the existence of mammalian cells, including tumor ones. It is known that the level of enzymes in this system is elevated in various types of malignant neoplasms.[497] The thiol-containing tripeptide glutathione (γ-glutamylcysteinylglycine, GSH) plays an important role in the detoxification of xenobiotics, free radical control, maintenance of the cell redox balance, formation of multiple drug resistance (MDR), *etc*.[498] This makes it promising to aim pharmacological compounds at the glutathione system as a biological target in order to damage the enzymes of this system, which would favor the vulnerability of tumor cells to oxidative stress.[499]

Two main enzymes are responsible for the biosynthesis of glutathione in a cell: first, γ-glutamylcysteine ligase (GCL, EC 6.3.2.2), which catalyzes the reaction between glutamate and cysteine, followed by the addition of a glycine residue to the resulting dipeptide with involvement of glutathione synthetase (GSS, EC 6.3.2.3).[500,501] Cellular glutathione participates in binding to various xenobiotics with involvement of enzymes of the glutathione S-transferase family, being an important regulator of intracellular metabolism.[502] Glutathione binding to reactive oxygen species (ROS), which is necessary for the protection against oxidative stress and regulation of the cell redox balance, is catalyzed by GST or by specific enzymes of the glutathione peroxidase family (GPx, EC 1.11.1.9).[503] Upon interaction with ROS, glutathione is converted to an oxidized dimeric form (GSSG), which, under the action of glutathione reductase (GR, EC 1.8.1.7), is reduced into the GSH monomer, thus closing the redox cycle.[504,505]

An important metabolic pathway that uses glutathione for detoxification of metabolites is the glyoxalase system consisting of glyoxalase I (GloI, EC 4.4.1.5) and glyoxalase II enzymes (GloII, EC 3.1.2.6).[506-508] This system catalyzes the conversion of methylglyoxal, a highly toxic glycolysis product, to D-lactate via the S-D-lactoylglutathione intermediate. The energy metabolism of the majority of tumor cells is based on the Warburg effect, i.e., aerobic glycolysis where glucose is converted to lactate in the presence of oxygen. This process in tumor cells is characterized by much higher activity (up to 200-fold) in comparison with normal cells.[509,510] Such a rate of glycolytic transformations results in a higher formation rate of glycolysis side products, including methylglyoxal (MG), a cytotoxic metabolite. Therefore, tumor cells are more sensitive to MG compared to healthy cells, and the glyoxalase system is a promising target for anticancer agents.

A number of inhibitors of glutathione system enzymes are currently known that make it possible to control its function at different stages of the metabolic pathway. GCL is the most promising target for the disruption of glutathione biosynthesis in the course of anti-tumor therapy by hindering and disruption of oncogenesis.[500] The best known inhibitors of γ-glutamylcysteine ligase include methionine and buthionine sulfoximines (MSO and BSO, respectively). *In vitro* and *in vivo* studies have shown the prospects of using MSO and BSO in combination with the known chemotherapeutic agents.[511] Moreover, clinical studies showed the safety of BSO administered intravenously.[512]

The inhibition of the glyoxalase system mainly involves the inhibition of the rate-limiting enzyme GloI. The best known GloI inhibitors include S-conjugated glutathione derivatives such as S-alkylglutathiones, S-*p*-bromobenzylglutathione, *etc*.[513] It was shown in *in vitro* studies that S-*p*-bromobenzylglutathione made it possible to overcome multiple drug resistance (MDR) and recover the sensitivity of tumor cells to therapy.[514] Subsequent studies have shown that tumor cell lines with high GloI expression are resistant to current clinical antitumor drugs but sensitive to GloI inhibitors.[515,516]

One of the promising ways for increasing the PDT efficiency is to create combined-action drugs comprising a photosensitizer and a chemotherapeutic agent.[92,517] Examples are known where the chemotherapeutic agent in a combined drug manifests pro-oxidant action that includes the inhibition of the tumor cell defense system against oxidative stress.[518,519]

The purpose of this work was to synthesize and study the photoinduced cytotoxicity of photosensitizers based on natural bacteriochlorins with sulfur-containing molecules capable of affecting the glutathione and glyoxalase systems for photodynamic efficiency improvement. All experimental details are presented in *Supporting Information*.

The sulfur-containing proteinogenic amino acids cysteine and cystine are among the key compounds involved in the redox processes in malignant cells. They undergo reversible enzymatic reactions with glutathione, thus weakening the antioxidant defense of tumor cells. The use of sulfur-containing amino acids in the development of antitumor drugs may shift the redox equilibrium in a tumor cell toward the generation of oxidative stress, which increases the

PDT efficiency.[524,525] Unlike cysteine and cystine, methionine has a methylated thiol group that cannot directly interact with the molecules of the cell's glutathione antioxidant system. However, some tumor cell lines are characterized by enhanced consumption of this amino acid, a phenomenon called "methionine dependence".[626] Therefore, creating a conjugate with this amino acid would increase the tropism of the entire molecule to tumor tissues. Moreover, methionine derivatives, such as L-methionine- and L-butyonine-sulfoximine, are selective inhibitors of the glutathione antioxidant system, including γ-glutamylcysteine synthase. Based on all of the above, it is obvious that creating bacteriochlorin conjugates with sulfur-containing amino acids (cysteine, cystine, methionine and its derivatives) may enhance the photoinduced effect of antitumor therapy due to the action on the redox system of malignancies and enhanced tropism to the latter.

Previously we reported a synthesis of derivatives of *O*-propyloxime-*N*-propoxybacteriopurinimide with cysteine (**2a**), cystine (**2b**), methionine (**3**), methioninesulfoximine (**4**), and buthioninesulfoximine (**5**),[520,521] that involved addition of the above aminoacids and their derivatives to the carboxyl group of the propionic residue at macrocycle position 17 (Scheme 74).

At the first stage of this work, we optimized the conditions for the preparation of DPBP conjugates with esters of sulfur-containing amino acids presented in Scheme 74. The reaction yield was taken as the optimization criterion. To increase it, various agents activating the carboxyl group were studied (Table 6).

Table 6. Reaction conditions in the synthesis of DPBP conjugates with sulfur-containing derivatives (all in inert argon atmosphere during 15 min).

Compound	Reaction conditions, *i*	Yield, %
DPBP-Cys (**2a**)	EEDQ, CH_2Cl_2, 25°C	27
	NHS, CH_2Cl_2, 0°C	19
	DCC, CH_2Cl_2, 0°C	17
	EDC, CH_2Cl_2, 0°C	25
	DCC, NHS, CH_2Cl_2, 0°C	21
	EDC, NHS, CH_2Cl_2, 0°C	41
DPBP-Cys-Cys-DPBP (**2b**)	EEDQ, CH_2Cl_2, 25°C	33
	EDC, CH_2Cl_2, 0°C	28
	EDC, NHS, CH_2Cl_2, 0°C	56
DPBP-Met (**3**)	EEDQ, CH_2Cl_2, 25°C	29
	EDC, CH_2Cl_2, 0°C	28
	EDC, NHS, CH_2Cl_2, 0°C	46
DPBP-MSO (**4**)	EEDQ, CH_2Cl_2, 25°C	31
	EDC, CH_2Cl_2, 0°C	28
	EDC, NHS, CH_2Cl_2, 0°C	48
DPBP-BSO (**5**)	EEDQ, CH_2Cl_2, 25°C	24
	EDC, CH_2Cl_2, 0°C	27
	EDC, NHS, CH_2Cl_2, 0°C	50

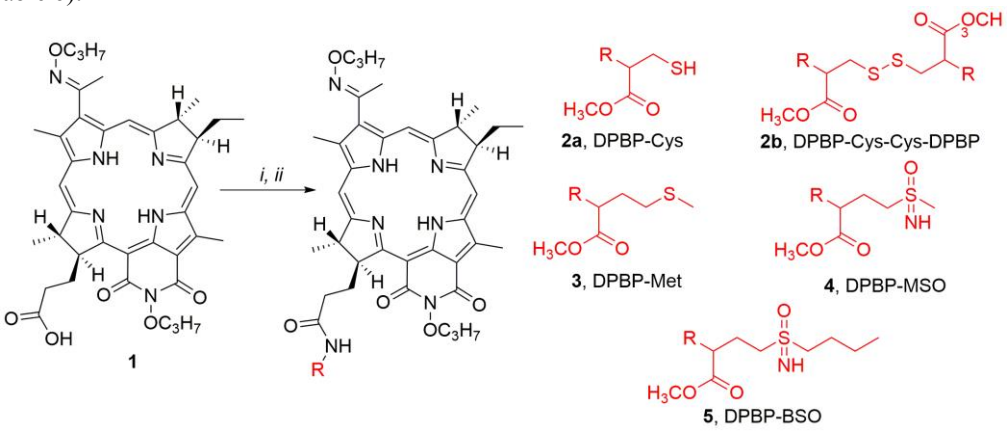

Scheme 74. Reagents and conditions: *i*: provided in the Table 6; *ii*: NH_2-R, CH_2Cl_2, inert argon atmosphere, 25°C, 48 h.

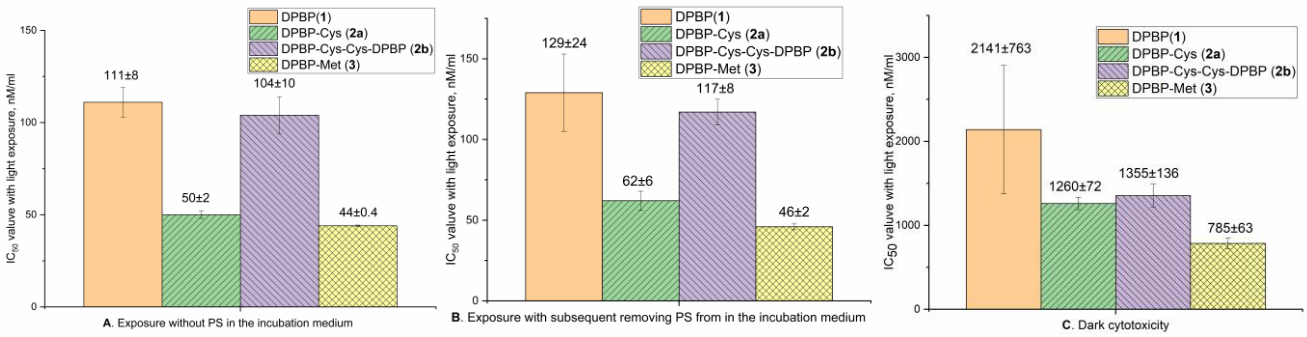

Figure 29. A study photoinduced activity of compounds 1, 2a,b, 3 *in vitro* on HeLa tumor cell line. All compounds were used as Kolliphor ELP 4% micellar solutions: A. Exposure in the presence of PS in the incubation medium. The time of incubation with photosensitizers before exposure to light was 4 h. The power density was 21.0 ± 1.0 mW/cm^2 and the calculated light dose was 10 J/cm^2; B. Exposure without PS in the incubation medium. The time of incubation with photosensitizers before exposure to light was 4 h. The power density was 21.0 ± 1.0 mW/cm^2 and the calculated light dose was 10 J/cm^2; C. Dark cytotoxicity.

The combination of 1-ethyl-3-(3-dimethylaminop-ropyl)-carbodiimide (EDC) and *N*-hydroxysuccinimide (NHS) as the activating agents was found to be the best. They were considerably superior to *N*-ethoxycarbonyl-2-ethoxy-1,2-dihydroquinoline (EEDQ) and 1,3-dicyclohexylcarbodiimide (DCC) and allowed the reaction yield to be increased by a factor of 1.5-2. Due to the high solubility of EDC in water, multiple extractions can be avoided, while addition of NHS produces a stable activated derivative of *O*-propyloxime-*N*-propoxybacteriopurpurinimide with *N*-succinimide.

In the previous model experiments, we observed a reversible transition of the free thiol group to the oxidized disulfide form.[520] Therefore, in this work we were the first to estimate the *in vitro* antitumor photodynamic efficacy of DPBP-Cys (**2a**), DPBP-Cys-Cys-DPBP (**2b**), and DPBP-Met (**3**) derivatives that can affect the glutathione system of tumor cells.

*Study of photo-induced antitumor activity of DPBP-Cys (**2a**), DPBP-Cys-Cys-DPBP (**2b**), and DPBP-Met (**3**) in vitro*

The HeLa cell line with elevated levels of intracellular glutathione was selected for *in vitro* biological tests.[497] The time of incubation with compounds before light exposure was 4 h, while the incubation time of cells after irradiation was 24 h. The cells were irradiated with a standard light dose of 10 J/cm^2 with an exposure time of 13 min. The starting compound, *O*-propyloxime-*N*-propoxybacteriopurpurinimide (**1**), was chosen as the reference compound. The survival of tumor cells was assessed both visually using an inverted microscope and by the MTT test. The results of the latter are shown in Figure 29.

The half-maximum inhibition concentration (IC_{50}) of compounds (**2a**) and (**3**) after 4 hours of cell incubation was 2-3 times smaller than that of the reference compound *O*-propyloxime-*N*-propoxybacteriopurinimide (**1**), both under exposure to light in the presence of PS in the incubation medium (Figure 29A) and under exposure to light after PS removal from the incubation medium (Figure 29B). The IC_{50} of the dimeric compound (**2b**) was slightly larger and comparable to that of the original compound (**1**). The dark cytotoxicity of compounds (**2a**) and (**2b**) was slightly higher than that of derivative (**3**) (Figure 29C).

Since the photoinduced IC_{50} of DPBP-Cys-Cys-DPBP (**2b**) was higher than that of cysteine (**2a**) and methionine (**3**), only DPBP-Cys (**2a**) and DPBP-Met (**3**) were selected for *in vivo* biological studies.

*Study of the photoinduced antitumor activity of DPBP-Cys (**2a**), DPBP-Met (**3**) in vivo*

The accumulation kinetics of DPBP-Cys (**2a**) and DPBP-Met (**3**) in a tumor compared to healthy tissues was studied on a tumor model of mouse sarcoma S37 using local electron spectroscopy. After intravenous injection, both drugs showed accumulation of the compounds of interest in the tumor with the maximum accumulation at 180 and 270 min, respectively (Figure 30). The fluorescence contrast in the accumulation maxima was 3.09 and 5.86 for DPBP-Cys (**2a**) and DPBP-Met (**3**), respectively.

The data obtained indicate that accumulation of DPBP-Cys (**2a**) and DPBP-Met (**3**) in the tissues of malignant neoplasms occurs, which, in combination with the restricted area of light exposure, provides an efficient tool for tumor targeting. Moreover, the maximum accumulation times of the compounds lie in the range convenient for the photodynamic therapy procedure.

At the next step, the photoinduced antitumor activity of DPBP-Cys (**2a**) and DPBP-Met (**3**) was studied *in vivo* using various irradiation modes. The dose of both photosensitizers was 5 mg/kg; DPBP (**1**) whose accumulation kinetics was studied previously was taken as the reference drug.[527] To select the optimal light dose, two irradiation modes with light doses of 150 J/cm^2 and 300 J/cm^2 at a radiation power density of 0.2 W/cm^2 were used. The PDT procedure was performed at the time points when the maximum accumulation of drugs took place (15 min, 180 min, and 270 min after intravenous injection of DPBP (**1**), DPBP-Cys (**2a**), and DPBP-Met (**3**), respectively).

Analysis of the growth dynamics of the primary tumor node showed that the highest antitumor effect was shown by the DPBP-Met compound **3** (Figure 31). The optimal PDT conditions for this compound are: a photosensitizer dose of 5 mg/kg, an interval of 270 min between its injection and the beginning of irradiation, and a light dose of 300 J/cm^2.

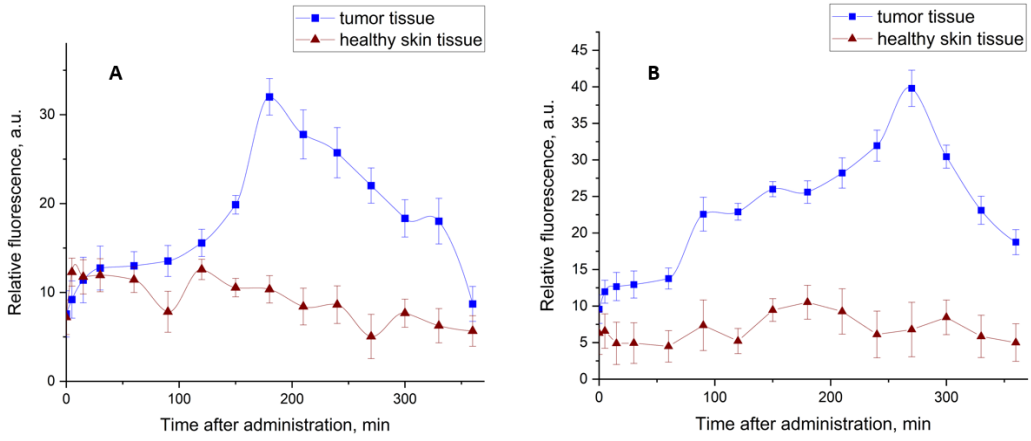

Figure 30. Accumulation kinetics of compounds **2a** (A) and **3** (B). The content of compounds in the samples was determined *in vivo* by local electron spectroscopy on sarcoma S37 tumor-bearing mice. The ratio of areas under the curves of fluorescence and laser reflection peaks was estimated.

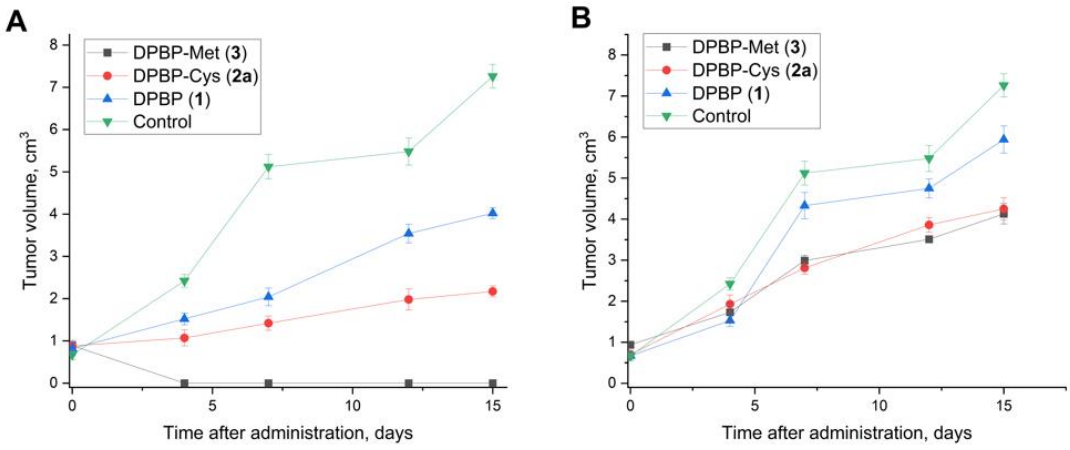

Figure 31. The growth dynamics of the primary tumor node in irradiation modes of 300 J/cm^2 (A) and 150 J/cm^2 (B) and at a photosensitizer dose of 5 mg/kg. The animals were monitored for 15 days after the PDT procedure. The anti-tumor effect was estimated from the dynamics of primary tumor growth in the experimental and control groups.

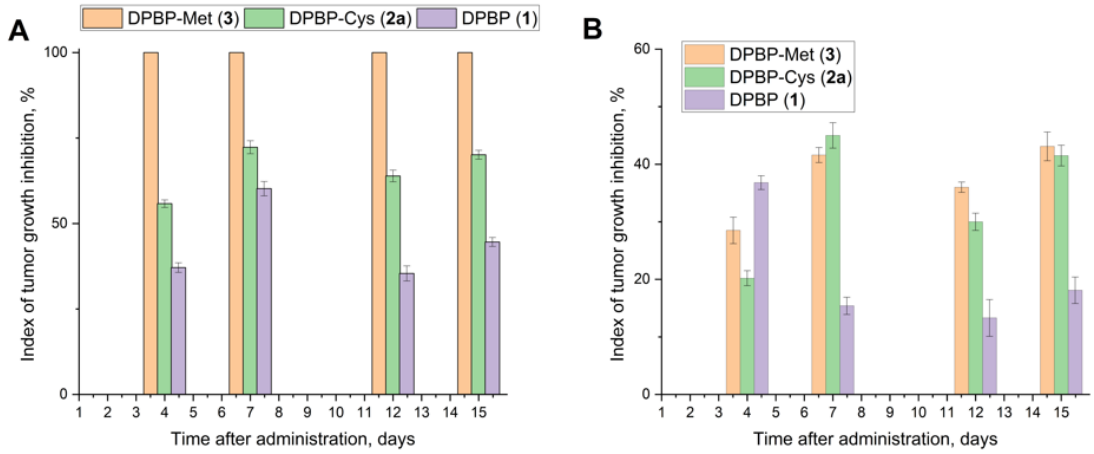

Figure 32. Tumor growth inhibition in experimental and comparison groups in irradiation modes of 300 J/cm^2 (A) and 150 J/cm^2 (B) and at a photosensitizer dose of 5 mg/kg. The animals were monitored for 15 days after the PDT procedure.

Using this PDT mode with DPBP-Met (**3**), complete resorption of the tumor node was achieved on day 4 after the treatment. The figure shows the tumor growth inhibition (TGI) data in two irradiation modes, 150 J/cm^2 (A) and 300 J/cm^2 (B) (Figure 32).

Thus, the *in vivo* studies on the biological properties of DPBP-Cys (**2a**) and DPBP-Met (**3**) indicated that the methionine methyl ester derivative (DPBP-Met (**3**)) has a two times higher selectivity of accumulation in the tumor tissue than the cysteine derivative **2a**. Moreover, the photoinduced antitumor activity of the DPBP-Met derivative (**3**) at a light dose of 300 J/cm^2 was higher than that of DPBP (**1**) and DPBP-Cys (**2a**).

Synthesis of DPBP conjugates with sulfur-containing inhibitors of enzymes of the glutathione and glyoxalase systems

Inhibitors of γ-glutamylcysteine synthase and glyoxalase I were used as sulfur-containing molecules capable of affecting the glutathione and glyoxalase systems and possessing antitumor activity. Inhibition of these enzymes should increase the efficiency of photoinduced antitumor therapy and reduce dark toxicity through the intracellular targeted impact on tumor cells.

Methionine and buthionine sulfoximines were chosen as potent γ-glutamylcysteine synthase inhibitors. Their conjugation with DPBP (**1**) was performed as described in our previously studies and resulted in conjugates DPBP-MSO (**4**) and DPBP-BSO (**5**).

S-Hexylglutathione dimethyl ester (**8**) was chosen as the glyoxalase I inhibitor. The esters of this class of compounds are known to have greater antitumor activity than the analogues with free carboxyl groups.[528] Initial attempts to obtain S-hexylglutathione dimethyl ether (**8**) by a conventional technique in acid medium failed to give the expected result, which seems to be due to the formation of a side product of S-hexylglutathione cyclization. Therefore, dimethyl ether (**8**) was obtained using diazomethane (Scheme 75).

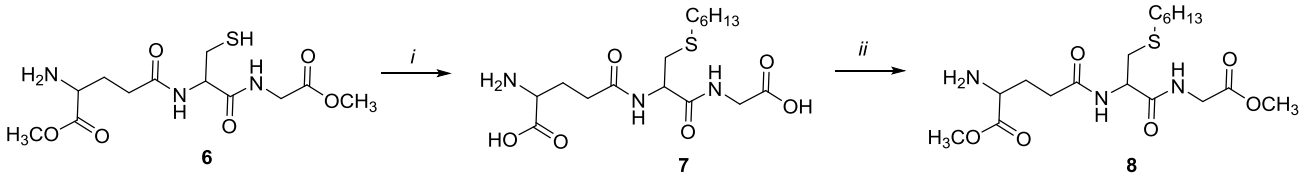

Scheme 75. Synthesis of S-hexylglutathione dimethyl ether (8). Reagents and conditions: *i*: 1-iodohexane, 1M aqueous NaOH, EtOH, inert argon atmosphere, 25°C; *ii*: CH_2N_2, Et_2O.

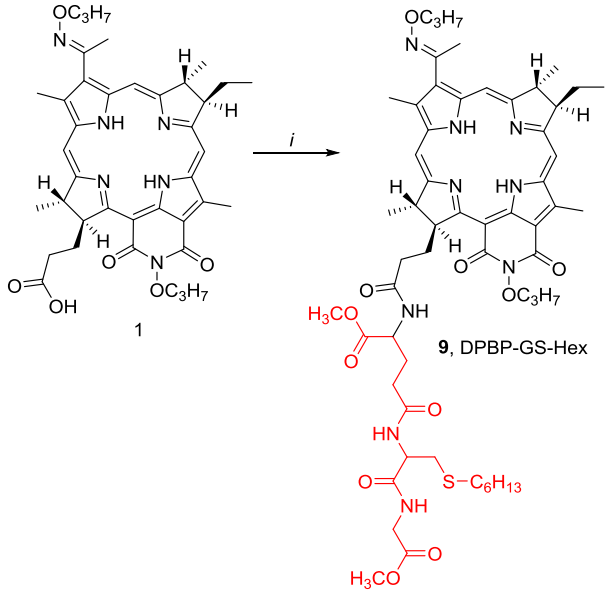

Scheme 76. Reagents and conditions: *i*: compound 8, EDC, NHS, CH_2Cl_2, inert argon atmosphere, 25°C.

At the next step, S-hexylglutathione dimethyl ether was added to the free carboxyl group of O-propyloxime-N-propoxybacteriopurinimide (**1**) using the optimized reaction conditions shown in Table 6 (Scheme 76).

The spectral characteristics of the pigment thus obtained did not differ from those of the original DPBP (**1**). The absorption maximum in the long-wave spectrum region for all the sulfur-containing conjugates (**2-5**, **9**) was 800 nm.

Study of the photoinduced antitumor activity of DPBP-GS-Hex, DPBP-MSO and DPBP-BSO in vitro

At the final stage of this work, the photoinduced cytotoxicity of all the resulting conjugates of *O*-propyloxime-*N*-propoxybacteriopurinimide with sulfur-containing amino acids (**2-5**) and with S-hexylglutathione dimethyl ether (**9**) was studied *in vitro* on the Hela tumor cell line. The time of incubation with compounds before light exposure was 4 h, while the incubation time after irradiation was 24 h. Cells were irradiated with a standard light dose of 10 J/cm^2, the exposure time was 13 min. The starting compound, *O*-propyloxime-*N*-propoxybacteriopurpurinimide (**1**), was chosen for comparison. Tumor cell survival was estimated both visually using an inverted microscope and by the MTT test whose results are presented in Table 7.

The highest photoinduced cytotoxicity *in vitro* was observed for compounds DPBP-MSO (**4**), DPBP-BSO (**5**), and DPBP-GS-Hex (**9**) than have 5-6 times lower IC_{50} than *O*-propyloxime-*N*-propoxybacteriopurinimide (**1**) and 2-3 times lower IC_{50} than the conjugates with cysteine (**2a**) and methionine (**3**), both upon exposure to light in the presence of PS in the incubation medium and upon exposure to light followed by removal of PS from the incubation medium. The lowest cytotoxicity without light exposure (dark cytotoxicity) was shown by DPBP-GS-Hex (**9**).

In conclusion, DPBP derivatives with sulfur-containing amino acids were obtained previously in our works.[520,521] In this work, we have optimized the reaction conditions for the amidation of *O*-propyloxime-*N*-propoxybacteriopurinimide with sulfur-containing amino acids and modified glutathione, which allowed us to increase the yield of the target derivatives by a factor of 1.5-2.

Table 7. Photoinduced cytotoxicity *in vitro* of sulfur-containing compounds on HeLa tumor cells.

Compound	Exposure in the presence of PS in the incubation medium	Exposure with subsequent removing PS from in the incubation medium	Dark cytotoxicity
	IC_{50} value, nM		
DPBP (**1**)	111 ± 8	129 ± 24	2141 ± 763
DPBP-Cys (**2a**)	50 ± 2	62 ± 6	1260 ± 72
DPBP-Cys-Cys-DPBP (**2b**)	104 ± 10	117 ± 8	1355 ± 136
DPBP-Met (**3**)	44 ± 0.4	46 ± 2	785 ± 63
DPBP-MSO (**4**)	16 ± 1	20 ± 5	232±27
DPBP-BSO (**5**)	20 ± 0.7	21 ± 2	485±63
DPBP-GS-Hex (**9**)	24 ± 4	27 ± 3	2042±981

The *in vivo* biological studies of solubilized DPBP conjugates with methyl esters of cysteine **2a** and methionine **3** on tumor-bearing mice with subcutaneously inoculated sarcoma S37 were performed for the first time. Methionine derivative **3** was found to have a 1.9-fold higher selectivity of accumulation in tumor tissue than cysteine derivative **2a**. Moreover, the photoinduced antitumor activity of compound **3** under the conditions used (5 mg/kg, light dose 300 J/cm^2) was found to be higher than that of the reference compound DPBP **1** and cysteine-based pigment **2a**.

A new derivative **9** of natural bacteriochlorophyll *a* with an inhibitor of the glutathione-dependent enzyme glyoxalase I, was obtained.

All the sulfur-containing bacteriochlorin conjugates obtained were studied *in vitro* on Hela tumor cells, and their photoinduced cytotoxicity was shown to increase in comparison with the parent compound **1**. This pattern shows a beneficial role of sulfur-containing compounds in the manifestation of photodynamic activity and suggests that the development of such PS for antitumor PDT is a promising approach.

12. Antitumour Efficacy of Photodynamic Therapy of Experimental Laboratory Animal Tumours with a New Photosensitizer of Chlorin Series

Most photosensitizers used for photodynamic therapy in clinical practice are derivatives of chlorin e_6. To date, research aimed at increasing the anti-tumour efficiency of PS continues. It is known that only high-purity chlorin e_6 has the most pronounced photodynamic properties, and the presence of related chlorine and the other ingredients in the dosage form significantly impairs the properties of the photosensitizer. Concomitant chlorines have a much lower quantum output of singlet oxygen and less accumulation in tumour tissues. This requires the application of a higher light dose and leads to blurring of the clear boundary during the PDT session and, as a result, significant damage to healthy tissues adjacent to the tumour node.[529] The presence of polyvinylpyrrolidone in the composition of the medicinal form of the photosensitizer leads to increased viscosity of the injectable solutions and makes it impossible to apply a rapid and convenient method of jet administration, replacing it with only drip intravenous administration. Thus the presence of impurities reduces the effectiveness of chlorine PSs. As a result, the improvement of PS is now on course to achieve the highest possible purity of chlorin e_6 in a sustainable form.

The new photosensitizer Heliochlorin, developed by Professor G.V. Ponomarev and co-authors,[70] is available in a lyophilically dried form, including trismeglumin salt of chlorin e_6 and meglumin as a cryostabilizer. Heliochlorin is a PS based on highly purified chlorin e_6 from methyl pheopharbide *a*, with a high core content of 93-98%.

The study of the antitumor efficacy of PDT with the Heliochlorin on the models of murine Erlich carcinoma and rat sarcoma M-1 showed that treatment at the optimal time after intravenous administration of PS with certain parameters of laser exposure allowed to achieve complete regression of tumour nodes and no recurrence within 90 days after therapy in 100% of animals.

The animal experiments were conducted in a strict accordance with the Guidelines for the Care and Use of Laboratory Animals of the National Medical Research Radiological Centre of the Ministry of Health of the Russian Federation and in accordance with the rules and requirements of the European Convention ETS/STE No. 123 and international standard GLP (OECD Guide 1:1998).

Table 8. Experiment Design.

Tumour	Test system	Group	PS dose, mg/kg	Mode of administration	Laser action parameters	
					E, J/cm^2	Ps, W/cm^2
Ehrlich's carcinoma	mice	1 group-PDT	2.5	intravenously	150	0.48
		1 control	-	-	-	-
		2 group-PDT	5.0	intravenously	150	0.48
		2 control	-	-	-	-
Sarcoma M-1	rats	3 group-PDT	2.5	intravenously	150	0.48
		3 control	-	-	-	-
		4 group-PDT	5.0	intravenously	150	0.48
		4 control	-	-	-	-

This study was performed using sarcoma M-1 bearing outbred female rats (totally 32 animals) at three months of age weighting on average 180-200 g and 48 female outbred mice two months old, 19-20 g weight with implanted Erlich carcinoma. The animals were housed in T-3, T-4 cages under the natural light conditions with the forced ventilation of 16 times/h, at a room temperature and relative humidity of 50–70%. The animals had free access to water and PK-120-1 feed for rodents (Laboratorsnab Ltd., Moscow, Russia). The tumour strains was obtained from the tumor bank of the N.N. Blokhin National Medical Research Center of Oncology of the Ministry of Health of Russian Federation. Sarcoma M-1 was implanted subcutaneously as a 1.0 mm^3 piece of donor tumour into the outer side of the left thigh. The experiment was started 8-9 days after transplantation, when the largest diameter of the tumour nodes reached 0.8-1.0 cm. Erlich's ascitic carcinoma liquid with 2.5×10^6 tumour cells from the donor mice was injected subcutaneously into the area of the lateral surface of the left thigh of mice. The experiment was started 4 days after transplantation, when

the largest diameter of the tumour nodes reached 0.4-0.6 cm. The experimental and control groups containing eight rats and twelve mice each. As the series with the different treatment regimens were not performed simultaneously, each series had its own control. As a control, we studied tumour-bearing animals without any exposure. The session of photodynamic therapy was performed, as described previously.[530] The animals of the experimental groups received the PS in doses of 2.5 and 5.0 mg/kg into the caudal vein. The tumours were exposed to the laser irradiation using an Atkus-2 semiconductor device (Atkus, Russia; λ = 662 nm, diameter of the light spot = 1 cm for mice and 1.5 cm for rats). The following doses of laser irradiation were tested: E = 150 J/cm^2; Ps = 0.48 W/cm^2 (Table 8). In our preliminary studies the optimal time of beginning of laser action after administration of the drug (drug-light interval) was determined: 45-60 min after intravenous administration of PS to mice and 60-75 min to rats.[531] The results were analyzed in the seventh, fourteenth, twenty-first and ninetieth days and compiled in Table 9. The antitumor efficacy of the PDT was assessed according to the criteria described earlier.[532,533]

After the PDT, there was a pronounced swelling of soft tissue in the irradiation zone, which is a natural reaction to photodynamic tumor damage with any known PS. The swelling was accompanied by hyperemia of the radiation zone and surrounding soft tissue. Tissue alteration was observed and, depending on the size of the surface to be irradiated, a thick scab of dark color was formed for 2-4 days after treatment.

Up to 21 days after photodynamic exposure (with a PS dose of 5.0 mg/kg and laser exposure parameters: E=150 J/cm^2; Ps=0.48 W/cm^2) an inhibition effect was observed on murine Erlich carcinoma in all experimental animals, and remained up to 3 months in 100% of animals. When the PS dose was reduced to 2.5 mg/kg at the same light dose, the complete tumour regression was observed to 21 days. Later on, some animals relapsed into tumour for 90 days after therapy, however, the percentage of cured animals was 66.7% (Table 9) and 33.3% of mice with relapse tumors increased their life expectancy by 45% compared to control (Table 10). All the control groups mentioned above demonstrate continuous tumor growth (see Table 9).

After PDT of rat sarcoma M-1 with the following parameters: the PS doses 2.5 and 5.0 mg/kg and dose of light: E=150 J/cm^2; Ps=0.48 W/cm^2 up to 90 days after therapy total regression of tumor in 100% of animals was observed (Table. 9).

Table 9. Anti-tumour efficacy of murine Erlich carcinoma and rat sarcoma M-1 PDT with intravenous administration of Heliochlorin (laser action parameters E = 150 J/cm^2; Ps = 0.48 W/cm^2).

No. gr.	PS dose, mg/kg	Observation period, days of			
		7	14	21	90
		Erlich's carcinoma of mice			
1	2.5		(2 and 3) 100%		(4) 67%
2	5.0		(2 and 3) 100%		(4) 100%
Control 1+2		(1) 0.09±0,02	(1) 0.94±0,16	(1) 4.05±2.43	-
		Sarcoma M-1 rats			
3	2.5		(2 and 3) 100%		(4) 100%
4	5.0		(2 and 3) 100%		(4) 100%
Control 3+4		(1) 2.7±0.5	(1) 10.2±2.1	(1) 17.1±4.2	-

Note: (1) Tumor volume (V, cm^3); (2) Tumor growth inhibition (TGI, %); (3) Percentage of animals with full tumor regression (R); (4) Percentage of completely cured animals.

Table 10. The life expectancy of animals (days) and an increase in the mean life span of animals (%) after PDT compared to control.

PS dose, mg/kg	Life expectancy	Increase in the mean life span of animals, %
	Mice	
2.5	86.0±4.0	45
5.0	>90	>100*
control	59.3±3.0	-
	Rats	
2.5	>90	>100*
5.0	>90	>100*
control	37.3±2.2	-

*Significant increase in the mean life span of animals compared to control;
>90 days and > 100% of animals with full tumour regression, no recurrence until 90 days after PDT, are removed from the experiment with the help of essential anesthesia.

Thus, the new chlorin e_6 derivative drug - Heliochlorin is an effective photosensitizer. Photodynamic therapy of experimental malignant tumours: murine Erlich carcinoma and rat sarcoma M-1 showed high photodynamic activity of the drug. Treatment involving intravenous administration of Heliochlorin at doses of 5.0 mg/kg (murine Erlich carcinoma) and 2.5 mg/kg (rat sarcoma M-1) at optimal time between administration of the drug and laser treatment with energy density 150 J/cm^2 and power density 0.48 W/cm^2 allowed to achieve the maximum therapeutic effect - complete tumor regression in 100% of animals and no recurrence of neoplasms up to 90 days after treatment. It has thus been shown that Heliochlorin has a pronounced antitumor activity for photodynamic therapy when administered at lower doses and at lower laser effects than other known chlorin drugs, clinical.

13. Clinical Application of Photodynamic Therapy

To date, in clinical practice, new methods of treatment based on the photochemistry achievements, photobiology and quantum physics are increasingly spreading. Photodynamic therapy (PDT) is a completely new technology used in the treatment of various diseases.[534-536]

Photodynamic therapy is highly effective and side effects and complications are minimal at the same time. This method is based on the selective accumulation of a photosensitizing substance in the tissue of a malignant tumor, followed by the chemical reaction development that causes the destruction of sensitized substances under the influence of a laser beam of a certain wavelength and power. PDT has no negative effect on nearby tissues and organs. Healing occurs according to the type of natural reparative processes; therefore, the method is organ-preserving, well-tolerated and permissible with repeated use.[537,538]

In the last decade, an increasing number of specialists have turned to studying the possibilities of this method in various fields of medicine.

Photodynamic therapy is widely and successfully used in purulent surgery; there is a pronounced antibacterial and anti-inflammatory effect. Resistance to PDT in the treatment of chronic infectious processes in pathogenic microorganisms does not develop. Recently, PDT of purulent wounds has been carried out using photosensitizers of the chlorin series and has a positive effect on the course of the wound process which is manifested by a pronounced antibacterial effect accelerating the cleansing of wounds from purulent-necrotic detritus and shortening the healing time of wound defects.[539]

By A.V. Heinz and co. a clinical study was conducted on the treatment of 120 patients with purulent and long-term non-healing soft tissue wounds of various etiologies and localization using the photoditazin photosensitizer (VETA-GRAND LLC, Russia, registration certificate No. LS 001246 of 18.05.2012) in the form of a gel. According to the results, it was concluded that this method of treatment contributes to reducing the time of wound cleansing from purulent-necrotic detritus, the appearance of granulations and reducing the timing of the epithelialization onset by 1.5–2 times. It also reduces the time of complete healing of purulent wounds by 5-7 days compared with traditional treatment.

It is important to note that the developed PDT method of purulent wounds using photosensitizers of the chlorin series provides a reduction in the time of granulation and complete healing of purulent wounds.

The effectiveness of PDT does not depend on the spectrum of sensitivity of pathogenic microorganisms to antibiotics and has a detrimental effect on antibiotic-resistant strains of *Staphylococcus aureus, Pseudomonas aeruginosa* and other bacteria. Photodynamic damage is caused by the cytotoxic effect of singlet oxygen and free radicals, therefore, the development of resistance of microorganisms to PDT is minimal. It should be noted that with prolonged treatment of local infectious processes, the antimicrobial effect of PDT does not weaken, and the bactericidal effect is local in nature and does not have a systemic detrimental effect on the saprophytic flora of the body.

In the field of endocrinology, the results of treatment of 72 patients with trophic ulcers who underwent PDT with photoditazine in the form of a gel, both in an independent version and in combination with NO-plasma therapy were analyzed. It was concluded that PDT accelerates the cleansing of wounds from devitalized tissues, normalizes microcirculatory disorders and stimulates fibroblast proliferation and granulation tissue maturation. It also enhances phagocytosis promotes the epithelization of ulcerative defect on the 12th-15th day.[540]

Of no small importance is the use of PDT in arthroscopy for the arthrosis treatment and other inflammatory processes in large human joints. The results of treatment of 11 patients with deforming arthrosis, synovitis and bursitis who underwent PDT with the drug photoditazine have been published. The drug was administered intravenously at the rate of 0.05 mg/kg of the patient's body weight. After PDT, the swelling in the projection of the lesion decreased; the intensity of the severity of the pain syndrome and the local temperature reaction of the skin was normalized.[543] Treatment results analysis of 86 patients aged 4 to 17 years with a clinical diagnosis of rheumatoid arthritis, who underwent PDT with the drug photoditazine in the form of a gel, showed that this method eliminates the main clinical symptoms and is highly effective in the treatment of inflammatory diseases of the joints.

Clinical trials have been successfully launched in many countries of the world to study the effectiveness of PDT in the treatment of ophthalmic diseases, in particular, such as neovascularization.

The results of PDT treatment effectiveness study in Russia with photosens (FSUE "SSC "NIOPIC", Russia, registration certificate RN000199/02 dated 04.03.2010) as monotherapy and combination of PDT with anti-VEGF in 38 patients with age-related macular degeneration have been published. According to the angiographic picture of the fundus and the average thickness of the retina in the foveolus, patients have increased visual acuity, the activity of the subretinal neovascular membrane has decreased after treatment.[541]

These guides indicate the effectiveness of the PDT method with the drug photosens in the treatment of patients with subretinal neovascular membrane against the background of age-related macular degeneration.

PDT is used in otorhinolaryngology to improve the treatment effectiveness of patients with ear throat and nose purulent-inflammatory diseases, in conditions of reduced immunity and increased resistance to antibiotics. The results of PDT in the treatment of purulent sinusitis in 41 patients with the photosensitizer radachlorin (LLC "RADA-PHARMA", Russia, registration certificate No.LS-001868 dated 12/16/2011) have been published. Treatment results analysis showed high efficiency of PDT. 38 patients had a complete cure; in 3 patients, a significant decrease in the titers of the detected pathogen was noted in the absence of clinical signs of the disease.[542]

Data from a number of studies confirm that the use of PDT in the toxic-allergic form allows to achieve stable remission and in simple forms of chronic tonsillitis to complete cure of the disease.

For many years, specialists have been investigating the problem of respiratory papillomatosis. Laryngeal papilloma is a benign tumor but is prone to rapid growth and frequent recurrence. Etiotropic therapy of this disease does not exist to this day. Photodynamic therapy is actively used

as an alternative method of treating this disease. Russian authors report on the results of treatment of 19 patients diagnosed with respiratory papillomatosis by PDT with radachlorin. After PDT, therapeutic effect was registered in all patients; complete eradication of PVI was 77%. The appearance of scars in the larynx and trachea or the aggravation of the existing scarring process has not been recorded.[543]

Currently, the main role in the pathogenesis of the precancerous and tumor pathology of the cervix development belongs to HPV of high oncogenic risk, namely 16, 18, 31, 33, 45 and 52 types. Russian authors report on the treatment results of 104 patients diagnosed with dysplasia of the II-III stage and cancer in situ of the cervix associated with highly oncogenic HPV genotypes with the drug photogem. After PDT, complete eradication of HPV DNA was achieved in 94% of cases and partial eradication of HPV was diagnosed in 6% of cases. This is the evidence of a pronounced antiviral effect of treatment.[544]

The incidence of epithelial malignant neoplasms of the skin is increasing annually. Basal cell skin cancer (BCC) accounts for a large proportion of them. One of the most effective, minimally invasive and organ-preserving methods of skin epithelial malignant neoplasms treatment is PDT. Photodynamic damage effectively destroys the tumor and pathological tissues preserving the surrounding healthy ones as much as possible.[545]

The positive effect in the treatment of skin cancer by PDT varies between 70-100% and depends on the localization of the tumor process and the stage, the dose of the photosensitizer and the chemical structure as well as the parameters of laser irradiation. Complete regression of tumors is registered in 75-80% of patients, and the duration of the relapse-free period ranges from 2 months to 5 years.[546,547]

The PDT method is successfully used for inconvenient localization of tumors with the absence of cosmetic defects in the form of gross deformation. PDT is indicated for tumors resistant to previously conducted methods of traditional therapy.

Along with primary and recurrent malignant tumors, a special place is occupied by metastatic lesions of the skin. According to the literature, the frequency of metastases of cancer of internal organs to the skin ranges from 0.29 to 3.3%.[548] Of the metastatic malignant skin tumors, the largest group is breast cancer.

A group of authors performed PDT with domestic photosensitizers in 36 patients with intradermal metastases. When using prolonged PDT in patients with intradermal metastases of breast cancer and melanoma, complete regression of tumors was obtained in 39.3% and 38%, respectively, partial – in 46% and 52.4%. Against the background of previously conducted traditional therapy, tumor resistance to traditional treatment was noted in all patients.[549]

Kaposi's sarcoma is a rare angioproliferative disease that is associated with human type 8 herpesvirus. PDT is the most promising method of its treatment. According to the results of treatment of 15 patients with intra-tumor administration of domestic photosensitizers using PDT, a positive clinical effect was noted by improving the general condition of patients and reducing the area of tumor lesion, which in turn leads to an improvement in the patients life quality.

Lung cancer occupies the first place in the structure of morbidity and mortality from malignant neoplasms. The surgical method of treatment is used for early central lung cancer. At the same time, about 20-50% of patients are inoperable. Photodynamic therapy can be used in combination with classical methods; therefore, it is more promising.[550] Some authors argue that the effectiveness of PDT in early central lung cancer (CRL) depends on the form of growth and size of primary bronchial cancer. Thus, with a superficial type of tumor (up to 5 mm), complete regression with PDT is achieved in 91% of cases, from 5 to 10 mm — in 89.4%. In nodular and polypoid types of tumors with a diameter of up to 5 mm, complete regression was noted in 93.7% of cases, and in tumors from 5 to 10 mm — in 62.0%.[551] A number of other authors after PDT in 99 patients with early CRL in art. IA with tumors up to 1 cm in diameter, complete regression was observed in 95% of patients, with tumors of 2 cm or more — in 46%. An excellent PDT result was indicated when the tumor size was up to 1 cm when the distal border of the tumor was clearly visible during bronchoscopy. In this case, full regression was achieved in 98% of the observations. Tumor recurrence was diagnosed in 13% of patients.[552] Experts from the UK noted that 517 patients had a 5-year survival rate of 70% with complete regression of the tumor. In the USA, in one of the PDT clinics, complete tumor regression was achieved in 69.5% of cases. A new focus of metachronous lung cancer was detected in 24% during further follow-up.[553]

A number of Russian researchers report the results of PDT of early CRL in 37 patients with domestic photosensitizers (photogem, radachlorin, photosens). In 87% of patients, complete regression of the tumor was noted.

According to the data of many authors, PDT CRL is a highly effective method and has no equal analogues, especially in patients with primary multiple bronchial lesions as well as with a high risk of complications of surgical treatment.

PDT is an alternative method for the stenosing malignant neoplasms treatment of the respiratory tract, such as lung atelectasis and pneumonia. There is information about PDT with domestic photosensitizers in 55 patients with stenosing malignant lung tumors of central localization. This group of patients had a positive clinical effect after treatment.

Recently, intrapleural prolonged PDT with the drug photosens has been used to treat tumor pleurisy in primary and metastatic lesions of the pleura. According to some authors, conducting such therapy in patients with mesothelioma and metastatic pleural lesion makes it possible to achieve a stable cessation of intrapleural exudation in 92% of patients with a follow-up period of up to 3.5 years.

To date, serious experience has been accumulated in the use of PDT in the early cancer treatment of the esophagus and stomach. This method allows to be applied repeatedly in the form of multi-course treatment with an interval of several months. Conducting a multi-course PDT is possible for many years.

In 116 patients (121 tumor foci), photodynamic therapy was performed for initial cancer of the esophagus and stomach with intravenous administration of domestic photosensitizers. Complete regression was achieved in 90 (74.4%) foci and partial regression was achieved in 31 (25.6%) tumor foci.[554]

Based on the above, it can be concluded that with the use of PDT, high oncological results can be achieved in the treatment of initial forms of esophageal and stomach cancer.

Tumor lesion of the digestive tract aggravates the condition of patients and reduces the quality of life. PDT is an alternative method of palliative care in inoperable patients with stenosing cancer of the upper digestive tract. The only method of eliminating tumor stricture is photodynamic therapy for recurrent dysphagia after stenting due to tumor germination through the walls of the prosthesis or tumor growth above or below the stent. The recanalization effect lasts on average 3 months. Repeated PDT also has a beneficial effect on the recurrence of dysphagia. To achieve the highest quality of life in patients of this group, a multicourse PDT is recommended.[555,556]

Stomach cancer ranks second in the structure of cancer mortality. At the time of diagnosis, in 70% of patients, the tumor process is locally widespread and is the cause of high mortality in the first year after diagnosis. A search is underway for new methods of specialized therapeutic effects on the area of the surgical field and peritoneum. Intraoperative PDT is one of such methods. The researchers note that the use of intraoperative PDT with domestic photosensitizers in patients with peritoneal dissemination in disseminated gastric cancer in combination with palliative surgical treatment to increase the duration of the relapse-free period and the overall survival of patients in this group is effective and safe.

Among all malignant neoplasms of the genitourinary system, bladder cancer accounts for 70%. Surgical treatment in the volume of transurethral resection within healthy tissues to the muscle layer is the main method of treatment. But at the same time, the percentage of relapses does not decrease and is 40-90% in the first year of follow-up. Currently, PDT is one of the most promising areas of relapse prevention.

A number of experts indicate that when using PDT with 5-aminolevulinic acid as adjuvant therapy, the relapse-free survival was more than 2.3 years in every second patient.[557]

Some authors report surgical treatment (transurethral resection of the bladder) followed by adjuvant PDT with domestic photosensitizers and intravesical chemotherapy in 35 patients with non-muscularly invasive bladder cancer. During the observation period, no signs of progression or recurrence of the tumor process were found.[558]

Therefore, as an adjuvant treatment, PDT in combination with chemotherapy or bladder TUR is a promising method that allows achieving high oncological results in the treatment of initial forms of bladder cancer.

The high frequency of precancerous diseases and early cervical cancer in the structure of gynecological pathology in young women significantly disrupts reproductive function and is an urgent problem. The human papillomavirus (HPV) plays a major role in the carcinogenesis of the cervix.

One of the newest approaches to the treatment of cervical pathology, combining optimal therapeutic effect and the absence of undesirable complications, is PDT. This method has both antitumor and antiviral effects aimed at both the lesion site and the source of permanent HPV infection of the epithelial layers.

In the study of B. Monk, PDT of dysplastic changes in the cervical epithelium and preinvasive cancer was performed with local application of photophrine with an exposure time of 24 h and an energy density of 100-140 J/cm2. Out the 11 patients (73%), 8 showed complete regression of pathological changes.

Russian researchers conducted a comparative analysis of PDT results in 195 women with dysplastic changes and early cervical cancer with intravenous administration of domestic photosensitizers. All patients were diagnosed with HPV types 16/18. Antitumor and antiviral effects were evaluated after PDT. A complete regression of the tumor was diagnosed in 178 people, partial – in 6, stabilization - in 11 people. Complete eradication of the virus was diagnosed in 182 people, partial – in 8 people and no effect in 5 patients.

It is important to note that PDT for precancerous and early cervical cancer is an effective organ-sparing treatment method that allows the patient to be cured, as well as contributes to her medical and social rehabilitation.

In addition, PDT can be considered as a method of secondary prevention of cervical cancer in viruspositive women and used as an independent method of treatment in this contingent of patients. PDT is an alternative method of treatment of precancerous and initial tumor pathology of the cervix with preservation of anatomical and functional integrity of the organ, which is important for the realization of reproductive function in women.

An urgent problem of modern clinical oncogynecology is the treatment of dystrophic diseases, intraepithelial neoplasia and initial vulvar cancer. Vulvar cancer among malignant tumors of the female genital organs is 5-8%. Vulvar cancer is most often preceded by a variety of background and precancerous diseases. Surgical intervention is complicated by the fact that the tumor is often localized in close proximity to important anatomical structures (urethra, vagina, rectum) or passes to them. The use of photodynamic therapy has expanded the possibilities of therapy for cancer and precancerous vulva.

In one of the works of Russian authors, the results of patients treatment with dystrophic diseases of the vulva, who underwent PDT using domestic photosensitizers, were analyzed. Treatment was carried out in 30 patients with vulvar lesions. By the nature of the revealed pathology of the vulva, 20 patients (66.7%) had verified sclerotic lichen of the vulva, 8 (26.6%) had squamous cell hyperplasia of the vulva, 2 patients (6.7%) had mixed dystrophy. The age of the patients ranged from 33 to 80 years, the average age was 56.5 years. Complete clinical remission in the vulvar pathology group was noted in 27 (90%) of 30 patients. In 3 (10%) patients with vulvar lichen sclerosis, a second PDT session was required, after which a clinical cure was diagnosed. In all cases, a good cosmetic effect was recorded which is especially important for women of reproductive age.[559]

According to another clinical study, the results of PDT in 67 patients were analyzed. In 36 patients (53.7%), vulvar lichen sclerosis was verified, in 16 (23.9%) – squamous cell hyperplasia of the vulva and in 15 patients (22.4%) – intaepithelial neoplasia of the vulva I-III art. Complete clinical remission was noted in 59 (88.1%) of 67 patients. 8 (11.9%) patients had partial remission, which required a repeat PDT session. After that clinical cure was diagnosed.

PDT of the affected vulva area attacked by the dystrophic process prevented the progression of the disease and achieved clinical recovery in 92.5% of patients.[560]

The analysis of the obtained PDT results using domestic photosensitizers in the treatment of dystrophic diseases and intraepithelial neoplasia of the vulva showed high therapeutic efficacy with minimal side effects and no complications after the treatment. The PDT method allows performing organ-preserving treatment in patients with vulvar diseases without deterioration of their quality of life. All this indicates the high efficiency of this method in the treatment of patients with vulvar diseases and the prospects for further development of this direction in oncogynecology.

14. PDT for Activation of Antitumor Immune Response

Cancer is one of the leading causes of death worldwide, being the cause of death for nearly 10 million people in 2020, or nearly one in six deaths.[561] The global cancer burden is expected to be 28.4 million cases in 2040, a 47% increase from 2020.[562] Despite significant scientific and financial efforts to improve five-year survival rates, statistics for many types of cancer are improving only slightly. This includes the bronchial, lung, esophageal, stomach, pancreas, liver, bile ducts, and brain cancers.[563] Other types of cancer have better survival parameters, which experts explain either by a good response to chemotherapy or by late activation of metastasis. This makes it possible to identify the tumor with instrumental methods before the metastatic stage and surgically remove it. According to the American authors, the minimum tumor size diagnosed with nuclear medicine techniques is 15 mm on average in U.S. clinics.[564] Impossibility of early detection is a major reason for treatment failures of tumors that begin to metastasize at smaller sizes.

In light of this, an important scientific challenge is finding sensitive methods and tools to diagnose minimally sized tumors. It is important for early-stage tumors diagnosis. Another major scientific problem is the development of minimally invasive method for evaluating the direction of the tumor process evolution and the possibility of changing this direction towards to the destruction of the tumor and metastases. This is especially important for actively metastasizing tumors, which include most of the types of tumors with a low five-year survival.

Increasingly popular optical diagnostic techniques using absorptive and fluorescent dyes have significantly advanced 5-year survival rates for several types of cancer.[565,566] Tissue spectral and video fluorescence analysis devices, with fluorescence excitation in the red and near-infrared ranges of the spectrum, have significantly advanced the diagnostic capabilities of optical methods.[567,568] For example, in neurosurgical intraoperative navigation during tumor removal, small bleeding completely blocks the possibility of fluorescence registration with excitation in the blue range, whereas with red range radiation, fluorescence registration is possible even under a layer of blood up to 1 mm.[569] The most commonly used near-infrared fluorophores in clinical practice today are protoporphyrin IX induced by 5-aminolevulinic acid,[570] methylene blue,[571,572] fluorescein[573,574] and indocyanine green.[575] One of the main directions of PDT development is the creation of photosensitizers that allow using infrared laser radiation for excitation, which has a greater depth of penetration into biological tissues. Currently promising infrared photosensitizers are products of bacteriochlorin series, the absorption maximums of which lie in the range of 760–820 nm,[576–578] products based on nanostructured forms of phthalocyanine derivatives.[579,580] Indocyanine green with an absorption maximum around 780 nm, widely used for fluorescent blood flow studies and identification of diseased lymph nodes,[581] also has photodynamic effects, as demonstrated in experimental models of skin cancer[582,583] and infectious pneumonia.[584]

Tumor stroma

It is known that any primary tumor consists not only of neoplastic cells, but also of a supporting stroma, the main elements of which are cells of the hematopoietic system (in particular neutrophils and macrophages).[585] A change in the phenotype of cells in the tumor microenvironment gives the tumor the opportunity to grow and invade. That is why the study of the transformed cells interactions with the stroma seems relevant and clinically important. Despite the emergence of various targeted drugs on the market, which have made a big breakthrough in the treatment of certain types of oncology, but such diseases as cancer of the stomach, liver, bile ducts, brain and spinal cord are still in the shadow of scientific progress and can not be treated with most drugs. The same applies to the skin melanoma. To date, particularly relevant is the search for new approaches to therapy, namely, new specific methods of influencing tumor stromal cells.[586]

Over the past decade, it has been shown that the stroma is an active and decisive component of tumor growth and its progression. Stromal cells, such as immune, mesenchymal and endothelial cells, can account for more than half of the cellular contents of the tumor. Their activation and function are the determining factor for regression or, conversely, growth of tumors. Further research should provide a better understanding of the interaction between tumors and the immune system, and this knowledge should be used to optimize cancer treatments.[587,588]

By secreting immunosuppressive cytokines or other pro-tumor molecules, tumor cells can create a microenvironment that inhibits antitumor immunity and promotes malignancy. Among the cells recruited by the tumor, macrophages are particularly numerous and are present on all stages of tumor progression. In the primary tumor, macrophages (so-called tumor-associated macrophages or TAM) can stimulate angiogenesis and enhance the invasion of tumor cells, their mobility and the ability to penetrate into the vessels.[589] During metastasis, metastasis-associated macrophages (MAM) contribute to extravasation of tumor cells, their survival and sustained growth.[590] Tumor-associated macrophages also suppress immunity by preventing the attack by natural killers and T-cells on tumor cells during tumor progression and after recovery from chemo- or immunotherapy. Thus, macrophages are attractive targets for cancer treatment.

Selective accumulation of PS by macrophages

According to literature, the amount of tumor-associated macrophages in the tumor microenvironment is 20 to 80% of the total number of cells,[591] while the accumulation of a photosensitizer in them can be up to 9 times higher (for porphyrin series) than in tumor cells.[592] This is due to the fact that during intravenous administration the photosensitizers bind to low-density lipoproteins, on the capture of which macrophages are oriented.

The scientific community already have developments on the selective accumulation of photosensitizers in tumor-associated macrophages. A group led Professor Hamblin conducted studies of targeted photodynamic therapy aimed at tumor-associated macrophages. A photosensitizer was developed based on chlorin e_6 bound to albumin, which selectively accumulated in TAM with intracutaneous administration and provided high PDT efficiency.[593,594] Another group of Japanese researchers suggested using chlorin conjugated with mannose for selective accumulation in TAM (M-chlorin), selectivity of the accumulation was demonstrated on cells *in vitro*.[595] Particularly successful in terms of accumulation in macrophage cells are nanoparticles. As such, it was shown that the use of photosensitizers in the nanoform allows selective accumulation in tumor-associated macrophages and tumor cells and the effectiveness of photodynamic therapy in melanoma B16F10 was demonstrated.[596]

In recent years, the possibility of using photosensitizers in the form of molecular nanocrystals for fluorescent diagnosis and photodynamic therapy has been investigated.[597] When such molecular aluminum phthalocyanine nanocrystals came in contact with the surrounding biological cells, the effect of fluorescence "kindling" and singlet oxygen generation was recorded.[598] he manifestation of the photoactive properties of mTHPC nanoparticle colloid, as well as the ability to change cellular functions, has been demonstrated in interaction with polarized macrophages.[599]

PDT-induced immune response

Although the researchers initially focused their efforts on increasing the direct cytotoxicity for tumor cells subjected to photodynamic effects (including increasing the generation efficiency of singlet oxygen by photosensitizers), there has recently been growing interest in developing methods and approaches for further studying and enhancing the immunostimulatory properties of PDT. During PDT, apoptosis and / or necrosis of tumor cells, destruction of the tumor-associated vasculature, as well as inflammation that can induce an immune response in the patient, which subsequently also leads to the death of tumor cells due to their destruction by their own immune cells, arises directly.[600,601]

PDT induced immune response not only increases the effectiveness of the therapy performed by systemically eliminating residual tumor lesions and thus controlling the primary growth of the tumor, but also has a certain potential to fight cancer cells at the metastatic stage and relapse of the disease.[602] Phototoxic damage to tumor cells and vessels induces the release of mediators provoking a local inflammatory reaction, resulting in the activation of innate immunity and the recruitment of phagocytes (macrophages, neutrophils, dendritic and mast cells), and natural killer (NK) that capture damaged and / or dying tumor cells.[603,604] Mediators of inflammation are perceived by immune cells as danger signals and can be recognized and neutralized by phagocytes, which leads to induced cytotoxic activity of immune cells against tumor cells.[605] In the event that a disrupting tumor cell is captured by an antigen-presenting cell (for example, dendritic cell), an effective antitumor immune response is triggered by activating a specific T-cell response: converting naïve T-cells into cytotoxic tumor-specific T-lymphocytes.[606]

From the point of view of fundamental medicine, when approaching anti-tumor therapy as the management of the immune response, many questions arise: how the PDT affects the polarization of macrophages, which populations of macrophages die first during PDT and whether the surviving populations of cells change their functions, whether anti-tumor immunity is acquired as a result of PDT, is it possible to evaluate non-invasively the quantitative ratio of macrophages of different polarizations before and after the PDT is performed directly in the tumor in vivo, how to neutralize the microglia of the brain activated as a result of PDT into the proinflammatory phenotype after tumor resorption, *etc*.

Vascular effect of PDT, oxygenation, effect of hypoxia on immune antitumor response

As a result of the vascular mechanism of PDT and the destruction of the tumor-associated vascular network, the nutrition of the tumor ceases, which contributes to its regression.[607] However, since in practice, during the treatment, an evaluation of the state of the vessels is not carried out, their destruction is often incomplete. An important tool for evaluating the vascular effect of PDT should be the measurement of tissue oxygenation during and after therapy, with the possibility of evaluating deep-seated tumor layers.[608] At the moment, separate studies are under way to monitor the oxygenation of tissues during PDT. The studies on experimental animals demonstrated the possibility of monitoring changes in the vascular bed and saturation with oxygen using photoacoustic microscopy during PDT with Verteporfin at a resolution of 60 μm.[609] Similar studies are conducted using optical coherent angiography.[610] In the past few years, there have been reports of laser speckle visualization in real time, a method developed for non-invasive monitoring of in vivo blood flow dynamics and vascular structure with high spatial and temporal resolution.[611] The possibility of conducting classical PDT in combination with the use of specific PET radiopharmaceuticals to evaluate the effect on cells (apoptosis, necrosis, proliferation, metabolism) or vascular damage was demonstrated.[612] However, to be widespread clinical practice, the method of monitoring blood flow parameters should be simple in management, inexpensive and allow assessing not only the dynamics of blood vessels of the tumor, but also their oxygenation which is relevant for PDT with non-vascular drugs.

Premise of PDT activation of immunity in brain tumors

Fluorescent diagnosis of brain tumors received wide development in the clinical practice of the Russian Federation, especially to conduct intraoperative navigation.[613,614]

Towards PDT methods Russian and Western doctors exhibit a more cautious attitude. This is due to the fact that microglia cells, acting as phagocytic macrophages in the activated state, can stay in this state for a long time and phagocytize healthy cells.[615] Microglia cells are activated by mechanical, radiation, or photodynamic effects on brain tissue.[616] One of the first photosensitizers, methylene blue, found neuroprotective effects on the central nervous system in traumatic brain injury by increasing autophagy, reducing brain edema and inhibiting microglia activation.[617,618] It should be noted that the photodynamic properties of methylene blue (and it has a rather significant photodynamic effect[619]) have not been used or discussed. Another point of caution in the use of PDT for brain tumors is that, in accordance with the effect mechanism, the irradiation zone will be destroyed and this will facilitate the migration of non-killed cancer cells to other areas for continued growth. In fact, PDT appears to be an assistant to tumor-associated microglial cells that express matrix metalloproteinases (MMPs) to destroy the matrix in the microenvironment of tumor cells, facilitating their migration and, consequently, metastasis. To mitigate these effects, it is necessary to evaluate the accumulation of a photosensitizer in microglia cells of different polarization and to select the light doses necessary for their deactivation. When the blood-brain barrier is compromised, which often occurs with malignant growth, monocytes enter the tumor stroma, which may polarize into pro-tumor or pro-inflammatory phenotypes upon extravasation, which also requires a separate study of their interaction with photosensitizers.[620]

Thus, PDT, depending on the time after the introduction of the photosensitizer and its redistribution between the cells of the stroma and the tumor, as well as the irradiation mode, stimulates a cascade of response reactions, the strength of which can already be controlled at the irradiation stage. For brain tumors, especially for 3-rd and 4-th stages gliomas, precise and long-term monitoring of the tumor bed condition is necessary not only during surgery, but also during remission. The most promising for this purpose are fiber-optic implants, installed for a long time in the projection of the tumor bed.[621]

15. Multifunctional Agents Based on Tetrapyrroles for Magnetic Resonance Imaging Guided Photodynamic Therapy

Despite significant progress in the study of the cancer biochemical mechanisms and the development of antitumor drugs, cancer remains one of the leading causes of morbidity and mortality worldwide.[622] Traditional methods – surgery, chemotherapy and radiotherapy are widely used to treat oncological diseases, but these methods don't always allow the tumors to be completely removed and have serious side effects. There is an extensive search for safe and cost-effective approaches to improve the effectiveness of traditional cancer therapies and to find new alternative approaches to its treatment.[623-625] Early diagnosis and detection of the pathological mass are the key to successful cancer therapy. Diagnostic imaging implies selective detection of pathological processes at the cellular and molecular levels, as well as their real-time monitoring with high sensitivity.[627] Over the years, cancer imaging techniques have progressed significantly from traditional methods providing structural information to more advanced and relatively new functional and molecular imaging technologies. In this regard, the concept of theranostics assuming application of the advantages of molecular imaging agents and tumor therapy with a single drug is a promising strategy.[628,629]

Integration of optical imaging and phototherapy methods have recently initiated phototheranostics.[629-631] Thus, the combination of optical fluorescence imaging (FLI) in the near infrared (NIR) (650-1700 nm) window of "optical tissue permeability", and PS action could be a promising approach in clinical practice. The combination of PDT and the magnetic resonance imaging procedure (MRI), which is widely used in clinical diagnostics due to its high three-dimensional spatial resolution and ability to penetrate into deep tissues, is of particular interest.[632,633] The relevance of MRI is due to its non-invasiveness, non-ionizing, and non-radiating modality, its ability to provide detailed information on tissue anatomy, function, and metabolism *in vivo* with excellent anatomical resolution.[634] Non-specific contrast agents based on paramagnetic metals (Gd(III), Mn(II), Fe(III)) are effective for improving sensitivity in clinical diagnostics, they account for approximately 25-30% of all MRI scans.[635-637] However, the application of such drugs is associated with the danger of increased nephrotoxicity due to the release of metal ion from the chelating complex, therefore, one of the most important tasks of the creation of contrast agents is to achieve stable metal chelation. In connection with the above, the design of multifunctional diagnostic systems for the combined diagnosis and therapy of cancer using PDT and MRI methods is a promising approach in clinical practice.

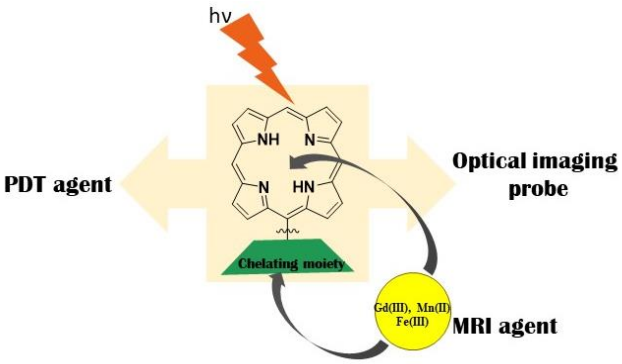

Figure 33. The chemical structure of theranostic agents for MRI guided PDT.

The introduction of contrast agent and PS as individual objects leads to limitations in their pharmacodynamics and pharmacokinetics, and, as a consequence, to differences in imaging based on their biodistribution. The inclusion of MRI contrast agent and PS in one theranostic agent has been shown to overcome this limitation, when the contrast agent and PS have the same biodistribution patterns, thus PDT treatment is further optimized.[638] Furthermore, this strategy of bimodal agents combining within a single molecular object provides the additional benefits of enhanced PS hydrophilicity in biological fluids and improved proton

relaxation for MRI efficiency due to the increased molecular weight.[639] In addition, the growing interest in the development of effective PS-based contrast agents is related to the fact that no commercially available contrast agent is effective enough for accurate detection of malignant neoplastic tissue.

In the past few years, agents for phototheranostics based on tetrapyrrole structures that could combine MRI diagnosis and PDT have been actively developed.[631,640-643] The limited cavity size of tetrapyrrole macrocycles cannot ensure stable binding to the large radius metal ions used in MRI, it was proposed to introduce an external chelating fragment into the PS molecule to create the drug-theranostics (Figure 33).[644-646]

This review is devoted to recent advances in the application of tetrapyrrole compounds for MRI guided PDT. It emphasizes that the introduction of an external chelating fragment into the structure of tetrapyrroles leads to generation of promising agents for phototheranostics. Data on the available contrast agents as well as PS based on tetrapyrroles containing Gd(III) for MR diagnostics are presented, methods of inclusion of metal atoms into such systems are analyzed.

Types of contrast probes used in MRI diagnosis

The principle of MRI is based on the phenomenon of nuclear magnetic resonance and proton spin relaxation in the magnetic field divided into 2 types: 1) longitudinal relaxation called T1 relaxation or spin-lattice relaxation arising from the dissipation of absorbed radiofrequency pulse energy in the surrounding tissue; 2) transverse relaxation, called T2 relaxation or spin-spin relaxation arising from the loss of phase coherence during spin precession. Longitudinal and transverse relaxations are two synchronous magnetic processes, each of which provides its own type of contrast: T1 recovery and T2 attenuation have brightening (positive contrast) and darkening (negative contrast) effects, respectively.[639,647]

The amount of intrinsic contrast between tissues produced on an MR image depends on the differences in T1 and/or T2 relaxation times of the observed tissues. In some cases, the difference in signals between diseased and healthy tissue is difficult to detect on the MR image. Pathological tissues may have no significant difference in T1 or T2 signals from the surrounding normal tissues. This signal distinction can be increased by introduction of an exogenous contrast agent (CA contrast agent).[632] The exogenous contrast agents improve MR images by locally decreasing T1 and T2 proton relaxation times.

Two main types of magnetic resonance probes are paramagnetic and superparamagnetic agents with unpaired electrons, and the corresponding magnetic moments engage in dipolar and scalar interactions with nearby water protons.[639] Then the local water protons relax and quickly exchange with other unrelaxed water protons reducing the average relaxation time. The amplification of the signal contrast can be achieved in two ways: either by higher tissue vascularization, which, for example, is typical for tumors, or by increased affinity of CA to the target area.

The contrast agent (CA) should have high relaxation ability, stability, specific biodistribution, rapid clearance, low osmolality and viscosity, as well as low toxicity. All these contrast agents have their advantages and drawbacks.[636] The typical CA is a chelated metal ion with a constant magnetic moment.[632,636, 639,643] The acute and chronic toxic side effects caused by the metal ion as well as the chelating agent are significantly reduced due to complexation.

T1 contrast agents are called positive CAs, and they are mostly compounds with paramagnetic metals. The investigated tissues absorbing such contrast agents become bright on T1-weighted images and can be distinguished from other pathological and normal physiological states, T1-weighted images are usually more preferable to T2 contrast agents. T1-type agents contain paramagnetic ions (Gd^{3+} and Mn^{2+}), which have high electron spin and constant magnetic moment due to seven and five unpaired electrons, respectively. T2 contrast agents are classified as negative CAs, they are derived from iron(III) compounds in most cases. The negative contrast agents reduce T2 signals by shortening the T2 relaxation time, which leads to a strong decrease in the MR signal and thus to the negative contrast *in vivo*.[29,632,636,639,647]

Gadolinium-based contrast agents

Gadolinium-based CAs are the basis of clinically used MRI contrast agents due to its properties: the high magnetic moment and the long electron spin relaxation time.[648-649] The contrast agents containing gadolinium reduce the T1 and T2 relaxation times of neighboring water protons, which increases the signal intensity of T1-weighted images and decreases the signal intensity of T2-weighted images. The contrast agents containing gadolinium reduce the T1 and T2 relaxation times of adjoining water protons, that increases the signal intensity of T1-weighted images and decreases the signal intensity of T2-weighted images. However, there are some physical restrictions, for example, the short half-life complicates the differentiation of benign and malignant tumors. In addition, gadolinium binds weakly to serum proteins, its salts are usually hydrolyzed and converted to hydroxides, which are absorbed by the reticuloendothelial system (RES) and accumulate in the body, especially in the liver, spleen and bones, thereby imparting potential toxicity to the drug. To partially overcome these problems, Gd is introduced in the chelated forms. Currently nine Gd contrast compounds with multidentate chelating ligands have been approved for the clinical practice. Generally, the cyclic ligand is more stable than the linear ligand. The ionic compounds are slightly more stable than nonionic compounds, but they have a higher osmolality at the same time. The ionic and hydrophilic complexes comprise gadolinium (III) diethylentriamine pentaacetate (Gd-DTPA, referred to as gadopentetate dimeglumine), Gd(III) 1,4,7,10-tetrazacyclododecane-1,4,7,10-tetraacetate (Gd-DOTA, gadoterate) and polyaspartate Gd(III). The nonionic hydrophilic gadolinium (III) chelates are Gd(III)-diethylene-triamine pentaacetate-*bis*(methylamide) (Gd-DTPA-BMA, gadodiamide) and macrocyclic chelate Gd-DOTA, in which the acetic acid functional group is substituted with 2-propanol radical (Gd-HP-DO3A, gadoteridol). The ionic and lipophilic gadolinium complexes comprise Gd-benzyl-oxymethyl derivative of dimethylglucamine salt of diethyltriaminepentaacetate (Gd-BOPTA, gadobenate

dimeglumine) and Gd-ethoxybenzyl diethylentriaminepentaacetate (Gd-EOB-DTPA, gadoxetate) (Figure 34).[648]

Although clinically used Gd chelates are relatively safe and generally tolerated by patients well, there have been some recent concerns about nephrogenic systemic fibrosis and nephrogenic fibrosing dermopathy in some patients, as well as retention of small quantities of Gd in bone and brain tissue has been found. These side effects have been identified in patients with impaired renal function and patients, who have been exposed to MRI scans with contrast repeatedly. However, there is no evidence that the application of approved gadolinium-based contrast agents can lead to pathological changes in the body.

Manganese-based contrast agents

Great attention has been recently paid to the development of the contrast agents based on Mn, which is an endogenous metal and has less toxicity. Mn(II) forms a Mn(II) high-spin d^5-cation (S = 5/2) and Mn(III) d^4-cation (S = 2). Mn(II) can act as a strong paramagnetic ion generating T1 signal amplification *in vivo*.[650,651] Manganese dipyridoxyldiphosphate (Mn-DPDP, Teslascan) and manganese(II) chloride tetrahydrate (LumenHance) are the only clinically approved Mn-based contrast agents.[652] Manganese in ionic form and manganese chelates have a short half-life. Manganese compounds are excreted primarily through the gastrointestinal tract and the biliary tract unlike gadolinium contrast agents. However, high concentrations of manganese have neurotoxic effects similar to Parkinson's disease. Mn-based contrast agent, manganese-N-picolyl-N,N',N'-*trans*-1,2-cyclohexenediamin triacetate (Mn-Py-C3A), has been recently proposed, and it provides high spin relaxation and resistance to Mn dissociation simultaneously. The application of Mn-Py-C3A exhibited the tumor contrast enhancement comparable to gadoterate meglumine in an animal model of breast cancer, and its partial hepatobiliary elimination allowed visualization of liver tumors in a model of the metastasis (Figure 35).[653] However, despite the rather high efficiency of the proposed Mn(II)-based MRI contrast agents, the problems of thermodynamic stability and kinetic inertness of these complexes remain unresolved, that calls into question their clinical application.

Iron-based contrast agents

The iron-based preparations were proposed as a potential alternative to gadolinium contrast compounds more than thirty years ago. It has led to extensive preclinical and clinical studies, but today the only commercially available contrast agent for MRI is Combidex® (iron oxide nanoparticles), approved exclusively in the Netherlands. Magnetic nanoparticles of iron (III) oxide are T2 contrast agent, and also Fe^{3+} ion has a significant T1 contrast enhancement effect.[639] The magnetic properties of Fe^{3+} are due to external unpaired electrons unlike the Gd^{3+} ion, so they depend strongly on the coordination method of the metal with the ligand. Iron is a widespread and endogenous element in the human body, so high-spin Fe(III) complexes are very promising as contrast agents for MRI, they have the best biocompatibility and safety profiles as compared to other metal complexes.[654]

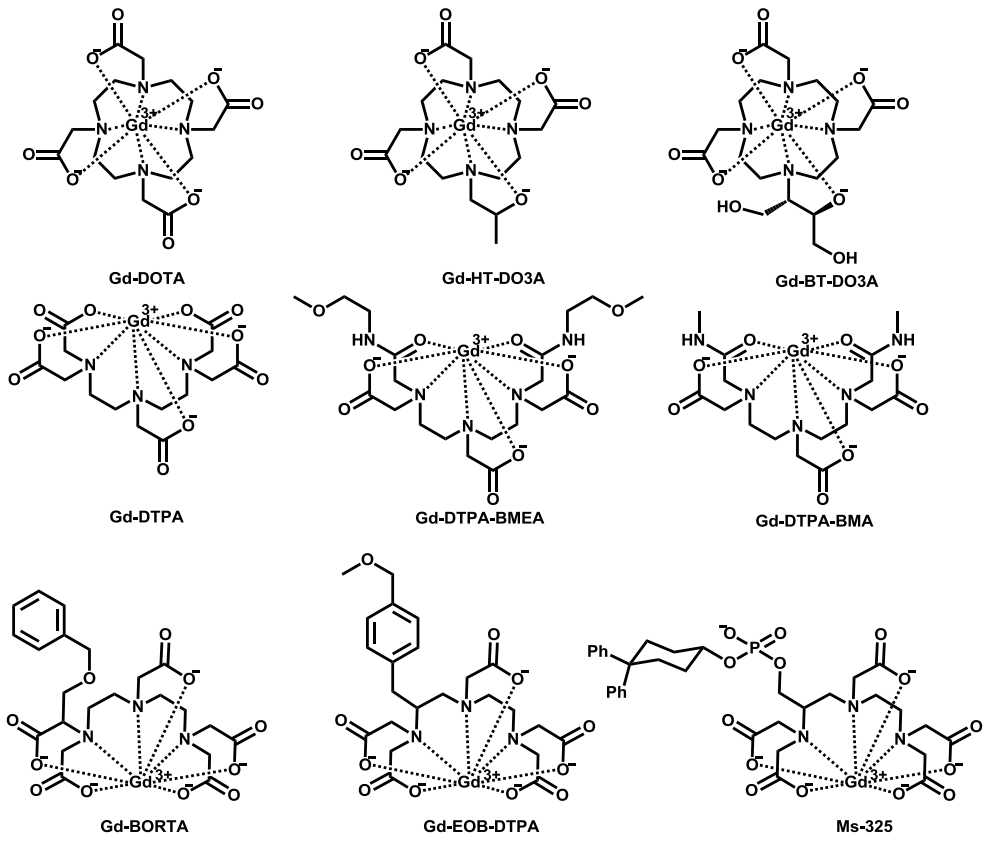

Figure 34. Gadolinium-based contrast agents approved for clinical application.[648]

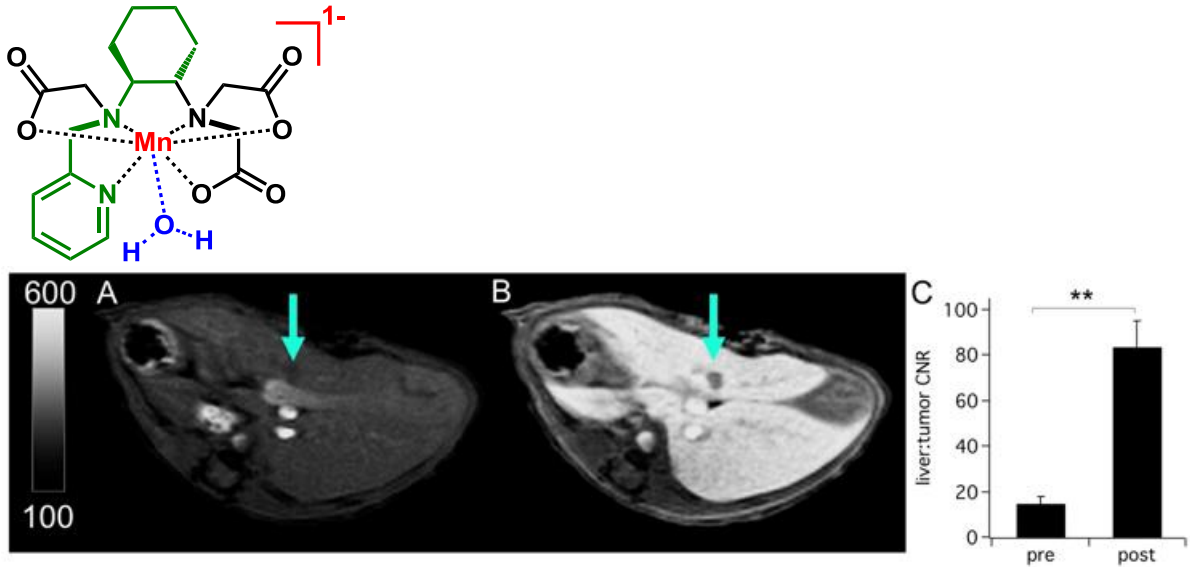

Figure 35. Liver imaging of an orthotopic mouse model of colorectal liver metastasis with complex Mn-Py-C3A at 4.7 T. (A and B) T1-weighted axial images of the liver at the level of the tumor (arrow) prior to and during the hepatocellular phase after injection of Mn-Py-C3A, respectively. (C) Liver parenchyma *vs*. tumor CNR prior to and following treatment with Mn-Py-C3A. Reprinted with permission from [653]. Copyright 2018 American Chemical Society.[653]

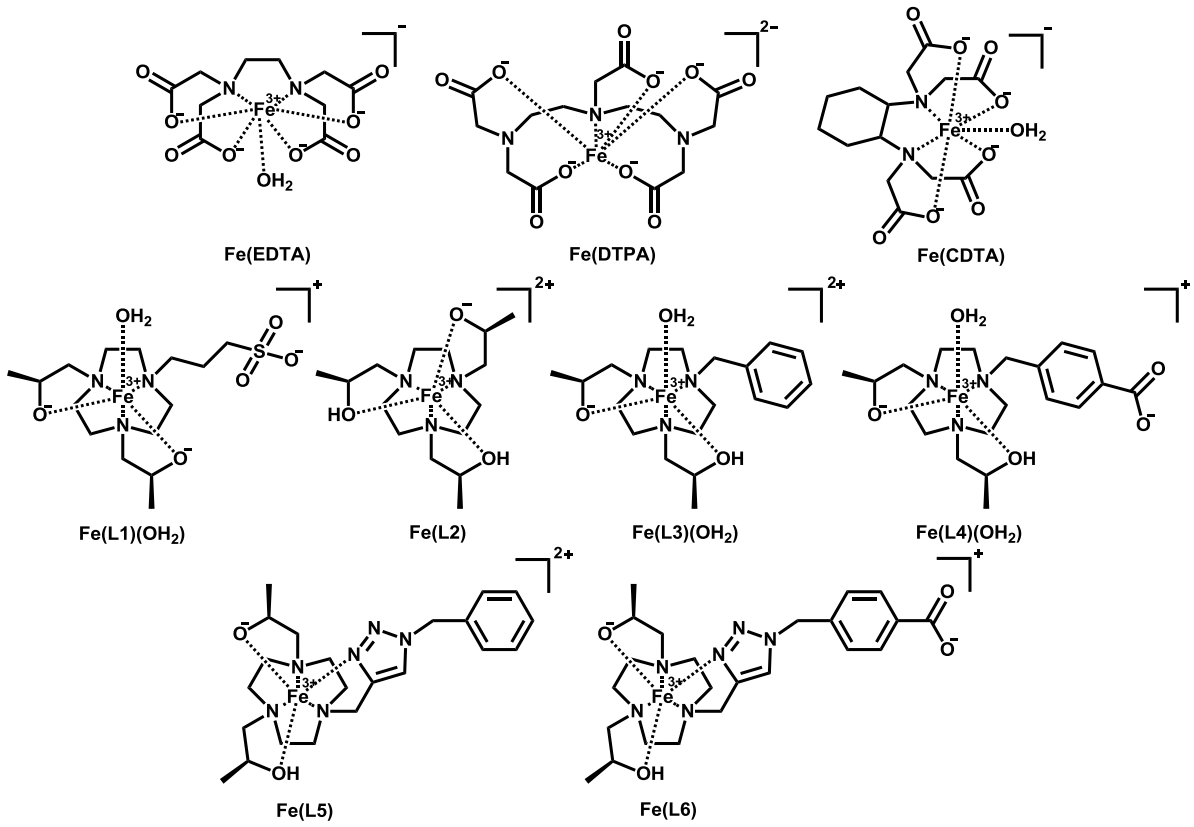

Figure 36. Potential MRI contrast agents based on Fe(III) complexes.[657]

There are two types of iron oxide-based contrast agents: superparamagnetic iron oxide (SPIO) and ultra-small superparamagnetic iron oxide (USPIO), which are colloidal suspensions of iron oxide nanoparticles. SPIO and USPIO have been successfully used to diagnose liver tumors in some cases. The superparamagnetic iron oxide particles or their ultra-small forms are removed from the blood by the reticuloendothelial system of the liver, spleen and lymph nodes after intravenous injection. Due to this specific biodistribution, these preparations can be used for the

organ imaging and the evaluation of metastasis spread, the macrophage labeling in the vulnerable atherosclerotic plaques, and the detection of inflammatory lesions after transplantations. This explains the recent increased interest in the application of iron-based preparations for MRI.[653] In terms of the development of new contrast agents, Schellenberger *et al.* have shown that low molecular weight Fe(III) complexes such as Fe-CDTA (Magnevist®) provide significant contrast imaging *in vivo* and exhibit enhancement kinetics similar to the data for the clinically used agent Gd-DTPA (Figure 36).[656,657]

The main problem of iron nanoparticles application in medical practice is related to the fact that nanoparticles tend to accumulate in vessels, causing their embolization and blocking the blood flow [654, 657].

Design of tetrapyrroles conjugates with Gd(III) for phototheranostics

Tetrapyrrole compounds can become a versatile platform for creating such agents due to their structure, functionalization ability, photophysical properties, and affinity for the tumor. The conjugation of tetrapyrrole PS with MRI-contrasts seems to be a particularly promising approach for the theranostics purposes.[658] Since unsubstituted tetrapyrroles are poorly soluble in aqueous media, the presence of hydrophilic complexes of Gd(III) and other paramagnetic metals makes PS soluble under physiological conditions and improves tissue distribution and excretion *in vivo*. In this regard, the molecular design of the therapeutic molecule, in particular, the selection of the optimal number and type of paramagnetic metal complexes within the conjugate to fulfill all the requirements for a drug and diagnostic drug is a critical point. PS for PDT, in turn, should have an amphiphilic structure, be non-toxic and have a strong absorption in the window of biological transparency to achieve the required depth of the tissue penetration and accumulation in the tumor.[659] In addition, the growing interest in the development of effective PS-based contrast agents is related to the fact that, to date, no commercially available contrast agent is sufficiently effective for the accurate detection of malignant neoplastic tissues.

Despite the well-known coordination abilities of tetrapyrroles, there are limitations in obtaining stable complexes with large radius paramagnetic metals, such as Gd(III) ions. The limited cavity size of the porphyrin macrocycle makes it very difficult to obtain stable compounds with metals used in MRI. Therefore, the introduction of an external chelating fragment into the structure of the molecule became necessary to realize the porphyrin-based theranostics concept, and most of the publications involve the conjugation of the tetrapyrrole cycle with an external chelating agent.

Previously, bifunctional agent **1** (Gd2(DTPA)4TPP) based on *meso*-5,10,15,20-tetrakis(4-aminophenyl)porphyrin bound to 4 DTPA complexes, two of which were metallated with Gd(III) ions, was first proposed in 1993.[660] It was found that the relaxation value for the obtained conjugate with Gd(III) was twice as high as for GdDTPA at 20 MHz, and a significant enhancement of the contrast image of the tumor compared to the adjacent normal tissues in mice was indicative of the affinity of the compound to the tumor tissue (Figure 37). Photoinduced toxicity studies performed

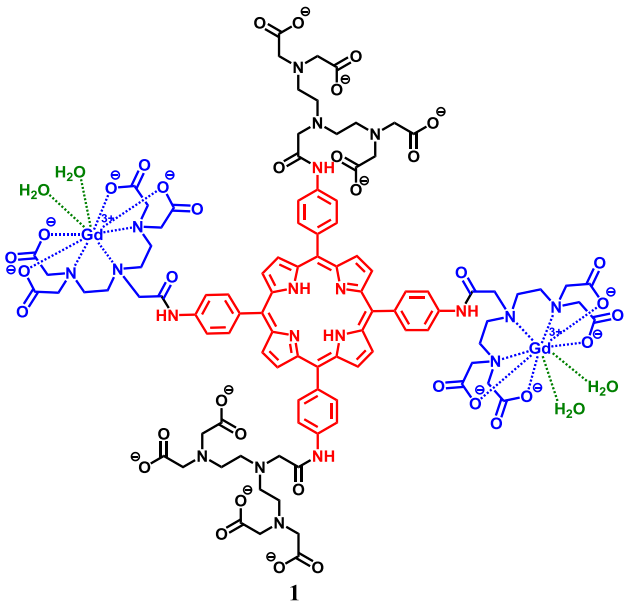

Figure 37. Structure of a new bimodal agent.[660]

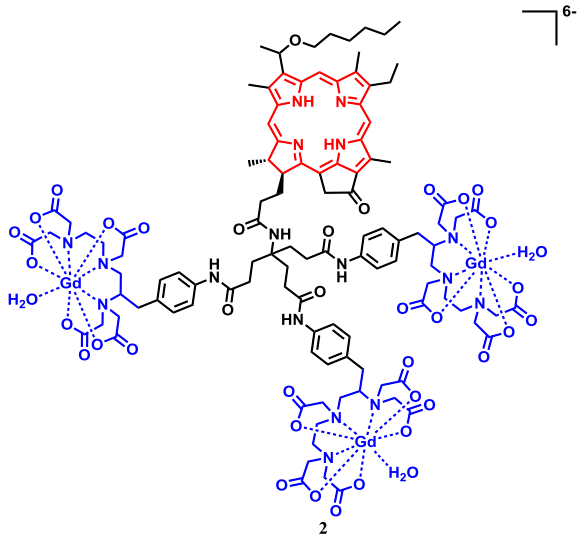

Figure 38. Chemical structure of the leader theranostic compound **2**.[661]

on two cell lines (HT29 and L1210) under multi-wavelength laser irradiation with λ=488 nm and 514 nm showed phototoxicity of the Gd2(DTPA)4TPP conjugate comparable to values for the commercially available PS hematoporphyrin. This Gd2(DTPA)4TPP conjugate was the first bimodal agent prototype developed for the MRI-controlled PDT.

More than ten years later Pandey *et al.* developed and investigated several theranostic agents based on the natural porphyrin pyropheoforbide with substituents of lipophilic or hydrophilic nature.[661] These porphyrins were conjugated to one, two, three, or six GdDTPA complexes. The conjugate design included the creation of a chelating agent bond by an additional branched linker away from the macrocycle, and the stability of the GdDTPA core was maintained by chelation with five anionic carboxyl groups.

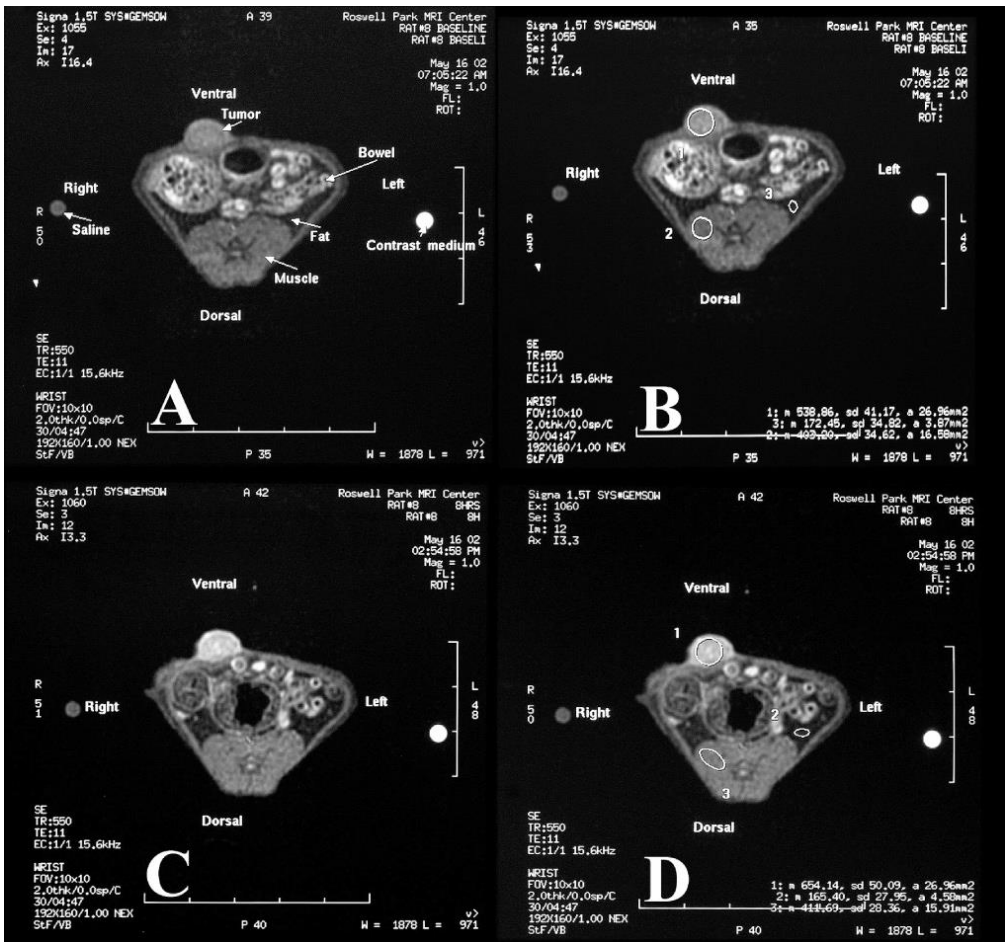

Figure 39. Magnetic resonance (MR) images of rat (Fischer) with Ward's colon tumors before (left) and 24 h after (right) injection of HPPH-3-GdDTPA conjugate (dose: 10 μmol/kg). Reprinted with permission from [661]. Copyright 2018, American Chemical Society.[661]

Theranostics containing one or two Gd complexes required the use of a liposomal composition to impart water solubility. With three (compound **2**) and six GdDTPA fragments in the conjugate molecule, water solubility was significantly improved. Compound **2** (HPPH-3GdDTPA) with three chelating fragments (Figure 38), was found to be the best candidate with respect to imaging and treatment results. This conjugate showed a marked enhancement of MR contrast in tumors in mice 24 h after injection at a dose 10 times lower than the clinical dose used with Magnevist® (Figure 39).

Fluorescence imaging obtained from the emission of light by the HPPH derivative also showed maximum intensity 24 h after injection. Also, this compound showed an effective PDT effect after a single irradiation at 665 nm (70 J/cm^2) 24 h after injection.

In the following work, conjugates of tetra- and monosubstituted *meso*-arylporphyrins **3** with GdDTPA residues were obtained (Figure 40).[662] Measurement of the longitudinal relaxation capacity of the products showed 154% and 251% enhancement over the commonly used Gd-DTPA for the mono- and tetrasubstituted derivatives, respectively, and their relaxation times were r1 7.82 mM^{-1}s^{-1} and 14.8 mM^{-1}s^{-1}.

Research [663] describes the production of potential theranostic drugs based on zinc phthalocyanine complexes conjugated with one molecule of the GdDO3A complex (Figure 41). To reduce the degree of aggregation in aqueous media and increase the solubility, the PS macrocycles were modified with peripheral hydrophilic substituents. The ZnPht-1Gd conjugate **4** showed a lower proton relaxation value (1.43 mM^{-1}s^{-1} at 128 MHz) compared to the commercial preparation Omniscan™ (3.23 mM^{-1}s^{-1} at 128 MHz). This phenomenon may be due to steric hindrances that make it difficult for water molecules to access the metal center. At the same time, the ZnPht-1Gd compound produced cytotoxic singlet oxygen quite efficiently in DMSO medium when irradiated with a quantum yield of 0.67.[663]

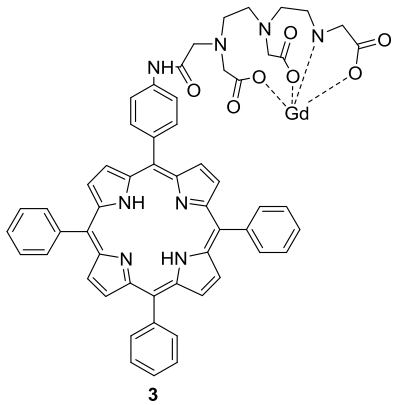

3

Figure 40. Structure of the new monosubstituted contrast agent **3**.[662]

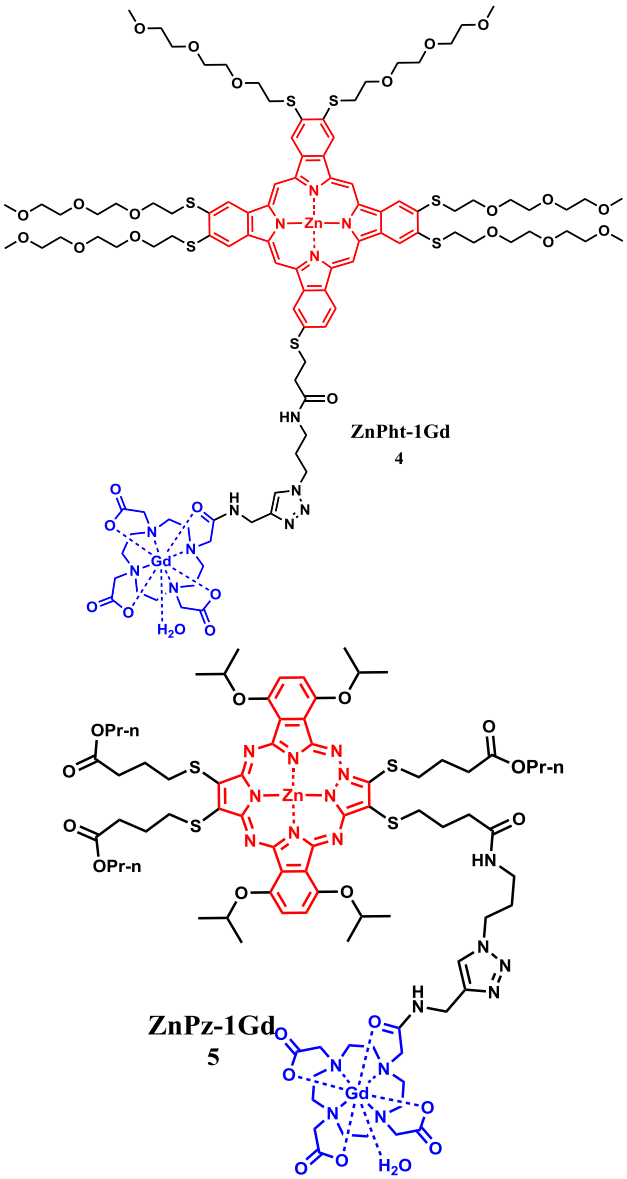

Figure 41. Chemical structure of **4** (ZnPht-1Gd) [663] and **5** (ZnPz-1Gd).[664]

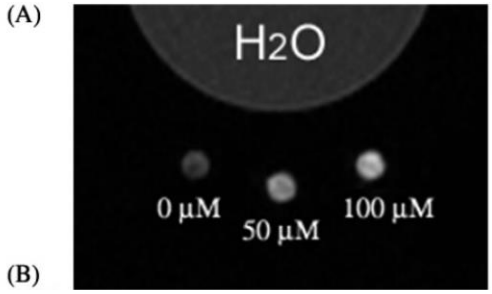

Figure 42. T1 weighted MR image of WI-38 VA13 cells incubated with 0.50, and 100 μM of Zn-Pz-1Gd(III) for 24 h at 4.7 T. Copyright © 2010, American Chemical Society.[663]

The zinc-based porphyrazine complex PS was bound to one, four, and eight GdDO3A complexes to form bifunctional conjugates (ZnPz-Gd) (Figure 41). These compounds showed a strong increase in relaxation (up to 12.8 $mM^{-1}s^{-1}$ for ZnPz-8Gd at 60 MHz and 37 °C) with an increase in the number of Gd-complexes attached to the PS (Figure 42). Cellular uptake was observed only for compounds containing a single Gd complex (ZnPz-1Gd). A noticeable phototoxic effect (with 50% cell destruction) was observed after 10-min white light irradiation.[664]

Porphyrin derivatives incorporating the Gd(III) ion into their cavity are an attractive agents due to their simplified structure and lower synthetic costs. However, numerous studies *in vivo* demonstrate problems associated with the reduced stability of these compounds caused by the dissociation of gadolinium ions from the porphyrin cavity [665]. Nevertheless, two compounds based on substituted porphyrazines **6-7** (GdPz1 and GdPz2), differing in the nature of the peripheral groups and containing a Gd(III) ion in the macrocycle cavity were obtained (Figure 43)[665]. Significant accumulation of the agent in the tumor *in vivo* was confirmed by fluorescence and MRI methods for both compounds. A good relaxation value under very strong magnetic field conditions (4.67 $mM^{-1}s^{-1}$ at 9.4 Tesla) was obtained for compound GdPz1, and cellular uptake, photodynamic activity and fluorescence *in vivo* were also studied. PDT activity was evaluated on CT26 cell line when irradiated with 615-635 nm light (10-20 J/cm^2, incubation concentration from 10^{-7} to 10^{-4} M). Moderate tumor death was observed, so further optimization of various parameters such as drug dose and light application was necessary.

The use of the multifunctionalized PS for the treatment of tumors with PDT and chemotherapy, as well as for MRI imaging, has also been reported.[666] Functionalized *meso*-arylporphyrin including gadolinium ion in the macrocycle cavity was covalently bound to chemotoxic platinum(II) complexes. The Gd/Pt-P1 compound **8** was obtained from 5,10,15,20-tetra(4-pyridyl)porphyrin (P1) coordinated with four Pt(II) complexes (Pt-P1) and one Gd(III) ion (Figure 44). The new polyfunctional agent showed almost doubled relaxation capacity at 3 Tesla compared to commercial GdDTPA. The phototoxic effect was studied on the C6 cell line after a 10-minute irradiation at 630 nm. A synergistic chemophotodynamic antitumor effect was observed in cells from C6 tumor-bearing mice.

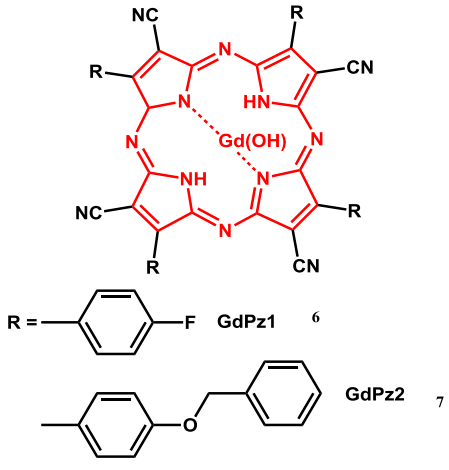

Figure 43. Molecular structure of GdPz1 and GdPz2.[665]

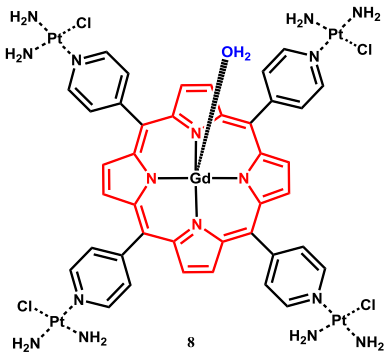

Figure 44. Molecular structure of **8**.[666]

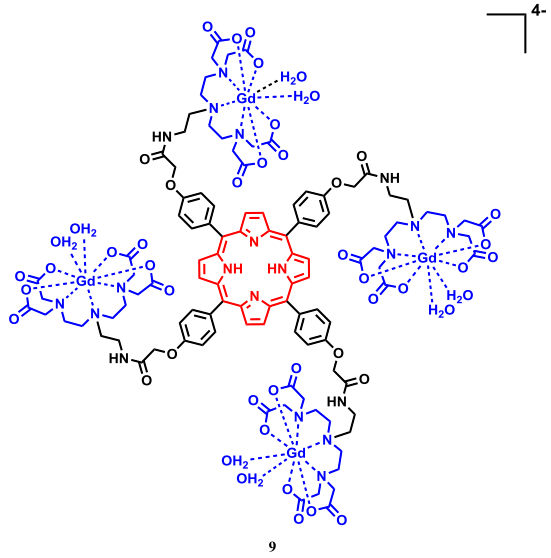

Figure 45. Chemical structure of the theranostic compound **9** developed by Chen *et al*.[667]

Increasing the number of coordinated water molecules near Gd(III) contrast agents is particularly attractive strategy to receive agents with high relaxation in a strong magnetic field. In this case, careful design of the structure of hepta- or hexadentate ligands is necessary in order to obtain Gd(III) complexes with good thermodynamic stability and kinetic inertness and to avoid the formation of ternary complexes with endogenous molecules. Chen *et al.* proposed a new structure of potential theranostics **9** (Figure 45) consisting of a central core-tetraphenylporphyrin bound to four GdDTTA complexes.[667]

This compound showed a high relaxation value (14.1 $mM^{-1}s^{-1}$ at 0.55 Tesla), which doubled in the presence of human serum albumin, indicating a high affinity of the obtained conjugate for this blood transport protein (Figure 46). Uptake of H1299 cell line was confirmed by confocal microscopy. Effective formation of singlet oxygen was observed under irradiation at 650 nm. The results demonstrated high potential of this compound as a contrast agent for multimodal (MR and luminescence) imaging and as a PS for PDT.[667]

In the following work, a number of theranostics based on zinc porphyrin complexes with an extended π-system with the external chelate ligand GdDOTA **10-12** were obtained, and the properties of the synthesized single- and two-photon activated PS as imaging probes were studied (Figure 47).[668,669] The attachment of GdDOTA to PS was realized using the commercial ligand DOTAGA (1,4,7,10-tetraazacyclodododecane-1-glutar-4,7,10-triacetic acid), which provided local flexibility while maintaining the stability of the GdDOTA fragment.

High relaxation r_1 values were obtained for **10-12**, which were 19.32, 19.94, and 14.33 mM^{-1}-s^{-1} at 20 MHz, respectively, which is 4-5 times higher for known contrast agents. A 20% increase in relaxation was also observed in the presence of BSA. Compound **10** had a strong single-photon absorption capacity (εmax = 41000 M^{-1} cm-1 at 667 nm in water).

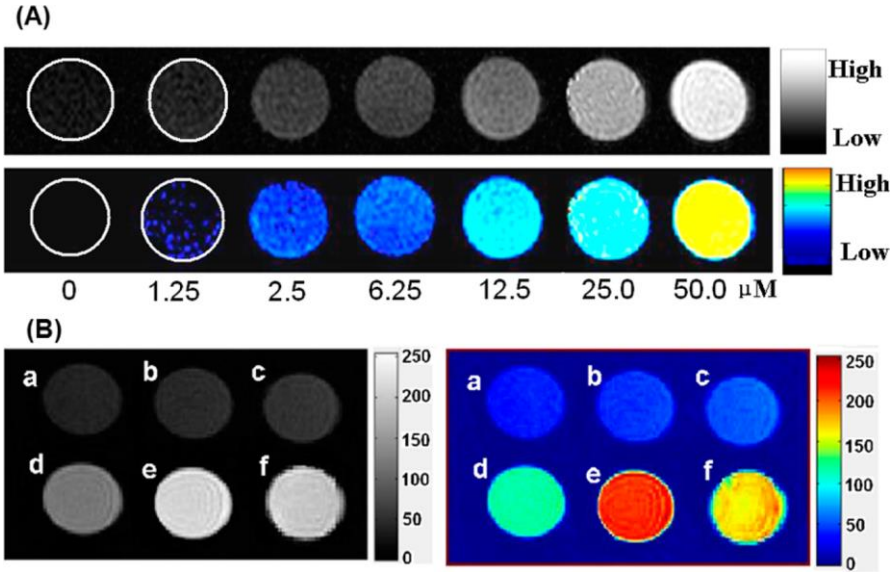

Figure 46. (A) T1-weighted phantom MR images for complex **9** with a concentration of 0−50.0 μM. (B) T1-weighted phantom MR images for complex **9**. Copyright © 2014, American Chemical Society.[667]

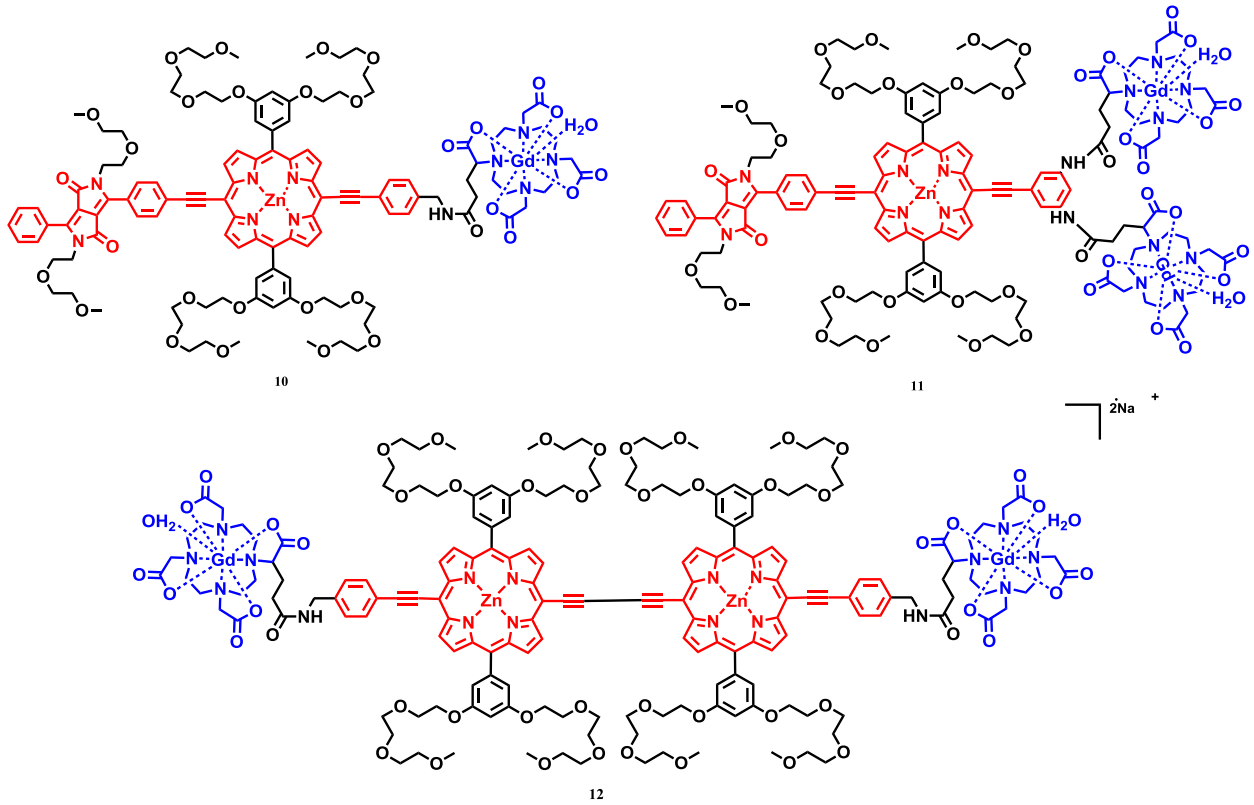

Figure 47. Chemical structure of theranostics **10-12** developed by Heitz *et al.*[668,669]

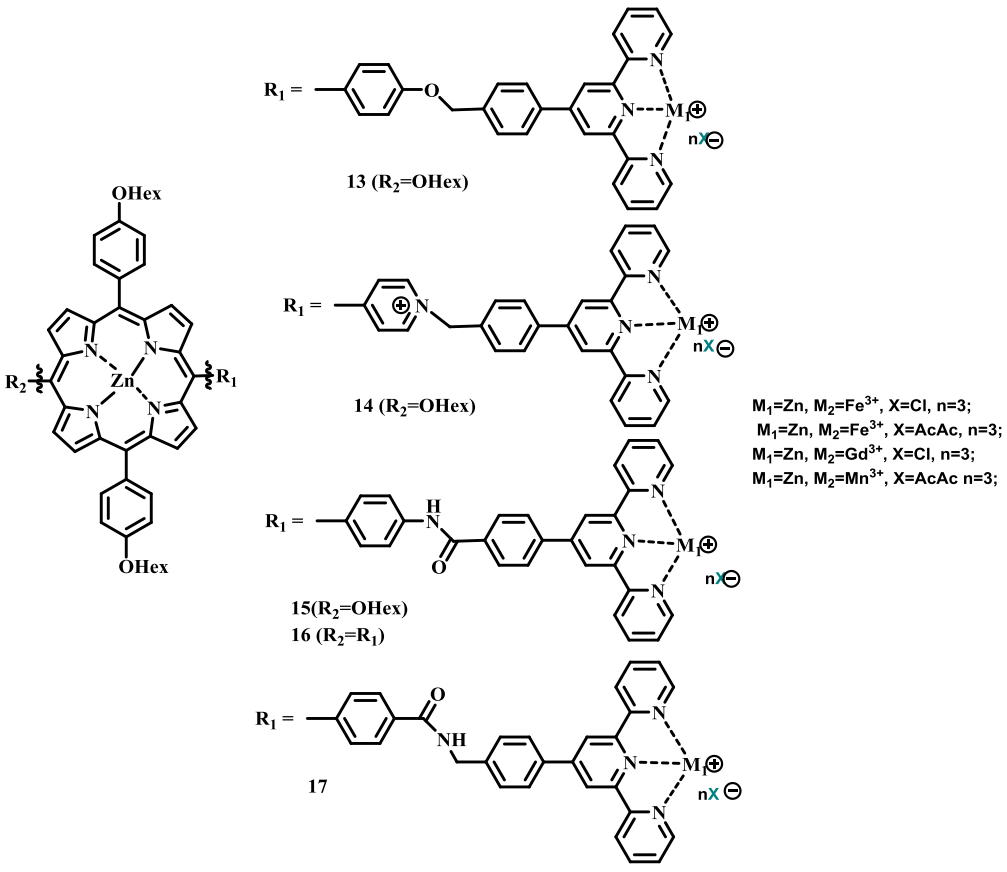

Figure 48. Structure of complexes with Gd(III), Fe(III), Mn(III).

The high PDT effect evaluated in HeLa cells was observed with single-photon excitation at 660 nm (1 h, 1 μM incubation), and a moderate two-photon PDT effect was achieved at 930 nm (300 scans, 1 μM incubation). High PDT effect was observed in HeLa cells after single-photon irradiation at 740 nm (30 min, incubation concentration of 1 μM). The effect of two-photon PDT was observed at 910 nm (300 scans, incubation concentration 2 μM) as a function of light power, and 100% cell death was observed at an average power of 108 mW.

In our work, terpyridine derivatives were used as an external chelating agent to obtain conjugates of *meso*-arylporphyrins with Gd(III), Fe(III), and Mn(III).[670] Terpyridine belongs to the type of linear pincer (claw-shaped) ligands and forms coordination chelates of the tridentate type with various metal cations in an almost flat geometry due to the presence of three conjugated nitrogen atoms in the molecule.[671] We have developed synthetic approaches for the preparation of conjugates based on porphyrins of A2B2 and A3B type with an active functional groups (NH_2, COOH, OH, Py) (Figure 48).

The highest yields were achieved when the amide bond between the porphyrin and terpyridine fragments was created. Thus, the yields of conjugates **15-17** were 90-95%. The conditions for obtaining conjugates **13-17** with paramagnetic ions Gd(III), Fe(III), Mn(III) for the subsequent creation of MRI-agents were established. Thus, it appeared that conjugate complexes with Fe(III) and Mn(III) salts were formed under mild conditions in an inert atmosphere at room temperature with the addition of sodium acetate as a catalyst, while the introduction of gadolinium under mild conditions was not effective enough and required harsher reaction conditions. To obtain Gd(III) complexes, the reaction was carried out in an inert box in an autoclave when heated well above the boiling point of the solvents (80°C).

To assess the safety of the obtained conjugates, it was important to evaluate the effect of the newly synthesized compounds on the ability to disrupt the integrity of intercellular contacts (test for inhibition of metabolic cooperation or for promoter activity). The study demonstrated that compounds **13-17** do not exhibit promoter activity in the given concentration ranges, i.e., they do not disrupt intercellular contacts. Thus, when exposed to compound **14** at concentrations of 4.5 μM; 2.25 μM; 1.125 μM and 0.56 μM, the degree of cell cooperation was 109%, 105%, 101%, 111% relative to untreated cells (Figure 49). At the same time, the degree of cell cooperation in the samples treated with TPA at a final concentration of 5 μg/ml was 15% to 20%, which is statistically significantly different from the control ($p<0.01$). Figure 49 shows microphotographs of the cell monolayer in the scratch region from the control and experimental samples.

The dark and light-induced toxicity of the obtained conjugates was evaluated *in vitro* on the Hep-2 cell line with and without irradiation for 1.5 and 24 h. The absence of dark and light-induced toxicity of the obtained compounds after 1.5 h was shown. However, an increase in dark-induced toxicity was observed with prolonged incubation. Moreover, for the conjugates linked by an amide bond, the toxicity was lower. Thus, for conjugate **13** after 24 h of incubation the IC50 was 2.47±0.233 μM (irradiation dose 8.073 J/cm^2) and 2.55±0.28 μM (no irradiation). For conjugate **15**, the IC50 was 1.55±0.15 μM (irradiation dose 8.073 J/cm^2) and 4.17±0.251 μM (no irradiation) (Figure 50). Such an effect may be related to the better biocompatibility (lower toxicity) of the amide bond for cells.

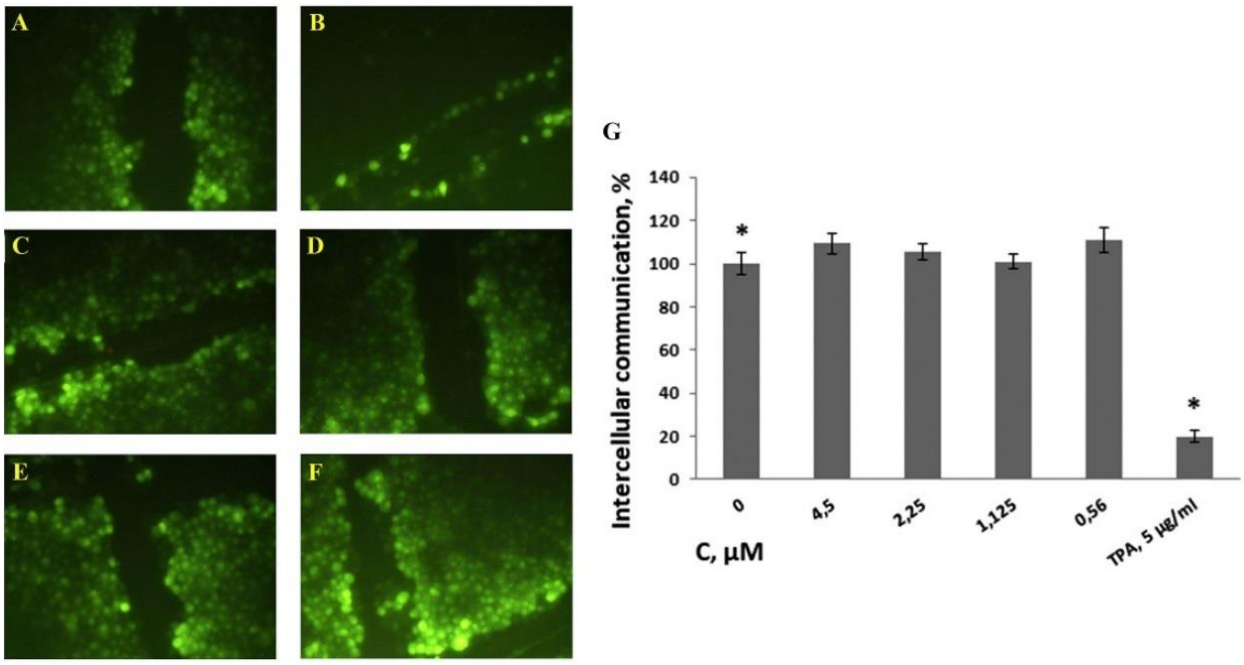

Figure 49. Micrographs of cell monolayer in the scratch area of control and experimental samples. A. Negative control (dH2O). B. Positive control (TPA, 5 μg/ml). Compound **12**: 4.5 μM (C); 2.25 μM (D); 1.125 μM (E) and 0.56 μM (F). LV propagation length in 4 minutes.

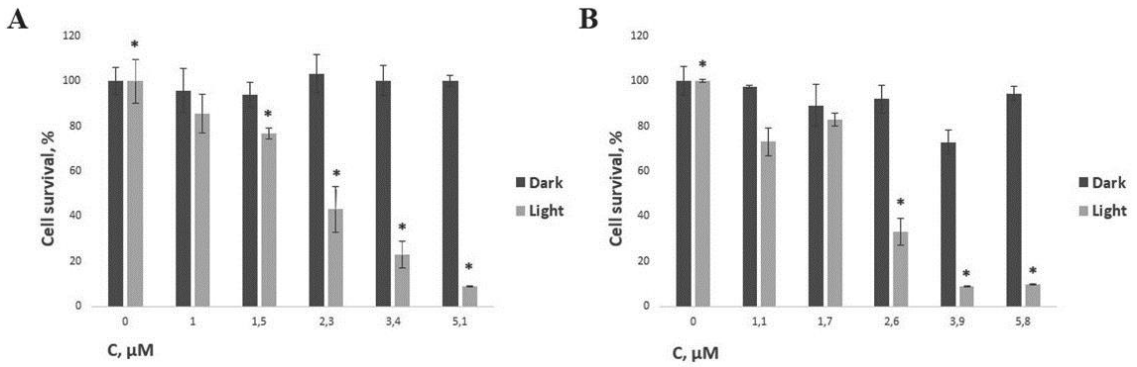

Figure 50. Effect of compounds on the viability of Hep2 cell line. Cells were irradiated for 90 min using the Medical Therapy Philips TL 20W/52 lamp (irradiation dose of 8.073 J/cm^2). Incubation of cells with the compound without irradiation in the dark for 90 min. * statistically significant differences in cell survival relative to values with zero concentration of the compound ($p<0.01$) were noted. A) conjugate **13**; B) conjugate **15**.

In conclusion, increasing interest in the development of effective contrast agents for MRI diagnostics based on tetrapyrrole PS is related to the fact that, to date, no commercially available contrast agent is effective enough for accurate detection of malignant neoplastic tissues. Analysis of the literature has shown that the development of multifunctional theranostic systems for combined diagnosis and therapy of cancer using PDT and MRI methods is a promising approach in clinical practice. Tetrapyrrole PSs are a suitable chemical platform for the design of multimodal agents for PDT. The strategy of combining bimodal agents in the structure of a single molecular object provides additional advantages of increased hydrophilicity of the PS in biological fluids and improved proton relaxation for MRI efficiency due to the increased molecular weight.

16. Effect of Amphiphilic Polymers and Polysaccharides on the Photosensitizing Activity of Porphyrin and Non-Porphyrin Dyes

One of the most important priorities of the Strategy for Scientific and Technological Development of the Russian Federation is the "Transition to personalized medicine, high-tech healthcare and health-saving technologies, including through the rational use of drugs (primarily antibacterial drugs)". Antibacterial photodynamic therapy (aPDT) can be considered not only in connection with the problem of the growth of resistance of pathogenic microorganisms to antimicrobial drugs, but also as a certain niche in antibiotic therapy, the relevance of which is associated with the loss of antibiotic effectiveness, as a result of which “common infections and minor injuries that have been curable for decades can now kill again” (opinion of WHO Assistant Director-General for Health Security Dr. Keiji Fukuda). It is precisely because of this circumstance that researchers from scientific and medical centers in Japan, the USA, South Korea, France, Australia, *etc*., begin to develop ideas about the use of aPDT instead of antibiotic therapy in the treatment of dental and some other types of chronic inflammatory processes. Approaches to the use of aPDT in the fight against wound infections, trophic ulcers and bedsores are also being developed. This is evidenced by the growing number of publications and relevant international symposiums. There is also a growing awareness that photodynamic therapy (PDT), including aPDT, should be understood not only as photoinduced effects on pathological tissues with necrosis or apoptosis of affected cells, but also as a targeted initiation of the effective dynamics of subsequent regenerative processes of tissue granulation and epithelialisation.[448,673] Such processes are initiated, among other things, by the body's immune system in the tissues adjacent to the pathologically developing tissues of the affected objects. And the task of PDT should be to choose the optimal regimes of photodynamic effects on pathological tissues so that the regenerative systems of the body can show their activity to the full extent. It is for this reason that the level of energy effects during PDT of affected objects should be minimized to a certain level in order to initiate, but not suppress, the possibilities of the body's regenerative systems. First of all, a controlled decrease in the level of light exposure during aPDT can be associated with a certain decrease in the concentration of photosensitizers (PS) introduced into the corresponding drugs, which is extremely important for reducing the phototoxicity of such dosage forms. As it was shown earlier,[674] the solution of such problems can be achieved by using PS with amphiphilic polymers (AP), with fragments of which PS molecules can form conformational complexes. In this case, the specific activity of the PS in the composition of such complexes with AP can exceed the specific activity of the initial PS molecules by an order of magnitude or more (“polymer effect”). Since photoinduced effects on pathological tissues during PDT are associated with photosensitized (with the participation of PS molecules, usually porphyrins, their chlorine derivatives, phthalocyanines) generation of singlet oxygen and its other reactive forms (ROS), conclusions about the "polymer effect" were made preliminary on the basis of the values of effective rate constant k_{eff} of photooxidation of a model substrate, tryptophan, and confirmed by aPDT of infected wounds in laboratory animals.[674,675] The idea of using PS together with polymeric components in the preparation of medicinal drugs for aPDT lies in the development of an integrated approach to the creation of effective photosensitizing systems. This is, first of all, the search for new components for the developed photosensitizing compositions

PS-AP, where PS is a photosensitizer; AP is an amphiphilic polymer. At the same time, it is possible to use not only traditional PS, such as phthalocyanine, porphyrin and chlorine derivatives, but also non-porphyrin compounds - dyes that not only show a high activity in the photogeneration of reactive oxygen species (ROS), primarily singlet oxygen $^1O_2$ with a quantum yield ΦΔ =0.75-0.76, but also exhibiting their own bactericidal activity (which is traditionally used in medical practice).[320,676,677] This, in particular, applies to methylene blue (MB) and rose bengal (RB).[678–680] These PS are currently used in aPDT of bacterial, viral and fungal infections, and their cost is significantly less than the cost of porphyrin compounds. It was shown in [673] that MB and RB dyes, as well as porphyrin compounds, can become the basis for the search for effective polymer-containing PS systems for aPDT. Methylene blue (Figure 51,a) is an organic dye of the thiazine dyes group, which has long been known as an effective photogenerator of singlet oxygen. Recently, it has attracted attention as a promising photosensitizer for PDT of cancer and infectious diseases.[681,682] Methylene blue is used as a PS for the destruction of Mycobacterium tuberculosis by aPDT.[683] However, unlike porphyrin derivatives, which require a long incubation period for photosensitization, phenothiazine derivatives, such as MB, do not require such a long pretreatment. Rose bengal (Figure 51,b) is a dianionic xanthene dye, also used in photodynamic therapy of certain types of cancer and fungal diseases.[684,685] The structure of MB and RB is represented by polycyclic aromatic compounds, which tend to form stable aggregates with low PS activity in aqueous solutions. In addition, due to its anionic nature, RB hardly penetrates through the cell walls of bacteria.

Studies have shown that ternary block copolymers of oxyethylene and oxypropylene, pluronics F127 and F108, polyvinylpyrrolidone, polyethylene glycol (PEG), and polyvinyl alcohol, may be of interest as AP for PS systems for aPDT. Naturally, the necessary (preliminary) condition for the use of such AP in PS systems is their promoting role in the model process of tryptophan photooxidation, which occurs during the photosensitized energy transfer of triplet excited PS molecules to molecular oxygen with the formation of singlet oxygen in aqueous media. The kinetic regularities of tryptophan photooxidation catalyzed by methylene blue and rose bengal in the presence (and absence) of the indicated AP, as well as an assessment of the effect of AP on the absorption and fluorescence spectra of the dyes, are presented below.

As shown earlier, amphiphilic polymers can initiate the deaggregation of porphyrins or dyes in an aqueous medium, thereby increasing the proportion of PS molecules that are effectively involved in the process of photosensitizing oxidation of substrate molecules. It is known that the aggregation of porphyrins in aqueous media, which reduces their photosensitizing activity due to the internal dissipation of photoexcitation energy, is due to hydrophobic interactions of their macrocycles, while the aggregation of these dyes is associated with their substituted anthracene structure. The magnitude of the effect of AP on the state of PS associates in all cases was analyzed by the value of the effective rate constant k_{eff} of the rate of tryptophan photooxidation in the presence of these PS and AP. At the same time, the measure of the ability of amphiphilic polymers to deaggregate the associates of these dyes when interacting with MB and RB, a kind of "activity series" of AP in the process of deaggregation, does not coincide with the similar series of AP activity during the destruction of aggregates of water-soluble porphyrin PS.[686 -688]

Thus, according to the ability to cause deaggregation of porphyrin water-soluble PS, in particular, photoditazine and dimegin, that is, to increase the value of k_{eff}, amphiphilic polymers are arranged as follows: PVP > F127 > > F108 > PEG > PVA. A similar pattern for MB and RB looks somewhat different: PVA > F108 > F127 > PEG > > PVP. These differences in the nature of the interaction of amphiphilic polymers with porphyrin PS and dyes are apparently related to the difference in the structures of macrocyclic PS and anthracene derivatives, which have small sizes.

The main interactions that determine the supramolecular structural organization of macrocyclic porphyrin compounds (including photoditazine and dimegine) in aqueous solutions are associated with hydrophobic, hydrogen, and donor-acceptor bonds. At the same time, the nature of intermolecular interactions of anthracene derivatives should be greatly influenced by the presence of positively charged (MB) or electronegative (RB) groups. Indeed, anionic RB, depending on the p*H* of the medium, can exist in cationic, neutral (lactone), and anionic forms (Figure 52). In a neutral photoinactive form, rose bengal exists in a slightly acidic environment (pH < 5) (Figure 52,II). In a neutral and weakly alkaline medium (p*H* 7.2–7.6), RB has a characteristic absorption spectrum with two bands (550 and 515 nm), corresponding to the dianionic form of RB (Figure 52,III). Thus, RB works as a PS only in a neutral and weakly alkaline medium (p*H* 7.2-7.6).[689,690] Another issue that is usually discussed in connection with the development of effective PS systems for aPDT is associated with the simultaneous use of biologically active molecules - proteins, proteolytic enzymes, polysaccharides with their own bactericidal activity during aPDT procedures. However, such biopolymers can reduce and even suppress the activity of dyes in $^1O_2$ photogeneration. It is shown below that one of the possible ways to solve these problems, specifically, when using natural polysaccharides with wound healing ability - chitosan (CHT) and sodium alginate (SA) in aPDT procedures - is the formation of conjugates of PS (in this case, MB and RB) with the indicated polysaccharides. Such conjugates provide better penetration of PS through bacterial cell walls, the structure of which includes polysaccharides and their complexes with proteins,[691] directly into the cell.

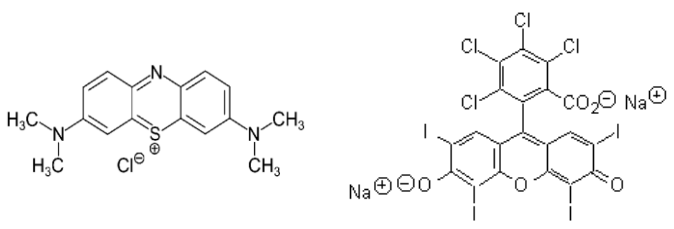

Figure 51. Structural formula of methylene blue (a) and rose bengal (b).

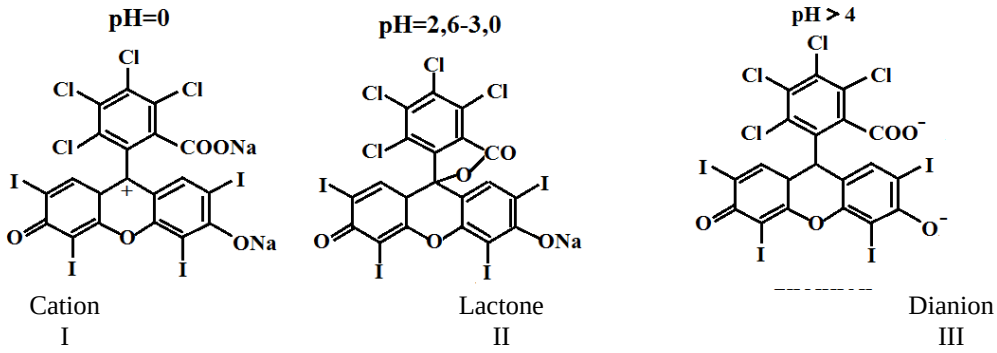

Figure 52. Tautomeric forms of rose Bengal.

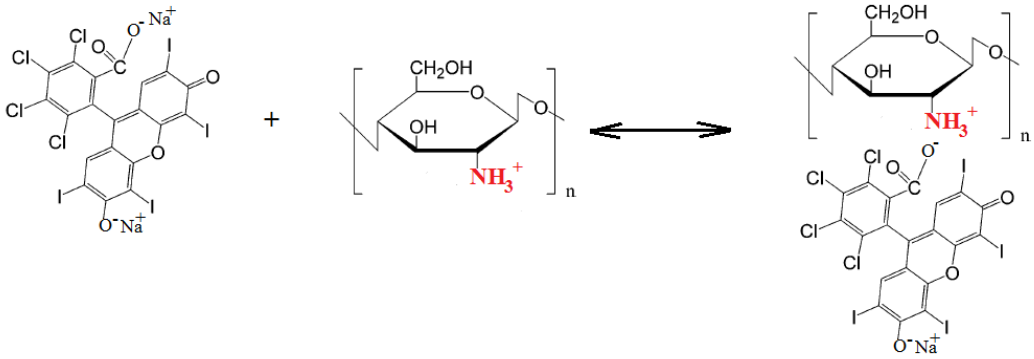

Figure 53. Schematic representation of the formation of the RB conjugate - a fragment of CHT.

Among microbial pathogens, gram-negative bacteria have the highest antibiotic resistance, and therefore the diseases caused by such microflora are extremely difficult to treat with antimicrobial therapy. They are also considered to be sufficiently resistant to photodynamic effects,[692] which is associated with the low permeability of their outer membrane for PS. It is known that cationic PS can most effectively interact with gram-negative bacteria.[210] Currently, PS covalently bound to polymeric polycations (natural and synthetic) are also used in aPDT. Thus, it was shown in [693] that the treatment of deuteroporphyrin with the polycationic peptide polymyxin *B* promotes the penetration of the formed complex through the membrane of gram-negative bacteria. The use of conjugates of anionic dyes (phthalocyanines) with cationic polylysine leads to an increase in their photobactericidal activity.[694] It was also shown that the binding of photosensitizers used in medical practice, in particular, photohem and photoditazine, with chitosan gel reduced the toxicity of the photosensitizer and significantly reduced hemorrhagic phenomena in the wound.[695-697] In this case, the interaction of polycationic chitosan and porphyrin PS significantly reduces their activity in the processes of generation of singlet oxygen.[698] It was shown that such a decrease is due to the aggregation of porphyrin molecules near the protonated amino groups of chitosan.[699,700] Moreover, as we demonstrated earlier, the activity of PS-chitosan systems in $^1O_2$ photogeneration in the aqueous phase can be increased by adding AP, specifically, polyvinylpyrrolidone or Pluronic F127.[701,702] It was shown by the proton NMR method that in the presence of the indicated AP, the photosensitizer is coordinated with the molecules of the amphiphilic polymer (formation due to hydrophobic and hydrogen bonds), which promotes PS disaggregation and, obviously, prevents its interaction with chitosan molecules.[686]

At the same time, the anionic dye RB interacts with protonated amino groups of chitosan macromolecules to form ionically bound conjugates (Figure 53), which leads to a decrease in the value of the effective photooxidation rate constant k_{eff} by 2.5–3 times.

In addition, it was shown that RB molecules that do not interact with chitosan macromolecules retain their photocatalytic activity. It should be emphasized that this equilibrium can exist only in a buffer solution, where the p*H* for the RB-CHT system cannot be lower than 4.5–4.0. When this reaction is carried out in an aqueous solution, the introduction of chitosan almost completely inhibits the process of photocatalytic oxidation of tryptophan. Since chitosan becomes soluble only in a slightly acidic medium (0.2–0.5% acetic acid, p*H* 4.5), it is also necessary to establish the role of acetic acid in the observed effect of chitosan on the PS activity of porphyrin and nonporphyrin photosensitizers, as well as the effect of acetic acid on the structure of the amphiphilic polymer, which determines the activity of PS-AP systems under such conditions. It turned out that in the case of rose bengal in an acetic acid medium, a slight

decrease in the value of k_{eff} (by approximately 1.3 times) is observed, i.e. the main role in reducing the photocatalytic activity of RB belongs to chitosan. At the same time, in the presence of PVP, the photocatalytic activity of RB is practically restored to its original value. A similar effect on the value of k_{eff} in the presence of chitosan is observed when MB is used as a PS. In this case, the drop in k_{eff} is 25-35%. A different picture is observed for PS of porphyrin and chlorine nature. It is shown that in a solution of 0.2% acetic acid (p*H*~4) both the photocatalytic activity of PPS and their complexes with AP and the spectral properties of dimegin and chlorin e_6 change. Under these conditions, PS is protonated to form a monoprotonated form. The photocatalytic activity of the monoprotonated form of DMG increases by ~1.4 times, while the photoactivity of protonated Ce6 decreases by ~1.2 times.[701] Due to the decrease of the k_{eff} value of tryptophan photooxidation catalyzed by MB and RB in the presence of chitosan, experiments on the use of sodium alginate as a polysaccharide (a biopolymer with wound healing properties) were carried out; Pluronic F127, PVA, CHT and PVP were used as amphiphilic polymers. The obtained results are shown in Table 11.

Table 11. Values of k_{eff} for MB, RB systems in the presence of polymers. The concentrations of polymers indicated in parentheses are given in mass fractions. [PS] = $5 \cdot 10^{-6}$ M, [Trp] = $1 \cdot 10^{-4}$ M, Trp-tryptophan.

The composition of the system in the order of mixing	k_{eff}, L/(mol·s)
MB	1500
MB, SA (0.001)	400
MB, SA (0.0001)	900
MB, PVA (0.04), SA (0.001)	800
MB, PVP (0.04), SA (0.001)	500
MB, F127 (1.30) SA (0.001)	800
MB, F127 (1.30) SA (0.0001)	1450
MB, CHT (0.01)	200
MB, F127 (1.30) CHT (0.01)	700
RB	1600
RB, SA (0.01)	1550
RB, SA, PVA	1800
RB, CHT (0.01)	50
RB, PVP (1.30), CHT (0.01)	1400

As follows from the data in Table 11, sodium alginate, as well as CHT, can significantly reduce the photocatalytic activity of MB, while the addition of amphiphilic polymers to the CHT-PS mixture can almost completely neutralize the effect of polysaccharides. The most active in these systems are PVP, F127, and PVA. It is interesting to note that sodium alginate in the case of RB practically does not reduce the value of keff. Possibly, this is due to the absence of interaction between the SA polyanion and the anionic RB. It should also be noted that in PS systems based on porphyrin photosensitizers, polyvinyl alcohol is completely inactive. Thus, in order to obtain effective PS polymer compositions containing polysaccharides and amphiphilic polymers, it is necessary, starting from the choice of PS, to carry out a targeted selection of AP and polysaccharide components.

Acknowledgements. The review was financially supported by a number of foundations, programs and grants: Section 1 (Koifman O.I. *et al.*) – by Ministry of Science and Higher Education of the Russian Federation (grant agreement No FZZW-2020-0008); Section 2 (Fedorov A.Yu. *et al.*) – by the Russian Science Foundation under Grant No. 21-73-10230 (https://rscf.ru/en/project/21-73-10230/) and by State assignment via the Research scientific laboratory of "Chemistry of natural products and their synthetic analogues" of Scientific Educational Centre "Technoplatform 2035" (FSWR-2021-014); Section 3 (Belykh D.V.) – The work was carried out within the framework of the state tasks of the Institute of Chemistry of the Komi Research Center of the Ural Branch of the Russian Academy of Sciences (Syktyvkar) No. 122040600073-3; Section 4 (Lebedeva N.Sh. *et al.*) – by the Russian Science Foundation (grant no. 21-73-20140); Section 5 (Gorbunova Yu.G. *et al.*) – by the Russian Science Foundation (project no. 19-13-00410-P); Section 6 (Dudkin S.V.) – by the Ministry of Science and Higher Education of the Russian Federation (Contract/agreement No. 075-00697-22-00); Section 7 (Lyubimtsev A.V., Maiorova L.A. *et al.*) – by the grant of the Russian Science Foundation (20-12-00175), and Ministry of Science and Higher Education of the Russian Federation (FZZW-2020-0008, synthesis of the compounds); Section 8 (Tyurin V.S. *et al.*) – by the Russian Science Foundation, grant 22-23-00903; Section 9 (Zenkevich E.I.) – by the BSPSR program "Photonics and Electronics for Innovations (2021-2025, Belarus)", Volkswagen Foundation (Project "New Functionalities of Semiconductor Nanocrystals by Controllable Coupling to Molecules"), and Visiting Scholar Program of TU Chemnitz, Germany (E.Z., 2020-2021); Section 10 (Berezin D.B. *et al.*) – by Russian Foundation for Basic Research, project number 20-03-00153. Authors are grateful to the Centers for Shared Use of Scientific Equipment of ISUCT (support of the Ministry of Science and Higher Education of Russia, project number 075-15-2021-671) and ISC RAS. The authors are grateful to Dr. I.I. Hludeev and Dr. V.P. Zorin (Belorussian State University) for their assistance in realization of gel-chromatographic experiments. Section 11 (Grin M.A. *et al.*) – Chemical synthesis and article preparation was performed as a part of the project "Radiopharmaceuticals" during realization of the RTU MIREA university development program (Federal academic leadership program Priority 2030). Biological studies were supported by the Ministry of Science and Higher Education of the Russian Federation (project № 0706-2020-0019). NMR spectra were performed using the equipment of the Shared Science and Training Center for Collective Use RTU MIREA and supported by the Ministry of Science and Higher Education of the Russian Federation. Section 14 (Loschenov V. B. *et al.*) – by the Ministry of Education and Science of the Russian Federation, grant for the creation and development of world-class research centers No. 075-15-2022- 315 "Photonics" and by the Russian Foundation for Basic Research, grant 20-02-00928. Section 15 (Zhdanova K.A. *et al.*) – by the Russian Science Foundation (project no. 22-73-10176); Section 16 (Solovieva A.N. *et al.*) – by state order No. 122040400099-5 of the N.N. Semenov Federal Research Center for Chemical Physics RAS.

References

1. Sausville E.A. Anticancer Drug Development: An Introduction. In: *Cancer Pharmacology: An Illustrated Manual of Anticancer Drugs*, Springer Publishing Company, **2019**. Ch. 1, 1–10.
2. Laxmikeshav K., Kumari P., Shankaraiah N. *Med. Res. Rev.* **2022**, *42*, 513-575.
3. Liu Y., Qin R., Zaat S.A.J., Breukink E., Heger M. *J. Clin. Transl. Res.* **2015**, *1*, 140–167.
4. Algorri J.F., Ochoa M., Roldán-Varona P., Rodríguez-Cobo L., López-Higuera J.M. *Cancers (Basel)* **2021**, *13*.
5. Hamblin M. *Curr. Opin. Microbiol.* **2016**, *33*, 67–73.
6. Kustov A.V., Berezin D.B., Strel'nikov A.I., Lapochkina N.P. *Antitumor and Antimicrobial Photodynamic Therapy: Mechanisms, Targets, Clinical and Laboratory Studies. A Guide* (Gagua A.K., Ed.), Moscow: Largo, **2020**, 108 p.
7. Van Straten D., Mashayekhi V., De Bruijn H.S., Oliveira S., Robinson D.J. *Cancers* **2017**, *9*, 1–54.
8. Caterino M., D'Aria F., Kustov A.V., Belykh D.V., Khudyaeva I.S., Startseva O.M., Berezin D.B., Pylina Ya.I., Usacheva T.R., Amato J., Giancola C. *Int. J. Biol. Macromol.* **2020**, *145*, 244–251.
9. Kustov A.V., Privalov O.A., Strelnikov A.I., Koifman O.I., Lubimtsev A.V., Morshnev Ph.K., Moryganova T.M., Kustova T.V., Berezin D.B. *J. Clin. Med.* **2022**, *11*, 233.
10. Bonnett R. *Chem. Soc. Rev.* **1995**, *24*, 19–33.
11. Venediktov E.A., Tulikova E.Yu., Rozhkova E.P., Belykh D.V., Khudyaeva I.S., Berezin D.B. *Macroheterocycles* **2017**, *10*, 295–300.
12. Zenkevich E., Sagun E., Knyukshto V., Shulga A., Mironov A., Efremova O., Bonnett R., Songca S.P., Kassem M.J. *Photochem. Photobiol. B* **1996**, *33*, 171–180.
13. Kustov A.V., Morshnev Ph.K., Kukushkina N.V., Krestyaninov M.A., Smirnova N.L., Berezin D.B., Kokurina G.N., Belykh D.V. *Comptes Rendus Chimie* **2022**, *25*, 97–102.
14. Bonnett R. *Chemical Aspects of Photodynamic Therapy*. Amsterdam: Science Publishers, **2000**.
15. Allison R.R., Moghissi K. *Clin. Endosc*. **2013**, *46*, 24–29.
16. Gogoi A., Kao F.-J., Liu Y.-L., Zhuo G.-Y. *Front. Phys.* **2022**, *10*, 977683.
17. Kou J., Dou D., Yang L. *Oncotarget* **2017**, *8*, 81591–81603.
18. Ochsner M. *J. Photochem. Photobiol. B* **1997**, *39*, 1–18.
19. Zenkevich E., Sagun E., Knyukshto V., Shulga A., Mironov A., Efremova O., Bonnett R., Pinda Songca S., Kassem M. *J. Phochem. Photobiol., B* **1996**, *33*, 171–180.
20. Isakau H.A., Parkhats M.V., Knyukshto V.N., Dzhagarov B.M., Petrov E.P., Petrov P.T. *J. Photochem. Photobiol., B* **2008**, *92*, 165–174.
21. Parkhats M.V., Galievskiy V.A., Stasheuski A.S., Trukacheva T.V., Dzhagarov B.M. *Opt. Spectrosc*. **2009**, *107*, 1026–1032.
22. Dadeko A., Murav'eva T.D., Starodubtsev A.M., Gorelov S.I., Dobrun M.V., Kris'ko T.K., Bagrov I.V., Belousova I., Ponomarev G.V. *Opt. Spectrosc.* **2015**, *119*, 633–637.
23. Zhang J., Jiang C., Longo J.P.F., Azevedo R.B., Zhang H., L.A. Muehlmann. *Acta Pharmaceutica Sinica B* **2018**, *8*, 137–146.
24. Amos-Tautua B.M., Pinda Songca S., Oluwafemi O.S. *Molecules* **2019**, *24*, 2456.
25. Krasnovsky Jr. A.A., Kozlov A.S., Benditkis A.S. *Macroheterocycles* **2019**, *12*, 171–180.
26. Soy R.C., Babu B., Oluwole D.O., Nwaji N., Oyim J., Amuhaya E., Prinsloo E., Mack J., Nyokong T. *J. Porphyrins Phthalocyanines* **2019**, *23*, 34–45.
27. Szurko A., Rams-Baron M., Montforts F.P., Bauer D., Kozub P., Gubernator J., Altmann S., Stanek A., Sieron A., Ratuszna A. *Photodiagn. Photodyn.* **2020**, *30*, 101799.
28. Zhang Q., He J., Yu W., Li Y., Liu Z., Zhou B., Liu Y. *RSC Med. Chem*. **2020**, *11*, 427–437.
29. Xiao-An Z., Lovejoy K.S., Jasanoff A., Lippard S.J. *Proc. Natl. Acad. Sci. U. S. A.* **2007**, 104, 10780–10785.
30. Xiaolong L., Xiaoda L., Lijia J., Xiuli Y., Zhifei D. *Biomaterials* **2014**, *35*, 6379–6388.
31. Lovell J.F., Pui-Chi L. *Theranostics* **2012**, *2*, 815–816.
32. Huang H., Song W., Rieffel J., Lovell J.F. *Front. Phys.* **2015**, *3*, 23–29.
33. Bhupathiraju N.V.S.D.K., Rizvi W., Batteas J.D., Drain C.M. *Org. Biomol. Chem.* **2016**, *14*, 389–408.
34. Mamardashvili G.M., Mamardashvili N.Zh., Koifman O.I. *Russ. Chem. Rev.* **2008**, *77*, 59–75.
35. Koifman O.I., Mamardashvili N.Zh. *Nanotechnologies in Russia* **2009**, *4*, 253–261.
36. Beletskaya I., Tyurin V.S., Tsivadze A.Y., Guilard R., Stern C. *Chem. Rev*. **2009**, *109*, 1659–1713.
37. *Handbook of Porphyrin Science, Vol. 4* (Kadish K.M., Smith K.M., Guilard R., Eds.), World Scientific Publishing Co., Singapore, **2010**.
38. *Handbook of Porphyrin Science, Vol. 27* (Kadish K.M., Smith K.M., Guilard R., Eds.), World Scientific Publishing Co., Singapore, **2014**.
39. Pereira P.M.R., Tomé J.P.C., Fernandes R., Molecular Targeted Photodynamic Therapy for Cancer. In: *Handbook of Porphyrin Science, Vol. 39* (Kadish K.M., Smith K.M., Guilard R., Eds.), World Scientific Publishing Co., Singapore, **2016**. 127–169.
40. Lupu M., Thomas C.D., Poyer F., Mispelter J., Rosilio V., Maillard P., Photobiology and Photochemistry Hand-in-Hand in Targeted Antitumoral Therapies. In: *Handbook of Porphyrin Science, Vol. 39* (Kadish K.M., Smith K.M., Guilard R., Eds.), World Scientific Publishing Co., Singapore, **2016**. 171–356.
41. Mfouo-Tynga I.S., Dias L.D., Inada N.M., Kurachi C. *Photodiagn. Photodyn.* **2021**, *34*, 102091.
42. Patent RU 2 128 993 C1, **1999**.
43. Lovell J.F., Liu T.W.B., Chen J., Zheng G. *Chem. Rev*. **2010**, *110*, 2839–2857.
44. Celli J.P., Spring B.Q., Rizvi I., Evans C.L., Samkoe K.S., Verma S., Pogu B.W., Hasan T. *Chem. Rev*. **2010**, *110*, 2795–2838.
45. Ethirajan M., Chen Y., Joshi P., Pandey R.K. *Chem. Soc. Rev*. **2011**, *40*, 340–362.
46. Ormond A.B., Freeman H.S. *Materials* **2013**, *6*, 817–840.
47. Habermeyer B., Guilard R. *Photochem. Photobiol. Sci*. **2018**, *17*, 675–1690.
48. Gomes A.T.P.C., Neves M.G.P.M.S., Cavaleiro J.A.S. *An Acad Bras Cienc* **2018**, *90* (1 Suppl. 2), 993–1026.
49. Li X., Lee S., Yoon J. *Chem. Soc. Rev*. **2018**, *47*, 1174–1188.
50. Zhao X., Liu J., Fan J., Chao H., Peng X. *Chem. Soc. Rev*. **2021**, *50*, 4185–4219.
51. Tian J., Huang B., Nawaz M.H., Zhang W. *Coord. Chem. Rev*. **2020**, *420*, 213410
52. Wang B., Zu G., Sun Y., Zhang Y., Wang X., Han J., Zhang C. *J. Liaon. Shihua Univ.* **2020**, *40*, 29–38.
53. Park W., Cho S., Han J., Shin H., Na K., Lee B., Kim D.H. *Biomater. Sci.* **2018**, *6*, 79–90.
54. Rajora M.A., Louac J.W.H., Zheng G. *Chem. Soc. Rev.* **2017**, *46*, 6433–6469.
55. Fernandes S.R.G., Fernandes R., Sarmento B., Pereira P.M.R., Tomé J.P.C. *Org. Biomol. Chem.* **2019**, *17*, 2579–2593.
56. Zhou J., Rao L., Yu G., Cook T.R., Chen X., Huang F. *Chem. Soc. Rev*. **2021**, *50*, 2839–2891.
57. Zhang H., Han J. *Org. Biomol. Chem.* **2020**, *18*, 4894–4905.
58. Hao M., Chen B., Zhao X., Zhao N., Xu F.-J. *Mater. Chem. Front.* **2020**, *4*, 2571–2609.
59. Escudero A., Carrillo-Carrión C., Castillejos M.C., Romero-Ben E., Rosales-Barrios C., Khiar N.A. *Mater. Chem. Front.* **2021**, *5*, 3788–3812.

60. Zheng Q., Liu X., Zheng Y., Yeung K.W.K., Cui Z., Liang Y., Li Z., Zhu S., Wang X., Wu S. *Chem. Soc. Rev.* **2021**, *50*, 5086–5125.
61. Policard A. *Compt. Rend. Soc. Biol*. **1924**, *91*, 1423–1424.
62. Auler H., Banzer G. *Z. Krebsforsch*. **1942**, *53*, 65–68.
63. Lipson R.L., Pratt J.H., Baldes E.J., Dockerty M.B. *Obstet. Gynecol.* **1964**, *24*, 78–84.
64. Dougherty T.J., Kaufman J.E., Goldfarb A., Weishaupt K.R., Boyle D., Mittleman A. *Cancer. Res.* **1978**, *38*, 2628–2635.
65. Filonenko E.V. *Russ. J. Gen. Chem*. **2015**, *85*, 211–216.
66. Patent RU 2183635 C2, 1999.
67. Patent RU 2183956, 2002.
68. Patent RU 2276976, 2004.
69. Patent RU 2523380, 2014.
70. Morozova N.B., Pankratov A.A., Plotnikova E.A., Vorontsova M.S., Makarova E., Lukyanets E.A., Kaprin A. *Research and Practical Medicine Journal* **2019**, *6*(4), 67–83.
71. Fukuzumi S., Lee Y.-M., Nam W. *ChemPhotoChem* **2018**, *2*, 121–135.
72. Lee H., Hong K.I., Jang W.D. *Coord. Chem. Rev.* **2018**, *354*, 46–73.
73. Zenkevich E.I., von Borczyskowski C. Photoinduced relaxation processes in self-assembled nanostructures: multiporphyrin complexes and composites “CdSe/ZnS quantum dot-porphyrin”. In: *Multiporphyrin Arrays: Fundamentals and Applications* (Kim D., Ed.) Singapore: Pan Stanford Publishing Pte. Ltd., **2012**, Chapter 5, 217.
74. Koifman O.I., Ageeva T.A., Beletskaya I.P., Averin A.D., Yakushev A.A., Tomilova L.G., Dubinina T.V., Tsivadze A.Yu., Gorbunova Yu.G., Martynov A.G., Konarev D.V., Khasanov S.S., Lyubovskaya R.N., Lomova T.N., Korolev V.V., Zenkevich E.I., Blaudeck T. , Ch. von Borczyskowski, Zahn D.R.T., Mironov A.F., Bragina N.A., Ezhov A.V., Zhdanova K.A., Stuzhin P.A., Pakhomov G.L., Rusakova N.V., Semenishyn N.N., Smola S.S., Parfenyuk V.I., Vashurin A.S., Makarov S.V., Dereven’kov I.A., Mamardashvili N.Zh., Kurtikyan T.S., Martirosyan G.G., Burmistrov V.A., Aleksandriiskii V.V., Novikov I.V., Pritmov D.A., Grin M.A., Suvorov N.V., Tsigankov A.A., Fedorov A.Yu., Kuzmina N.S., Nyuchev A.V., Otvagin V.F., Kustov A.V., Belykh D.V., Berezin D.B., Solovieva A.B., Timashev P.S., Milaeva E.R., Gracheva Yu.A., Dodokhova M.A., Safronenko A.V., Shpakovsky D.B., Syrbu S.A., Gubarev Yu.A., Kiselev A.N., Koifman M.O., Lebedeva N.Sh., Yurina E.S. *Macroheterocycles* **2020**, *13*, 311–467.
75. Jing H., Rong J., Taniguchi M., Liey J.S. *Coord. Chem. Rev.* **2022**, *456*, 214278.
76. Huang L., Asghar S., Zhu T., Ye P., Hu Z., Chen Z., Xiao Y. *Expert Opin. Drug Del.* **2021**, *18*, 1473–1500.
77. Chen J., Fan T., Xie Z., Zeng Q., Xue P., Zheng T., Chen Y., Luo X., Zhang H. *Biomaterials* **2020**, *237*, 119827.
78. Zenkevich E.I., Sagun E.I., Knyukshto V.N., Stasheuski A.S., Galievsky V.A., Stupak A.P., Blaudeck T., von Borczyskowski C. *J. Phys. Chem. C* **2011**, *115*, 21535-21545.
79. *Self-Assembled Organic-Inorganic Nanostructures: Optics and Dynamics* (Zenkevich E., von Borczyskowski C., Eds.), Singapore: Pan Stanford, **2016**.
80. Martynenko I.V., Orlova A.O., Maslov V.G., Baranov A.V., Fedorov A.V., Artemyev M. *Beilstein J. Nanotechnol*. **2013**, *4*, 895–902.
81. Rakovich Yu.P. Organic-Inorganic Hybrid Nanosystems for Photodynamic Therapy. In: *The 2nd International Symposium on Physics, Engineering and Technologies for Biomedicine, KnE Energy & Physics*, **2018**, 416–419.
82. Moghassemi S., Dadashzadeh A., Azevedo R.B., Feron O., Amorim C.A. *J. Control Release* **2021**, *339*, 75-90.
83. Yakavets I., Millard M., Zorin V., Lassalle H.P., Bezdetnaya L. *J. Control Release* **2019**, *304*, 268-287.
84. Sun C.Y, Cao Z., Zhang X.J., Sun R., Yu C.S., Yang X. *Theranostics* **2018**, *8*, 2939-2953.
85. Sewid F.A., Annas K.I., Dubavik A., Veniaminov A.V., Maslov V.G., Orlova A.O. *RSC Advances* **2022**, 12, 899-906.
86. Rybkin A.Y., Belik A.Y., Goryachev N.S., Mikhaylov P.A., Kraevaya O.A., Filatova N.V., Parkhomenko I.I., Peregudov A.S., Terent'ev A.A., Larkina E.A., Mironov A F., Troshin P.A., Kotelnikov A.I. *Dyes Pigm.* **2020**, *180*, 108411.
87. Zenkevich E., Blaudeck T., Sheinin V., Kulikova O., Selyshchev O., Dzhagan V., Koifman O., von Borczyskowski C., Zahn D.R.T. *J. Mol. Struct.* **2021**, *1244*, 131239.
88. Yu X.-T., Sui S.-Y., He Y.X., Yu C.-H., Peng Q. *Biomater Adv.* **2022**, *135*, 212725.
89. Mokhtari R.B., Homayouni T.S., Baluch N., Morgatskaya E., Kumar S., Das B., Yeger H. *Oncotarget*. **2017**, *8*, 38022–38043.
90. Khdair A., Chen D., Patil Y., Ma L., Dou Q.P., Shekhar M.P., Panyam J. *J. Control. Release* **2010**, *141*, 137–144.
91. Otvagin V.F., Kuzmina N.S., Kudriashova E.S., Nyuchev A.V., Gavryushin A.E., Fedorov A.Yu. *J. Med. Chem*. **2022,** *65* 1695–1734.
92. Hu X., Ogawa K., Li S., Kiwada T., Odani A. *Chem. Lett*. **2017,** *46*, 764–766.
93. Thapa P., Li M., Bio M., Rajaputra P., Nkepang G., Sun Y., Woo S., You Y. *J. Med. Chem*. **2016**, *59*, 3204–3214.
94. Kwiatkowski S., Knap B., Przystupski D., Saczko J., Kędzierska E., Knap-Czop K., Kotlińska J., Michel O., Kotowski K., Kulbacka Ju. *Biomed. Pharmacother.* **2018**, *106*, 1098–1107.
95. Hiyama K., Matsui H., Tamura M., Shimokawa O., Hiyama M., Kaneko T., Nagano Y., Hyodo I., Tanaka J., Miwa Y., Ogawa T., Nakanishi T., Tamai I. *J. Porphyrins Phthalocyanines* **2013**, *17*, 36–43.
96. Chen Y., Zheng X., Dobhal M.P., Gryshuk A., Morgan J., Dougherty T.J., Oseroff A., Pandey R.K. *J. Med. Chem*. **2005**, *48*, 3692–3695.
97. Dąbrowski J.M., Pucelik B., Regiel-Futyra A., Brindell M., Mazuryk O., Kyzioł A., Stochel G., Macyk W., Arnaut L.G. *Coord. Chem. Rev.* **2016**, *325*, 67–101.
98. Ye Y., Wang L.-X., Zhang D.-P., Yan Y.-J., Chen Z.-L. *J. Innov. Opt. Health Sci*. **2015**, 8, 1540001.
99. Dąbrowski J.M., Arnaut L.G. *Photochem. Photobiol. Sci.* **2015**, *14*, 1765–1780.
100. Pinto da Silva L., Magalhães C.M., Núñez-Montenegro A., Ferreira P.J.O., Duarte D., Rodríguez-Borges J.E., Vale N., Esteves da Silva J.C.G. *Biomolecules* **2019**, *9*, 384.
101. Li Q., Li W., Di H., Luo L., Zhu C., Yang J., Yin X., Yin H., Gao J., Du Y., You J. *J. Control Release* **2018**, *277*, 114–125.
102. Ulfo L., Costantini P.E., Di Giosia M., Danielli A., Calvaresi M. *Pharmaceutics* **2022**, *14*, 241.
103. Nyuchev A.V., Otvagin V.F., Gavryushin A.E., Romanenko Y.I., Koifman O.I., Belykh D.V., Schmalz H.-G., Fedorov A.Yu. *Synthesis* **2015**, *47*, 3717–3726.
104. Hu X., Ogawa K., Li S., Kiwada T., Odani A. *Bull. Chem. Soc. Jpn*. **2019**, *92*, 790–796.
105. Cheruku R.R., Cacaccio J., Durrani F.A., Tabaczynski W.A., Watson R., Siters KMissert., J.R., Tracy E.C., Dukh M., Guru K., Koya R.C., Kalinski P., Baumann H., Pandey R.K. *J. Med. Chem*. **2021**, *64*, 741−767.
106. Huang L., Wei G., Sun X., Jiang Y., Huang Z., Huang Y., Shen Y., Xu X., Liao Y., Zhao C. *Eur. J. Med. Chem.* **2018**, *151*, 294–303.
107. Simões J.C.S., Sarpaki S., Papadimitroulas P., Therrien B., Loudos G. *J. Med. Chem.* **2020**, *63*, 14119–14150.
108. Zhao X., Ma H., Chen J., Zhang F., Jia X., Xue J. *Eur. J. Med. Chem.* **2019**, *182*, 111625.
109. Otvagin V.F., Nyuchev A.V., Kuzmina N.S., Grishin I.D., Gavryushin A.E., Romanenko Y.V., Koifman O.I., Belykh

D.V., Peskova N.N., Shilyagina N.Y., Balalaeva I.V., Fedorov A.Yu. *Eur. J. Med. Chem.* **2018**, *144*, 740–750.
110. Otvagin V.F., Kuzmina N.S., Krylova L.V., Volovetsky A.B., Nyuchev A.V., Gavryushin A.E., Meshkov I.N., Gorbunova Y.G., Romanenko Y.V., Koifman O.I., Balalaeva I.V., Fedorov A.Yu. *J. Med. Chem*. **2019**, *62*, 11182–11193.
111. Huang K., Niu Y., Yuan G., Yan M., Xue J., Chen J. *Sensor Actuat B-Chem.* **2022**, *355*, 131275.
112. Musallam L., Ethier C., Haddad P.S., Bilodeau M. *J. Cell. Physiol.* **2004**, *198*, 62–72.
113. Zhang W., Lu J., Gao X.N., Li P., Zhang W., Ma Y., Wang H., Tang B. *Angew. Chem. Int. Ed.* **2018**, *57*, 4891-4896.
114. Brave S.R., Odedra R., James N.H., Smith N.R., Marshall G.B., Acheson K.L., Baker D., Howard Z., Jackson L., Ratcliffe K., Wainwright A., Lovick S.C., Hickinson D.M., Wilkinson R.W., Barry S.T., Speake G., Ryan A.J. *Int. J. Oncol*. **2011**, *39*, 271–278.
115. Leriche G., Chisholm L., Wagner A. *Bioorganic Med. Chem.* **2012**, *20*, 571–582.
116. Krylova L.V., Peskova N.N., Otvagin V.F., Kuzmina N.S., Nyuchev A.V., Fedorov A.Yu., Balalaeva I.V., *Opera Med. Physiol*. **2022**, *9*, 5–14.
117. Kuzmina N.S., Otvagin V.F., Krylova L.V., Nyuchev A.V., Romanenko Yu.V., Koifman O.I., Balalaeva I.V., Fedorov A.Yu. *Mendeleev Commun.* **2020**, *30*, 159–161.
118. Singh S., Aggarwal A., Bhupathiraju N.V.S.D.K., Arianna G., Tiwari K., Drain C.M. *Chem. Rev.* **2015**, *115*, 10261–10306.
119. Zaki M., Arjmand F., Tabassum S. *Inorg. Chim. Acta* **2016**, *444*, 1–22.
120. Muhammad N., Guo Z. *Curr Opin Chem Biol*. **2014**, 144–153.
121. Hadi A.G., Jawad K., Ahmed D.S., Yousif E. *Syst. Rev. Pharm*. **2019**, *10*, 26–31.
122. Khan A., Parveen S., Khalid A., Shafi S. *Inorg. Chim. Acta*. **2020**, *505*, 119464.
123. Shaheen F., Sirajuddin M., Ali S., Rehman Z.-U., Dyson P.J., Shah N.A., Tahir M.N. *J. Organomet. Chem.* **2018**, *856*, 13–22.
124. Tikhonov S., Ostroverkhov P., Suvorov N., Mironov A., Efimova Yu., Plutinskaya A., Pankratov A., Ignatova A., Feofanov A., Diachkova E., Vasil'ev Yu., Grin M. *Int. J. Mol. Sci*. **2021**, *22*, 13563.
125. Witt O., Deubzer H.E., Milde T., Oehme I. Cancer Lett. **2009**, *277*, 8–21.
126. Eckschlager T., Plch J., Stiborova M., Hrabeta J. *Int. J. Mol. Sci*. **2017**, *18*, 1414.
127. Halsall J.A., Turner B.M. *BioEssays* **2016**, *38*, 1102–1110.
128. Banik D., Noonepalle S., Hadley M., Palmer E., Gracia-Hernandez M., Zevallos-Delgado C., Manhas N., Simonyan H., Young C.N., Popratiloff A., Chiappinelli K.B., Fernandes R., Sotomayor E.M., Villagra A. *Cancer Res.* **2020**, *80*, 3649–3662.
129. Aru B., Günay A., Şenkuytu E., Yanıkkaya Demirel G., Gürek A.G., Atilla D. *ACS Omega* **2020**, *5*, 25854−25867.
130. Rakha E.A., El-Sayed M.E., Green A.R., Lee A.H.S., Robertson J.F., Ellis I.O. *Cancer* **2007**, *109*, 25–32.
131. Aru B., Günay A., Yanıkkaya Demirel G.Y., Gürek A.G., Atilla D. *RSC Adv*. **2021**, *11*, 34963–34978.
132. Thomas C.J., Rahier N.J., Hecht S.M. *Bioorg. Med. Chem*. **2004**, *12*, 1585–1604.
133. Zhang H.-X., Lin H.-H., Su D., Yang D.-C., Liu J.-Y. *Mol. Pharmaceut.* **2022**, *19*, 630–641.
134. Pettit G.R., Singh S.B., Hamel E., Lin C.M., Alberts D.S., Garcia-Kendal D. *Experientia* **1989**, *45*, 209–211.
135. Nam N.H. *Curr. Med. Chem*. **2003**, *10*, 1697–1722.
136. Bio M., Rajaputra P., Nkepang G., Awuah S.G., Hossion A.M.L., You Y. *J. Med. Chem.* **2013**, *56*, 3936–3942.
137. Ha S.Y.Y., Zhou Y., Fong W.P., Ng D.K.P. *J. Med. Chem.* **2020**, *63*, 8512–8523.
138. Chou T.C. *Pharmacol. Rev.* **2006**, *58*, 621–681.
139. Gaukroger K., Hadfield J., Lawrence N.J., Nolan S., McGown A.T. *Org. Biomol. Chem.* **2003**, *1*, 3033–3037.
140. Hadfield J.A., McGown A.T., Mayalarp S.P., Land E.J., Hamblett I., Gaukroger K., Lawrence N.J., Hepworth L.A., Butler J. *Substituted Stilbenes and Their Reactions*, US7220784B2, **2007**.
141. Klán P., Šolomek T., Bochet C.G., Blanc A., Givens R., Rubina M., Popik V., Kostikov A., Wirz J. *Chem. Rev.* **2012**, *113*, 119−191.
142. Kuzmina N.S., Otvagin V.F., Maleev A.A., Urazaeva M.A., Nyuchev A.V., Ignatov S.K., Gavryushin A.E., Fedorov A.Yu. *J. Photochem. Photobiol. A* **2022**, *433*, 114138.
143. Lin W., Peng D., Wang B., Long L., Guo C., Yuan J. *Eur. J. Org. Chem*. **2008**, *2008*, 793–796.
144. Sheldon J.E., Dcona M.M., Lyons C.E., Hackett J.C., Hartman M.C.T. *Org. Biomol. Chem*. **2016**, *14*, 40–49.
145. Malatesti N., Munitic I., Jurak I. *Biophys Rev*. **2017**, *9*, 149–168.
146. Feng Y., Tonon C.C., Ashraf Sh., Hasan T. *Adv. Drug Delivery Rev.* **2021**, *177*, 113941.
147. Pucelik B., Sułek A., Dabrowski J.M. *Coord. Chem. Rev.* **2020**, *416*, 213340.
148. Sharma S.K., Dai T., Kharkwal G.B., Huang Y.-Y., Huang L., Bil De Arce V.J., Tegos G.P., Hamblin M.R. *Curr. Pharm. Des.* **2011**, *17*(13), 1303–1319.
149. Sobotta L., Skupin-Mrugalska P., Piskorz J., Mielcarek J. *Eur. J. Med. Chem*. **2019**, *175*, 72-106.
150. Dharmaratne P., Sapugahawatte D.N., Wang B., Chan C.L., Lau K.-M., Lau C.B.S., Fung K.P., KP D., IP M. *Eur. J. Med. Chem.* **2020**, *200*, 112341.
151. Takahashi T., Ogasawara Sh., Shinozaki Y., Tamiaki H. *Eur. J. Org. Chem.* **2019**, *37*, 6333-6340.
152. Suvorov N., Pogorilyy V., Diachkova E., Vasil'ev Y., Mironov A., Grin M. *Int. J. Mol. Sci*. **2021**, *22*, 6392.
153. Kustov A.V., Morshnev P.K., Kukushkina N.V., Smirnova N.L., Berezin D.B., Karimov D.R., Shukhto O.V., Kustova T.V., Belykh D.V., Mal'shakova M.V., Zorin V.P., Zorina T.E. *Int. J. Mol. Sci*. **2022**, *23*, 5294.
154. Cai J.-Q., Liu X.-M., Gao Z.-J., Li L.-L., Wang H. *Materials Today* **2021**, *45*, 77-92.
155. Awad M., Thomas N., Barnes T.J., Prestidge C.A. *J. Control. Release* **2022**, *346*, 300–316.
156. Anas A., Sobhanan J., Sulfiya K.M., Jasmin C., Sreelakshmi P.K., Biju V. *J. Photochem. Photobiol. C* **2021**, *49*, 100452.
157. Aroso R.T., Piccirillo G., Arnaut Z.A., Gonzalez A.C.S., Rodrigues F.M.S., Pereira M.M. *J. Photochem. Photobiol.* **2021**, *7*, 100043.
158. Luciano M., Brückner C. *Molecules* **2017**, *22*, 980.
159. Wiehe A., O'Brien J.M., Senge M.O. *Photochem. Photobiol. Sci.* **2019**, *18*, 2565-2612.
160. Huang L., Wang M., Huang Y.-Y., El-Hussein A., Wolf L., Chiang L. Y., Hamblin M. R. *Photochem. Photobiol. Sci*. **2018**, *17*, 638–651.
161. Tegos G.P., Anbe M., Yang Ch., Demidova T.N., Satti M., Mroz P., Janjua S., Gad F., Hamblin M.R. *Antimicrob. Agents Ch.* **2006**, *50*, 1402–1410.
162. Le Guern F., Ouk T.-S., Grenier K., Joly N., Lequartb V., Sol V. *J. Mater. Chem. B* **2017**, *5*, 6953–6962.
163. Yin R., Dai T., Avci P., Jorge A.E.S., CMA de Melo W., Vecchio D., Huang Y.-Y., Gupta A., Hamblin M. R. *Curr. Opin. Pharmacol.* **2013**, *13*, 1–32.
164. Huang L., Huang Y.-Y., Mroz P., Tegos G.P., Zhiyentayev T., Sharma S.K., Lu Z., Balasubramanian T., Krayer M., Ruzie C., Yang E., Kee H.L., Kirmaier C., Diers J.R., Bocian D.F., Holten D., Lindsey J.S., Hamblin M.R. *Antimicrob. Agents Ch.* **2010**, 3834–3841.
165. Taima H., Okubo A., Yoshioka N., Inoue H. *Tetrahedron Lett.* **2005**, *46*, 4161–4164.
166. Ryazanova O., Voloshin I., Dubey I., Dubey L., Zozulya V. *Ann. N.Y. Acad. Sci.* **2008**, *1130*, 293–299.

167. Miyatake T., Hasunuma Y., Mukai Y., Oki H., Watanabe M., Yamazaki S. *Bioorg. Med. Chem*. **2016**, *24*, 1155–1161.
168. Miyatake T., Tamiaki H., Shinoda H., Fujiwara M., Matsushita T. *Tetrahedron* **2002**, *58*, 9989–10000.
169. Saenz C., Ethirajan M., Tracy E.C., Bowman M.-J., Cacaccio J., Ohulchanskyy T., Baumann H., Pandey R.K. *J. Photochem. Photobiol. B* **2022**, *227*, 112375.
170. Mironov A.F., Nechaev A.V. *Russ. J. Bioorg. Chem*. **2003**, *29*, 96–98.
171. Mironov A.F., Nechaev A.V. *Russ. J. Bioorg. Chem.* **2001**, *27*, 120–123.
172. Nechaev A.V., Mironov A.F. *Russ. J. Bioorg. Chem.* **2008**, *34*, 245–251.
173. Gushchina O.I., Gramma V.A., Larkina E.A., Mironov A.F. *Mendeleev Commun*. **2017**, *27*, 50–52. DOI: 10.1016/j.mencom.2017.01.015
174. Mal'shakova M.V., Frolova L.L., Alekseev I.N., Kutchin A.V., Patov S.A., Belykh D.V. *Russ. Chem. Bull*. **2018**, *67*, 1467–1475.
175. Khudyaeva I.S., Shevchenko O.G., Belykh D.V. *Russ. Chem. Bull*. **2020**, *69*, 742–750.
176. Gradova M.A., Movchan T.G., Khudyaeva I.S., Chernyad'ev A.Yu., Plotnikova E.V., Lobanov A.V., Belykh D.V. *Macroheterocycles* **2020**, *13*, 23-32.
177. Pylina Y.I., Khudyaeva I.S., Startseva O.M., Shadrin D.M., Shevchenko O.G., Velegzhaninov I.O., Kukushkina N.V., Berezin D.B., Belykh D.V. *Macroheterocycles* **2021**, *14*, 317-322.
178. Gushchina O.I., Larkina E.A., Mironov A.F. *Macroheterocycles* **2014**, *7*, 414-416.
179. Li J., Zhang X., Liu Y., Yoon I., Kim D.-K., Yin J.-G., Wang J.-J., Shim Y. K. *Bioorg. Med. Chem*. **2015**, *23*, 1684–1690.
180. Gushchina O.I. *Synthesis and properties of amide derivatives of the chlorin series*, Diss. Cand. Chem. Sci. Moscow, **2019**, 130.
181. Mironov A.F., Ruziev R.D., Lebedeva V.S. *Russ. J. Bioorg. Chem.* **2004**, *30*, 466–476.
182. Pantiushenko I.V., Rudakovskaya P.G., Starovoytova A.V. *et al. Biochemistry (Moscow)* **2015**, *80*, 752–762.
183. Mironov A.F., Grin M.A., Tsiprovskii A.G., Titeev R.A., Nizhnik E.A., Lonin I.S. *Mendeleev Commun.* **2004**, *14*, 204-207.
184. Grin M.A., Mironov A.F. *Russ. Chem. Bull*. **2016**, *65*, 333–349.
185. Mal'shakova M.V., Belykh D.V. *J. Porphyrins Phthalocyanines* **2022**, *26*, 403–406.
186. Takahashi T., Ogasawara Sh., Shinozaki Y., Tamiaki H. *Bull. Chem. Soc. Jpn*. **2020**, *93*, 467–476.
187. Ogasawara S., Tamiaki H. *Bull. Chem. Soc. Jpn*. **2018**, *91*, 1724-1730.
188. Pandey R.K., Smith N.W., Shiau F.-Y., Dougherty T.J., Smith K.M. *J. Chem. Soc., Chem. Commun*. **1991**, 1637-1638.
189. Pandey R.K., Shiau F.U., Smith N.N., Dougherty D.J., Smith K.M. *Tetrahedron* **1992**, *48*, 7591-7600.
190. Pavlov V.Y., Ponomarev G.V. *Chem. Heterocycl. Compd*. **2004**, *40*, 393-425.
191. Ponomarev G.V. *Chem. Heterocycl. Compd.* **1997**, *33*, 1127–1166.
192. Belykh D.V. *Russ. J. Gen. Chem.* **2019**, *89*, 2604–2649.
193. Belykh D.V., Tarabukina I.S., Gruzdev I.V., Kodess M.I., Kutchin A.V. *J. Porphyrins Phthalocyanines* **2009**, *13*, 949–956.
194. Belykh D.V., Tarabukina I.S., Gruzdev I.V., Kuchin A.V. *Macroheterocycles* **2010**, *3*, 145-149.
195. Belykh D.V., Khudyaeva I.S., Startceva O.M., Gruzdev I.V., Romanenko Y.V. *Macroheterocycles* **2016**, *9*, 366-372.
196. Tarabukina I.S., Startseva O.M., Patov S.A., Belykh D.V. *Macroheterocycles* **2015**, *8*, 168-176.
197. Kustov A.V., Kustova T.V., Belykh D.V., Khudyaeva I.S., Berezin D.B. *Dyes Pigm.* **2020**, *173*, 107948.
198. Stamati I., Kuimova M. K., Lion M., Yahioglu G., Phillipsb D., Deonarain M.P. *Photochem. Photobiol. Sci*. **2010**, *9*, 1033-1041.
199. Phillips D. *Pure Appl. Chem.* **2011**, *83*, 733–748.
200. Stamati I. *Targeted Photodynamic Therapy of cancer using photoimmunoconjugates based on pyropheophorbide a derivatives*. PhD thesis, Imperial College, London September, **2010**.
201. Li J.Z., Wang J.J., Yoon I., Cui B.C., Shim Y.K. *Bioorg. Med. Chem. Lett*. **2012**, *22*, 1846–1849.
202. Casteel M.J., Jayaraj K., Gold A., Ball L.M., Sobsey M.D. *Photochem. Photobiol.* **2004**, *80*, 294
203. Costa L., Alves E., Carvalho C., Tomé J.P., Faustino M.A., Neves M.G., Tome A.C., Cavaleiro J.A., Cunha Â., Almeida A. *Photochem. Photobiol. Sci.* **2008**, *7*, 415.
204. Martins D., Mesquita M.Q., Neves M.G., Faustino M.A., Reis L., Figueira E., Almeida A. *Planta* **2018**, *248*, 409.
205. Lebedeva N.S., Koifman O. *Russ. J. Bioorg. Chem.* **2022**, *48*, 1.
206. Lebedeva N., Gubarev Y., Koifman M., Koifman O. *Molecules* **2020**, *25*, 4368.
207. Ergaieg K., Seux R. *Desalination* **2009**, *246*, 353.
208. Merchat M., Bertolini G., Giacomini P., Villaneuva A., Jori G. *J. Photochem. Photobiol. B: Biol.* **1996**, *32*, 153.
209. Hamblin M.R., Hasan T. *Photochem. Photobiol. Sci.* **2004**, *3*, 436.
210. Costerton J., Ingram J., Cheng K. *Bacteriol. Rev.* **1974**, *38*, 87.
211. Nikaido H. *Rev. Infect. Dis.* **1988**, S279.
212. Hamblin M.R., O'Donnell D.A., Murthy N., Rajagopalan K., Michaud N., Sherwood M.E., Hasan T. *J. Antimicrob. Chemother*. **2002**, *49*, 941.
213. Lebedeva N.S., Yurina E.S., Lubimtsev A.V., Gubarev Y.A., Syrbu S.A. *Chem. Phys. Lett.* **2022**, 140090.
214. Lebedeva N.S., Yurina E.S., Gubarev Y.A., Syrbu S.A. *Spectrochim. Acta, A* **2018**, *199*, 235.
215. Rapacka-Zdończyk A., Woźniak A., Michalska K., Pierański M., Ogonowska P., Grinholc M., Nakonieczna J. *Front. Med.* **2021**, *8*, 642609.
216. Vaara M. *Microbiol. Rev.* **1992**, *56*, 395.
217. Carvalho C.M., Gomes A.T., Fernandes S.C., Prata A.C., Almeida M.A., Cunha M.A., Tomé J.P., Faustino M.A., Neves M.G., Tomé A.C. *J. Photochem. Photobiol. B: Biol.* **2007**, *88*, 112.
218. Alves E., Costa L., Carvalho C., Tomé J.P., Faustino M.A., Neves M.G., Tomé A.C., Cavaleiro J.A., Cunha Â., Almeida A. *BMC Microbiol.* **2009**, *9*, 1.
219. Spesia M.B., Lazzeri D., Pascual L., Rovera M., Durantini E.N. *Fems Immunol. Med. Mic.* **2005**, *44*, 289.
220. Gyulkhandanyan A.G., Paronyan M.H., Gyulkhandanyan A.G., Ghazaryan K.R., Parkhats M.V., Dzhagarov B.M., Korchenova M.V., Lazareva E.N., Tuchina E.S., Gyulkhandanyan G.V. *J. Innov. Opt. Health Sci.* **2022**, *15*, 2142007.
221. Reddi E., Ceccon M., Valduga G., Jori G., Bommer J.C., Elisei F., Latterini L., Mazzucato U. *Photochem. Photobiol.* **2002**, *75*, 462.
222. Boyle R.W., Dolphin D. *Photochem. Photobiol.* **1996**, *64*, 469.
223. Lazzeri D., Rovera M., Pascual L., Durantini E.N. *Photochem. Photobiol.* **2004**, *80*, 286.
224. Marciel L., Mesquita M.Q., Ferreira R., Moreira B., Neves M.G.P.M.S., Faustino M.A.F., Almeida A. *Future Med. Chem* **2018**, *10*, 1821.
225. Goncalves P.J., Bezzerra F.C., Teles A.V., Menezes L.B., Alves K.M., Alonso L., Alonso A., Andrade M.A., Borissevitch I.E., Souza G.R. *J. Photochem. Photobiol. A: Chem.* **2020**, *391*, 112375.
226. Ribeiro C.P., Gamelas S.R., Faustino M.A., Gomes A.T., Tome J.P., Almeida A., Lourenco L.M. *Photodiagn. Photodyn. Ther.* **2020**, *31*, 101788.

227. Ribeiro C.P., Faustino M.A., Almeida A., Lourenço L.M. *Microorganisms* **2022**, *10*, 718.
228. Maisch T., Bosl C., Szeimies R.-M., Lehn N., Abels C. *Antimicrob. Agents Chemother.* **2005**, *49*, 1542.
229. Guterres K.B., Rossi G.G., Moreira K.S., Burgo T.A.L., Iglesias B.A. *BioMetals* **2020**, *33*, 269.
230. Guterres K.B., Rossi G.G., de Campos M.M.A., Moreira K.S., Burgo T.A.L., Iglesias B.A. *Photodiagn. Photodyn. Ther.* **2022**, *38*, 102770.
231. Rossi G.G., Guterres K.B., Moreira K.S., Burgo T.A.L., de Campos M.M.A., Iglesias B.A. *Photodiagn. Photodyn. Ther.* **2021**, *36*, 102514.
232. Nitzan Y., Ashkenazi H. *Curr. Microbiol.* **2001**, *42*, 408.
233. Oriel S., Nitzan Y. *Photochem. Photobiol.* **2012**, *88*, 604.
234. Gubarev Y.A., Lebedeva N.S., Yurina E.S., Syrbu S.S., Kiselev A.N., Lebedev M.A. *J. Pharmaceut. Anal.* **2021**, *11*, 691-698.
235. Koifman O.I., Lebedeva N. S., Gubarev Y. A., Koifman M. O. *Chem. Heterocycl. Compd.* **2021**, *57*, 423.
236. Lebedeva N.S., Gubarev Y.A., Mamardashvili G.M., Zaitceva S.V., Zdanovich S.A., Malyasova A.S., Romanenko J.V., Koifman M.O., Koifman O.I. *Scientific Reports* **2021**, *11*, 1.
237. Koifman M., Malyasova A., Romanenko Y.V., Yurina E., Lebedeva N.S., Gubarev Y.A., Koifman O. *Spectrochim. Acta, A* **2022**, *279*, 121403.
238. Gubarev Y.A., Lebedeva N.S., Yurina E.S., Mamardashvili G.M., Zaitceva S.V., Zdanovich S.A., Koifman O.I. *J. Biomol. Struct. Dyn.* **2022**, 1.
239. Kiselev A.N., Syrbu S.A., Lebedeva N.S., Gubarev Y.A. *Inorganics* **2022**, *10*, 63.
240. Syrbu S.A., Kiselev A.N., Lebedev M.A., Gubarev Y.A., Lebedeva N.Sh., *Russ. J. Gen. Chem.* **2021**, *91*, 1039–1049.
241. Lebedeva N.S., Gubarev Y.A., Lyubimtsev A.V., Yurina E.S., Koifman O.I. *Macroheterocycles* **2017**, *10*, 37.
242. Syrbu S.A., Kiselev A., Lebedev M.A., Gubarev Y.A., Yurina E.S., Lebedeva N.S. *Russ. J. Gen. Chem*. **2022**, *92*, 1005–1010.
243. Shang J., Ye G., Shi K., Wan Y., Luo C., Aihara H., Geng Q., Auerbach A., Li F. *Nature* **2020**, *581*, 221.
244. DeRosa M. C., Crutchley R. J. *Coord. Chem. Rev.* **2002**, *233–234*, 351–371
245. *Photosensitizers in Medicine, Environment and Security* (Nyokong T., Ahsen V., Eds.), Springer, **2012**.
246. Dąbrowski J.M., Pucelik B., Regiel-Futyra A., Brindell M., Mazuryk O., Kyzioł A., Stochel G.G., Macyk W., Arnaut L.G., DeRosa M.C., Crutchley R.J., Gouterman R., Sekkat N., Van Den Bergh H., Nyokong T., Lange N. *Molecules* **2012**, *17*, 98–144.
247. Nyokong T. *Pure Appl. Chem*. **2011**, *83*, 1763–1779.
248. Gouterman R. *J. Mol. Spectrosc*. **1968**, *27*, 225–235.
249. Martynov A.G., Mack J., May A.K., Nyokong T., Gorbunova Y.G., Tsivadze A.Y. *ACS Omega* **2019**, *4*, 7265–7284.
250. Pereira G.F.M., Tasso T.T. *Inorg. Chim. Acta* **2021**, *519*, 120271.
251. Ogunsipe A., Maree D., Nyokong T. *J. Mol. Struct*. **2003**, *650*, 131–140.
252. Juríček M., Kouwer P.H.J., Rehák J., Sly J., Rowan A.E. *J. Org. Chem*. **2009**, *74*, 21–25.
253. Dilber G., Durmuş M., Kantekin H. *Dyes Pigm.* **2019**, *160*, 267–284.
254. Kollar J., Machacek M., Halaskova M., Lenco J., Kucera R., Demuth J., Rohlickova M., Hasonova K., Miletin M., Novakova V., Zimcik P. *J. Med. Chem.* **2020**, *63*, 7616–7632.
255. Bunin D.A., Martynov A.G., Safonova E.A., Tsivadze A.Y., Gorbunova Y.G. *Dyes Pigm.* **2022**, *207*, 110768.
256. Halaskova M., Rahali A., Almeida-Marrero V., Machacek M., Kucera R., Jamoussi B., Torres T., Novakova V., De La Escosura A., Zimcik P. *ACS Med. Chem. Lett.* **2021**, *12*, 502–507.
257. Lioret V., Saou S., Berrou A., Lernerman L., Arnould C., Decréau R.A. *Photochem. Photobiol. Sci*. **2022**, 0–6.
258. Schneider L., Larocca M., Wu W., Babu V., Padrutt R., Slyshkina E., König C., Ferrari S., Spingler B. *Photochem. Photobiol. Sci.* **2019**, *18*, 2792–2803.
259. Kobayashi N., Furuyama T., Satoh K. *J. Am. Chem. Soc*. **2011**, *133*, 19642–19645.
260. Furuyama T., Satoh K., Kushiya T., Kobayashi N. *J. Am. Chem. Soc.* **2014**, *136*, 765–776.
261. Yoshida T., Furuyama T., Kobayashi N. *Tetrahedron Lett*. **2015**, *56*, 1671–1674.
262. Furuyama T., Yoshida T., Hashizume D., Kobayashi N. *Chem. Sci.* **2014**, *5*, 2466–2474.
263. Kolomeychuk F.M., Safonova E.A., Polovkova M.A., Sinelshchikova A.A., Martynov A.G., Shokurov A.V., Kirakosyan G.A., Efimov N.N., Tsivadze A.Y., Gorbunova Y.G. *J. Am. Chem. Soc*. **2021**, *143*, 14053–14058.
264. Safonova E.A., Martynov A.G., Nefedov S.E., Kirakosyan G.A., Gorbunova Y.G., Tsivadze A.Y. *Inorg. Chem*. **2016**, *55*, 2450–2459.
265. Dumoulin F., Durmuş M., Ahsen V., Nyokong T. *Coord. Chem. Rev.* **2010**, *254*, 2792–2847.
266. Ribeiro C.P.S., Lourenço L.M.O. *J. Photochem. Photobiol. C Photochem. Rev*. **2021**, *48*, 100422.
267. Anaya-Plaza E., Aljarilla A., Beaune G., Nonappa, Timonen J.V.I., de la Escosura A., Torres T., Kostiainen M.A. *Adv. Mater*. **2019**, *31*, 1902582.
268. Nene L.C., Magadla A., Nyokong T. *J. Photochem. Photobiol. B Biol.* **2022**, *235*, 112553.
269. Scalise I., Durantini E.N. *Bioorg. Med. Chem*. **2005**, *13*, 3037–3045.
270. Sindelo A., Kobayashi N., Kimura M., Nyokong T. *J. Photochem. Photobiol. A Chem*. **2019**, *374*, 58–67.
271. Meshkov I.N., Bulach V.V., Gorbunova Y.G., Gostev F.E., Nadtochenko V.A., Tsivadze A.Y., Hosseini M.W. *Chem. Commun*. **2017**, *53*, 9918–9921.
272. Meshkov I.N., Bulach V., Gorbunova Y.G., Kyritsakas N., Grigoriev M.S., Tsivadze A.Y., Hosseini M.W. *Inorg. Chem.* **2016**, *55*, 10774–10782.
273. Stuzhin P.A. *J. Porphyrins Phthalocyanines* **1999**, *3*, 500–513.
274. Donzello M.P., Ercolani C., Gaberkorn A.A., Kudrik E.V., Meneghetti M., Marcolongo G., Rizzoli C., Stuzhin P.A. *Chem. - A Eur. J.* **2003**, *9*, 4009–4024.
275. Safonova E.A., Meshkov I.N., Polovkova M.A., Volostnykh M.V., Tsivadze A.Y., Gorbunova Y.G. *Mendeleev Commun*. **2018**, *28*, 275–277.
276. Martynov A.G., Safonova E.A., Tsivadze A.Y., Gorbunova Y.G. *Coord. Chem. Rev*. **2019**, *387*, 325–347.
277. Chen Y., Li G., Pandey R.K. *Curr. Org. Chem.* **2004**, *8*, 1105-1134.
278. Huang Y.-Y., Luo D., Hamblin M.R. *Curr. Org. Chem*. **2015**, *19*, 948-957.
279. Martinez De Pinillos Bayona A., Mroz P., Thunshelle C., Hamblin M.R. *Chem. Biol. Drug Design* **2017**, *89*, 192-206.
280. Aggarwal A., Samaroo D., Jovanovic I.R., Singh S., Tuz M.P., Mackiewicz M.R. *J. Porphyrins Phthalocyanines* **2019**, *23*, 729-765.
281. Senge M.O., Brandt J.C. *Photochem. Photobiol*. **2011**, *87*, 1240-1296.
282. Senge M.O. *Photodiagn. PDT* **2012**, *9*, 170-179.
283. Hu Z., Rao B., Chen S., Duanmu J. *BMC Cancer* **2010**, *10*, 235.
284. Mazor O., Brandis A., Plaks V., Neumark E., Rosenbach-Belkin V., Salomon Y., Scherz A. *Photochem. Photobiol*. **2005**, *81*, 342-351.
285. Scherz A., Salomon Y., Lindner U., Coleman J. *Comprehen. Ser. Photochem. Photobiol. Sci.* **2016**, *15*, 461-480.
286. Gouterman M. In: *The Porphyrins* (Dolphin D., Ed.). Academic Press, New York, **1978**, pp. 1-165.

287. Juselius J., Sundholm D. *Phys. Chem. Chem. Phys*. **2000**, *2*, 2145-2151.
288. Otero N., Fias S., Rodenković S., Bultinck P., Grana A.M., Mandado M. *Chem. Eur. J.* **2011**, *17*, 3274-3286.
289. Fliegel H., Sundholm D. *J. Org. Chem.* **2012**, *77*, 3408-3414.
290. Moss G.P. *Pure Appl. Chem*. **1987**, *59*, 779-832.
291. Lindsey J.S. *Chem. Rev.* **2015**, *115*, 6534-6620.
292. Dudkin S.V., Makarova E.A., Lukyanets E.A. *Russ. Chem. Rev.* **2016**, *85*, 700-730.
293. Taniguchi M., Lindsey J.S. *Chem. Rev*. **2017**, *117*, 344-535.
294. Whitlock Jr. H.W., Hanauer R., Oester M.Y., Bower B.K. *J. Am. Chem. Soc.* **1969**, *91*, 7485-7489.
295. Konan Y.N., Gurny R., Alleman E. *J. Photochem. Photobiol. B. Biol.* **2002**, *66*, 89-106.
296. Pushpan S.K., Venkatraman S., Anand V.G., Sankar J., Parmeswaran D., Ganesan S., Chandrashekar T.K. *Curr. Med. Chem. Anti-Cancer Agents* **2002**, *2*, 187-207.
297. Allison R.R., Downie G.H., Cuenca R., Hu X.-H., Childs C.J.H., Sibata C.H. *Photodiagn. PDT* **2004**, *1*, 27-42.
298. Wainwright M. *Photosensitisers in Biomedicine*. Wiley-Blackwell, **2009**, 269 p.
299. Patent RU 2479585 C1, **2013**.
300. Patent US 6410586 B1, **2002**.
301. Lyubimtsev A.V., Semeikin A.S., Syrbu S.A., Koifman O.I. *Book of abstracts of the 14th International conference Synthesis and application of porphyrins and their analogues (ICPC-14)*, Ivanovo. **2022**, p. 47.
302. Riyad Y.M., Naumov S., Schastak S., Griebel J., Kahnt A., Häupl T., Neuhaus J., Abel B., Hermann R. *J. Phys. Chem. B* **2014**, *118*, 11646−11658
303. Sharma S.K., Mroz P., Dai T., Huang Y.-Y., Denis T. G. St., Hamblin M.R. *Isr. J. Chem*. **2012**, *52*, 691-705.
304. Dąbrowski J. M. *Adv. Inorg. Chem*. **2017**, *70*, 343-394.
305. Oertel M. Schastak S.I., Tannapfel A., Hermann R., Sack U., Mössner J., Berr F. *J. Photochem. Photobiol. B Biol.* **2003**, *71*, 1-10.
306. Schastak S., Jean B., Handzel R., Kostenich G., Hermann R., Sack U., Orenstein A., Wang Y., Wiedemann P. *J. Photochem. Photobiol. B Biol.* **2005**, *78*, 203-213.
307. Yakubovskaya R.I., Plotnikova E.A., Plyutinskaya A.D., Morozova N.B., Chissov V.I., Makarova E.A., Dudkin S.V. Lukyanets E.A., Vorozhtsov G.N. *J. Photochem. Photobiol. B: Biol.* **2014**, *130*, 109-114.
308. Schastak S., Gitter B., Handzel R., Hermann R., Wiedemann P. *Methods Find. Exp. Clin. Pharmacol*. **2008**, *30*, 129-133.
309. Schastak S., Ziganshyna S., Gitter B., Wiedemann P., Claudepierre T. *PLoS ONE* **2010**, 5, e11674.
310. Patent RU 2663900 C1, **2018**.
311. Pankratov A.A., Andreeva T.N., Plotnikova E.A., Morozova N.B., Vorontsova M.S., Merkulova I.B., Abramova T.V., Starkova N.N., Kalinichenko V.N., Yakubovskaya R.I. *Russ. J. Biotherapy* **2017**, *16*(s1), 60.
312. Plyutinskaya A.D., Plotnikova E.A., Stramova V.O., Yakubovskaya R.I. *Russ. J. Biotherapy* **2017**, 16(s1), 63.
313. Maklygina Yu.S., Sharova A.S., Kundu B., Balla V.K., Steiner R., Loschenov V.B. *Biomedical Photonics* **2016**, *5*, 4-12.
314. Patent RU 2537759 C1, **2013**.
315. Patent RU 2535097 C1, **2014**.
316. Koifman O.I., Ponomarev G.V., Sergeeva T.V., Ivanov A.V., Tsitrin E.B. *Russ. J. Biotherapy* **2017**, *16*(s1), 43.
317. Sergeeva T.V., Zharov E.V., Bogatyrev O.P., Ivanov A.V., Zinov'ev S.V., Koifman O.I., Krasnovsky A.A. *Russ. J. Biotherapy* **2015**, *14*(1), 130.
318. Rzhevskii D.I., Ivanov A.V., Rodionov I.V., Dyachenko I.A., Murashev A.N. *Biomedical Photonics* **2019**, *8*(4s), 35-36.
319. Ghorbani J., Rahban D., Aghamiri Sh., Teymouri A., Bahador A. *Laser Ther.* **2018**, *27*, 293–302.
320. Collins T.L., Markus E.A., Hassett D.J., Robinson J.B. *Curr. Microbiol.* **2010**, *61*, 411-416.
321. Cieplik F., Tabenski L., Buchalla W., Maisch T. *Front. Microbiol.* **2014**, *5*, 405.
322. Patent RU 2523380 C1, **2014**.
323. Patent RU 2647588 C1, **2018**.
324. Meng Sh., Xu Z., Hong G., Zhao L., Zhao Zh., Guo J., Ji H., Liu T. *Eur. J. Med. Chem.* **2015**, *92*, 35-48.
325. Parthiban V., Yen P. Y. M., Uruma Y., Lai P-Sh. *Bull. Chem. Soc. Jpn.* **2020**, *93*, 978-984.
326. Khan R., Özkan M., Khaligh A., Tuncel D. *Photochem. Photobiol. Sci.* **2019**, *18*, 1147-1155.
327. Hamblin M.R., Chiang L.Y., Lakshmanan S., Huang Y-Y., Garcia-Diaz M., Karimi M., *et al. Nanotechnol. Rev.* **2015**, *4*, 359-372.
328. Tutt L.W., Boggess T.F. *Progress in Quantum Electronics* **1993**, *17*(4), 299-338.
329. Algethami N., Sadeghi H., Sangtarash S., Lambert C.J. *Nano Lett.* **2018**, *18*, 4482−4486.
330. Bellamy-Carter A., Roche C., Anderson H.L., Saywell A. *Sci. Rep.* **2021**, *11*, 20388.
331. Wang D., Niu L., Qiao Z. Y., Cheng D. B., Wang J., Zhong Y. A. *CS Nano* **2018**, *12*, 3796–3803.
332. Stoffelen C., Huskens J. *Soft Small* **2016**, *12*, 96−119.
333. Ariga K., Nishikawa M., Mori T., Takeya J., Shrestha L.K., Hill J.P. *Sci. Technol. Adv. Mater*. **2019**, *20*, 51–95.
334. Webre W.A., Gobeze H.B., Shao S., Karr P.A., Ariga K., Hill J.P., D'Souza F. *Chem Commun*. **2018**, *54*, 1351–1354.
335. Oldacre A.N., Friedman A.E., Cook T.R. *J. Am. Chem. Soc*. **2017**, *139*, 1424−1427.
336. Huang Z., Qin B., Chen L., Xu J.F., Faul C.F., Zhang X. *Macromol. Rapid Commun*. **2017**, *38*, 1700312−1700326.
337. Yang L., Tan X., Wang Z., Zhang X. *Chem. Rev.* **2015**, *115*, 7196−7239.
338. Rubia-Payá C., De Miguel G., Martín-Romero M. T., Giner-Casares J. J., Camacho L. *Adv. Colloid Interface Sci.* **2015**, *225*, 134−145.
339. Kuzmin S.M., Chulovskaya S.A., Parfenyuk V.I. *Electrochimica Acta* **2020**, *342*, 136064.
340. Mon M., Bruno R., Ferrando-Soria J., Armentano D., Pardo E. *J. Mater. Chem. A* **2018**, *6*, 4912–4947.
341. Maiorova L.A., Kobayashi N., Zyablov S.V., Bykov V.A., Nesterov S.I., Kozlov A.V., Koifman O.I. *Langmuir* **2018**, *34*, 9322-9329.
342. Karlyuk M.V., Krygin Y.Y., Maiorova-Valkova L.A., Ageeva T.A., Koifman O.I. *Russ. Chem. Bull.* **2013**, *62*(2), 471-479.
343. Vu T.T., Maiorova L.A., Berezin D.B., Koifman O.I. *Macroheterocycles* **2016**, *9*, 73-79.
344. Valkova L.A., Glibin A.S., Koifman O.I. *Macroheterocycles* **2011**, *4*, 222-226.
345. Valkova L.A., Erokhin V.V., Glibin A.S., Koifman O.I. *J. Porphyrins Phthalocyanines* **2011**, *15*, 1044-1051.
346. Valkova L.A., Shabyshev L.S., Feigin L.A., Akopova O.B. *Molecular Crystals and Liquid Crystals Science and Technology. Section C, Molecular Materials* **1996**, *6*(4), 291-298.
347. Maiorova L.A., Koifman O.I., Burmistrov V.A., Kuvshinova S.A., Mamontov A.O. *Protection of Metals and Physical Chemistry of Surfaces* **2015**, *51*(1), 85-92.
348. Valkova L.A., Shabyshev L.S., Feigin L.A., Akopova O.B. *Izv. Akad. Nauk Ser. Fiz.* **1997**, *61*(3), 631-636.
349. Kharitonova N.V., Maiorova L.A., Koifman O.I. *J. Porphyrins Phthalocyanines* **2018**, *22*, 509-520.
350. Gromova O.A., Maiorova L.A., Salnikov D.S., Demidov V.I., Kalacheva A.G., Torshin I.Yu., Bogacheva T.E., Gromov A.N., Limanova O.A., Grishina T.R., Jafari S.M., Koifman O.I. *BioNanoSci.* **2022**, *12*, 74–82.
351. Erokhina S., Pastorino L., Di Lisa D., Kiiamov A.G., Tayurskii D.A., Iannotta S., Erokhin V., Faizullina A.R. *MethodsX* **2021**, *8*, 101230.

352. Rikhtegarana S., Katouzianbc I., Jafari S.M., Kiani H, Maiorova L.A., Takbirgou H. *Food Structure* **2021**, *30*, 100227.
353. Maiorova L.A., Erokhina S.I., Pisani M., Barucca G., Marcaccio M., *et al. Colloids Surf. B* **2019**, *182C*, 110366.
354. Semeikin A.S., Koifman O.I., Berezin B.D. *Chem. Heterocycl. Compd.* **1982**, *18*, 1046–1047.
355. Dudkin S., Makarova E., Slivka L., Lukyanets E. *J. Porphyrins Phthalocyanines* **2014**, *18*, 107-114.
356. Koifman O.I., Ageeva T.A. *Russ. J. Org. Chem.* **2022**, *58*, 443-479.
357. Beletskaya I.P., Tyurin V.S., Uglov A., Stern C., Guilard R. In: *Handbook of Porphyrin Science*, Vol. 23 (Kadish K.M., Smith K.M., Guilard R., Eds.), World Scientific: Singapore, **2012**. Ch. 108, pp. 81-279.
358. Vicente M. da G.H., Smith K.M. *Curr. Org. Synt.* **2014**, *11*, 3-28.
359. Senge M.O. *Chem. Commun.* **2011**, *47*, 1943-1960.
360. Ponomarev G.V. *Chem. Heterocycl. Compd.* **1994**, *30*, 1444-1465.
361. Burrell A.K., Officer D.L. *Synlett* **1998**, *1998*(12), 1297-1307.
362. Ando A., Yamazaki M., Komura M., Sano Y., Hattori N., Omote M., Kumadaki I. *Heterocycles* **1999**, *50*, 913-918.
363. Dahms K., Senge M.O., Bakri Bakar M. *Eur. J. Org. Chem.* **2007**, *2007*, 3833-3848.
364. Runge S., Senge M.O. *Tetrahedron* **1999**, *55*, 10375-10390.
365. Arnold D.P., Johnson A.W., Mahendran M. *J. Chem. Soc., Perkin Trans. 1* **1978**, 366-370.
366. Smith K.M. In: *Synthesis and Modifications of Porphyrinoids* (Paolesse R., Ed), Springer, Berlin, Heidelberg, **2014**. 1-34.
367. Tkachenko N.V., Lemmetyinen H., Sonoda J., Ohkubo K., Sato T., Imahori H., Fukuzumi S. *J. Phys. Chem. A* **2003**, 1*07*, 8834-8844.
368. Fuhrhop J.-H., Witte L., Sheldrick W.S. *Justus Liebigs Annalen der Chemie* **1976**, *1976*, 1537-1559.
369. Ponomarev G.V. *Chem. Heterocycl. Compd.* **1996**, *32*, 1263-1280.
370. Paolesse R., Nardis S., Monti D., Stefanelli M., Di Natale C. *Chem. Rev.* **2017**, *117*, 2517-2583.
371. Nyman E.S., Hynninen P.H. *J. Photochem. Photobiol. B: Biol.* **2004**, *73*, 1-28.
372. Sternberg E.D., Dolphin D., Brückn C. *Tetrahedron* **1998**, *54*, 4151-4202.
373. Cerqueira A.F.R., Moura N.M.M., Serra V.V., Faustino M.A.F., Tomé A.C., Cavaleiro J.A.S., Neves M.G.P.M.S. *Molecules* **2017**, *22*, 1269.
374. Vicente M.G.H., Smith K.M. *J. Org. Chem.* **1991**, *56*, 4407-4418.
375. Glowacka-Sobotta A., Wrotynski M., Kryjewski M., Sobotta L., Mielcarek J. *J. Porphyrins Phthalocyanines* **2019**, *23*, 1-10.
376. Moreira L.M., Vieira dos Santos F., Lyon J.P., Maftoum-Costa M., Pacheco-Soares C., Soares da Silva N. *Austral. J. Chem.* **2008**, *61*, 741-754.
377. Morgan A., Garbo G., Rampersaud A., Skalkos D., Keck R., Selman S. *Photodynamic Action of Benzochlorins*. SPIE: **1989**,Vol. 1065.
378. Li G., Pandey S.K., Graham A., Dobhal M.P., Mehta R., Chen Y., Gryshuk A., Rittenhouse-Olson K., Oseroff A., Pande R.K. *J. Org. Chem.* **2004**, *69*, 158-172.
379. Belyaev E.S., Kozhemyakin G.L., Tyurin V.S., Frolova V.V., Lonin I.S., Ponomarev G.V., Buryak A.K., Zamilatskov I.A. *Org. Biomol. Chem.* **2022**, *20*, 1926-1932.
380. Orlova E.A., Romanenko Y.V., Tyurin V.S., Shkirdova A.O., Belyaev E.S., Grigoriev M.S., Koifman O.I., Zamilatskov I.A. *Macroheterocycles* **2022**, *15*, 139-146.
381. van der Haas R.N.S., de Jong R.L.P., Noushazar M., Erkelens K., Smijs T.G.M., Liu Y.,Gast P., Schuitmaker H.J., Lugtenburg J. *Eur. J. Org. Chem.* **2004**, *2004*, 4024-4038.
382. Morgan A.R., Rampersaud A., Garbo G.M., Keck R.W., Selman S.H. *J. Med. Chem.* **1989**, *32*, 904-908.
383. Muthiah C., Taniguchi M., Kim H.-J., Schmidt I., Kee H.L., Holten D., Bocian D.F., Lindsey J.S. *Photochem. Photobiol.* **2007**, *83*, 1513-1528.
384. Wang Q., Ma F., Tang W., Zhao S., Li C., Xie Y. *Dyes Pigm.* **2018**, *148*, 437-443.
385. Chen B., Ding Y., Li X., Zhu W., Hill J.P., Ariga K., Xie Y. *Chem. Commun.* **2013**, *49*, 10136-10138.
386. Shkirdova A.O., Orlova E.A., Ponomarev G.V., Tyurin V.S., Zamilatskov I.A., Buryak A.K. *Macroheterocycles* **2021**, *14*, 208-212.
387. Tyurin V.S., Erzina D.R., Zamilatskov I.A., Chernyadyev A.Y., Ponomarev G.V., Yashunskiy D.V., Maksimova A.V., Krasnovskiy A.A., Tsivadze A.Y. *Macroheterocycles* **2015**, *8*, 376-383.
388. Ponomarev G.V., Rozynov B.V. *Chem. Heterocycl.Comp.* **1973**, *9*, 1065-1068.
389. Yashunsky D.V., Morozova Y.V., Ponomarev G.V. *Chem. Heterocycl. Compd.* **2000**, *36*, 485-486.
390. Yashunsky D.V., Morozova Y.V., Ponomarev G.V. *Chem. Heterocycl. Compd.* **2000**, *36*, 487-488.
391. Yashunsky D.V., Morozova Y.V., Ponomarev G.V. *Chem. Heterocycl. Compd.* **2001**, *37*, 380-381.
392. Morozova Y.V., Yashunsky D.V., Maksimov B.I., Ponomarev G.V. *Chem. Heterocycl. Compd.* **2003**, *39*, 388-389.
393. Volov A.N., Zamilatskov I.A., Mikhel I.S., Erzina D.R., Ponomarev G.V., Koifman O.I., Tsivadze A.Y. *Macroheterocycles* **2014**, *7*, 256-261.
394. Erzina D.R., Zamilatskov I.A., Stanetskaya N.M., Tyurin V.S., Kozhemyakin G.L., Ponomarev G.V., Chernyshev V.V., Fitch A.N. *Eur. J. Org. Chem.* **2019**, *2019*, 1508-1522.
395. Papkovsky D.B., Ponomarev G.V., Wolfbeis O.S. *J. Photochem. Photobiol A: Chem.* **1997**, *104*, 151-158.
396. Borchert N.B., Ponomarev G.V., Kerry J.P., Papkovsky D.B. *Analyt. Chem.* **2011**, *83*, 18-22.
397. Zhdanov A.V., Li L., Yang P., Shkirdova A.O., Tang S., Yashunsky D.V., Ponomarev G.V., Zamilatskov I.A., Papkovsky D.B. *Sensor. Actuat. B-Chem.* **2022**, *355*, 131116.
398. Ponomarev G.V., Shul'ga A.M. *Chem. Heterocycl. Compd.* **1984**, *20*, 383-388.
399. Ponomarev G.V., Shul'ga A.M. *Chem. Heterocycl. Compd.* **1987**, *23*, 757-762.
400. Ponomarev G.V., Shul'ga A.M., Rozynov B.V. *Chem. Heterocycl. Compd.* **1993**, *29*, 155-162.
401. Shkirdova A.O., Zamilatskov I.A., Stanetskaya N.M., Tafeenko V.A., Tyurin V.S., Chernyshev V.V., Ponomarev G.V., Tsivadze A.Y. *Macroheterocycles* **2017**, *10*, 480-486.
402. Kozhemyakin G.L., Tyurin V.S., Shkirdova A.O., Belyaev E.S., Kirinova E.S., Ponomarev G.V., Chistov A.A., Aralov A.V., Tafeenko V.A., Zamilatskov I.A. *Org. Biomol. Chem.* **2021**, *19*, 9199-9210.
403. Harper S.R., Pfrunder M.C., Esdaile L.J., Jensen P., McMurtrie J.C., Arnold D.P. *Eur. J. Org. Chem.* **2015**, *2015*, 2807-2825.
404. Dahlstedt E., Collins H.A., Balaz M., Kuimova M.K., Khurana M., Wilson B.C., Phillips D., Anderson H.L. *Org. Biomol. Chem.* **2009**, *7*, 897-904.
405. Belyaev E.S., Shkirdova A.O., Kozhemyakin G.L., Tyurin V.S., Emets V.V., Grinberg V.A., Cheshkov D.A., Ponomarev G.V., Tafeenko V.A., Radchenko A.S., Kostyukov A.A., Egorov A.E., Kuzmin V.A., Zamilatskov I.A. *Dyes Pigm.* **2021**, *191*, 109354.
406. Andreeva V.D., Ponomarev G.V., Shkirdova A.O., Tyurin V.S., Zamilatskova I.A. *Macroheterocycles* **2021**, *14*, 201-207.
407. Smith M.J., Blake I.M., Clegg W., Anderson H.L. *Org. Biomol. Chem.* **2018**, *16*, 3648-3654.
408. Birin K.P., Gorbunova Y.G., Tsivadze A.Y. *RSC Adv.* **2015**, *5*, 67242-67246.

409. Jiang J., Liu D., Zhao Y., Wu F., Yang K., Wang K. *Appl. Organomet. Chem.* **2018**, *32*(9), e4468.
410. Chen C., Zhu Y.-Z., Fan Q.-J., Song H.-B., Zheng J.-Y. *Chem. Lett.* **2013**, *42*, 936-938.
411. Murugavel M., Reddy R.V.R., Sankar J. *RSC Advances* **2014**, *4*, 13669-13672.
412. Hong S.-K., Jeoung E., Lee C.-H. *J. Porphyrins Phthalocyanines* **2005**, *9*, 285-289.
413. Higashino T., Imahori H. *ECS Meeting Abstracts* **2021**, MA2021-01, 769.
414. Sagun E.I., Zenkevich E.I., Knyukshto V.N., Shulga A.M. *Opt. Spectrosc.* **2011**, *110*, 251-256.
415. Sagun E.I., Ganzha V.A., Dzhagarov B.M., Shulga A.M. *Khimicheskaya Fizika* **1991**, *10*, 477-484.
416. Gijzeman O.L.J., Kaufman E., Porter G. *J. Chem. Soc. Farad. Trans. II* **1973**, *69*, 708-720.
417. Dzhagarov B.M., Sagun E.I., Ganzha V.A., Gurinovich G.P. *Khimicheskaya Fizika* **1987**, 6, 919-928.
418. Majranowski V.G. In: *Porphyrins: Spectroscopy, Photochemistry, Application* (Enikolopyan N.S., Ed.) Moscow: Nauka, **1987**, pp. 127-181.
419. Zenkevich E.I., von Borczyskowski C., Shulga A.M., Bachilo S.M, Rempel U., Willert A. *Chem. Phys*. **2002**, *275*, 185-209.
420. Zenkevich E.I., von Borczyskowski C., Shulga A.M. *J. Porphyrins Phthalocyanines* **2003**, *7*, 731-754.
421. Zenkevich E.I. *Macroheterocycles* **2016**, *9*, 121-140.
422. Zenkevich E.I., Willert A., Bachilo S.M., Rempel U., Kilin D.S., Shulga A.M., von Borczyskowski C. *Mater. Sci. Eng. C* **2001**, *18*, 99-111.
423. Zenkevich E.I., von Borczyskowski C. Surface Photochemistry of Quantum Dot-Porphyrin Nanoassemblies for Singlet Oxygen Generation. In: *Photoinduced Processes at Surfaces and in Nanomaterials, ACS Symposium Series* (Kilin D., Ed.) Washington: American Chemical Society. **2015**, Vol. 1196, Ch. 12, 235–272.
424. Blaudeck T., Zenkevich E.I., Cichos F., von Borczyskowski. C. *J. Phys. Chem. C.* **2008**, *112*, 20251-20257.
425. Lakowicz J.R. *Principles of Fluorescence Spectroscopy*. New York: Kluwer Academic/Plenum Publishers, **1999**, 2nd ed., 245 p.
426. Klimov V. *Nanocrystall Quantum Dots*. Washington: CRS Press LLC. **2010**, 410 p.
427. Lemon C.M., Karnas E., Bawendi M.G., Nocera D.G. *Inorg. Chem*. **2013**, *52*, 10394−10406.
428. Motevich I.G., Zenkevich E.I., Stroyuk O.L., Raievska O.E., Kulikova O.M., Sheinin V.B., Koifman O.I., Zahn D.R.T., Strekal N.D. *J. Appl. Spectrosc.* **2021**, *87*, 1057-1066.
429. Salokhiddinov K., Byteva I., Dzhagarov B. *Opt. Spectrosc.* **1979**, *47*, 881-884.
430. Krasnovsky A., Jr. *Photochem. Photobiol*. **1979**, *29*, 29-34.
431. Krasnovsky A., Jr. *Chem. Phys. Lett*. **1981**, *81*, 443-445.
432. Ogilby P.R., Foote C.S. *J. Am. Chem. Soc*. **1982**, *104*, 2069–2070.
433. Minaev B.F., Lunell S., Kobzev G.I. *J. Mol. Struct*. **1993**, *284*, 1–9.
434. Gaponenko S.V. *Introduction to Nanophotonics*, Cambridge: Cambridge University Press. **2010**.
435. Mogilevtsev D., Maloshtan A., Lepeshkevich S.V., Dzhagarov B.M. *J. Fluoresc*. **2012**, *22*, 1415—1419.
436. Dzhagarov B.M., Zharnikova E.S., Stasheuski A.S., Galievsky V.A., Parkhats M.V. *J. Appl. Spectrosc.* **2012**, *79*, 869-874.
437. Minaev B. *Chemistry and Chemical Technology* **2016**, *10*, 519-530.
438. Ivashin N.V., Shchupak E.E. *Opt. Spectrosc*. **2018**, *124*, 32–42.
439. Pham T.C., Nguyen V.N., Choi Y., Lee S., Yoon J. *Chem. Rev.* **2021**, *121*, 13454-13619.
440. Maisch T. *J. Photochem. Photobiol. B: Biol.* **2015**, *150*, 2-10.
441. Nguyen V.N., Yan Y., Zhao J., Yoon *J. Acc. Chem. Res.* **2021**, *54*, 207-220.
442. Moura N.M.M., Monteiro C.J.P., Tome A.C., Neves M.G.P.M.S., Cavaleiro J.A.S. *Arkivoc* **2022**, *2*, 54-98.
443. Kustov A.V., Belykh D.V., Startseva O.M., Kruchin S.O., Venediktov E.A., Berezin D.B. *Pharm. Anal. Acta.* **2016**, *7*, 1000480.
444. Sobotta L., Skupin-Mrugalska P., Mielcarek J., Goslinski T., Balzarini J. *Mini Rev. Med. Chem.* **2015**, *15*, 503-521.
445. Sobotta L., Skupin-Mrugalska P., Piskorz J., Mielcarek J. *Dyes Pigm.* **2019**, *163*, 337-355.
446. Sobotta L., Skupin-Mrugalska P., Piskorz J., Mielcarek J. *Eur. J. Med. Chem.* **2019**, *175*, 72-106.
447. Castano A.P., Demidova T.N., Hamblin M.R. *Photodiagn. Photodyn. Ther.* **2004**, *1*, 279-293.
448. Castano A.P., Demidova T.N., Hamblin M.R. *Photodiagn. Photodyn. Ther.* **2005**, *2*, 91-106.
449. Bonneau S., Vever-Bizet C. *Exp. Opin. Ther. Patents* **2008**, *18*, 1011-1025.
450. Malatesti N., Munitic I., Jurak I. *Biophys. Rev.* **2017**, *9*, 149-168.
451. Kustov A.V., Morshnev P.K., Kukushkina N.V., Smirnova N.L., Berezin D.B., Karimov D.R., Shukhto O.V., Kustova T.V., Belykh D.V., Mal'shakova M.V., Zorin V.P., Zorina T.E. *Int. J. Mol. Sci.* **2022**, *23*, 5294.
452. Smith D.A., van de Waterbeemd, Walker D.K., Mannhold R., Kubinyi H., Timmerman H. In: *Methods and Principles in Medicinal Chemistry* (Mannhold R., Kubinyi H., Timmerman H., Eds.), Wiley–VCH Verlag: Weinheim **2001**, 141 p.
453. Gerola A.P., Tsubone T.M., Santana A., de Oliveira H.P.M., Hioka N., Caetano W. *J. Phys. Chem. B* **2011**, *115*, 7364-7373.
454. Kustov A.V., Belykh D.V., Smirnova N.L., Khudyaeva I.S., Berezin D.B. *J. Chem. Thermodyn.* **2017**, *115*, 302-306.
455. Kim J., Santos O.A., Park J.H. *J. Control Release* **2014**, *191*, 98-104.
456. Zeinali M., Abbaspour-Ravasjani S., Ghorbani M., Babazadeh A., Soltanfam T., Santos A.C., Hamblin M.R. *Drug Discov. Today* **2020**, *25*, 1416-1430.
457. Berezin D.B., Kustov A.V., Krestyaninov M.A, Batov D.V., Kukushkina N.V., Shukhto O.V. *J. Mol. Liq.* **2019**, *283*, 532-536.
458. Berezin D.B., Makarov V.V., Znoyko S.A., Mayzlish V.E., Kustov A.V. *Mend. Commun.* **2020**, *30*, 621-623.
459. Kustov A.V., Krestyaninov M.A., Kruchin S.O., Shukhto O.V., Kustova T.V., Belykh D.V., Khudyaeva I.S., Koifman M.O., Razgovorov P.B., Berezin D.B. *Mendeleev Commun*. **2021**, *31*, 65-67.
460. Shukhto O.V., Khudyaeva I.S., Belykh D.V., Berezin D.B. *ChemChemTech* **2021**, *64*(11), 86-96.
461. Kustov A.V., Smirnova N.L., Berezin D.B., Berezin M.B. *J. Chem. Thermodyn.* **2015**, *83*, 104-109.
462. Kustov A.V., Smirnova N.L., Berezin D.B., Berezin M.B. *J. Chem. Thermodyn.* **2015**, *89*, 123-126.
463. Zhidomorov N.Yu., Nazarenko O.A., Demidov V.I., Kustov A.V., Kukushkina N.V., Koifman O.I., Gagua A.K., Tomilova I.K., Berezin D.B. *Biomed. Photonics* **2022**, *11*, 23-32.
464. O'Connor A.E., Gallagher W.M., Byrne A.T. *Photochem. Photobiol.* **2009**, *85*, 1053-1074.
465. Rezende L.G., Tasso T.T., Candido P.H.S., Baptista M.S. *Photochem. Photobiol.* **2022**, *98*, 572-590.
466. Tsubone T.M., Martins W.K., Pavani C., Junqueira H.C., Itri R., Baptista M.S. *Sci. Reports* **2017**, *7*, 1-19.
467. Di Mascio P., Martinez G.R., Miyamoto S., Ronsein G.E., Medeiros M.H.G. *Chem. Rev.* **2019**, *119*, 2043-2086.
468. Itri R., Junqueira H.C., Mertins O., Baptista M.S. *Biophys. Rev.* **2014**, *6*, 47-61.
469. Bacellar I.O.L., Oliveira M.C., Dantas L.S., Costa E.B., Junqueira H.C., Martins W.K., Durantini A.M., Cosa G., Di

Mascio P., Wainwright M., Miotto R., Cordeiro R.M., Miyamoto S., Baptista M.S. *J. Am. Chem. Soc.* **2018**, *140*, 9606-9615.
470. Tsubone T.M., Baptista M.S., Itri R. *Biophys. Chem.* **2019**, *254*, 106263.
471. Berezin D.B., Solodukhin T.N., Shukhto O.V., Belykh D.V., Startseva O.M., Khudyaeva I.S., Kustov A.V. *Russ. Chem. Bull.* **2018**, *67*, 1273-1279.
472. Belykh D.V., Startseva O.M., Patov S.A. *Macroheterocycles* **2014**, *7*, 401-413.
473. Kępczyński M., Pandian R.P., Smith K.M., Ehrenberg B. *Photochem. Photobiol.* **2002**, *76*, 127-134.
474. Abraham M.H., Acree W.E. *New J. Chem*. **2016**, *40*, 9945-9950.
475. Čunderlíková B., Gangeskar L., Moan J. *J. Photochem. Photobiol. B* **1999**, *53*, 81-90.
476. Kustov A.V., Belykh D.V., Smirnova N.L., Venediktov E.A., Kudayarova T.V., Kruchin S.O., Berezin D.B. *Dyes Pigm.* **2018**, *149*, 553-559.
477. Kustov A.V., Berezin D.B., Kruchin S.O., Batov D.V. *Russ. J. Phys. Chem.* **2022**, *96*, 793-799.
478. Khludeev I.I., Kozyr' L.A., Zorina T.E., Zorin V.P. *Bull. Exp. Biol. Med.* **2015**, *160*, 208-212.
479. Berezin D.B., Kustov A.V., Kukushkina N.V., Morshnev Ph.K., Karimov D.R., Belykh D.V., Belykh E.S., Zorina T.E., Zorin V.P. In: *12th Int. Conference on Porphyrins and Phthalocyanines (ICPP-12)*, Madrid, **2022**, p. 331.
480. Samaroo D., Zahran M., Wills A.C., Guevara J., Tatonetti A. *Porphyrin Science by Women* **2021**, *3*, 266-281.
481. Ghosh S., Chakrabarty S., Bhowmik D., Kumar G.S., Chattopadhyay N. *J. Phys. Chem. B* **2015**, *119*, 2090-2102.
482. Hamblin M.R., Newman E.L. *J. Photochem. Photobiol. B* **1994**, *26*, 45-56.
483. Hamblin M.R., Newman E.L. *J. Photochem. Photobiol. B* **1994**, *26*, 147-157.
484. Polo L., Valduga G., Jori G., Reddi E. *Int. J. Biochem. Cell Biol.* **2002**, *34*, 10-23.
485. Reshetov V., Zorin V., Siupa A., D'Hallewin M.A., Guillemin F., Bezdetnaya L. *Photochem. Photobiol.* **2012**, *88*, 1256-1264.
486. Ossoli A., Wolska A., Remaley A.T., Gomaraschi M. *Biochim. Biophys. Acta (BBA) - Molec. Cell Biol. Lipids* **2022**, *1867*, 159068.
487. Hadi T., Ramseyer C., Gautier T., Bellaye P.S., Lopez T., Schmitt A., Lirussi F. *JCI Insight* **2020**, *5*(24), e140280.
488. Cruz P.M.R., Mo H., McConathy W.J., Sabnis N., Lacko A.G. *Front. Pharmacol.* **2013**, *4*, 119.
489. Jori G. In: *In vivo transport and pharmacokinetic behavior of tumor photosensitizers. Photosensitizing compounds: their chemistry, biological and clinical use.* Wiley, Chichester (Ciba foundation symposium). **2007**, pp. 78-94.
490. Williamson M.P. *Prog. Nucl. Magn. Reson. Spectrosc.* **2013**, *73*, 1-16.
491. Barut B., Demirbaş Ü., Şenocak A., Özel A., Kantekin H. *Synth. Met.* **2017**, *229*, 22-32.
492. Duong-Ly K.C., Gabelli S.B. *Methods in enzymology. Academic Press* **2014**, *541*, 105-114.
493. Feng M., Tang B., Liang, S.H., Jiang X. *Curr. Top. Med. Chem.* **2016**, *16*, 1200-1216.
494. Plekhova N., Shevchenko O., Korshunova O., Stepanyugina A., Tananaev I., Apanasevich V. *Bioengineering* **2022**, *9*(2), 82.
495. Kessel D., Smith K.M., Pandey R.K., Shiau F.Y., Henderson B. *Photochem. Photobiol.* **1993**, *58*, 200-203.
496. Balendiran G.K., Dabur R., Fraser D. *Cell Biochemistry and Function* **2004**, 22, 343-352.
497. Gamcsik M.P., Kasibhatla M.S., Teeter S.D., Colvin O.M. *Biomarkers* **2012**, *17*, 671-691.
498. Lu S.C. *Mol. Aspects Med.* **2009**, *30*(1-2), 42-59.
499. Brozovic A., Ambriović-Ristov A., Osmak M. *Crit. Rev. Toxicol.* **2010**, *40*, 347-359.
500. Asantewaa G., Harris I.S. *Curr. Opin. Biotech.* **2021**, *68*, 292-299.
501. Kalinina E.V., Gavriliuk L.A. *Biochemistry (Moscow)* **2020**, *85*, 895-907.
502. Townsend D.M., Findlay V.L., Tew K.D. *Method. Enzymol.* **2005**, *401*, 287-307.
503. Flohé L., Toppo S., Orian L. *Free Radical Bio. Med.* **2022**, *187*, 113-122.
504. Couto N., Wood J., Barber J. *Free Radical Bio. Med.* **2016**, *95*, 27-42.
505. Miller C.G., Schmidt E.E. *Brit. J. Pharmacol.* **2019**, *176*, 532-543.
506. Thornalley P.J. *Biochem. Soc. Trans.* **2003**, *31*, 1343-1348.
507. He Y., Zhou C., Huang M., Tang C., Liu X., Yue Y., Qingchun D., Zhebin Z., Liu D. *Biomed. Pharmacother.* **2020**, *131*, 110663.
508. Morgenstern J., Campos M., Nawroth P., Fleming T. *Antioxidants* **2020**, *9*, 939.
509. Liberti M.V., Locasale J.W. *Trends Biochem. Sci.* **2016**, *41*, 211-218.
510. Yu L., Chen X., Sun X., Wang L., Chen S. *J. Cancer* **2017**, *8*(17), 3430.
511. Bailey H.H. *Chem.-Biol. Interact.* **1998**, *111*, 239-254.
512. Bailey H.H., Mulcahy R.T., Tutsch K.D., Arzoomanian R.Z., Alberti D., Tombes M.B., Wilding G., Pomplun M., Spriggs D.R. *J. Clin. Oncol.* **1994**, *12*(1), 194-205.
513. Vince R., Daluge S., Wadd W.B. *J. Med. Chem.* **1971**, *14*, 402-404.
514. Thornalley P.J., Edwards L.G., Kang Y., Wyatt C., Davies N., Ladan M.J., Double J. *Biochem. Pharmacol.* **1996**, *51*, 1365-1372.
515. Santarius T., Bignell G.R., Greenman C.D., Widaa S., Chen L., Mahoney C.L., Butler A., Edkins S., Waris S., Thornalley P.J., Futreal A.P., Stratton M.R. *Gene. Chromosome. Canc.* **2010**, *49*, 711-725.
516. Rabbani N., Thornalley P.J. *Int. J. Molecular Sci.* **2022**, *23*, 2453.
517. Grin M., Suvorov N., Ostroverkhov P., Pogorilyy V., Kirin N., Popov A., Sazonova A., Filonenko E. *Biophys. Rev.* **2022**, 1-23.
518. Tikhonov S., Ostroverkhov P., Suvorov N., Mironov A., Efímova Y., Plutinskaya A., Pankratov A., Ignatova A., Feofanov A., Diachkova A., Vasil'ev Y., Grin M. *Int. J. Mol. Sci.* **2021**, *22*, 13563.
519. Hu F., Yuan Y., Mao D., Wu W., Liu B. *Biomaterials* **2017**, *144*, 53-59.
520. Grin M.A., Pogorilyy V.A., Noev A.N., Tikhonov S.I., Majouga A.G., Mironov A.F. *Macroheterocycles* **2018**, *11*, 89-94.
521. Mironov A.F., Ostroverkhov P.V., Tikhonov S.I., Pogorilyy V.A., Kirin N.S., Chudakova O.O., Tsygankov A.A., Grin M. A. *Fine Chemical Technologies* **2021**, *15*(6), 16-33.
522. Liu L., Huang J., Li K., Hu X., Sun C. *J. Chromatogr. B* **2011**, 879, 56-60.
523. Percie du Sert N., Hurst V., Ahluwalia A., Alam S., Avey M.T., Baker M., Würbel H. *J. Cerebr. Blood Flow Met.* **2020**, *40*, 1769-1777.
524. Berk M., Copolov D., Dean O., Lu K., Jeavons S., Schapkaitz I., Anderson-Hunt M., Judd F., Katz F., Katz P., Ording-Jespersen S., Little J., Conus P., Cuenod M., Do Q.K., Bush A.I. *Biol. Psychiat.* **2008**, *64*(5), 361-368.
525. Yu M., Liu Y., Duan Y., Chen Y., Han J., Sun L., Yang X. *Biochem. Biophys. Res. Commun.* **2017**, *484*(1), 56-63.
526. Cavuoto P., Fenech M.F. *Cancer Treat. Rev.* **2012**, *38*, 726-736.
527. Patent RU 2521327C1, **2012**.
528. Levy E.J., Anderson M.E., Meister A. *Proceedings of the National Academy of Sciences* **1993**, *90*, 9171-9175.

529. Belyii Yu.A., Tereshchenko A.V., Volodin P.L. *et al. Refract. Surg. Ophthalmol*. **2006**, *6*, 55-57.
530. Abramova O.B., Demyashkin G.A., Drozhzhina V.V. *et al. Molecules* **2022**, *27*, 3445.
531. Abramova O.B., Drozhzhina V.V., Kozlovtseva E.A. *et al. Macroheterocycles* **2021**, *14*, 312-316.
532. Abramova O.B., Yuzhakov V.V., Kaplan M.A. *et al. Bull. Exp. Biol. Med*. **2021**, *170*, 479–484.
533. Abramova O.B., Kaplan M.A., Yuzhakov V.V. *et al. Bull. Exp. Biol. Med*. **2021**, *171*, 468–471.
534. Sokolov V.V., Chissov V.I., Filonenko E.V. *et al. Proceedings of SPIE - The International Society for Optical Engineering* **1995**, *2325*, 364–366.
535. Sokolov V.V., Filonenko E.V., Telegina L.V. *et al. Quantum Electronics* **2002**, *32*, 963–969.
536. Filonenko E.V. *Bio-Medical Photonics* **2021**, *10*, 4–22.
537. Zharkova N.N., Kozlov D.N., Smirnov V.V., Sokolov V.V., Chissov V.I., Filonenko E.V., Sukhin G.M., Galpern M.G., Vorozhtsov G.N. *Proceedings of SPIE - Photodynamic Therapy of Cancer II* **1995**, *2325*, 400-403.
538. Chissov V.I., Skobelkin O.K., Mironov A.F., Smirnov V.V., Sokolov V.V., Sukhin G.M., Filonenko E.V., Litvin D.G., Stranadko E.F., Kolobanov A.S., Astrakhankina T.A., Nokel Yu., A., Zharkova N.N., Kozlov D.N. *Surgery* [*Хирургия*] **1994**, *70*, 3-6.
539. Tolstykh P.I., Derbenov V.A., Kuleshov I.Yu. *Surgery* [*Хирургия*] **2010**, *12*, 17-22.
540. Tamrazova O.B., Molochkov A.V., Bagramova G.E., Pomerantsev O.N. *Clinical Dermatology and Venereology* [*Клиническая дерматология и венерология*] **2013**, *11*(4), 62-67.
541. Hopley C., Salkeld G. *Br. J. Ophthalmol.* **2004***, 88*, 982-987.
542. Isaev V.M., Nasedkin A.N., Ashurov Z.M., Reshetnikov A.V. *Russian Otorhinolaryngology* **2004**, *5*, 76-79.
543. Nasedkin A.N., Grachev N.S., Logunova E.V. *Photodynamic Therapy and Photodiagnostics* [*Фотодинамическая терапия и фотодиагностика*] **2013**, (3), 59.
544. Trushina O.I., Novikova E.G., Sokolov V.V., Filonenko E.V., Chissov V.I., Vorozhtsov G.N. *Photodiagnosis and Photodynamic Therapy* **2008**, 5, 256-259.
545. Kapinus V.N., Kaplan M.A., Kudryavtseva G.T., Khnychev S.S., Yakovlev V.V., Romanko Yu.S. In: *Modern methods of photodynamic (fluorescent) diagnostics and photodynamic therapy*. Obninsk, **2001**, p. 36-41.
546. Romanko Yu.S., Kaplan M.A., Popuchiev V.V. *Russian Journal of Skin and Venereal Diseases* **2004**, *6*, 6-10.
547. Lehmann P. *Br. J. Dermatol.* **2007**, *156*, 793-801.
548. Kaplan M.A., Kapinus V.N., Goranskaya E.V. *Tumors of the Female Reproductive System* [*Опухоли женской репродуктивной системы*] **2011**, *4*, 28-31.
549. Filonenko E.V., Okushko A.N., Sukhin D.G., Yanikova A.G. *P.A. Herzen Journal of Oncology* [*Онкология. Журнал им. П.А. Герцена*] **2012**, *3*, 52-54.
550. Simone C.B., Friedberg J.S., Glatstein E., Stevenson J.P., Sterman D.H., Hahn S.M., Cengel K.A. *J. Thorac. Dis.* **2012**, *4*, 63-75.
551. Hayata Y., Kato H., Konaka C., Ono J., Takizawa N. *Chest* **1982**, *81*, 269-277.
552. Mathur P.N., Edell E., Sutedja T., Vergnon J.M. *Chest* **2003**, *123*, 176-180.
553. Cortese D.A., Edell E.S., Kinsey J.H. *Mayo Clin. Proc.* **1997**, *72*, 595-602.
554. Filonenko E.V., Vashakhmadze L.A., Khomyakov V.M. *Siberian Journal of Oncology* [*Сибирский онкологический журнал*] **2012**, 2, 84-89.
555. Sokolov V.V., Pavlov P.V., Karpova E.S., Pirogov S.S. *Photodynamic Therapy and Photodiagnostics* [*Фотодинамическая терапия и фотодиагностика*] **2014**, (1), 33-34.
556. Filonenko E.V. *Photodynamic Therapy and Photodiagnostics* [*Фотодинамическая терапия и фотодиагностика*] **2015**, (1), 22-25.
557. Berger A.P., Steiner H., Stenzi A., Akkad T., Bartsch G., Holtl L. *Urology* **2003**, *61*, 338-341.
558. Zubkov A.Yu., Nuriev I.R., Sitdykov E.N. *Onkourologiya* **2014**, (2), 26-28.
559. Monk A., Brewer C., Van Nostrand K., Bems M. *Gynecol. Oncol.* **1997**, *64*(1), 70-75.
560. Novikova E.G., Sokolov V.V., Sidorova I.S., Chulkova E.A. *Russian Journal of Oncology* **2009**, (2), 12-19.
561. Ferlay J., Ervik M., Lam F., *et al. Global Cancer Observatory: Cancer Today* **2020**. http://gco.iarc.fr/today.
562. Sung H., Ferlay J., Siegel R.L., *et al. CA: A Cancer J. Clinicians* **2021**, *71*, 209–249.
563. Jemal A., Ward E.M., Johnson C.J., *et al. JNCI: J. National Cancer Institute* **2017**, *109*, djx030.
564. Erdi Y.E. *Mol. Imaging Radionucl. Ther.* **2012**, *21*, 23–28.
565. Stummer W., Pichlmeier U., Meinel T., *et al. Lancet Oncology* **2006**, *7*, 392–401.
566. Kausch I., Sommerauer M., Montorsi F., *et al. Eur. Urol.* **2010**, *57*, 595–606.
567. Liu R., Xu Y., Xu K., Dai Z. *Aggregate* **2021**, *2*, e23.
568. Craig S.E.L., Wright J., Sloan A.E., Brady-Kalnay S.M. *World Neurosurg* **2016**, *90*, 154–163.
569. Loshchenov M., Zelenkov P., Potapov A., Goryajnov S., Borodkin A. *Photonics Lasers in Medicine* **2014**, *3*, 159–170.
570. Harada Y., Murayama Y., Takamatsu T., Otsuji E., Tanaka H. *Int. J. Mol. Sci.* **2022**, *23*, 6478.
571. Barnes T.G., Hompes R., Birks J., *et al. Surg. Endosc.* **2018**, *32*, 4036–4043.
572. Hillary S.L., Guillermet S., Brown N.J., Balasubramanian S.P. *Langenbecks Arch. Surg.* **2018**, *403*, 111–118.
573. Schebesch K.-M., Brawanski A., Hohenberger C., Hohne J. *Turk Neurosurg.* **2016**, *26*, 185–194.
574. Sun Z., Jing L., Fan Y., *et al. Int. Rev. Neurobiol.* **2020**, *151*, 139–154.
575. Morales-Conde S., Alarcón I., Yang T., *et al. Surg. Endosc.* **2020**, *34*, 3897–3907.
576. Martinez De Pinillos Bayona A., Mroz P., Thunshelle C., Hamblin M.R. *Chem. Biol. Drug Des.* **2017**, *89*, 192–206.
577. Mroz P., Huang Y., Szokalska A., *et al. FASEB J.* **2010**, *24*, 3160–3170.
578. Sharma S.K., Krayer M., Sperandio F.F., *et al. J. Porphyrins Phthalocyanines* **2013**, *17*, 73–85.
579. Meerovich I.G., Sanarova E.V., Oborotova N.A., *et al. Russ. J. Gen. Chem.* **2015**, *85*, 280-288.
580. Baldea I., Ion R.-M., Olteanu D.E., *et al. Med. Pharm. Rep.* **2015**, *88*, 175–180.
581. Skubleny D., Dang J.T., Skulsky S., *et al. Surg. Endosc.* **2018**, *32*, 2620–2631.
582. Maruyama T., Akutsu Y., Suganami A., *et al. PLoS ONE* **2015**, *10*, e0122849.
583. Urbanska K., Romanowska-Dixon B., Matuszak Z., *et al. Acta Biochim. Pol.* **2002**, *49*, 387–391.
584. Geralde M.C., Leite I.S., Inada N.M., *et al. Physiological Reports* **2017**, *5*, e13190.
585. Mansouri S., Heylmann D., Stiewe T., Kracht M., Savai R. *eLife* **2022**, *11*, e79895.
586. Engblom C., Pfirschke C., Pittet M.J. *Nat. Rev. Cancer* **2016**, *16*, 447–462.
587. Perentes J.Y., Duda D.G., Jain R.K. *Dis. Model. Mech.* **2009**, *2*, 107–110.
588. Turley S.J., Cremasco V., Astarita J.L. *Nat. Rev. Immunol.* **2015**, *15*, 669–682.
589. Noy R., Pollard J.W. *Immunity* **2014**, *41*, 49–61.
590. Kitamura T., Qian B.-Z., Pollard J.W. *Nat. Rev. Immunol.* **2015**, *15*, 73–86.
591. Milas L., Wike J., Hunter N., Volpe J., Basic I. *Cancer Research* **1987**, *47*, 1069–1075.

592. Korbelik M., Krosl G., Olive P.L., Chaplin D.J. *Br. J. Cancer* **1991**, *64*, 508–512.
593. Anatelli F., Mroz P., Liu Q., *et al. Mol. Pharm.* **2006**, *3*, 654–664.
594. Korbelik M., Hamblin M.R. *Photochem. Photobiol. Sci.* **2015**, *14*, 1403–1409.
595. Hayashi N., Kataoka H., Yano S., *et al. Mol. Cancer Ther.* **2015**, *14*, 452–460.
596. Wen A.M., Lee K.L., Cao P., *et al*. *Bioconjugate Chem.* **2016**, *27*, 1227–1235.
597. Scalfi-Happ C., Zhu Z., Graefe S., *et al. Photodiagn. Photodyn. Ther.* **2018**, *22*, 106–114.
598. Makarov V.I., Pominova D.V., Ryabova A.V., *et al. Pharmaceutics* **2022**, *14*, 2122.
599. Zhu Z., Scalfi-Happ C., Ryabova A., *et al*. *J. Photochem. Photobiol. B: Biol.* **2018**, *185*, 215–222.
600. Agostinis P., Berg K., Cengel K.A., *et al*. *CA Cancer J. Clin.* **2011**, *61*, 250–281.
601. Castano A.P., Demidova T.N., Hamblin M.R. *Photodiagn. Photodyn. Ther.* **2005**, *2*, 91–106.
602. Shams M., Owczarczak B., Manderscheid-Kern P., Bellnier D.A., Gollnick S.O. *Cancer Immunol. Immunother.* **2015**, *64*, 287–297.
603. Jalili A., Makowski M., Świtaj T., *et al*. *Clin. Cancer Res.* **2004**, *10*, 4498–4508.
604. Saji H., Song W., Furumoto K., Kato H., Engleman E.G. *Clin. Cancer Res.* **2006**, *12*, 2568–2574.
605. Piette J. *Photochem. Photobiol. Sci.* **2015**, *14*, 1510–1517.
606. Anzengruber F., Avci P., de Freitas L.F., Hamblin M.R. *Photochem. Photobiol. Sci.* **2015**, *14*, 1492–1509.
607. Azzouzi A.-R., Vincendeau S., Barret E., *et al. The Lancet Oncology* **2017**, *18*, 181–191.
608. Mallidi S., Anbil S., Lee S., *et al*. *J. Biomed. Opt.* **2014**, *19*, 028001.
609. Shao P., Chapman D.W., Moore R.B., Zemp R.J. *J. Biomed. Opt.* **2015**, *20*, 106012.
610. Sirotkina M.A., Matveev L.A., Shirmanova M.V., *et al. Sci. Rep.* **2017**, *7*, 41506.
611. Goldschmidt R., Kalchenko V., Scherz A. In: *Optical Methods for Tumor Treatment and Detection: Mechanisms and Techniques in Photodynamic Therapy XXVI* (Kessel D.H., Hasan T., Eds.), SPIE, San Francisco, California, United States, **2017**, *10047*, 100470M.
612. Lakouas D.K., Huglo D., Mordon S., Vermandel M. *Photodiagn. Photodyn. Ther.* **2017**, *18*, 236–243.
613. Potapov A.A., Goryaynov S.A., Okhlopkov V.A., *et al. Neurosurg. Rev.* **2016**, *39*, 437–447.
614. Zelenkov P., Shevelev I., Potapov A., *et al. Photodiagn. Photodyn. Ther.* **2011**, *8*, 163.
615. Xu H., Wang Z., Li J., *et al. Neural Plasticity* **2017**, *2017*, 1–11.
616. von Leden R.E., Cooney S.J., Ferrara T.M., *et al*. *Lasers Surg. Med.* **2013**, *45*, 253–263.
617. Zhao M., Liang F., Xu H., Yan W., Zhang J. *Mol. Med. Rep.* **2016**, *13*, 13–20.
618. Wang Y.-C., Cui Y., Cui J.-Z., *et al. Mol. Med. Rep.* **2015**, *12*, 2149–2154.
619. Tardivo J.P., Del Giglio A., de Oliveira C.S., *et al*. *Photodiagn. Photodyn. Ther.* **2005**, *2*, 175–191.
620. Chekhonin V.P., Baklaushev V.P., Yusubalieva G.M., Volgina N.E., Gurina O.I. *Annals of the Russian Academy of Medical Sciences* **2012**, *67*, 66–78.
621. Jain A., Betancur M., Patel G.D., *et al*. *Nature Mater.* **2014**, *13*, 308–316.
622. Siegel R.L., Miller K.D., Fuchs H.E., Jemal A. *CA Cancer J. Clin.* **2022**, *72*, 7–33
623. Wicki A., Witzigmann D., Balasubramanian V., Huwyler J. *J. Control. Release* **2015**, *200*, 138–157.
624. Liu W., Liu C., Wang H., Xu L., Zhou J., Li S., Cheng Y., Zhou R., Zhao L. *Comput. Struct. Biotechnol. J.* **2022**, *20*, 5150-5161.
625. Ashrafizadeh M., Aghamiri S., Tan S.C., Zarrabi A., Sharifi E., Rabiee N., Kadumudi F.B., Pirouz A.D., Delfi M., Byrappa K., Thakur V.K., Kumar K.S.S., Girish Y.R., Zandsalimi F., Zare E.N., Orive G., Tay F., Hushmandi K., Kumar A.P., Karaman C., Karimi-Maleh H., Mostafavi E., Makvandi P., Wang Y. *Nano Today* **2022**, *45*, 101532.
626. Jeong Y., Hwang H.S., Na K. *Biomater. Res.* **2022**, *26,* 27.
627. Aoun F., Kourie H.R., Artigas C., Roumeguère T. *Future Oncol*. **2015**, *11*, 2205–2219.
628. Gao M., Tang B.Z. *Coord. Chem. Rev*. **2020**, *402*, 213076.
629. Ng K.K., Zheng G. *Chem. Rev.* **2015**, *115*, 11012–11042.
630. Yin X., Cheng Y., Feng Y., Stiles W.R., Park S. H., Kang H., Choi H.S. *Adv. Drug Delivery Rev.* **2022**, *189*, 114483.
631. Gao D., Guo X., Zhang X., Chen S., Wang Y., Chen T., Huang G., Gao Y., Tian Z., Yang Z. *Materials Today Bio.* **2020**, *5*, 100035.
632. Terreno E., Castelli D.D., Viale A., Aime S. *Chem. Rev*. **2010**, *110*, 3019–3042.
633. Zhou Z., Bai R., Munasinghe J., Shen Z., Nie L., Chen X. *ACS Nano* **2017**, *11*, 5227–5232.
634. Ying Liu, Weiqiang Lin, Fang Yang, Tianfeng Chen *Appl. Mater. Today* **2022**, *28*, 101520.
635. Abakumova T.O., Nukolova N.V., Gusev E.I., Chekhonin V.P. *Neurosci. Behav. Physiol*. **2015**, *115*, 58-65.
636. Xiao Y.-D., Paudel R., Liu J., Ma C., Zhang Z.-S., Zhou S.-K. *Int. J. Mol. Med.* **2016**, *38,* 1319-1326.
637. Li J., Li X., Gong S., Zhang C., Qian C., Qiao H., Sun M. *Nano Lett.* **2020**, *20*, 4842–4849.
638. Xie J., Jiang J., Davoodi P., Srinivasan M.-P., Wang C.-H. *Chem. Eng. Sci*. **2015**, *125*, 32.
639. Zhang Z., Zhou F.-L., Davies G.-L., Williams G.R. *VIEW* **2022**, *3*, 20200134.
640. He M., Chen Y., Tao C., Tian Q., An L., Lin J., Tian Q., Yang H., Yang S. *ACS Appl. Mater. Inter.* **2019**, *11*(45), 41946-41956.
641. Brewster II J.T., Thiabaud G.D., Harvey P., Zafar H., Reuther J.F., Dell'Acqua S., Johnson R.M., Root H.D., Metola P., Jasanoff A., Casella L., Sessler J.L. *Chem* **2020**, *6*, 703-724.
642. Felder P.S., Keller S., Gasser G. *Advanced Therapeutics* **2020**, *3*(1), 1900139.
643. Schmitt J., Jenni S., Sour A., Heitz V., Bolze F., Pallier A., Bonnet C.S., Toth E., Ventura B. *Bioconjugate Chem.* **2018**, *29*, 3726-3738.
644. Tsolekile N., Nelana S., Oluwafemi O.S. *Molecules* **2019**, *24*, 2669.
645. Grin M.A., Brusov S.S., Shchepelina E.Yu., Ponomarev P.V., Khrenova M.K., Smirnov A.S., Lebedeva V.S., Mironov A.F. *Mendeleev Commun*. **2017**, *27*, 338-340.
646. Boros E., Gale E.-M., Caravan P. *Dalton Trans*. **2015**, *44*, 4804.
647. Vlaardingerbroek M.-T., Boer J.A. *Magnetic Resonance Imaging: Theory and Practice*. Springer Science & Business Media, United States, **2013**.
648. Chan K.W.-Y., Wong W.-T. *Coord. Chem. Rev.* **2007**, *251*, 2428-2451.
649. Guglielmo F.F., Mitchell D.G., Gupta S. *Radiologic Clinics of North America* **2014**, *52*, 637-656.
650. Botta M., Carniato F., Esteban-Gómez D., Platas-Iglesias C., Tei L. *Future Med. Chem*. **2019**, *11*, 1461–1483.
651. Geraldes C.F.G.C., Castro M.M.C.A., Peters J.A. *Coord. Chem. Rev*. **2021**, *445*, 214069.
652. Rocklage S.M., Cacheris W.P., Quay S.C., Hahn F.E., Raymond K.N. *Inorg. Chem*. **1989**, *28*, 477–485.
653. Wang J., Wang H., Ramsay I.A., Erstad D.J., Fuchs B.C., Tanabe K.K., Caravan P., Gale E.M. *J. Med. Chem.* **2018**, *61*(19), 8811–8824.
654. Jeon M., Halbert M.V., Stephen Z.R., Zhang M. *Adv. Mater*. **2020**, 1906539.

655. Shu G., Chen M., Song J., Xu X., Lu C., Du Y., Xu M., Zhao Z., Zhu M., Fan K., Fan X., Fang S., Tang B., Dai Y., Du Y., Ji J. *Bioact. Mater.* **2021**, *6*(5), 1423-1435.
656. Scharlach C., Warmuth C., Schellenberger E. *Magn. Reson. Imaging* **2015**, *33*, 1173-1177.
657. Wahsner J., Gale E.M., Rodríguez-Rodríguez A., Caravan P. *Chem. Rev*. **2019**, *119*, 957-1057.
658. Calvete M.J.F., Pinto S.M.A., Pereira M.M., Geraldes C.F.G.C. *Coord. Chem. Rev*. 2**017**, *333*, 82-107.
659. Mironov A.F., Zhdanova K.A., Bragina N.A. *Russ. Chem. Rev*. **2018**, *87*, 859–881.
660. Hindré F., *et al. J. Magn. Reson. Imaging* **1993**, *3*, 59-65.
661. Li G., Slansky A., Dobhal M.P., Goswami L.N., Graham A., Chen Y., Kanter P., Alberico R.A., Spernyak J., Morgan J., Mazurchuk R., Oseroff A., Grossman Z., Pandey R.K. *Bioconjugate Chem.* **2005**, *16*, 32-42.
662. Haroon-Ur-Rashid M.N., Umar K., Khan M.N., Yaseen M. *Anjum J. Struct. Chem*. **2014**, *55*, 910–915.
663. Tekdaş A.D., Garifullin R., Şentürk B., Zorlu Y., Gundogdu U., Atalar E., Tekinay A.B., Chernonosov A.A., Yerli Y., Dumoulin F., Guler M.O., Ahsen V., Gürek A.G. *Photochem. Photobiol.* **2014**, *90*, 1376-1386.
664. Song Y., Zong H., Trivedi E.R., Vesper B.J., Waters E.A., Barrett A.G.M., Radosevich J.A., Hoffman B.M., Meade T.J. *Bioconjugate Chem.* **2010**, *21*, 2267-2275.
665. Yuzhakova D.V., Lermontova S.A., Grigoryev I.S., Muravieva M.S., Gavrina A.I., Shirmanova M.V., Balalaeva I.V., Klapshina L.G., Zagaynova E.V. *Biochimica et Biophysica Acta (BBA) - General Subjects* **2017**, *1861*, 3120-3130.
666. Wu B., Li X., Huang T., Lu S., Wan B., Liao R., Li Y., Baidya A., Long Q., Xu H. *Biomater. Sci*. **2017**, *5*, 1746.
667. Luo J., Chen L.-F., Hu P., Chen Z.-N. *Inorg. Chem.* **2014**, *53*, 4184-4191.
668. Jenni S., Bolze F., Bonnet C.S., Pallier A., Sour A., Toth E., Ventura B., Heitz V. *Inorg. Chem.* **2020**, *59*, 14389-14398.
669. Schmitt J., Jenni S., Sour A., Heitz V., Bolze F., Pallier A., Bonnet C.S., Tóth É., Ventura B. *Bioconjugate Chem*. **2018**, *29*, 3726−3738.
670. Vyalba F.Yu., Ivantsova A.V., Zhdanova K.A., Usachev M.N., Gradova M.A., Bragina N.A. *Mendeleev Commun*. **2022**, *32*, 675-677.
671. Mefteh W.B., Touzi H., Bessueille F., Chevalier Y., Kalfat R., Jaffrezic-Renault N. *Electroanalysis* **2015**, *27(1)*, 84-92.
672. Oyama J., Fernandes Herculano Ramos-Milaré Á.C., Lopes Lera-Nonose D.S.S., Nesi-Reis V., Galhardo Demarchi I., Alessi Aristides S.M., Juarez Vieira Teixeira J., Gomes Verzignassi Silveira T., Campana Lonardoni M.V. *Photodiagn. Photodyn. Ther.* **2020**, *30*, 101682.
673. Solovieva A.B., Timashev S.F. *Russ. Chem. Rev*. **2003**, *72,* 965.
674. Solovieva A.B., Rudenko T.G., Shekhter A.B., Glagolev N.N., Spokoinyi A.L., Fayzullin A.L., Aksenova N.A., Shpichka A.I., Kardumyan V.V., Timashev P.S. *J. Photochem. Photobiol. B: Biol.* **2020**, *210*. 111954.
675. Günsel A., Taslimi P., Atmaca G.Y., Bilgiçli A.T., Pişkin H., Ceylan Y., Erdoğmuş A., Yarasir M.N., Gülçin İ. *J. Mol. Struct.* **2021**, *1237*, 130402.
676. Lee H.-J., Kang S.-M., Jeong S.-H., Chung K.-H., Kim B.-I. *Photodiagn. Photodyn. Ther.* **2017**, *20*, 116–119.
677. Méndez D.A.C., Gutierrez E., Dionísio E.J., Oliveira T.M., Buzalaf M.A.R., Rios D., Machado M.A.A.M., Cruvinel T. *Lasers Med. Sci.* **2018**, *33*, 479–487.
678. Pérez-Laguna V., García-Luque I., Ballesta S., Pérez-Artiaga L., Lampaya-Pérez V., Samper S., Soria-Lozano P., Rezusta A., Gilaberte Y. *Photodiagn. Photodyn. Ther.* **2018**, *21*, 211–216.
679. Usacheva M.N., Teichert M.C., Biel M.A. *J. Photochem. Photobiol. B: Biol.* **2003**, *71*, 87–98.
680. Lim E.J., Oak C.-H., Heo J., Kim Y.-H. *Oncology Reports* **2013**, *30*, 856–862.
681. Dos Santos A.F., Terra L.F., Wailemann R.A.M., Oliveira T.C., Gomes V. de M., Mineiro M.F., Meotti F.C., Bruni-Cardoso A., Baptista M.S., Labriola L. *BMC Cancer* **2017**, *17*, 194.
682. Shih M.H., Huang F.C. *Invest. Ophthalmol. Vis. Sci*. **2011**, *52*, 223–229.
683. Atenco-Cuautle J.C., Delgado-López M.G., Ramos-García R., Ramírez-San-Juan J.C., Ramirez-Ramirez J., Spezzia-Mazzocco T. *Proc. SPIE 11070, 17th International Photodynamic Association World Congress*, 11070A1, **2019**, 7 August.
684. Houang J., Perrone G.G., Pedrinazzi C., Longo L., Mawad D., Boughton P.C., Ruys A.J., Lauto A. *Adv. Therapeutics* **2018**, 1800105.
685. Aksenova A., Oles T., Sarna T., Glagolev N.N., Chernjak A.V., Volkov V.I., Kotova S.L., Melik-Nubarov N.S., Solovieva A.B. *Laser Physics* **2012**, *22*, 1642–1649.
686. Koifman O.I., Ageeva T.A. *Porphyrin Polymers: Synthesis, Properties, Applications*. Moscow: LENAND, **2018**. 304 p.
687. Koifman O.I., Ageeva T.A. *Polymer Sci. C* **2004**, *46*, 49-72.
688. Amat-Guerri F., López-González M.M.C., Sastre R., the late Martinez-Utrilla R. *Dyes Pigm.* **1990**, *13*, 219–232.
689. Martin M.M., Lindqvist L. *J. Luminescence* **1975**, *10*, 381–390.
690. Jiang C., Brown P.J., Ducret A., Brun Y.V. *Nature* **2014**, *506*, 489-493.
691. Malik Z., Hanania J., Nitzan Y. *J. Photochem. Photobiol. B: Biol.* **1990**, *5*, 281-293.
692. Nitzan Y. *Photochem Photobiol.* **1992**, *55*, 89-96.
693. Strakhovskaya M.G., Belenikina N., Nikitina V., Kovalenko S., Kovalenko I., Averyanov A., Rubin A., Galochkina T. *Clinical Practice* **2013,** *4*, 25-30.
694. Loke W.K., Lau S.K., Yong L.L., Khor E., Sum C.K. *J. Biomed. Mater. Res.* **2000**, *53*, 8.
695. Fontana C.R., dos Santos D.S. Jr., Bosco J.M., Spolidorio D.M., Marcantonio R.A. *Drug Deliv*. **2008**, *15*, 417-422.
696. Solovieva A.B., Rudenko T.G., Shekhter A.B., Glagolev N.N., Spokoinyi A.L., Fayzullin A.L., Aksenova N.A., Shpichka A.I., Kardumyan V.V., Timashev P.S. *J. Photochem. Photobiol., B: Biol*. **2020**, *210*, 111954.
697. Aksenova N.A., Timofeeva V.A., Rogovina S.Z., Timashev P.S., Glagolev N.N., Solov'eva A.B. *Polym. Sci. Ser. B* **2010**, *52*, 67–72.
698. Glagolev N.N., Rogovina S.Z., Solov'eva A.B., Aksenova N.A., Kotova S.L. *Russ. J. Phys. Chem*. **2006**, *80*. Suppl. 1., S72.
699. Glagolev N.N., Aksenova N.A., Rogovina S.Z., Solovieva A.B. *Reports of the Russian Academy of Sciences* **2007**, *416*, 57-59.
700. Kardumyan V.V., Aksenova N.A., Glagolev N.N., Timashev P.S., Solovieva A.B. *J. Chem. Phys*. **2020**, *152*, 194901.
701. Kuryanova A.S., Aksenova N.A., Savko M.A., Glagolev N.N., Dubovik A.S., Plashchina I.G., Timashev P.S., Solovieva A.B. *Russ. J. Phys. Chem*. **2022**, *96*, 747-753.

Received 11.10.2022
Accepted 15.12.2022